FHWA-NJ-2005-025

EVALUATION OF INTEGRAL ABUTMENTS

FINAL REPORT
September 2006

Submitted by

Sophia Hassiotis, Associate Professor
Yaser Khodair, Reasearch Assistant
Eugenia Roman, Research Assistant
Yousef Dehne, Research Assistant

Department of Civil, Environmental and Ocean Engineering
Stevens Institute of Technology
Hoboken, N.J. 07030

NJDOT RESEARCH PROJECT MANAGER

Mr. Vincent Nichnadowicz

In cooperation with

New Jersey
Department of Transportation
Division of Research and Technology
and
U.S. Department of Transportation
Federal Highway Administration

Disclaimer Statement

"The contents of this report reflect the views of the authors who are responsible for the facts and the accuracy of the data presented herein. The contents do not necessarily reflect the official views or policies of the New Jersey Department of Transportation or the Federal Highway Administration. This report does not constitute a standard, specification or regulation."

TECHNICAL REPORT STANDARD TITLE PAGE

1. Report No.	2.Government Accession No.	3. Recipient's Catalog No.
FHWA-NJ-2005-025		

4. Title and Subtitle	5. Report Date
FINAL REPORT **EVALUATION OF INTEGRAL ABUTMENTS**	**September, 2006**
	6. Performing Organization Code

7. Author(s)	8. Performing Organization Report No.
Sophia Hassiotis, Yaser Khodair, Eugenia Roman, Yousef Dehne	

9. Performing Organization Name and Address	10. Work Unit No.
Stevens Institute of Technology Castle Point on Hudson Hoboken, N.J. 07030	11. Contract or Grant No.

12. Sponsoring Agency Name and Address		13. Type of Report and Period Covered
New Jersey Department of Transportation PO 600 Trenton, NJ 08625	Federal Highway Administration U.S. Department of Transportation Washington, D.C.	14. Sponsoring Agency Code

15. Supplementary Notes

16. Abstract

An integral bridge is a single or multiple-span structure that is cast monolithically to its abutments. Stub abutments supported on a single row of vertical piles create a flexible connection that can accommodate the longitudinal displacements of the superstructure. The primary purpose of using integral abutments is the elimination of deck-movement joints and bearings that have been found expensive to maintain.

This research project is centered on the evaluation of integral abutments as a design alternative to the use of bearings in medium-length highway bridges. It includes: 1) an extensive literature search; 2) the instrumentation of Scotch-Road Bridge in Trenton, N.J. to obtain strain data on the piles, displacement and rotation data on the abutment, soil-pressure data on the abutments and the MSE wall, and strain data on deck connection; and 3) a finite element model of the system. The end result is the recommended design procedure for integral abutments of highway bridges.

Integral abutments have been found to be a safe alternative design. A step-by-step design procedure for piles to withstand the horizontal thermal loading is included.

17. Key Words	18. Distribution Statement
Integral Abutments, Bridge Testing, Horizontally Loaded Piles, Design Recommendations	

19. Security Classif (of this report)	20. Security Classif. (of this page)	21. No of Pages	22. Price
Unclassified	**Unclassified**		

Form DOT F 1700.7 (8-69)

ACKNOWLEDGEMENTS

The authors wish to acknowledge the commitment and support of the New Jersey Department of Transportation (NJDOT). In particular, we would like to thank Mr. Anthony Chmiel, Research Project Manager and Mr. Jose Lopez, Deputy Manager of the NJDOT Bridge Bureau for their technical support and guidance during the execution of this project. The authors would also like to thank our partners, Mr. Laverne Wallace and Mr. Ricardo Bermudez of the “Sensing Systems Corporation” for their excellent work in the data-gathering portion of this work.

TABLE OF CONTENTS

LIST OF FIGURES

LIST OF TABLES

CHAPTER 1 - EXECUTIVE SUMMARY

Integral abutment bridges have no expansion joints between the deck and the abutments. They have been in use since masonry arches were introduced thousands of years ago. Modern highway bridges have also been built with integral construction. However, an increasingly analytical approach to bridge design in recent years has resulted in the erection of many new highway bridges that use complicated movement joints and sliding bearings to accommodate calculated thermal effects and horizontal displacements. Unfortunately, many of these jointed bridges are exhibiting deterioration of beam ends, pedestals, and piers predominately caused by the flow, through the bridge joints, of deck drainage waters contaminated with deicing chemicals. Nationwide, rehabilitation costs for damaged bridge joints and substructures figure into millions of dollars annually. As a result, integral bridges are seen as a cost-effective alternative, and are becoming increasingly popular.

The New Jersey Department of Transportation (NJDOT) initiated a research project to:

1. Summarize and evaluate the present state of knowledge in the field of integral abutments.
2. Evaluate the design, details, and construction of a bridge with integral abutments.
3. Instrument the bridge and gather sufficient data to assess present design and construction practices.
4. Use measured data to evaluate and update numerical models, and further use these models to understand the behavior.
5. Use all knowledge gathered to modify the design codes and design assumptions.

To achieve the objectives, a comprehensive research plan has been accomplished. This includes instrumentation and monitoring of the Scotch Road Integral Abutment Bridge, (located in Mercer County, New Jersey, over I-95), literature search, numerical calculations, and ultimately, the presentation of design detailing and construction methods.

As a first step, an extensive literature review has been completed to gather information about integral abutments. We have studied journal papers, conference papers, educational theses, and have gathered and reviewed pertinent information of other Departments of Transportation. The entire system has been reviewed, which includes the abutment, piles, deck-abutment connection detailing, deck, approach slab, expansion joints at end of approach slab, construction practices, etc. A summary of these efforts is found in Chapter 2. The full literature review is found in Roman[1].

In addition, the Scotch Road Integral Abutment Bridge has been instrumented during construction. Data has been collected during 2003-2006 on its behavior under thermal cyclic loading. Numerical modeling using finite element and finite difference codes have been developed to further study the behavior of the bridge. A summary of these efforts is found in Chapter 3.

The research accumulated a set of design criteria for integral abutment bridges, summarized in Chapter 4. These are based on the design specifications of NJDOT, recommendations and practice of other researchers and transportation departments and on the research efforts of Stevens Institute of Technology at the Scotch Road Bridge. A full treatment of the subject is found in Dehne[(2)]

Chapter 5 summarizes the conclusions reached due to this research effort. The bibliography is found in Chapter 6.

The full research efforts are found in Appendix A to appendix I. The appendices are organized as follows:

Appendix A is a summary of the testing program: Description of the testing bridge at Scotch Road, gage description, gage installation, design of new gages, and data acquisition system.

Appendix B is the evaluation of commercially available software (such as L-PILE) that use p-y curves in the design of laterally loaded piles, for its ability to predict the behavior of the piles. A full treatment of the subject is found in Khodair [3]

Appendix C is the development of a finite element model using ABAQUS.[(96)] Specific studies are summarized on the bending of the piles, the influence of the sleeve diameter on the pile bending, and pile buckling. A full treatment of the subject is found in [3].

Appendix D is the summary of a study on the lateral earth pressure developed behind the abutment wall during the daily and yearly cycles of wall displacement.

Appendix E is a summary of the construction sequence used in the Scotch Road Bridge.

Appendix F is a summary of on-going laboratory and full-scale testing around the country.

Appendix G shows the plots of the data gathered during 2003 to 2006 at the Scotch Road Bridge.

CHAPTER 2 - INTEGRAL ABUTMENTS: STATE-OF-THE ART IN ENGINEERING PRACTICE

The use of integral abutments is not new. In the United States, there is evidence that Colorado used integral abutments as early as 1905. But it wasn't until the 1930's that state transportation departments accepted the concept, after the Hardy Cross Method for the analysis of continuous frames became available. Along with the development of a method to analyze continuous structures, the need for integral abutments was also identified. Engineers from the Ohio Department of Highways state that "… there is always the risk of water leakage and concrete deterioration at a joint … intermediate joints are unnecessary."[4] Ohio, South Dakota, and Oregon seem to have leaded the trend of using joint-less bridges in the 1930's and 1940's.

The National Interstate Highway System construction boom in the late 1950's and early 1960's prompted a significant growth in the understanding and design of integral abutment bridges. In the early 1960's, it was realized that joints and bearings were a major source of bridge maintenance problems and that bridges constructed without joints were outperforming jointed bridges. Integral bridges remain in service for longer periods of time with only moderate maintenance and occasional repairs.[5] In 1980, the FHWA recommended that bridges with overall lengths of 300 ft for steel bridges, 500 ft for cast-in-place concrete bridges and 600 ft for pre- and post-tensioned concrete be built as continuous and, if unrestrained, with integral abutments. It also recommended that greater span lengths be used, if experience indicated that such designs are satisfactory.[6] As a result, the construction of integral abutment bridges is becoming the standard in the majority of states.[7,8] A survey of transportation departments reported shows that 20 of 30 departments (60% of survey responses) were already using integral construction for continuous bridges.[5] Many states, including California, Colorado, Idaho, Iowa, Kansas, Missouri, Nebraska, New York, North Dakota, Ohio, Pennsylvania, South Dakota, Tennessee, Virginia and Wisconsin, have used joint-less bridges. New York began building integral bridges in the late 1970's.[9] By 1996, New York had constructed 155 integral bridges (112 pre-stressed-concrete, and 43 steel superstructures.)

In addition to building new bridges with integral construction, many states retrofit their existing bridges to eliminate the abutment joints, in an effort to reduce maintenance costs. A New York study in 1992 concluded that retrofitting designs can be implemented with minimal material and construction costs, resulting in an estimated annual savings of $0.5 to $1.25 million in maintenance cost to the state.[10] A national survey conducted by Rhode Island in 1995 revealed that 22 transportation agencies had eliminated bridge-deck joints on existing steel bridges, 19 of which had retrofitted these older bridges solely to eliminate deck joints.[11] The latest survey on the use of integral abutments is found in Maruri and Petro.[12]

To date, Tennessee holds the record for the longest joint-less bridge: a pre-cast concrete bridge on Tennessee State Route 50 over Happy Hollow Creek. It is a nine-span AASHTO 72 inches bulb-tee girder bridge with composite deck. Its overall length measures 1175 ft. The state of Colorado has built the longest integral bridge with cast-

in-place concrete beams, with a span of 952 ft., and the longest steel girder integral bridge, with a span of 1044 ft.

Advantages and Limitations of Integral Abutments

The absence of problems associated with deck joints and expansion bearings offer a significant maintenance cost savings over the life of the structure. There are additional advantages in the use of integral abutments. 1) Integral abutments eliminate uplift due to dead loads, which results in greater end-span ratios; 2) they increase capacity during seismic events, making integral abutment bridges the preferred structures in more active seismic regions;[13] 3) they provide a reserve live-load capacity to resist potentially damaging overloads, by distributing loads along the continuous and full-depth diaphragm at bridge ends;[14] 4) they lend themselves to a simpler, rapid construction sequence since only one row of vertical piles is used, a deck joint or bearing hardware does not need to be installed, cofferdams (for footing excavation/construction) are not necessary, and the entire end diaphragm/back-wall can be cast simultaneously and with less forming, eliminating the need to form bridge seats; 5) they result in a simplified bridge replacement scenario since integral abutments lack the large bulky footing that is typical for a jointed bridge. This allows integral bridges to be constructed behind existing buried foundations, eliminating the need for additional foundation excavation.

Limitations in the use of integral abutments include: the need for approach slabs, the inclusion of joints at the end of the approach slab, the uncertainty of the pile flexural stresses in the loaded piles, and the imposed limits on the length and skew of the structure.

Objectives

In what follows we will summarize the research projects of the past ten years and the empirical knowledge gained by experienced bridge engineers that helped shape a design method for integral abutments. We will report on: 1) abutment details, 2) the approach slab, 3) the pile design, 4) the behavior of the soil behind the abutment, 5) the details on the superstructure, and 6) the on-going research projects.

Design of Abutment

Figure 1 shows a typical integral abutment. The rigid connection allows the abutment and superstructure to act as a single structural unit by distributing the stiffness and flexibilities of the system throughout the soil/structure system so that all supports accommodate the thermal and braking loads.

Abutment Type

Most researchers agree that the stub-type abutment supported on a single row of piles is the most desirable end condition for an integral abutment.[15,16] While pile-supported integral abutments are desirable, stub abutments on spread footings supported on rock have also performed successfully for horizontal movements up to 0.25in.[14]

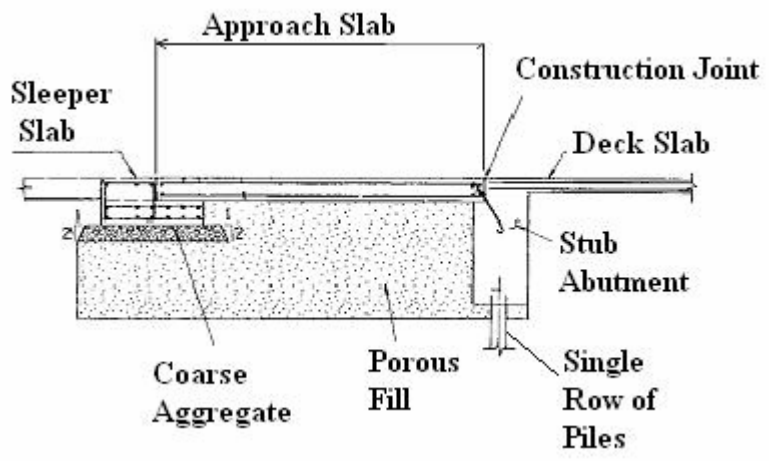

Figure 1. Diagram of the integral abutment system of the Scotch-Road Bridge

Connection Details

Abutment-to-Approach Slab and Deck

Detailing of the abutment-deck continuities have been standardized for a variety of range of applications and are available from a number of transportation departments.[8] Most connections are designed as rigid by using adequate reinforcement detailing between the slab, girders and abutment. Seismic design provisions usually require joint details that must have some level of rotational ductility for energy dissipation purposes.[13] The detailing may vary as a function of structure geometry.

Figure 2 shows a typical connection between an abutment, approach slab, and deck slab for integral bridges. All states use reinforcement bars to connect the slabs to the abutment. States such as Massachusetts, New Jersey, New York and Virginia use a diagonal bar. Others, like Colorado and Maine, use straight bars.

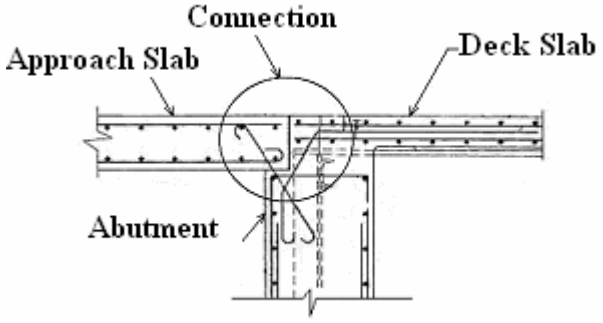

Figure 2. Approach slab connected to an integral abutment [17]

For comparison, a typical connection for a non-integral bridge is shown in Figure 3 where an expansion joint between the bridge deck and the approach slab is used and

the approach slab rests on a corbel. The state of Massachusetts uses such a corbel to seat the approach slab in integral bridges also.

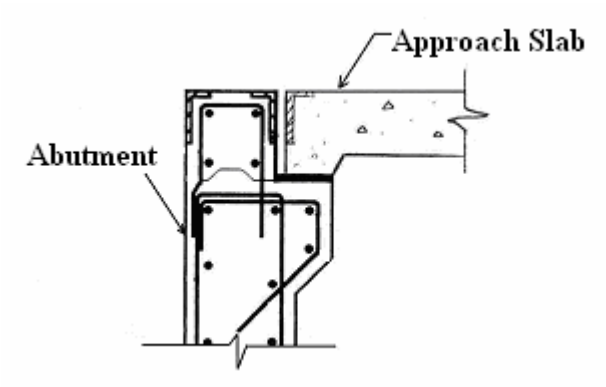

Figure 3. Approach slab connected to conventional abutment[17]

Abutment-to-Girder

A positive connection to the girder ends is usually provided by vertical and transverse reinforcing steel. This connection should fully transmit the temperature variations and the live load rotation that the superstructure experiences into the abutment piling.

Typically, the steel girder rests on a bearing pad or plate placed above the pile, and the bearing area is then cast into the abutment. Steel beams can be connected to the pile caps with anchor bolts prior to making the integral connection.[14] This ensures that the superstructure and the abutment move together. Another suggestion is that the girder is welded to the pile. In such cases, holes are cut through the girder web to allow for continuous transverse reinforcement.

Construction details for pre-stressed concrete girders are similar to that of steel girders. Supplementary details include using grouted pins to connect the beam to the lower portion of the abutment. Sometimes galvanized pipe is run through the web to provide a casing for transverse reinforcing steel.

Abutment-to-Piles

The pile is embedded into the abutment a suitable length to ensure fixity at the connection. Steel piles are typically embedded one-and-a half to two feet into the concrete abutment.[18] The pile should be embedded into the abutment pile cap approximately two-pile diameters to achieve pile fixity to the abutment.[19] In general, HP 10x42 piles embedded one foot into the abutment can accommodate approximately three inches of repeated movement without detriment to either the pile or the abutment.[20] Embedding the pile two feet resulted in significantly less cracking in the

concrete abutment and a correspondingly greater ability to develop a larger interface moment, as compared to a shallower embedment length.[21]

Some states such as Maine, Massachusetts, New Jersey, New York and Ohio require a minimum of two-feet pile embedment into the abutment, while Colorado and Virginia vary from one to one-and-a half feet for their required minimum depth of embedment.

Design of Approach Slab

Most states use an approach slab to mitigate the settlement of the backfill near the abutment and thus provide a smooth transition from the highway pavement to bridge deck.[22] This is in accordance with the FHWA Technical Advisory on integral construction that suggests "approach slabs are needed to span the area immediately behind integral abutments to prevent traffic compaction of material where the fill is partially disturbed by abutment movement. The approach slab should be anchored with reinforcing steel to the superstructure …" [23] A good review of approach slab performance and design is found in [24]. In what follows, we are summarizing the industry findings on accepted detailing of approach slabs in integral bridge construction.

Approach Slab Details

The approach slab should be doweled into the abutment back-wall to ensure a watertight joint.[25] In addition, the slab should be cantilevered over the wing-walls to minimize surface water infiltration. A rigid connection should be used at the approach slab to the abutment to prevent a shifting of the approach slab from its support. [14] It is suggested that the anchorage used to fasten the approach slab to the abutment should act as a hinge so that the slab can rotate downward without distress as the embankment soil settles. Anchorage of the approach slab to the bridge prevents vehicular traffic from consolidating the backfill adjacent to the abutments. [26]

Favorable approach slab details used by the NJDOT are found in Figure 2. New Jersey places the approach slab over a bond-breaking material, such as polyethylene, to reduce friction between the slab and the supporting soil, thus ensuring that the approach slab will move easily as the structures expands and contracts.

Figure 4 shows details used in Massachusetts. Massachusetts has a unique connection where the approach slab is below the finished grade and is not part of the wearing surface. The Ohio DOT places tie-bars diagonally through the slab seat to serve as both an approach slab anchorage and a hinge, which accommodates the settlement of the approach slab as the embankment material consolidates.[27]

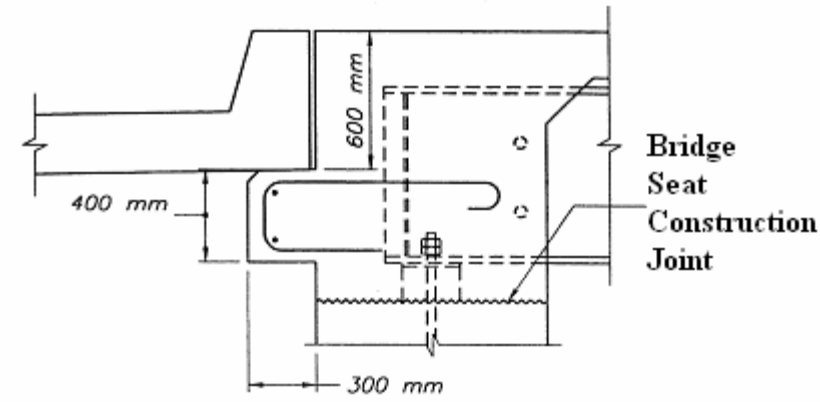

Figure 4. Approach slab details[28]

Length of Approach Slab

The length of the approach slab is often based on experience, finite element simulation and approximate calculations. In general, the length of an approach slab is compatible with the expected settlement. Longer approach slabs are considered in cases involving very soft foundation soils and/or high embankments to provide a more gradual transition in areas of potentially high settlement. A complete table of typical approach slab dimensions used by 35 different states is found in [29].

Using 30-feet long approach slabs supported on select backfill material has been recommended by researchers.[30] Others suggest that the length of the approach slab should be two to three times the height of the abutment. This argument follows from the rationale that displacing the abutment causes movement of a wedge of the backfill soil with a height equal to the height of the abutment and a length equal to tan (45 + F/2) times the height of the abutment, which is about twice the height of the abutment.[22] Here F is the angle of internal friction of the fill.

According to a survey fifty percent of respondents reported a commonly used slab length of 20 ft. [29] The shortest reported length was 10 ft., and the longest 40 ft. The reported thickness of the slabs varied from eight inches for a slab-length of 15 ft. to 17 in. for a slab-length of 30 ft. Approach slabs with a typical length of 20 ft were reported to have a thickness between nine and 15 inches, with an average of 12 in. Most respondents construct full-width (curb-to-curb) approach slabs.

Others recommend that approach slabs be designed to span various lengths, typically 13 to 23 ft.[31] The required design length of an approach slab (L) can be estimated as:

$$L \geq 200\,(S_f - S_a) \qquad (1)$$

where S_f is the estimated total fill settlement at the end of the approach slab, and S_a is the estimated settlement of the bridge abutment. Furthermore, if the bridge abutment is constructed on deep foundations, then the value of S_a can be assumed to be zero.

Slope of the Approach Slab

A 1/200 maximum change of slope in the approach slab has been recommended.[31] The recommendation is based on studies performed by Wahls[[32]and Stark et al. [33]. Less than 1/200 has been suggested to ensure rider comfort.[33] Changes in slope between 1/100 and 1/125 should be addressed with remedial measures.

Effects of Superstructure Type on the approach slab

There is a direct and significant correlation between the condition of the approach slabs and the expansion (span) length of a steel superstructure integral bridge.[9] The longer the span length, the lower the approach slab ratings. Washington State reports difficulties with approach slabs when the bridge length is more than 350 ft.

Design of Piles

Factors that affect pile behavior include loading conditions, pile type and spacing, length of pile-embedment into the abutment, use of prebored holes, and type of backfill. The behavior of abutment piles has been studied early on.[See references34,35,36, and 37] In what follows we will review the most recent conclusions reached by the research community on the design of the piles.

Accepted Analysis and Design Methods for Laterally Loaded Piles

The main form of loading in the piles of an integral abutment is the lateral displacement imposed on the stub abutment by the superstructure. A number of methods being used by different agencies to analyze lateral loads on piles are summarized in [38]. A simplified method that has been developed to design piles for integral bridges introduces an equivalent cantilever column to replace the actual pile-soil system. [39,40] The equivalent cantilever column model was experimentally evaluated and was found to be a sufficient method to accurately design piles for integral bridges.[41] A method for the design of pile caps in integral abutments, called the “group-equivalent pile (GEP)” method, has also been developed.[42]

In solving the soil-structure interaction problem, the p-y method is the most common method used in the United States.[14] It is the basis of proprietary software packages such as L-PILE [43] or COM624P [44].

Rotation and Vertical Loading

Piles embedded in the abutment experience some rotation during lateral loading, depending on the vertical capacity of the piles.[42] Rotation was attributed mainly to deformation or cracking of the concrete at the pile connection to the abutment. As such they suggest that reinforcement in both faces of the abutment be used and a minimum of five inches of cover around the piles be provided. The pile rotation was also attributed to the rotation of the abutment and the pile group as a result of the vertical movement of the piles.

The vertical load-carrying capacity of H-piles is not significantly affected by lateral displacements of up to two inches in soft clay, stiff clay, loose sand, medium sand, and dense sand.[45] However, in very stiff clay, it was found that the vertical load-carrying

capacity of the H-pile was reduced by approximately 50% for two inches lateral displacement and by 20% for one inch of lateral displacement. On the other hand, other researchers speculate that the vertical load-carrying capacity of piles may be reduced due to lateral displacements.[46,47] Additional research is recommended to determine the limitations on the axial load capacity of piles undergoing lateral movement.[48]

Forces in piles that resulted from subjecting a study bridge to one, two and three side-by-side HS20 trucks have been investigated.[18] Finite element analysis results indicated that the pile that was located at the free end of the wingwall was always the most heavily loaded pile in tension. Conversely, the maximum compression occurred in piles located under the abutment. These findings led the researchers to conclude that the conventional methods of computing pile forces under a footing subjected to vertical load and biaxial bending cannot be used to determine pile loads in integral bridges.

Types of Piles

Integral abutments are typically supported on a single row of vertical piles. Several different types of piles have been used, including steel H-piles, steel pipe piles (open-end or concrete filled), and prestressed concrete piles. Steel H-or HP-piles have been used most often.

Steel H-Piles

Steel H-piles oriented for weak-axis bending have been accepted in industry as the best pile type for integral abutments. Experimental data showed that H-piles supporting integral bridges could withstand cyclic loading as long as the maximum stresses remain equal to or less than the nominal yield stress of the pile material. [22,48]

Steel Pipe Piles

Steel pipe piles, either open-ended or filled with concrete, have also been used. Pipe piles filled with concrete have high resistance to local buckling. They also have large moment and shear capacity. [49,50] The pipe piles had high flexural stiffness, which developed large shear forces that could not be transmitted to the abutment. [48] Sites most suitable for pipe piles include soft clays, silts, and loose-to-medium dense sands underlain by dense-bearing granular material.[51] The same research indicates that pipe piles can be driven closed-end or open-end; they are typically economical in the range of 40 to 80 ft., and can carry loads as high as 250 kips.

Prestressed Concrete Piles

Prestressed concrete piles have also been used. An unacceptable amount of damage to a prestressed concrete pile under simulated temperature-induced cyclic loading has been recorded.[16] Concrete piles are too stiff to support integral abutments.[48] Under repeated lateral loads, tension cracks developed in the pile at the connection of the pile to the abutment.

Design Details Used to Reduce Stresses on Piles

The piles that support the abutments may be subjected to high stresses as a result of the cyclic expansion and contraction of the superstructure. Maximum pile stresses occur near the top of the pile. High stresses from cyclic expansion and contraction of

the superstructure can cause formation of plastic hinges in the piles and may ultimately reduce their axial capacity.

Use of Hinges

The current design practice allows for the construction of pile-abutment connection joints to develop full continuity. Consequently, bending moments at pile ends are produced due to longitudinal thermal cycling of the superstructure and dynamic end rotations are induced by the movement of vehicular traffic. These bending moments may be high enough to initiate plastic yielding of steel piles. (See references 34,35,37,46,40, and 41) In addition, the repetitive variation of the loads may cause low-cycle fatigue. (See references 52,53,54, and 55)

In an effort to reduce bending of the piles supporting integral abutments, the ODOT devised a concept that contains a hinge between the superstructure-encased stringers and the abutment pile caps. (53) This hinge accommodates rotation of the superstructures at the abutments due to concrete slab placement and movement of vehicular traffic across the structure. It also accommodates pile cap rotation caused by thermal expansion and contraction of superstructures. Unfortunately, no matter how many water-seepage prevention measures are used, ODOT has found that the water has seeped into the hinged joints and corroded the hinge reinforcement.

The use of hinges has also been recommended for longer integral bridges because they reduce pile stresses. As the need to build longer integral bridges grows, the role of integral bridges with hinges is expected to become more important.(48)

Pile Orientation

The orientation of a pile in an integral abutment system has a significant effect on the stresses generated in the piles. Various states have been known to orient their piles for either strong-axis or weak-axis bending.

- Strong-axis Bending

Strong-axis bending of a pile occurs when the web of the pile is parallel to the centerline of the beam. Piles oriented for strong-axis bending accommodate a greater total lateral displacement than piles oriented for weak-axis bending. Also, they have been shown to provide more rigidity for earthquake loads when liquefaction of the embankment soil is considered. Only a few states prefer to orient the piles for strong-axis bending. Among these are California, Idaho and Tennessee.

- Weak-axis Bending

Weak-axis bending of a pile occurs when the web of the pile is perpendicular to the centerline of the beam. Steel H-piles oriented on their weak-axis are the best pile type for the support of integral abutment bridges. (48) Weak-axis bending generates less stress in the piles and accommodates bridge displacements better, as compared with strong-axis bending. (56) In addition, the vertical load capacity is higher in the deflected piles oriented for weak axis bending. (20) A drawback in the weak-axis orientation is that the total lateral displacement that can be accommodated is limited because of the potential for flange buckling. (57)

New York State recommends constructing integral abutment bridges with lengths greater than 165 ft. using steel H-piles oriented for bending about the weak axis.[9] New Jersey, Iowa, North Dakota, South Dakota, Minnesota and West Virginia are among the states that prefer to orient the piles for weak-axis bending.[53]

Pre-drilling

Pre-drilling oversize holes and surrounding the piles with loose granular material has emerged as a common method to reduce stresses in the piles as well as to increase the vertical loading capacity of piles. (See references46, 56, 58,59,and 60) The pre-bored hole should be approximately twice the diameter of the pile. In theory, the pre-drilling procedure should yield the desired results if the stiffness of the removed soil is higher than that of the sand. [57] Therefore, it is safe to say that pre-drilling is appropriate in stiff soil conditions.

The depth of pre-drilling is an important factor. For example, an HP 10x42 steel H-pile required six to10 ft. of predrilled depth to achieve the desired results. [46] The pre-drilled holes need to be 10 to 20 ft. deep, measured from the pile head.[18] Others report that the pre-bored hole should be at least eight feet deep.[57] In Iowa, all integral abutment piling of bridges with an overall length greater 130 ft. must be driven through an oversize hole predrilled to a minimum of eight feet below the bottom of the pile cap. [56]

Eighteen out of 30 polled agencies did not pre-drill oversized holes for the piles.[38]

Length of Pile

Longer piles (around 20 ft.) experience slightly lower axial stresses than shorter piles (around 10 ft.)[18] Piles in tension, under the wingwalls, were more sensitive to changes in pile length that the piles that were located directly under the abutment beam. Integral abutments should not be used at sites where the abutment piles cannot be driven through at least 10 to 16 ft. of overburden.[26]

Pile Stiffness

The distribution of the forces and the moments in any frame depends on the relative stiffness of the frame members. Therefore, we can effectively reduce the shear and moment at the supporting piles by reducing the stiffness of the piles. To that end, increasing the effective length to the fixity point should decrease the pile stiffness. [59] The abutment movement is resisted if the abutment piles and surrounding soil are too stiff. [61] As a result, the abutment and superstructure are subjected to higher stresses.

Battered Piles

Some bridges have performed satisfactorily when their steel H-piles were battered in the direction of the movement of the bridge. However, battered piles may cause damage to the slab seat. Researchers have found that battering the front row of piles (of a two-row pile system) significantly increases the resistance of abutments to longitudinal shrinkage and cyclic thermal movement of the deck slab, causing a fracture of the slab seat.[19]

In addition, the piles experience reduction in the vertical load capacity due to the abutment movement. Overall, designers have been advised to avoid the use of battered piles in integral abutment construction.

Spacing and pile location

A small number of piles under the abutment significantly increases the compression load on each pile.[18]The number of piles used under the wingwalls does not have the same affect.

Piles in a group carry unequal amount of lateral loads, depending on their location within the group and the pile spacing.[42] The unequal lateral load distribution among the piles is called “shadowing”, which is a term that refers to the overlapping of shear zones and subsequent reduction of soil resistance. One popular method of accounting for the shadowing is to include p-multipliers in the p-y analysis of the piles. The value of the p-multiplier is dependent on the pile location within the group and the pile spacing. The p-multipliers to account for pile group effects by making adjustments to the p-y curves.[62] These multipliers are empirical reduction factors that have been derived from load tests on pile groups. The value of the multiplier is less than one, which results in a reduction in the ultimate soil resistance and consequently eases the shape of the p-y curve.

A diagram that represents the state-of-the-art values to be used in the analysis and design of laterally loaded pile groups can be found in [42].

Pile Fatigue

Two remedial measures that have been developed in an effort to protect the pile against the chance of fatigue damage.[19] These measures include: 1) installation of a hinge in the abutment between the piles and the superstructure, and 2) orientation of the piles for weak axis bending. A low-cycle fatigue damage model for the piles has been used to define length limits of integral bridges. [63]

Design of Wing-walls

Most states utilize wing-walls that are integral with the abutments in joint-less bridges.[14] Cantilever wing-walls up to 20 ft.-long and 10 ft.-high have been used successfully in Tennessee for over thirty years. The wing-walls should be parallel to the axis of the bridge, in order to take maximum advantage of the bending strength of the wing-walls as well as to minimize the exposed area to passive soil resistance during the expansion phase. As the length of the wing-wall increases, the pile loads decrease since the moment arm is longer over a constant applied moment.[18]

Effects of Cyclic Loading and Behavior of Soil

As temperatures change daily and seasonally, the abutment system is subject to cyclic loading and the effects of soil/structure interaction.

Development of Passive/Active pressures

The magnitude and mode of the abutment movement are primary factors that control the earth pressures. Earth pressures increase as the bridge expands and decreases

as the bridge contracts. As the superstructure moves away from the abutment during temperature decreases, we expect that the soil pressures behind the abutment approach an active condition, since it takes very little movement of the abutment to mobilize active pressures. As the superstructure moves towards the abutment, it is possible that the force exerted on the soil mass behind the abutment will mobilize passive forces. As temperature increases, passive pressures do develop.[59] The effect of passive pressure behind the abutments is one important factor that requires further research.[26]

England et al. (2000) and Lock (2002) report that an increase in the earth pressure behind the abutment with time can result in earth pressures that are significantly higher than design values. [64] This condition, which is termed "soil ratcheting", represents a potentially serious long-term source of problems for the integral abutment.

Effect of Approach Fill on Pile Stresses

Interaction between the approach fill and the foundation soil is instrumental in reducing the shear and moment in the piles. In a finite element analysis, they applied the same displacement at two sets of pile-heads: one without approach fill, one with approach fill.[48] Calculations indicate that the approach fill drags the foundation soil as it moves, resulting in less resistance of the foundation soil against pile displacement. Reductions in shear of 40% for loose sand and up to 64% for dense sand are reported.

Effect of Approach fill on Total Movement of Structure

The resistance provided by the approach fill to the expansion and contraction of the bridge is insignificant.[22] Therefore, the expansion and contraction of integral bridges can be calculated using the method recommended by AASHTO [65]

Effect of Approach fill on Structural Integrity of Abutment

The amount of cracking in an integral abutment, associated with horizontal displacement resulting from temperature variations, depends significantly on the stiffness of the soil behind the abutment. [66] Research suggest that red-clay soil, which is much stiffer that compacted fill, contributed to extensive cracking in the concrete abutment.

Effect of Approach fill on Settlement below Approach Slab

Settlement of the supporting soil is the leading cause of longitudinal cracks in approach slabs. [25,57,67] Such ground settlements can be attributed to consolidation of foundation soils, compression of embankment backfill, and localized settlements of the soil near the interface of the approach slab to the abutment.[25,68]

Design Recommendations on Approach Fill

A survey records that most states use a well-graded porous, granular backfill behind their integral abutments.[35] This type of backfill is more easily compacted and it aids in carrying water away from the abutments. Uniformly graded, free draining crushed stone backfill material was used on Virginia's Route 257 over I-81 Study Bridge. However, this is not typical for bridges in Virginia where New-Castle sand and crusher-run gravel are often used as backfill for pile caps, footings and other buried

structures.[26,42] Novel, compressible, elastic materials have been proposed for installation between the abutment and the surrounding backfill.[32] Geo-synthetics could be considered an option for backfill material behind the abutments.[69]

Settlement of the approach fill, “causing a bump at the end of the bridge”, is a common problem for both jointed and integral abutments. However, the problem is further complicated for integral bridges because of the cyclic loading on the backfill. Often a void develops between the backfill and the abutment as the abutments move back and forth. The approach slab is intended to span this void that may develop, to provide a smooth transition between the settled backfill and the abutment, and to deter water intrusion and erosion of the backfill material. Researchers have identified several design details that can be used to limit or eliminate the distress on the approach slab. These include using select backfill material for a distance material for a distance of 150 feet from the bridge as well as waterproofing the approach embankment to minimize the problem.[25] A 95% compaction of the backfill material eliminates settlement of the approach fill and approach slab.[70] The use of well-graded, porous, granular backfill since such material is easily compacted in close spaces and aids in carrying any water away from the abutments. Soil improvement techniques (such as preloading) and use of drainage can also be used to decrease settlement.[22,57]

Some states have resorted to using special details in order to accommodate the cyclic movement of the abutment. For example, North Dakota has a detail that provides an expansion joint material several inches thick behind the abutment back-wall with a piece of corrugated metal behind it.[71] This mechanism was designed to reduce the passive earth pressures on the abutment and to help avoid the formation of a void behind the abutment due to the expansion and contraction of the superstructure.

Superstructure Type

Either steel or concrete girders can be used in the superstructure of an integral bridge. Both materials have yielded long-span integral bridges. However, the type of superstructure will make a difference in the design and response of the integral abutment system. Results from the inspection of 84 integral bridges (30 steel, 54 pre-stressed concrete superstructures) and 105 joint-less decks in New York State show the following: [9]

For all bridges: 1) some cracking was observed on deck and approach slab, posing no structural problems; 2) approach slabs seem to deteriorate more than abutment stem and deck near the abutment; 3) steel superstructures fared better than concrete ones; 4) performance of bridges was poorer for skews greater than 30 degrees.

For concrete bridges: 1) transverse cracks were observed in deck slab; 2) minor settlement under approach slabs force the slabs to act as simply-supported beams, a condition they are not designed for. The additional bending moments create cracking; 3) the greater span lengths contribute to poorer performance of the deck; 4) skew significantly influences the condition of the deck and approach slabs; 5) abutment stems with straight wing-walls performed better than those with flared wing-walls.

For steel bridges: 1) the greater the expansion or span length, the lower is the rating for the approach slab (deck and abutment-stem ratings did not suffer); 2) the greater the skew, the lower were the ratings for the deck and the abutment stem.

Loading on Integral Abutment Bridges

A sufficient design of integral abutments must account for primary and secondary loads, as well as the distribution of these loads through the integral abutment system. In what follows we will summarize loading conditions that affect an integral bridge to a greater degree than a conventional bridge.

Primary Loads

Estimating analytically the effect of the integral abutment to the response of the superstructure is not easy because accurate methods to account for the stiffness of the abutment do not exist.(72)

The type of connection that exists between the superstructure and its foundation affects mainly the seismic loading. In general, integral abutments are preferred for more active seismic design regions, and have performed well in actual seismic events.(73)They are advantageous because they eliminate the possibility of girder support loss, the most common cause of damage to a bridge during a seismic event. Integral abutments also offer significant material reduction by eliminating the need for large bridge seats and restrainers.(See references 14,26,59 and 72)

AASHTO makes specific recommendations with respect to structural analysis and design of bridges for earthquake loading but they are not explicit with respect to foundation analysis and design. The significance of accounting for Soil-Structure Interaction on integral abutment bridges should be standardized. A vast amount of research exists on the subject that has not yet reached the design community. The soil-structure interaction problem for integral bridges is summarized in [74].

Several states have implemented modeling procedures and standard details in their design of integral abutments for earthquake loading. Massachusetts Highway evaluates seismic loadings on integral abutment bridges using finite-element analysis. Oregon DOT has included hooked dowels in the approach slab to restrain earthquake movement with respect to the bridge.(38) Integral abutment bridges should be proportioned to limit displacements to four inches or less in an effort to minimize damage due to earthquakes.(73)

Secondary Loads

Secondary forces due to a) temperature-induced expansion and contraction (thermal loading), b) shrinkage and creep, c) differential settlement, and d) pavement pressure can cause cracks and are of great importance in the design of integral abutments. However, the sum of these secondary effects is so small compared to the typical dead and live loads applied to the bridge, that they can be ignored for bridges less than 300-feet long. These effects should be considered for single spans, the continuity connection of continuous spans, for structures over 300 ft.-long, for structures where

passive pressure effects are greatest and for structures exposed to sustained high temperatures.[75]

Thermal Loading

The typical behavior of an integral abutment bridge depends primarily on the bridge temperature. Both daily and seasonal temperature changes affect integral bridges and cause the bridge to expand during temperature increases and to contract during temperature decreases. This cyclic behavior results in lateral displacements that must be accommodated by the pile/abutment system. These movements can cause 1) changes in the stresses and strains in the piles under the abutments; 2) changes in lateral earth pressures on the abutments, diaphragms and wing-walls; 3) changes in movement of the approach slabs; and 4) the development of a settlement trough adjacent to each abutment, caused by the backfill soil slumping downward and toward the back of each abutment.

In addition to lateral displacements and forces, thermal gradients through the depth of the superstructure generate secondary bending moments because the centroid of the temperature-distribution curve may not coincide with the centroid of the beam cross-section. Studies on the temperature distribution over the cross section of bridge beams indicate that the most important factors in temperature distribution are 1) the maximum temperature differential and 2) the distribution of this differential across the depth of the beams. (See references 76,77,78 and 79) For concrete structures in moderate climates, the moments induced by thermal gradients can be ignored.[75] The moments generated by the thermal gradient are similar to those generated by creep or shrinkage, and can be calculated according to AASHTO[65]

Shrinkage and Creep

Creep and shrinkage is a consideration in both integral and non-integral bridges. These effects are particularly important when integral abutments are used with concrete superstructures. The greatest effect of shrinkage is apparent on the positive moment of single spans and on the continuity connection at the abutment of continuous span integral bridges. Shrinkage has a lesser effect on the negative moments at piers of two and three span bridges and only a slight effect on the positive or negative moments at the mid-span of continuous spans. [75,80] Equations used to calculate the shear force and moment due to shrinkage can be found in [75].

Differential Settlement

Differential settlement is a concern for both jointed and integral bridges. Causes of differential settlement include:[31] 1) compression of the fill material, 2) settlement of the natural soil under the embankment, 3) poor construction practices, 4) high traffic loads, 5) poor drainage, 6) poor fill material and 7) loss of fill by erosion. We can add that plastic deformation and flow of granular soil under cyclic loading

Differential settlement can result in secondary bending moments in integral bridges. if the differential settlements are less than 1.5 in., the resulting induced secondary moments can be ignored.[80] Simple procedures to estimate differential settlement can be found in [81] and [82].

Pavement Pressure

Pavement pressure is a term for the compressive longitudinal force that develops within the approach pavement due to the cyclic movement of the approach pavement at debris-filled pavement joints. This pressure is typically transmitted to the adjacent approach pavement of the bridge. The cyclic movement of integral abutments amplifies this pressure generation. A pavement "blowup", or an instantaneous fracture or damage of the pavement, is evidence of the high compressive stresses that can be present within the pavement.(19) Pressure relief joints are typically incorporated into the approach system of integral abutment bridges to accommodate this pressure.

Transportation departments are aware that the design of approach pavements for integral bridges needs special consideration and provisions to avoid distress.(19) Pressure relief joints are typically installed in the approach system of jointed and joint-less bridges to relieve this residual pressure. A joint should be provided in all cases where the approach roadways or ramps are constructed of concrete and when the anticipated total movement at an abutment exceeds half-an-inch against an asphalt approach roadway.(57) However, using joints that contain metal hardware for anchorage is discouraged since laborious modifications to the joint hardware would be necessary if the roadway is repaved in the future. The Tennessee Department of Transportation (TDOT) routinely incorporates silicone expansion joints between the approach slabs and the asphalt pavement to account for the possibility of abutment movement and to relieve pavement pressure.

Skew and Geometry of Structure

Skew on jointed bridges is easily accommodated. However, the skew of an integral bridge presents a concern to designers because skew can affect the transfer of the loads.

Effect of Skew on Pile Stresses

Skewed integral abutment bridges generate thermal-induced biaxial bending stresses in the piles. When H-piles are used to support the abutment, the biaxial loading will translate into increased pile stresses depending on the pile orientation with respect to the skew. An analysis of this problem is found in [47].

Affect of skew on Soil Pressures behind Abutments

A 20^{o}-skewed bridge had significantly variable soil pressures, with the maximum value occurring at the obtuse corner and the minimum value occurring at the acute corner. This observation indicates that the obtuse corner moves into the backfill soil more than the acute corner.[83]

Condition Rating Based on Skew

Thirty steel superstructure bridges with integral abutments at varying skews were inspected and rated.(9) The research assigned a numerical rating to the condition of the bridge deck, the approach slab and the abutment stem. The numerical rating was based the scale of the State of New York, which rates the condition of a structural element according to the amount of visible deterioration/distress. Analysis of the

condition ratings of the bridges indicated that the greater the skew of the bridge deck, the lower the condition ratings were for the deck, approach slab and abutment stem. Field inspections of 84 steel and concrete integral bridges in New York State concluded that steel structures performed better than concrete structures without skew or with skews less than 30°. Both steel and concrete bridges performed poorly with skews greater than 30°.

Acceptable Skew Angles

Researchers do not seem to agree on a limit for skew angles. For example, some suggests that the sharper the skew, the more desirable it is to use integral abutments since the rugged integral connection of the abutment and deck can be mobilized to transmit horizontal forces to the abutment system.(84) However, others note that sharp skews are problematic to bridges of all types, with or without joints.(70)

Table 1 shows the limiting skew angles used by about 30 state agencies.(38) The majority of the states have limited the skew angle on integral bridges to 30°. Connecticut DOT and Oklahoma DOT do not allow integral abutments on skewed bridges while TDOT and Colorado DOT have no limit of skew on integral abutment bridges. Others suggest limiting the bridge skews to less than 30° to mitigate pile overstress.(26)

Table 1 - Maximum allowable limits(38)

		Length (feet)					**Height (feet)**	
State or Prov.	Thermal Movement (in)	Steel Girder	Precast-Concrete Girder	Cast-in-Place Concrete Girder	Skew Angle (Deg)	Tolerance for Pile Location, (in)	Abutmnt	Stem
AK	-	-	200	-	30	3	-	-
AR	-	300	300	-	15	Per Specs	No Lim.	No Lim.
CA	0.5	102	167	167	21	4	14	9
CO	4	300	600	500	No Lim.	6	No Lim.	No Lim.
GA	No Lim.	No Lim.	No Lim.	No Lim.	30	No Specs	No Lim.	No Lim.
IL	No Lim.	275	375	375	30	Standard	No Lim.	No Lim.
IA	Limited by Length	Undet.	500	500	30	3	3 to 5	Length Depend.
KS	2	300	500	500	45	3	By Design	By Design
KY	No Lim.	300	400	400	30	6	No Lim.	3 ft min. pile cap
ME	3.7	295	490	490	25	2	12	-

MD	1	-	60	-	30	6	10 to 15	10
MA	Not defined	325	325	325	30	3	Min.	Minimize
MI	No Lim.	No Lim.	No Lim.	No Lim.	30	6	-	-
MN	No Lim.	200	200	200	20	No Specs	3.2	3.2
NV	1	250	400	400	20-45	-	Design	Design
NH	1.5	150	80	-	10	-	-	-
NY	Limited by Length	460	460	460	30	1	-	1 to 2
ND	Limited by Length	400	400	160	30	No Specs	3.7	2 to 6
OK	-	300	400	-	0	6	3.1	6
OR	No Lim.	No Lim.	No Lim.	No Lim.	45	No Specs	No Lim.	No Lim.
PA	2	300 to 400	400	Not Used	20	-	-	-
QC	No Lim.	-	256	-	20°15'	2	10	6
SD	Limited by Length	350	700	700	30	6	No Lim.	-
TN	2	430	800	800	No Lim.	No Specs	-	No Lim.
VT	Limited by Length	80	-	-	15	Standard	No Lim.	No Lim.
VA	1.5	300/ 150[a]	500/ 260[a]	-	30	3	No Lim.	No Lim.
WA	No Lim.	Not used	350	200	30	6	-	12
WV	2	Movement is Limited, Not Length			30	3	No Lim.	No Lim.
WY	2	330	No Lim.	330	45	0.8	No Lim.	No Lim.
Max.	**No Lim.**	**No Lim.**	**No Lim.**	**No Lim.**	**No Lim.**	**Per Specs**	**No Lim.**	**No Lim.**
Min.	**0.5**	**80**	**60**	**160**	**No Skew**	**0.8**	**3**	**1**

[a]Lesser value used with maximum skew

Length of Structure

One of the main reasons for the increasing use of integral abutments is the long-term economy associated with joint-less bridges. The application of this type of construction

to longer and longer bridges suggests additional savings, but also may introduce unanticipated problems.

Maximum Length

A maximum length of integral bridge is very difficult to determine.[22] Many researchers agree that a thorough understanding of the complex soil/structure interaction of an integral bridge is necessary in order to expand the current limits on the lengths of integral bridges. Often, it is previous experience that encourages designers to extend the length of integral bridges.[26]

A low-cycle fatigue damage model for the piles has been used to define the maximum length limits of integral bridges.[54] The maximum strain amplitude has been calculated that a steel pile can sustain and retain a service life of 75 years. Accordingly, maximum bridge lengths have been proposed of concrete superstructures of 490 to 870 feet in cold climates, 590 to 1050 feet in moderate climates. For steel superstructures the bridges range between 260 and 475 feet in cold climates and 410 to 720 feet in moderate climates.

Maximum Horizontal Displacement

Usually, the maximum horizontal displacement that can be accommodated by the abutment and piles determine the acceptable length of the superstructure. For example, the TDOT permits one inch of horizontal pile movement at the ground surface in each direction. For steel bridges erected at 60^{o} F and expected to undergo a temperature range of 0 to 120^{o} F this leads to a total bridge length of 440 feet. For concrete bridges erected at 35^{o} F and expected to undergo a temperature range of 25 to 95^{o} F this leads to a total bridge length of 730 feet. Only minor cracking occurred at these displacements.[21] It is of interest to note that the TDOT has built longer integral bridges that perform adequately, namely a 525-foot long steel bridge and an 1175-foot long concrete bridge.

Integral abutments could easily accommodate up to two inches of total movement, if properly designed.[14]

Integral abutments with hinges may be used for longer integral bridges since the hinges have been found to reduce pile stress.[48] However, adequate research about the construction and performance of such hinges does not exist.

Curved Bridges

Research on the use of integral abutments on curved bridges is scarce and the problem is not well understood yet. It is difficult to anticipate the path of movement of curved structures.[20] For example, it could be along the radial axis of the deck or the chord line of the end span girders or along a chord struck from abutment to abutment.

Deck Design

Elimination of the joints will subject the superstructure to secondary stresses that are due to the response of the structure to thermal and moisture changes, settlements of the substructure, post-tensioning, and the cyclic movement of the bridge. These stresses can be significantly above those permitted by current design specifications,

and occasionally, the design is not sufficient to prevent structural distress and fracture of the structure.[5,7] A review of joint less deck designs is found in [85] The feasibility of joint-less bridge decks for rehabilitation projects is found in [10]. A survey on the elimination of deck joints in North America is found in [11].

Crack patterns

Minor cracking of the deck and approach slabs of integral abutment systems have been observed.[9] Transverse cracking has also been noticed 1) in the deck slab at the beginning of the notch-down and 2) at relatively uniform spacing along the deck. Although a minor structural problem, such cracking could affect the serviceability of the structures.

Typical patterns of early-age deck-slab cracking in integral bridges include diagonal cracks that occasionally develop at the acute corners, and transverse cracks that occasionally develop over (previously) placed concrete end-diaphragms.[53]

Secondary stresses in the bridge deck caused by thermal changes and settlement of the substructure can be significantly greater than those permitted by current design specifications and are responsible for deck cracking. It should be noted however that maximum transverse stresses in the deck slab can be 25-50% lower for integral bridges than the simply supported bridges.[18]

Deck cracking at abutments has also occurred as a result of insufficient continuous temperature and shrinkage reinforcement in the deck slabs over the end-diaphragms at the abutments. Connections between the static abutments and the moving deck/superstructure can be stressed and crack if a significant temperature change was to occur during the initial concrete setting or if proper construction inspection methods were not adhered to during the setting.

The condition of the deck can be correlated to the associated condition of the abutment stem and to the horizontal displacement.[9] A greater displacement results in an inferior condition of the deck and the abutment stem.

Skew angles also affect the condition of the deck and abutment stem. A greater skew results in lower condition ratings for the deck and abutment stem.[9]

Settlement of the soil beneath the approach slab has been linked to both transverse and longitudinal cracking of the concrete deck. For example, transverse cracking has been observed in all lanes that developed a void and experienced the loss of support under approach slabs.[67]

Design Detail to Avoid Deck Cracking

The state of Ohio has considered the potential deck-stresses that would be associated with integral abutments. Consequently, their standard integral abutment detail connects the deck slab to the abutment with an un-reinforced key. This detail has proven successful for bridges with a maximum length of 175 ft. and skew of up to 30^{o}.

Accepted Design Methods

Wolde-Tinsae and Klinger [36] offer a report on integral bridge design and construction. Wasserman [7,14,20,57] seems to have produced the most comprehensive design method

for integral abutments. A design approach for pre-stressed-concrete girder integral bridges is found in [55].

Conclusions

In this chapter we summarize the current state of knowledge and experience on the design of integral abutments. Although state agencies are surging ahead with the design and construction of longer integral bridges, it is evident that an accepted design process is not available, and recommendations on design are made mainly on the basis of practical experience.

In general, stub abutments supported on a single row of piles are used. An approach slab is included and provided with rotational degrees of freedom at the connection with the superstructure. In the design of piles under integral abutments, bridge engineers have taken the following general approach: 1) limited the horizontal displacement allowed; 2) limited the use of piles to only a single row of long, slender, vertical piles oriented on the weak axis of bending; 3) specified bored holes in stiff foundation materials and filled the holes with fine-grained material; 6) limited piles to steel “H” sections that may have a longer fatigue life; 7) reduced the penetration of abutments into embankments to reduce the resistance of surrounding soil to pile and abutment movement; 8) controlled the skew to minimize pile deflection in both longitudinal and lateral directions. The backfill soil behind the abutment is recommended to consist of well-compacted granular fill.

The development of standard details and design specifications would help in the acceptance and use of this design alternative. In addition, we recommend that further research is needed in several areas: 1) the development of passive pressures behind the abutment due to the cyclic loading; 2) the contribution of the abutment in reducing stresses and rotations on the pile tops; 3) possible fatigue effects at the pile/abutment connection; 4) simplified methods to take into account the soil/structure interaction for earthquake loading calculations.

CHAPTER 3 - SUMMARY OF RESEARCH ON SCOTCH ROAD BRIDGE

An integral-abutment bridge is designed to transfer the temperature and traffic-induced horizontal loading to its foundation. The mechanism eliminates bearings, which have been a source of expensive rehabilitation. Although integral abutments have been used successfully by many states, a nationally accepted design methodology does not exist for their design and construction. Instead, each highway department depends on the experience of its engineers to push the design envelope.

The New Jersey Department of Transportation is in the process of revising its design specifications on integral bridges, and to this end, it has funded an extensive testing program to monitor the Scotch Road Integral Abutment Bridge. The summary and most relevant conclusions of the research program are presented in this chapter.

The research can be broken down to four major components: 1) an extensive literature review; 2) the review of current design procedures and the introduction of a step-by-step procedure for the design of the integral abutment piling; 3) the instrumentation and data gathering of the Scotch Road Bridge; and 4) the analytical study of the bridge with finite elements.

Literature Review

For the literature review, the synopsis of the research in integral abutments since the 1990's has been given in chapter 1. Empirical knowledge, university research, design manuals, and any work that contributed into this area of engineering have been studied and the relevant conclusions summarized. The review includes all areas of the abutment such as detailing, approach slab, pile design, passive pressure behind the abutment, details on the superstructure, etc. Overall, it can be concluded that the use of integral abutments should be a preferred method of construction and that problems associated with integral abutments (such as skew, curvature, bridge length) can be overcome with smart design.

A Step-by-Step Procedure for the Design of Integral Abutments

A step-by-step procedure for the design of integral abutments is given in chapter 2. The procedure is based on current design measures by the NJDOT, the design practices of other transportation departments, and recent research by Stevens and other research groups. In general, it was found that the directives provided by the NJDOT have been among the most prevalent and accepted practices.

Instrumentation and data gathering at the Scotch Road Bridge

The test site, set up and instrumentation is summarized in appendix A. In summary, the Scotch Road Bride, which is located in an urban, 4-lane highway crossing Interstate 95 in the vicinity of Trenton, New Jersey, was chosen as the test structure. The existing highway bridge on Scotch Road was replaced with a new, wider structure. The new bridge is a 2-span continuous HPS70W steel- girder structure supported on a conventional pier with fixed bearings and integral abutments.

The bridge is 298 feet long, built of steel plate girders spaced at 11 feet on centers across a width of 104.3 feet. A multi-column bent supported on spread footings comprises the pier. The structure has a skew of about 15^{o} measured from the centerline of bearing to the centerline of bridge.

The abutments average 11 feet high and 3 feet thick. Each of the abutments is supported on a single row of 19 HP360x152 piles, oriented for weak-axis bending. The piles are approximately 38.5 feet long. A two-foot diameter corrugated steel sleeve was placed around each pile and subsequently backfilled with granular material to increase the flexibility of the system. Compacted crushed stone was used as a backfilling material between the piles and the steel mesh tying the components of the MSE wall. The soil behind the abutment and below the approach slab is well-compacted I-9 porous fill.

The bridge was instrumented during construction and has been monitored continually for the past three years. The following types of measuring devices were used: (1) strain gauges along the depth of the piles (as well as inside the abutment mass); (2) soil pressure cells for measuring the horizontal soil pressure behind the abutment, on the galvanized sleeves surrounding the piles, and at two elevations on the MSE wall; (3) inclinometers for measuring the rotations at the connection between the abutment and the stringers; (4) round displacement transducers connected to four strain gages for measuring the longitudinal displacement at the relief slab and (5) thermocouples to monitor the temperature of the concrete slab and the steel girders.

The following figures are given as a summary of the measurements obtained in this research effort. The full data is given in appendix G.

Figure 5 is a plot of the temperature variation with time. During the summer, the top of the deck reached up to 20^{o}F higher than ambient. In the mean time, highest and lowest temperatures in the girders were measured at the bottom and they were up to 10^{o}F higher than ambient. During the winter, the deck and the top and bottom of the girders were approximately at ambient temperatures.

Figure 6 is a plot of the bridge displacement during the daily and seasonal temperature variation. The bridge response to temperature variation is as expected. This displacement was used to study the pressure built up behind the abutment and the movement of the piles supporting the abutment.

Figure 7 is a plot of the rotation of the bridge. Rotation is not taken into consideration in the design of the substructure but it can be considerable especially in the summer months that see a rotation almost double the one measured in the winter. This is due to the fact that the temperature variation along the depth of the girder, which is the main cause of the rotation, is negligible during the winter.

Figure 8 is a plot of the axial stresses developed at the top of the piles due to the displacement and rotation of the abutment. In general we found that the expected values are below the measured values. This is due to the fact that the abutment is flexible and does not transmit all of the displacement to the piles.

Figure 9 shows the variation of pressure along the abutment wall. In general, we see a built up of pressure behind the abutment. A steady built up can be explained by

plastification and flow of granular material during cyclic loading, which is known in the literature as “strain ratcheting”. In addition, we see jumps in pressure after the winter months. During low temperatures, soil moves behind the abutment to fill the gap left by the shrinking structure. Daily cycles during these months set and densify this soil. During the spring months, as the temperatures start to increase, the bridge is pushing into dense ground and is meeting with high resistance. It is also possible that the top ground is semi-frozen during early spring. Further research is needed to isolate all the mechanisms responsible for the pressure built-up and to conclude on the possible ramifications on the integral abutment design.

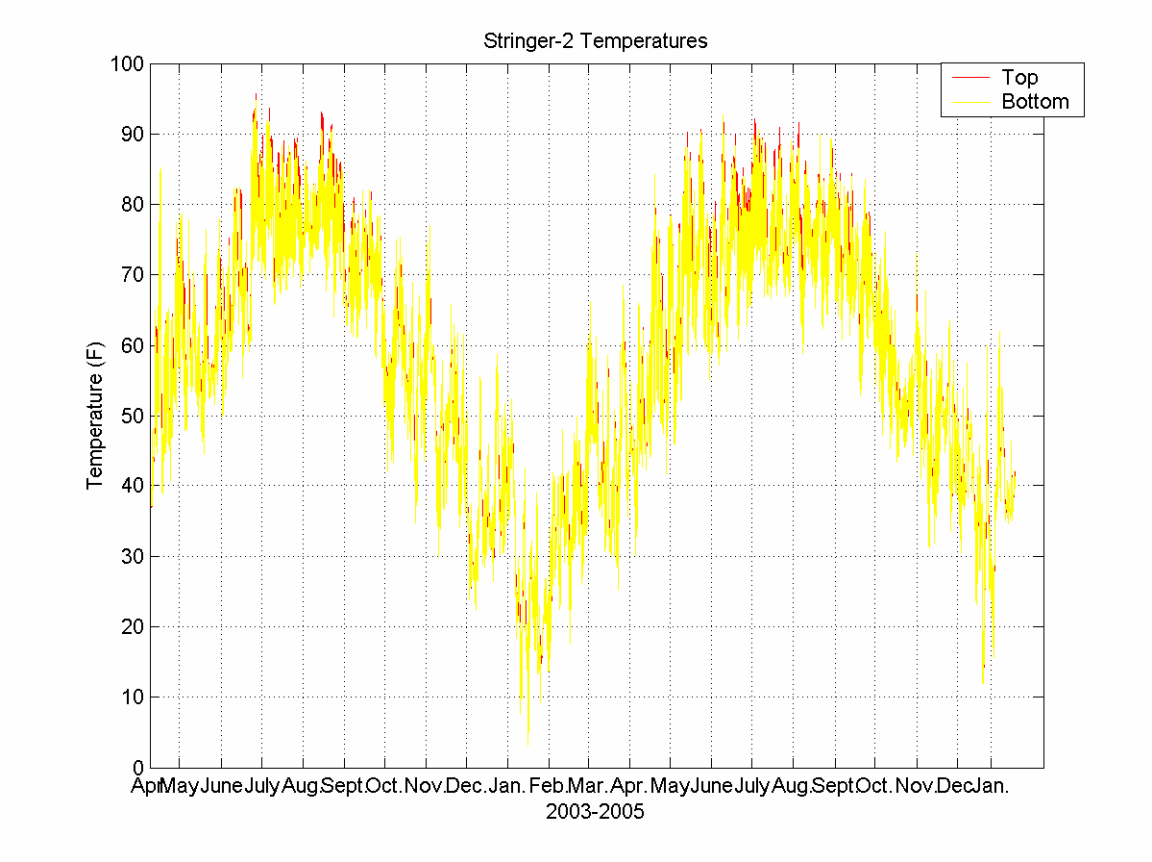

Figure 5. Temperature on top and bottom of Stringer 2

.

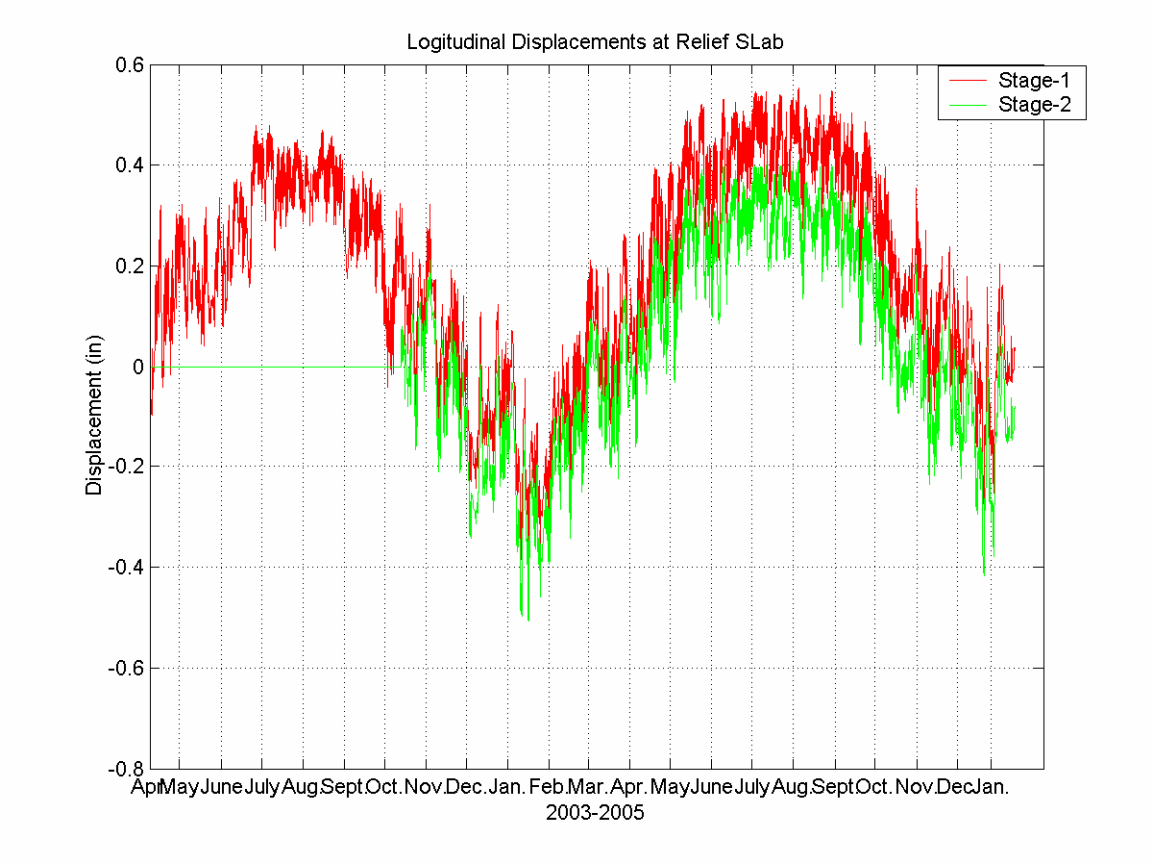

Figure 6. Longitudinal displacement at the relief slab

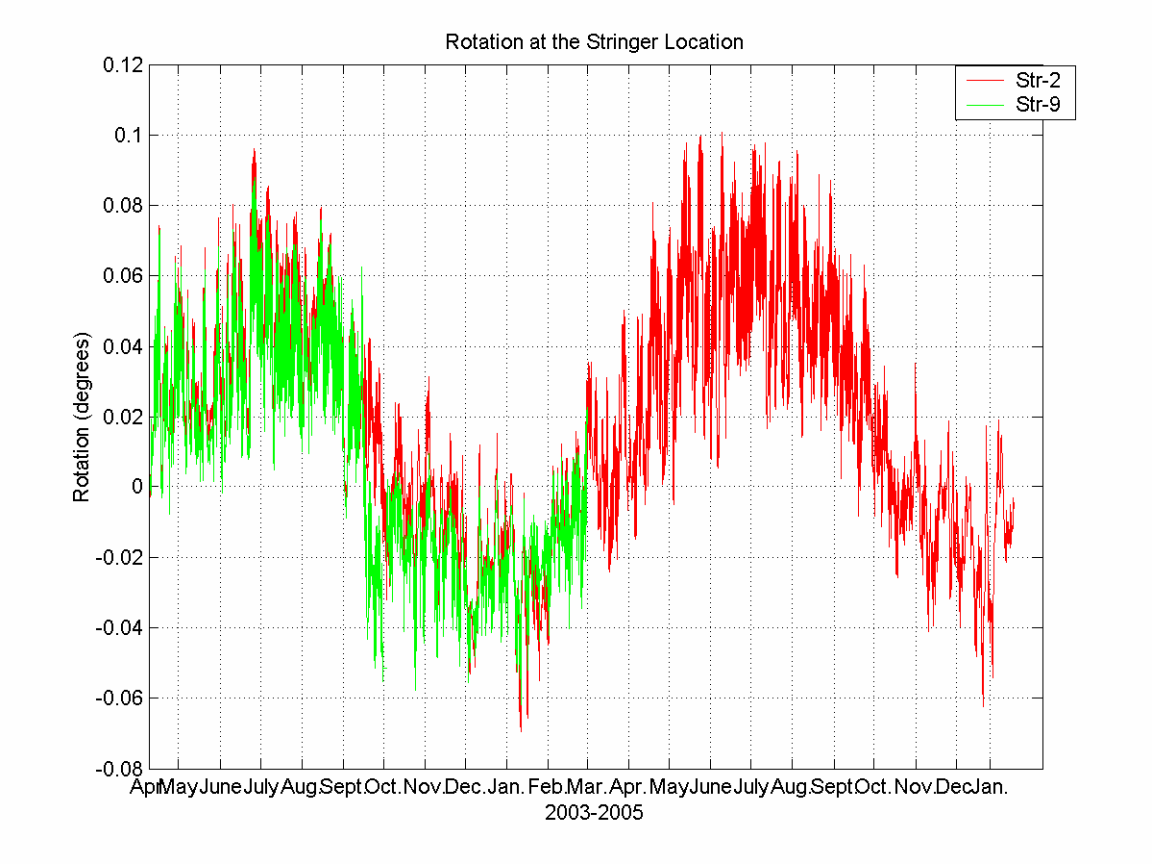

Figure 7. Rotation of the stringer at the connection with abutment

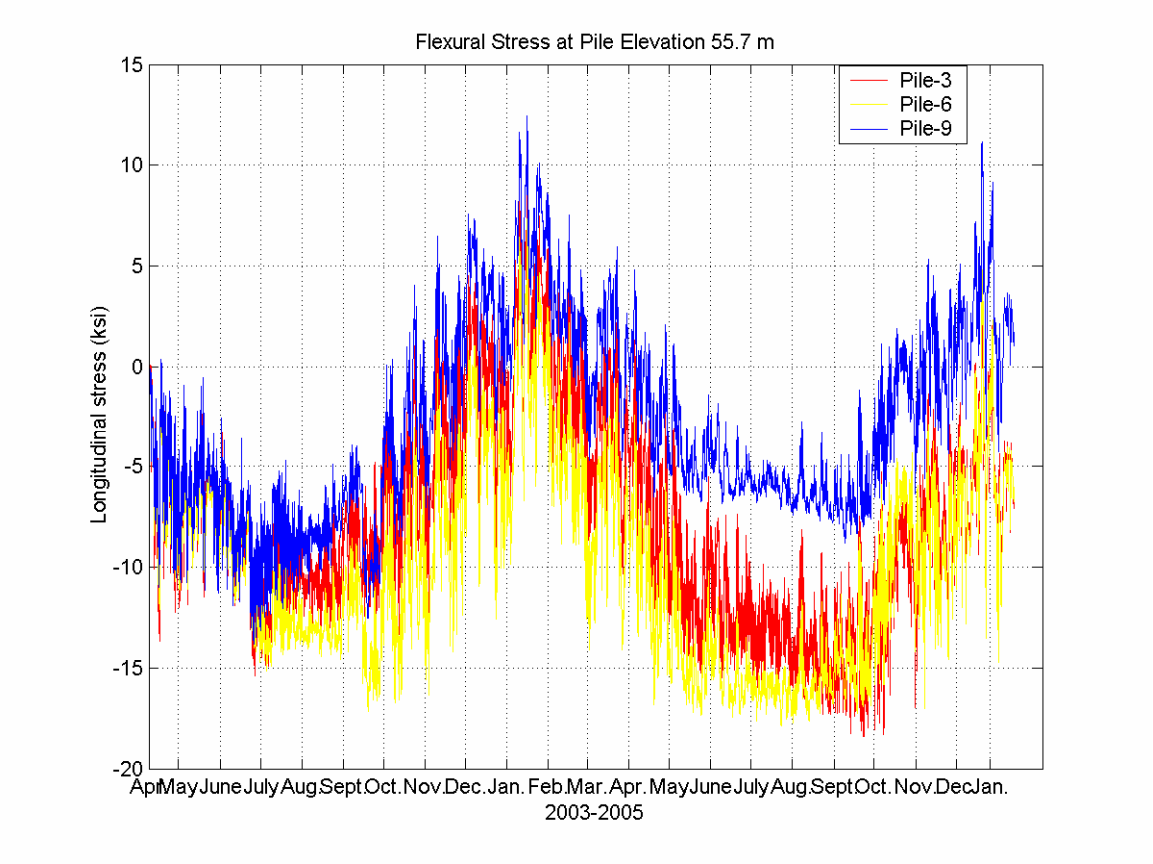

Figure 8. Axial stress at pile top

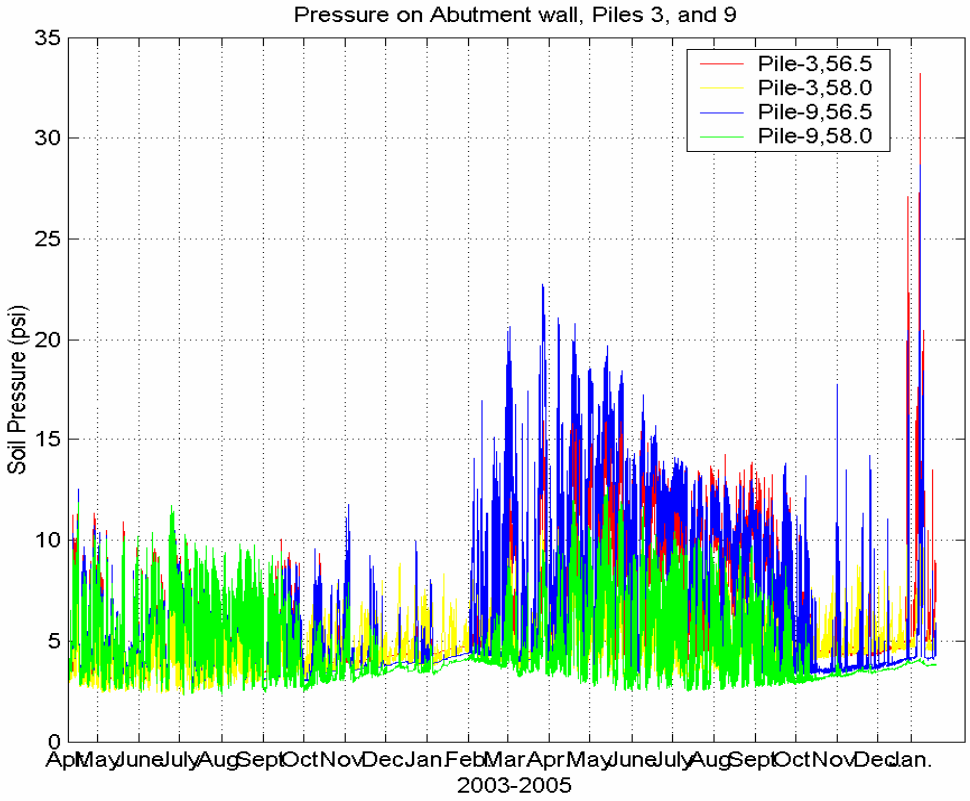

Figure 9. Soil pressure along the abutment wall

Analytical Study of the Bridge with Finite Elements

Three-dimensional finite element models were prepared using the commercially available software ABAQUS to study the behavior of the bridge substructure. Two distinct studies were undertaken: 1) parametric studies on the behavior of the piles in bending and 2) parametric studies on the buckling capacity of horizontally loaded piles.

The full treatment of the subject is found in Khodair[3] The detailed analysis is found in appendix C. In this section, a summary of the work is presented.

Parametric studies on the behavior of the piles in bending

A three-dimensional, nonlinear finite element (FE) model of an integral abutment bridge has been developed to study the effect of thermal loading on the soil/pile system using ABAQUS.[96] The finite element model consists of soil continuum elements. Material non-linearity is accounted for both, the piles and the soil. The measured displacements induced by temperature changes were used as an input to the analytical model. The analytical results were compared with experimental data

The objective in this work was to determine: 1) the stresses on the piles during thermal loading, and 2) the transfer of lateral loading from the piles to the MSE (Mechanically Stabilized Earth) wall that supports the foundation of the bridge.

The FE model includes the study of HP piles embedded in a single layer of sand confined within the corrugated galvanized steel sleeves. Each pile is modeled using eight-nodded solid continuum elements. The boundary conditions on the top of the pile ensure rigid translations and rotations. The rigid connection at the top of the pile was implemented through tying the top surface of the pile to the bottom surface of the abutment to ensure maintaining zero slope at the top of the pile, and hence full fixation of the piles into the abutment walls. The non-linear response of the soil was also modeled using solid continuum elements. The sand-pile interaction was modeled using the surface-to-surface contact algorithm found in ABAQUS.

One load case that is of major concern for integral abutment bridges is the loading associated with thermal expansions and contractions. The loading was implemented in the FE model as an imposed displacement and rotation boundary conditions. The material for the steel pile was assumed to be elastic perfectly plastic. An elastic-plastic model was adopted for the reinforced concrete integral abutment. The soil was modeled with strain hardening model according to Mohr Coulomb failure criterion. The FE results were compared to finite difference solutions.

The effect of the diameter of the galvanized steel sleeve surrounding the HP pile has been studied. The results from the FE model showed that the magnitude of the axial stresses in the pile decrease as the diameter of the sleeve increases and hence, the amount of sand surrounding the pile increases. However, the crushed stone pressures calculated at the perimeter of the galvanized steel sleeve are approximately zero in magnitudes regardless of the change in the diameter size. These results were substantiated by the pressure measurements recorded at the perimeter of the galvanized steel sleeves by the soil pressure cells. This part of the research suggests that providing a galvanized steel sleeve of one-foot in diameter filled with sand is sufficient for accommodating the pressure developing as a result of the expected thermal loading. In addition, it became evident that increasing the size of the diameter of the galvanized steel increases the capacity of piles to lateral loading.

Parametric studies on the buckling capacity of horizontally loaded piles

The buckling behavior of a single pile and a pile-bent was also studied using three-dimensional finite elements. An iterative linear analysis based on extracting the eigenvalues of the pile has been adopted. The finite element model consists of soil continuum elements. Material non-linearity is accounted for both, the piles and the soil in the base state of the model. A parametric study has been utilized to determine the effect of the geometric and material properties of the pile and the surrounding sand on the predicted critical buckling loads of the piles. We found that the group effect in the pile-bent increases the magnitude of the critical buckling loads as compared to single piles.

The FE model focuses on modeling HP steel piles supported laterally along their depths by sand confined within galvanized steel sleeves. Each pile is modeled using eight-nodded solid continuum elements. The sand bounding the piles was also modeled using solid continuum elements. The boundary conditions in the FE model were meant to emulate the restraints imposed on the piles and the surrounding soil in the construction site. The length of the pile adopted in the model is 17 feet, eliminating the

portion of the pile embedded in plain concrete. Accordingly, all the degrees of freedom of the nodes that belong to the bottom surface of the pile were restrained. The degrees of freedom of the nodes bordering the sand-sleeve were also restrained due to the confinement of the sleeves by the crushed stone backfilling. The surface-to-surface contact algorithm in ABAQUS/Standard was used to model the interaction between the steel pile and the surrounding sand. The friction coefficient estimated by the tangent of the friction angle between the steel pile and the encircling sand was used to define the tangential contact behavior between the two materials.

The material for the steel pile was assumed to be elastic perfectly plastic. An elastic-plastic model was adopted for the reinforced concrete integral abutment. The non-linear nature of the soil was included into the base state of the model. A strain-hardening model defined according to Mohr Coulomb failure criterion, was adopted.

A parametric study was conducted to study the effect of the stiffness of the soil surrounding the pile, the pile length, the boundary conditions at the top and bottom of pile, and the effect of combining axial and lateral loads. The parametric study revealed that all four factors studied significantly affected the magnitudes of the critical buckling load of the pile. The single-pile buckling model showed that the pile globally buckles at a vertical load of approximately 3000kips for (fixed with sway-fixed) boundary conditions. However, embedding the pile into a one-foot galvanized steel sleeve filled with sand increased the pile capacity against buckling by 17 times. The results from the parametric study for the pile-bent model also emphasized that the group effect substantially increases the buckling capacity for each of the piles (2.5 times that of a single pile embedded in sand with fixed with sway-fixed boundary conditions). However, applying combined axial and vertical loading has an adverse effect on the pile capacity for buckling, and the critical buckling load decreases significantly under this type of loading.

CHAPTER 4 - DESIGN RECOMMENDATIONS

Introduction

Integral bridges are single or multiple span continuous structures that are cast monolithically to their abutments. Stub abutments supported on a single row of vertical piles create a flexible connection that can accommodate the longitudinal displacements of the superstructure. The primary purpose of the integral abutments is the elimination of deck movement joints and bearings.

The integral abutment bridges are different than the traditional rigid frame bridges, which resist the longitudinal loading with full-height abutments, either fixed or pinned at the base.

Integral abutment bridges have been found to be economical to both, construct and maintain and should be considered as a viable option for slab and slab on stringer, steel or concrete bridges.

What follows is a set of design recommendations based on a combination of 1) the original design recommendations of the NJDOT; 2) the practice and experience of other engineering and transportations agencies in the United States and Europe; 3) the research of the last 10 years in the United States and Europe; and 4) the research conducted by Stevens Institute of Technology at the Scotch Road Bridge.

Initial Criteria

You may use an integral bridge option if the following guidelines are met.

1. Skew angles are less than 30^{o}.

***Commentary*:** Integral abutments for skewed bridges experience a component of soil passive pressure in the transverse direction during thermal elongation. A skew angle of 20^{o} does not mobilize the transverse pressures and is a reasonable theoretical upper limit for the skew. [86]. In the field, bridges with skews of more than 30^{o} did not perform as well. Results are based on inspection of 84 integral bridges in New York State.[9]

Integral bridges can accommodate greater skew angles. However, the transverse forces, the abutment rotation, and biaxial bending on the piles should be evaluated and details should be carefully engineered to accommodate the additional forces and displacements.

2. Total bridge length up to 460 feet.

***Commentary*:** The total bridge length that can be accommodated with fully integral abutments has not been established (see Table 1). For example, the VDOT allows for the following maximum lengths: (a) steel bridges less than 300ft at zero skew or less than 150 feet at 30^{o} skew; (b) concrete bridge 500 feet at zero skew or less than 250 feet at 30^{o} skew. [87]
However, the limits used by the NJDOT seem to be within accepted practice and should be used until further developments.

3. Curvature is limited to 5^{o}
4. The difference in the profile grade elevation at each abutment does not exceed 5% of bridge length.
5. The site is such that the abutment piles can be driven through at least 10 feet of overburden.

Commentary Some literature asserts that integral abutments should not be used at sites where the abutment piles cannot be driven through at least 10 to 16.5 ft. of overburden.[26] However, others show that stub abutments on spread footings supported on rock have also performed successfully for horizontal movements up to ¼ in.[14]

General Design Requirements

Abutment

The NJDOT Abutment details are shown in Figure 10. Connections are designed as rigid by using adequate reinforcement detailing between the slab, girders and abutment. Seismic design provisions usually require joint details that must have some level of rotational ductility for energy dissipation purposes.[13]

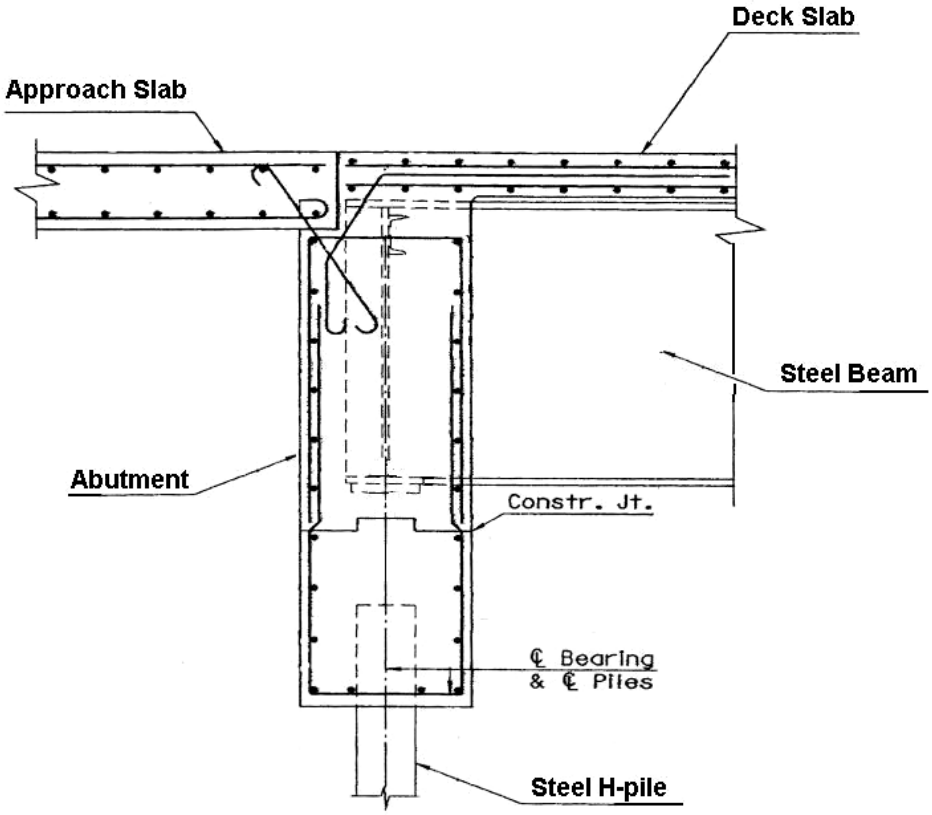

Figure 10. NJDOT abutment details

Abutment type

- Use a stub abutment supported on a single row of vertical piles.
- Abutment heights, measured from the roadway surface to the bottom of the cap should not exceed 13 feet. [28]

Connection details

- Moment connection between approach slab and abutment established as shown in Figure 10.
- Joint between slab and approach slab should be sealed.
- Provide a positive connection to the girder ends to fully transmit the temperature and live load from the superstructure into the abutment piling. See construction sequence in appendix E.
- Insert the pile into the abutment the maximum of two feet or two times the pile diameter.

Commentary: Embedding the pile two feet resulted in significantly less cracking in the concrete abutment and a correspondingly greater ability to develop a larger interface moment, as compared to a shallower embedment length.[66]

Approach Slab

- An approach slab should be used with integral abutment bridges.
- Design as simply supported span (as opposed to slab-on-grade) to avoid cracking when voids are created underneath due to soil flow and consolidation.
- The length will vary from a minimum of 10 feet to a maximum that is based on the intercept of a 1 to 1.5 line from the abutment excavation to the top of the highway pavement. This length is to be measured along the centerline of roadway.
- To ensure rider comfort, a slope of less than 1/200 should be used. [31,32] The approach slab shall be placed parallel to the skew. A width from face of rail to face of rail is recommended. Special provisions shall be made to allow free movement of the approach slab if curbs or barriers are present. Approach slabs shall always be separate pour from the superstructure slab, but shall be joined together.
- Place the approach slab over polyethylene sheets to reduce friction between the slab and the supporting soil, thus ensuring that the approach slab will move easily as the structures expands and contracts.

Commentary: The approach slab should be doweled into the back-wall to ensure a watertight joint. In addition, the slab should be cantilevered over the wing-walls to minimize surface water infiltration.[25]

Piles

- Use a single row of vertical piles. This arrangement increases the flexibility of the system and facilitates the longitudinal displacement of the structure.

Types of Piles

- Use steel H-piles oriented for weak-axis bending. Place H-Piles such that the web is perpendicular to the centerline of the bridge.

Commentary: Steel piles have been accepted as the best alternative by most researchers. Many DOTs place the piles on the strong-axis bending. However, it is reported that, in such orientation, they develop moments that may crack the concrete around the pile/abutment connection.

Many DOTs place the piles such that the web is parallel to the skew. This may induce small torsions on the pile.

Pre-drilling

- Use pre-drilled oversized holes and surround the piles with loose granular material to increase the flexibility of the system and reduce stresses in the piles.
- The pre-bored hole should be approximately twice the diameter of the pile. In stiff soils, the larger the diameter of the pre-bored holes, the smaller the stress on the pile.[108]
- The pre-bored hole should be at least 13 ft in length (as in Scotch Road.)
- The sand should be placed such that it is dense at the bottom and loose at the top of the pile (as in Scotch Road.)

Commentary: The depth of pre-drill is an important factor, and the literature is not conclusive about the exact depth needed. For example, an HP 10x42 steel H-pile required six to 10 feet of predrilled depth to achieve the desired results. [71] Others state that the pre-drilled holes need to be 10 to 20 feet deep, measured from the pile head. [18] In Iowa, all integral abutment-piling of bridges with an overall length greater than 130 feet must be driven through an oversize hole predrilled to a minimum of eight feet below the bottom of the pile cap. [56] The Mass. DOT also requires eight feet of pre-drilled holes.[28]

Eighteen out of 30 agencies polled did not pre-drill oversized holes for the piles [38]

Design procedure for horizontally-loaded piles

Several articles describe a conservative method that can be used to analyze/design integral abutments. Wasserman et al.[14] provides the most comprehensive procedure based on work by Wolde-Tinsae and Greinmann.[58] This procedure, which was closely followed for the design of the integral abutments used on the study bridge, is presented in the following section. These calculations are applicable to structures with steel superstructures, supported on steel H-piles oriented for bending in the weak axis.

Design Philosophy

The foundations of the Scotch Road Bridge were designed and built using the AASHTO ASD requirements, and the following recommendations compliment these requirements. However, the NJDOT requires that the AASHTO LRFD should be used in future designs. As a result, the following recommendations should be revised to reflect the new design requirements.

In either case, the design of integral bridges is based on the assertion that due to the flexibility of the piling, thermal stresses are transferred to the substructure by the rigid connection between the superstructure and substructure. Therefore, the design of the piles should be such that a certain degree of flexibility is achieved.

First, the piles must be able to develop sufficient resistance to the applied vertical loads (dead loads, live loads and impact). This information is available from the geo-technical investigation of the area. A number of different piles should be identified that can be used. Then from this group of piles one can choose a pile that will be studied for its capacity to create *a flexible foundation for horizontal loading*.

To assure strength and flexibility, the chosen pile must be able to develop a sizable resisting moment at its top as a response to a horizontal displacement. At the same time, it should be designed to achieve double curvature within its design length. The objective then is to choose a pile that will be at the verge of plastification at its top when the bridge experiences its design displacement, also, the pile is in double curvature.

Here, we present a flowchart of the steps needed to achieve an acceptable design for the piles. A design example based on calculations from the Scotch Road Bridge and summarized in Roman [1] follows. Full treatment of this subject can be found in Dehne [2].

DESIGN FLOWCHART FOR INTEGRAL ABUTMENT

Step 1. Superstructure design

The superstructure design is based on LRFD.

Step 2. Design the abutment piles for vertical load

2.1 Choose the pile that can carry the applied vertical loads (dead load+live load + impact)

- **Choose pile cross section.**
- **Allow 1/16" corrosion around the pile perimeter.**
- **Calculate the allowable pile stress for the corroded section.**
- **Check the axial load capacity: If the total pile design load is more than the allowable force on the pile corroded section,** Redesign.

Step 3. Design the piles for horizontal loading

3.1 Calculate the total thermal movement demand at the abutment

3.2 Calculate the plastic moment capacity of the section of the pile, M_P

3.3 Check the ability of the surrounding concrete to develop the plastic moment capacity within the embedded length of pile penetrating the abutment.

3.4 Calculate the displaced shape and the bending moment diagram of a horizontally loaded pile embedded in soil (using a program such as L-PILE)

- **The boundary condition needed to model the pile-abutment system is fixed head + displacement. Using L-PILE one can start modeling using fixed head condition (slope at the pile head =0) and then apply the lateral load that is needed to achieve the horizontal displacement.**
- **If** M^{TOP} **(moment at the top of pile) is less than the plastic moment** M_P **then reduce the pile section or the steel grade.** Redesign
- **If** M^{TOP} **is approximately equal to the plastic moment then we remodel the system as a free head with an applied** M_o **at the top.**

3.6 Check the unbraced length section of the pile as a beam column

- **Determine the applicable group load cases on the unbraced length (L_c) of the pile (unbraced = length of pile between zero moments)**
- **Calculate the pile capacities using the AASHTO LRFD and develop interaction diagram.**
- **Superimposed the group loading on the interaction diagram.**
  - **If the group loading is under the interaction diagram then ok.**
  - **If not then** Redesign **(increase pile cross section or the steel grade)**

Example of Integral Bridges Design Procedure (Scotch Road over I-95)

In this section, a step-by-step design procedure will be applied to the design of the Scotch Road Bridge piles. The numbers are taken from calculations by ARORA and ASSOCIATES[88]. The calculation steps have been summarized in Roman [1]. Equation numbers refer to AASHTO (1996)[89] and interims. The step numbers correspond to the steps in the flowchart.

Step 1. Superstructure design

The design of the superstructure follows the LRFD code. The loads are factored. The connection between the superstructure and its abutment is considered simply supported for the analysis and design of the superstructure. This is a conservative design since the frame action will reduce the actual moments on the superstructure, however, negative moments at the connection should be checked.

Step 2. Design the abutment piles for vertical load

Group load cases imposed on the piles are based on the profile of the soil that surrounds the buried pile and the project-specific design code (i.e. ASD, LFD, LRFD, un-factored LRFD loads, etc.) In this project, pile capacities are based on working stress design values. The loading will be un-factored LRFD loads incorporating the standard AASHTO specifications.[90] The piles will be designed for dead load, live loads and impact load as per NJDOT 1.15.3C8[17]

Step 2.1 Choose the pile that can carry the applied vertical load

In this design, we used un-factored AASHTO (1998) LRFD 3.6.2.1[90]. The total applied load per pile is:

V_{tot}= DL+ LL + Impact = *155 kips*

Choose pile cross section

From the geo-technical report different HP sections were studied. An HP14 × 102 was found adequate to carry the vertical loads. The section properties are:

- F_Y =36*ksi*……..Specified minimum yield stress for steel
- A_0= $30in^2$ ……..…Cross-sectional area
- S_Y= $51.4in^3$ ……Elastic section modulus with respect to minor (Y-Y) axis.
- r_y =3.56*in* …… Radius of gyration with respect to Y-Y axis
- $z_y = 78.8in^3$ ……Plastic section modulus with respect to minor (Y-Y) axis.
- $k = \frac{z_y}{S_Y} = 1.5248$ …….Shape factor
- b_f = = 14.248*in*……..Flange width
- d = 14*in*……Beam depth

- $t_f = 0.705in$ ……..Flange thickness

Allow 1/16 in corrosion around the pile perimeter

According to AASHTO recommendations, 1/16 inch should be deducted from the shell thickness of concrete-filled pipe piles to allow for reduction in section due to corrosion. Corrosion of the HP piles can also be expected in an integral abutment system. Therefore a reduction of 1/16 inch around the pile perimeter was also applied to the pile when determining its section properties and reduced axial and moment capacity, P_{cr} and M_{pcr}.

Original Section

$A_0 = 30in^2$

Perimeter $P = 2 \times b_f + 2 \times (b_f - t_w) + 2 \times (d - 2 \times t_f) = 82.93in$

Corroded Section

$A_{cr} = P \times 0.0625in = 82.93 \times 0.0625 = 5.18in^2$

$A' = A_0 - A_{cr} = 30 - 5.18 = 24.67in^2$

Calculate the allowable pile stress for the corroded section

- Allowable pile stress: $f_a = 0.25\ F_Y = 36ksi$ ……(AASHTO 4.5.7.3)
- Determine the pile allowable vertical capacity = 166*kips* for south abutment from the geotechnical report.

Check axial load capacity

Check that the allowable axial force on the corroded pile section is larger than the applied loads.

$Pa = A' \times f_a = 220.78kips > 155kips$ ……..……ok

Step 3. Design the piles for horizontal loading

Step 3.1. Calculate the thermal movement demand at each abutment

The maximum thermal movement, Δ_{ABUT}, for the design of integral abutment bridges shall be:

$$\Delta_{ABUT} = ½ \text{ L x } \alpha \text{ x } \Delta T \qquad (2)$$

where:

- L is the total length of the bridge between abutments
- ΔT is the difference between the temperature during which the bridge was set and a maximum or minimum temperature expected at the site. The temperature range expected is prescribed by AASHTO. For cold climates, steel structures,

AASHTO 3.12.2 and AASHTO Table 3.12.2.1 give the range of temperatures as –31°F to 122 °F (-35 °C to 50 °C)

- α is the coefficient of thermal expansion. For steel α=6.5E^{-6} / °F (11.7E^{-6} / °c), AASHTO 6.4.1.

In the design of the study bridge, the structure has two equal spans, a total length of 298 ft, and was set at 70°F. As such the design ΔT is 70-(-31)=101 °F and the displacement demand at the abutment is

$$\Delta_{ABUT} = \tfrac{1}{2} (298 \times 12) \times 6.5E^{-6} \times 101 = 1.17 \text{ in}$$

Maximum movement demand at the abutment will not be factored (LFRD load factor = 1) as per AASHTO[91], and NJDOT design manual.[17]

Step 3.2 Calculate the plastic moment capacity of pile

Moment capacity: For HP14 × 102 the plastic moment capacity is

$M_p = F_Y \times Z_Y = 36 \times 78.81 = 2{,}837.16 k - in$

Pile Section Properties for Corroded Section:

$$t_{fcr} = t_f - (2 \times 0.0625\ in) \quad t_{fcr} = 0.580\ in$$

$$w_{cr} = d - 2 \times t_f + 2 \times 0.0625\ in = 12.73\ in$$

$$I_{Ycr} = 2\left[\left(\tfrac{1}{12}\right) \times t_{fcr} \times b_f^3\right] + \left(\tfrac{1}{12} \times w_{cr} \times t_{fcr}^3\right) = 312.63\ in^4$$

$$S_{ycr} = \frac{I_{Ycr}}{\left(b_f / 2\right)} \quad \Rightarrow \quad S_{ycr} = 42.29 in^3$$

$$Z_{Ycr} = 2 \times \left[\frac{(b_f - 2 \times 0.0625in)^2 \times t_{fcr})}{2}\right] + \left[0.25 \times \left[(d - 2 \times 0.0625in) - t_{fcr}\right] \times (t_w - 2 \times 0.0625in)^2\right]$$

$$= 63.4 in^3$$

$$A_{cr} = \left(2 \times b_f \times t_{fcr}\right) + \left(w_{cr} \times t_{fcr}\right) = 24.53 in^2$$

$$M_p = F_Y \times Z_Y = 36 \times 63.4 = 2282.25 kip - in$$

$$r_{ycr} = \sqrt{\frac{I_{ycr}}{A_{scr}}} = 3.57\ in$$

Calculate the plastic moment capacity (M_p) of the embedded pile.

$M_P = F_Y \times Zycr \qquad M_P = 2282.25 kip.in$

Step 3.3. Check capacity of concrete to meet the plastic moment demand at connection

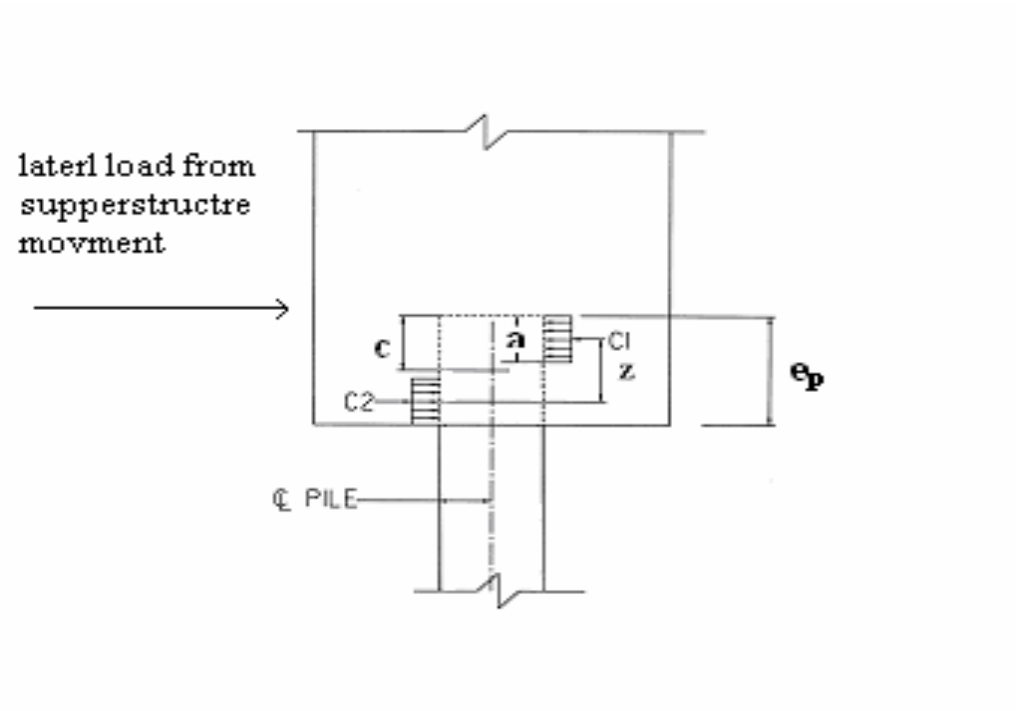

Figure 11. Schematic of embedded pile

Check the ability of the pile head to develop the plastic moment capacity, by calculating the maximum couple developed by the concrete in compression over a width equal to that of the HP14 × 102 web (since the piles are oriented to the weak axis). Referring to Figure 11, e_p is length of the embedded pile in abutment concrete (equal to 2 ft in this example) and C is the maximum compressive force developed by the concrete over a width equal to the pile web, b_w.

The maximum compressive force in the concrete is:

$C1 = C2 = 0.85 \times f_{cb} \times a \times b_w$

where f_{cb} is the strength of the concrete in bearing.

The neutral axis is at

$c = e_p \times 0.5 \qquad c = 12 in$

and the compressed depth is

$a = 0.85 \times c \qquad a = 10.2 in$

The web thickness is

$b_w = d - 2t_f \qquad b_w = 12.6in$

The developed compressive force is

$C1 = 0.85 \times a \times b_w \times f_{cb} \qquad C1 = 109.24in^2 f_{cb} \qquad C2 = -C1$

The maximum couple is

$Z = e_p - a \qquad Z = 13.8in$

$C = C1 \times Z \times f_{cb}$; $C = 1507.54in^3 f_{cb} \Rightarrow \max$ Couple.

The maximum couple, C should be equal to or greater than the required M_p.

The bearing capacity around large inserts can reach an average of 3.78f'c, (i.e. fcb = 3.78 f'c.) This value is based on research finding by Burdette et al [12]. A factor of safety, FS, greater that 1.0 indicates that the concrete around the embedded pile head is adequate.

Determine f_{cb} required to develop the plastic capacity in the pile:

$M_P = C$

$M_P = 2282.25Kip.in = C = 1507in^3 f_{cb}$

$f_{cb} = \frac{M_P}{C} \qquad f_{cb} = 1.51kip.in^{-2}$

$FS = \frac{3.78}{\frac{f_{cb}}{f_c}} \qquad FS = 7.49$ >> 1.0 <<<<< Verify using

Step 3.4. Calculate the displaced shape and bending moment diagram of the horizontally loaded pile

To assure the flexible behavior of the pile a plastic moment (plastic hinge) should develop at the pile top when the maximum displacement is applied, and a double curvature (two points of zero moment) must develop within the pile embedded length.

To check the ability of the pile to develop the plastic moment capacity at its top, we use L-PILE. We need to model a pile with a top-deflection equal to the longitudinal displacement expected at the bridge level, and with a slope of zero due to its fixity to the abutment. L-PILE cannot be immediately used to model the necessary kinematic boundary conditions shown in Figure 12(a). Instead, we start modeling using a fixed head condition (i.e. slope at the pile head =0) and we apply the lateral load, V that is needed to achieve the horizontal displacement Figure 12 (b). The objective at this point of the design is to choose a pile that will achieve plastic moment at its top when the required boundary conditions are applied.

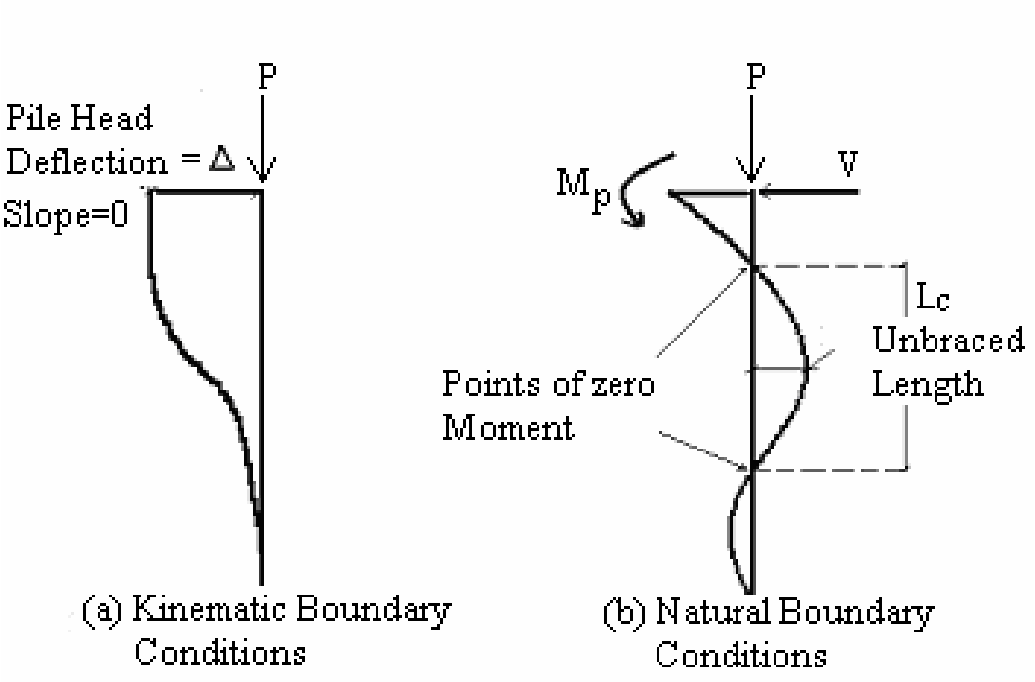

Figure 12. Typical integral pile boundary conditions

The design directive is:

- If M^{TOP} (moment at the top of pile) is less than the plastic moment M_P then reduce the pile section or the steel grade and redesign
- If M^{TOP} is slightly exceeding the plastic moment at the very top of the pile, then we accept the design and remodel the system as a free head with an applied M_P at the top.
- Use L-PILE to find the bending moment diagram as shown in Figure 12. From this we can pick the unbraced length L_c, and the maximum moment M_{max} This moment is due to the lateral loading, and it will be present in all load combinations that include lateral loading. L-PILE can also be used to find the p-y curves.

Step 3.5 Check the unbraced length of the pile as a beam column

From the previous step we determined the equivalent length of column L_c. This length will be checked as a beam–column. If the section is compact, all members subjected to both, axial loading and bending must satisfy section AASHTO 10-36, to meet the AASHTO ASD requirements.

In order to assure that the AASHTO ASD requirements are met for all possible load combinations on the L_c-section of the pile we will (a) use the AASHTO 10-36 to create an interaction diagram (i.e. a load-moment plot) for the pile which is now analyzed as a

beam-column; and (b) make sure that every possible load combination falls under the load–moment line. The imposed loads combinations are the unfactored LRFD loads.

Develop the column interaction diagram for the pile.

This step requires the execution of several steps in order to obtain all of the necessary information needed to develop the interaction diagram.

- **Calculate the maximum capacity under axial loading**, P_u, of the unbraced length of the pile, Lc, from AASHTO (1996), Article 10.54, and equation 10-150. To find $P_{u,}$ calculate the buckling stress in the column, F_{cr}, using the AASHTO equation 10-151. In this equation, the effective length factor, *K*, depends on the assumed end conditions of the pile. Wasserman [7] suggests *K* = 0.875. A factor of *K* = 1.0 was used by in the Scotch Road over I-95 calculations. Several valuable studies performed under actual field conditions concluded that the equations used to predict column buckling are extremely conservative. For this reason, we suggest that a value of 0.875 can be used in this part of the calculations in the future. For the example herein,

$L_c = 12.7\,ft$

$K = 1.0$

$\frac{KL_c}{r_y} \le \sqrt{\frac{2\pi^2 E}{F_y}}$ (AASHTO 10-152)

$v = \sqrt{\frac{2\pi^2 E}{F_y}}$ $v = 126.15$

$y = \frac{KL_c}{r_{ycr}}$ $y = 42.69$

Thus= if $y < v$ the design is acceptable. Otherwise, redesign.

$F_{cr} = F_y \cdot \left[1 - \frac{F_y \cdot \left(\frac{KL_c}{r_y}\right)^2}{4\pi^2 E}\right]$ $F_{cr} = 33.9271\,Kip \cdot in^{-2}$ (AASHTO 10-151)

$P_u = 0.85 \cdot A_{scr} \cdot F_{cr}$ $P_u = 707.43\,Kip$ (AASHTO 10-151)

Determine the maximum capacity under combined loading. The ultimate moment, M_u, and the Euler Buckling stress, F_e, assuming that the column is acting as a beam-column with eccentric loading. F_e can be calculated from AASHTO (1996), equation 10-157.

$M_{pcr} = F_y \cdot Z_{yer}$	$M_{pcr} = 2282.25 Kip \cdot in$
$M_u = F_y \cdot S_{ycr}$	$M_u = 1522.44 Kip \cdot in$
$F_e = \frac{E \cdot \pi^2}{\left(\frac{K \cdot L_c}{r_y}\right)^2}$	$F_e = 156.3 Kip \cdot in^{-2}$ (ASSHTO 10-157)

- **Develop the interaction diagram** using AASHTO (1996), equations 10-155 and 10-156 and the values previously calculated for P_u, M_u, M_p, A_{scr}, F_{cr}, F_e and F_y. An example load interaction diagram is shown in Figure 13.

Impose the critical load combination on the interaction diagram. One must examine the interaction diagram(Figure 13) to determine if the pile is capable of withstanding the displacement at the head of the pile and it is performing adequately as a compression member when driven through the soil. If the Load-Moment point (associated with the group loadings) is to the left of the diagonal, the pile is adequate. Otherwise, the pile must be redesigned or special remedial measures (i.e. use of pre-bored hole) must be considered.

In this example the critical load combinations are as follows:

- Load combination I is from the vertical loading. So, the load is $P = 692KN$ and the moment is zero.
- Load combination IV includes the maximum vertical load $P = 554KN$ and a maximum moment, applied on the unbraced length L_C of the pile, of $M_{MAX} = 113kn - m$. This load combination falls over the $P - M$ line and the pile must be redesigned.

Step 4. Design the abutment

For the stub abutment, we mainly design for the earth pressure, and seismic loads. Minimum steel is placed for temperature and shrinkage. The analysis depends on deep beam criteria, which the stub abutment usually meets. We will follow the 1998 AASHTO LRFD bridge design specifications(90). Figure 14 is a sketch of the abutment cross-section showing the passive earth pressure.

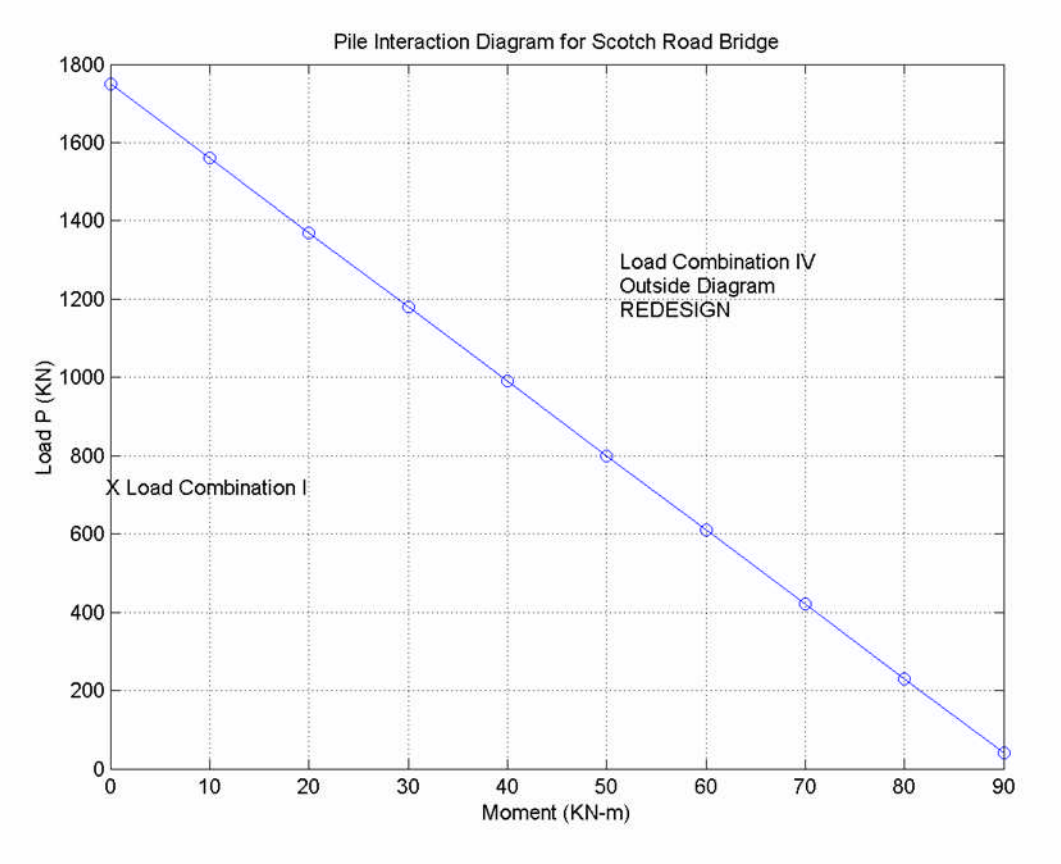

Figure 13. Example of moment interaction diagram with imposed group loadings

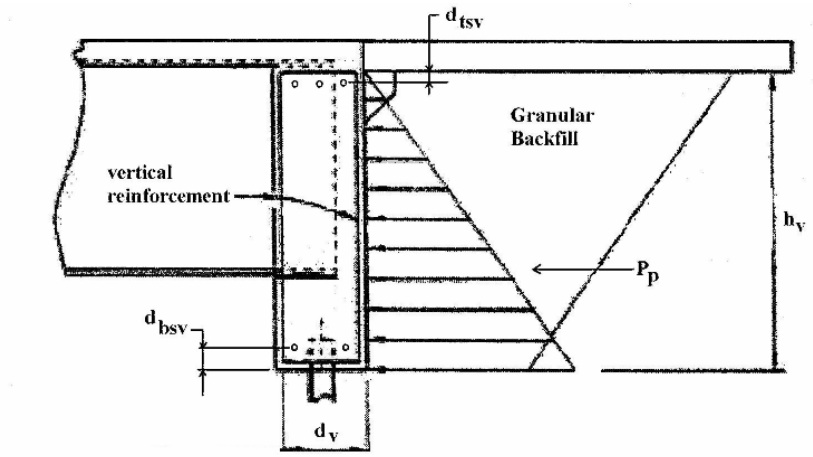

Figure 14. Schematic depicting dimensions for vertical bending analysis[57]

To calculate the passive earth pressure P_p, and the ultimate passive earth pressure, P_{pu}, Assume a uniformly increasing load applied to a simple beam (conservative result). In the case of bending analysis of an integral abutment, the simple beam can be

defined as the distance from the bottom of the approach slab to the bottom of the abutment beam.

$h_v = 11ft$

$\phi = 33.25$

$\gamma = 120pcf$

$P_p = 0.5\gamma_s h_v^2 \cdot \left(\frac{1+\sin(\phi)}{1-\sin(\phi)}\right)$ $\quad P_p = 24.88kip \cdot ft^{-1}$

$P_{pu} = 1.3 \cdot P_p$ $\quad P_{pu} = 32.35kip \cdot ft^{-1}$

A safety factor of 1.3 was used.

Commentary: For the first three yearly cycles of the abutment movement, the soil behind the abutment densifies and accrues plastic strains and induces a large pressure on the abutment. For this reason, we recommend that the largest angle of internal friction possible for the soil be used. For example, a ϕ of 45^o would have captured more closely the pressures measured behind the Scotch Road abutment.

CHAPTER 5 - SUMMARY AND CONCLUSIONS

This report summarizes the collective knowledge on the issues surrounding the design and construction of integral abutment bridges. Information from the New Jersey Department of Transportation was combined with the experience of other departments of transportation around the country, recent research and testing from several research teams around the country, and evidence gathered from the measurements of the Scotch Road Bridge, over I-95 in Trenton, New Jersey. The result is the accumulation of several observations and recommendations for a successful integral abutment design.

Based on this research project on integral abutments, our recommendations are:

1. Integral abutments constitute a preferable design for new bridge construction.
2. The major factors that limit integral abutment construction are the skew, curvature, and length of the bridge.
3. Another factor that should be considered in choosing an integral abutment is the available depth to the bedrock. The piles must be long to develop their curvature.
4. The limiting factors can be overcome with careful design.
5. Either steel or concrete superstructures can be candidates for integral-abutment construction.
6. Pile-supported, stub-type abutments are preferable.
7. A single row of long, slender, vertical steel H piles oriented for weak-axis bending is the best pile type for integral abutments.
8. Battered piles cause damage to the slab seat and should be avoided.
9. Pre-drilling oversize holes in stiff soils and surrounding the piles with loose sand is a common and advantageous method in reducing the stresses in the piles.
10. Calculations by this research team show that the larger the pre-drilled hole (in strong soils) the smaller the stresses on the piles.
11. Piles under the wing-walls can experience tension under vertical loading.
12. Calculations and measurements by this research team show that the p-y method (found in L-PILE, COM624P, etc) was an adequate method to analyze the piles for bending due to the horizontal movement of the bridge.
13. Calculations by this research team verified that piles in a group carry unequal amount of lateral loads due to “shadowing”. One can use p-multipliers to account for the difference.
14. Measurements taken herein show that piles directly under a girder experience higher displacements and rotations that are imparted to the pile from the girder.

15. Measurements taken herein verify that passive soil pressures develop behind the abutment due to densification and “soil ratcheting” during cyclic loading. The pressures were found to be much higher than usual design values.
16. Research completed after the present project shows that for longer bridges, the maximum passive pressure (after cyclic loading) can be assumed to be a Rankine pressure calculated with a maximum density of the soil and a K_p for a maximum angle of internal friction[92]. A conservative K_p can be found in NCHRP (1991) and can be used with a Rankine pressure distribution.
17. Measurements herein showed that the obtuse corner of the bridge experienced higher passive pressures. This was explained by the unequal movement of the bridge into the backfill soil due to the skew.
18. Geo-synthetics could be considered an option for backfill behind the abutments to reduce passive pressure built-up.
19. Porous, granular, well-compacted backfill should be used behind the abutment.
20. Measurements of stress taken around the pile sleeves and at the MSE wall, as well as calculations performed in this research effort show that the stresses that the piles impart to the surrounding soil due to their lateral movement dissipate quickly. As such, the MSE wall (or other retaining structure) is not loaded due to the movement of the bridge.
21. At the Scotch Road Bridge, temperatures at the deck reached up to 20^o F higher than ambient during the summer months. Temperature at the steel girder reached up to 10^o F higher than ambient. Both reached about ambient during the winter months.
22. The Scotch-Road Bridge experienced higher rotation during the summer months due to a higher variation of temperature along the depth of the girder. Such rotations can be transmitted to the piles during the summer months.
23. Calculations performed as part of this project show that the abutment is not rigid. It acts as a flexible member and does not transmit all of the top displacement/rotation to the pile top. This leads to a conservative design for the piles.

The wing walls and other construction peripheral to the bridge were not addressed herein. Anecdotal evidence and testimonials on such members have been summarized in the literature search.

Since the conclusion of this research, the LRFD method for the design of the foundations has been in effect. This should not compromise the overall design directive and method that has been given herein. However, 1) load factors, 2) resistance factors and 3) limit analysis have not been addressed for the piles in the presence of strong sand. These should be the subject of further research.

APPENDIX A - THE SCOTCH-ROAD BRIDGE INSTRUMENTATION AND DATA GATHERING

The Scotch-Road Bridge

This research project is based on a study bridge located on Scotch Road over I-95 in Ewing Township, Mercer County, New Jersey. The existing Scotch Road over I-95 Bridge was replaced with a 2-span continuous steel bridge with integral abutments.

The integral abutment bridge was designed by ARORA and ASSOCIATES Trenton, NJ in accordance with several design codes, including:

- The 1998 (2nd Edition) of the AASHTO LRFD Bridge Design Specifications, with current interims, as modified by Section 3 of the NJDOT Design Manual for Bridges and Structures.
- Design of pile foundations and MSE walls follows the Service Load Design Method as defined in the AASHTO Standard Specifications. The design method prescribed by Wasserman (2001) was closely followed and modified to reflect NJDOT integral abutment design requirements.

A cross section of the new bridge is shown in Figure 15. The bridge is 298 feet long. It is comprised of steel plate girders spaced at 11 feet on center across its width. It has a skew of 14°53'58" measured from the centerline of the bearing to the centerline of the bridge. The overall deck width is 104.3 feet. The deck will carry three 12 ft. travel lanes in each direction, two 10 ft. shoulders, and two six feet sidewalks flanked by two, one foot parapets. The single pier is a conventional multi-column bent supported on spread footings.

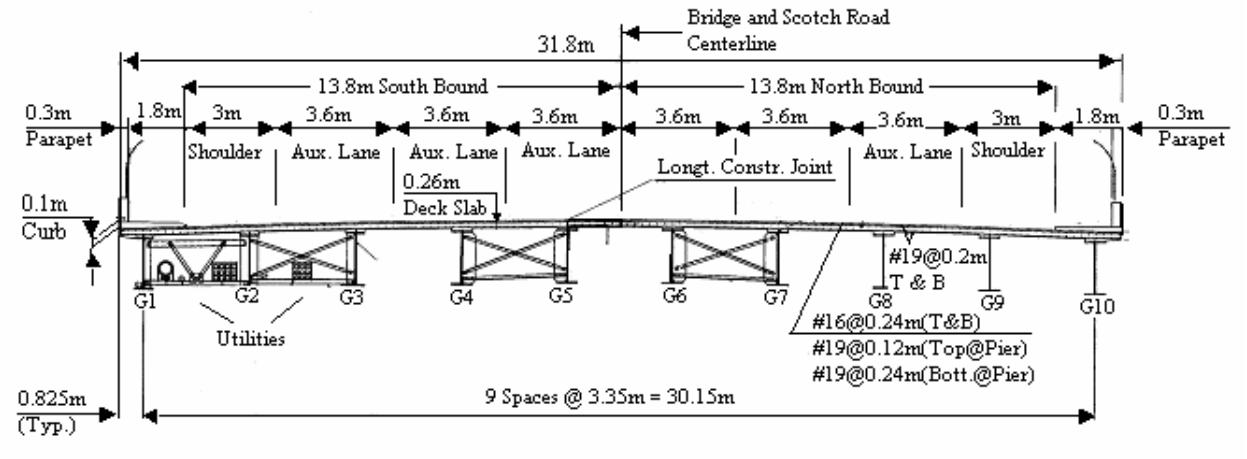

Figure 15. Typical section of the study bridge (Arora et al. 2001)

The abutment is about 11 feet high and three feet thick. It encompasses wing-walls that extend back from the bridge. Each of the abutments and wing-walls are supported on a single row of HP14x1102 piles, oriented for weak axis bending. A two-foot diameter corrugated steel sleeve was placed around each pile and subsequently backfilled with granular material. The piles are approximately 38.5 ft. long.

A relief slab (approach slab), 19.7 feet in length and 1.5 feet in thickness was tied to either abutment with epoxy-coated rebar. The approach slab rested on the abutment at one end and the sleeper slab at the other end. A full-depth armored joint is provided between the relief slab and the sleeper slab.

The integral abutment bridge has been instrumented during two construction stages (I and II). Instrumentation started in October 2001 along with the Stage I construction schedule. Data is gathered every two hours, at the top of the hour, since April 2003, for Stage-I and October 2003 for Stage-II.

Several types of electronic instruments have been used during the instrumentation process to gain full understanding of the behavior of the bridge. The cable number was used as the unique identifier for each electronic measurement. A total of 70 cables were installed.

Two major tests were held for the integral abutment bridge project: A) Test (1) was a static truck test, in which the truck was positioned immobile at specific locations (A through P) as shown in Figure 3.1. B) Test (2) was also a static test, where thermally induced strain data were measured over 24 hour period. During this test, no vehicles or heavy load were allowed on the bridge. The full report on gage preparation, calibration, placement, and measurement number assignments is found in [93].

Classification of Instruments

Six types of measuring devices were used to instrument the substructure of the Scotch Road, I-95 integral abutment bridge, Figure 16 and Figure 17:

- Fifteen electrical resistant strain gauges for measuring strains along the depth of the piles. Each strain gage is composed of four wires connected together to form a Wheatstone bridge.
- Eighteen soil pressure cells for measuring the horizontal soil pressure behind the abutment, on the galvanized sleeves surrounding the piles, and at two elevations on the MSE wall. The soil pressure cells were manufactured and calibrated in the laboratory before being installed on site.
- Two inclinometers for measuring the rotations at the connection between the abutment and stringers 2 and 5. The inclinometers were calibrated in the laboratory with a full-length cable attached. A tilt beam operated with a screw lift was used to set a known angle and to measure the output. The output from the inclinometers was compared to the manufacturer calibration.

- Two temperature sensors that output voltage signals that were converted into degrees F, to measure the temperature of the abutment at stringers 2 and 5.
- Two round displacement transducers were connected to four strain gages for measuring the displacement at the East and West ends of the North relief slab.
- Eight thermocouples to measure the temperature variations in the bridge deck at girders 2 and 6.

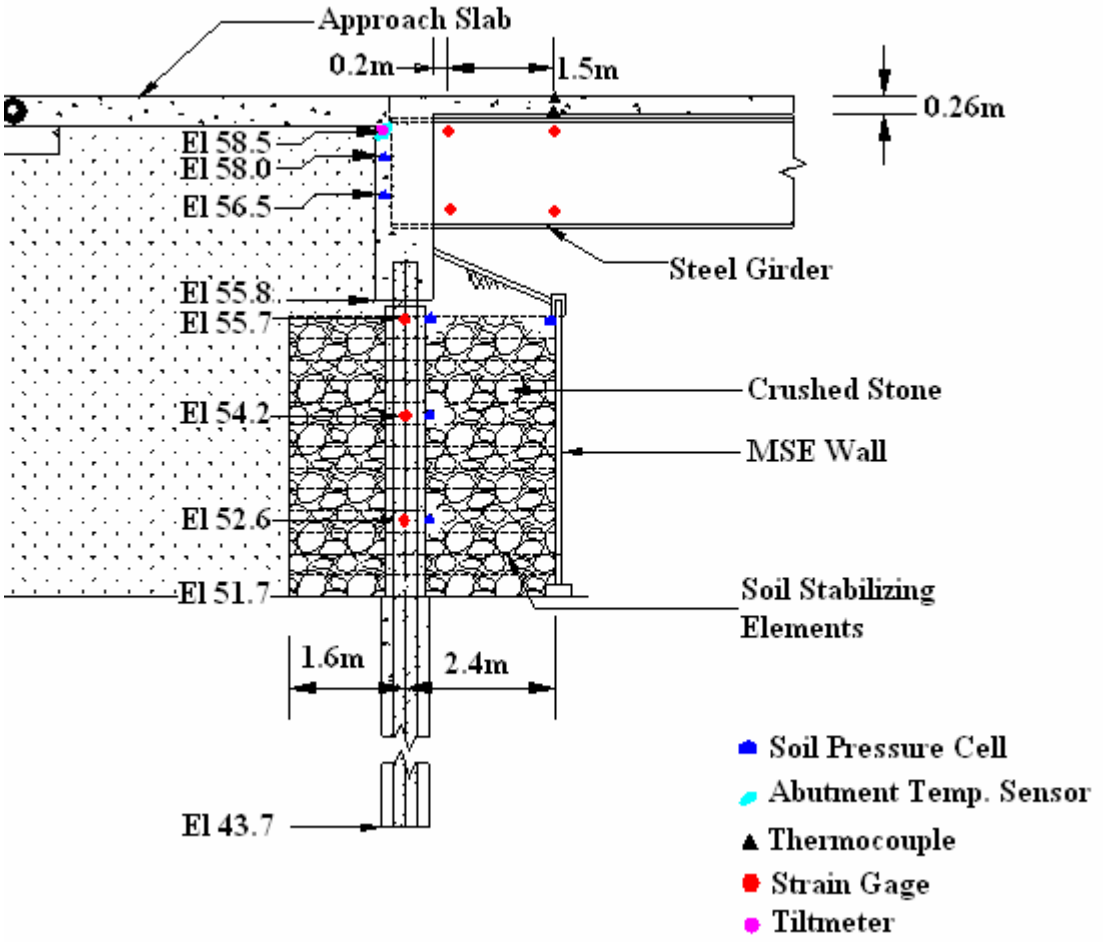

Figure 16. Cross-section at abutment showing gage locations

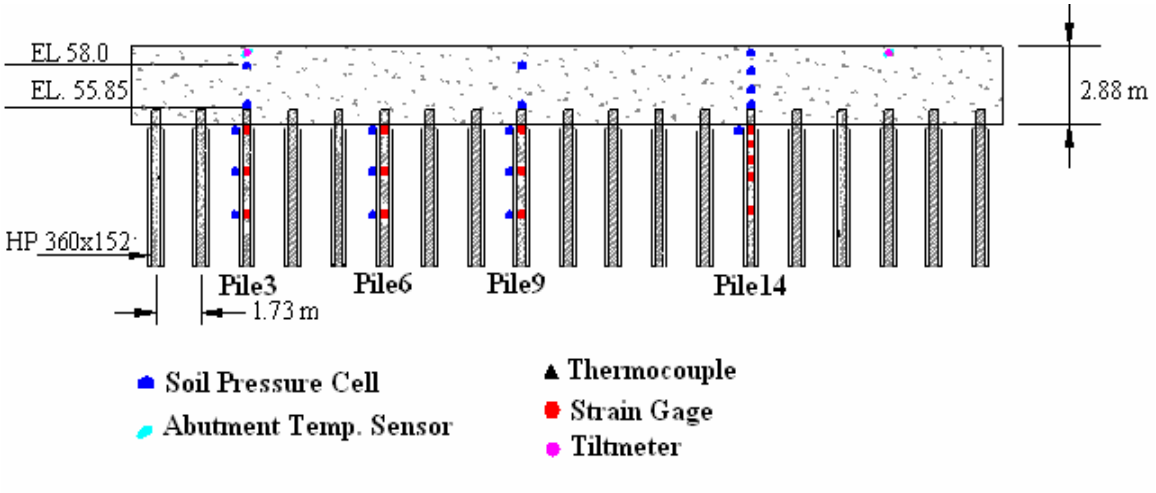

Figure 17. Side-view of Instrumentation

Two of the gages mentioned above were developed and calibrated for this specific project. Sensing Systems Corporation of New Bedford, Massachusetts has designed and manufactured 1) the structural movement sensor placed on the relief slab to measure the longitudinal movement of the superstructure and 2) the soil pressure gages shown in Figure 18. The development, calibration, placement and monitoring of all sensors are described in appendix A

Figure 18. Installation of soil pressure cell on the exterior surface of galvanized-steel sleeve

Data Acquisition System

The acquisition of data was accomplished using the CR 5000 Measurement and Control System manufactured by Campbell Scientific, Inc. “The CR5000 can measure nearly every commercially available sensor, usually without external signal conditioning and features programmable scan rates, measurement types, and recording intervals. On-board instruction sets contain statistical and mathematical functions that provide on-site data reduction and output results in the desired units of measure. The CR5000 performs measurement and control based on time or conditional events and is compatible with most wireless and hard-wire communications options”, (Campbell Scientific, Inc. website). The CR 5000 is a stand-alone system that can be connected to a personal or a laptop computer. The connection between the computer and the CR5000 system is achieved through a serial link interface. A programming code is written on the PC and downloaded on the CR5000 system via this serial link. This code controls the frequency at which the data is collected. Two codes were developed, one to limit the acquisition of data upon command from a laptop computer and the other to acquire data at two-hour intervals and at top of the hour. The duration of data acquisition lasts for ten seconds for every one-second interval. The data is then averaged and saved to the hard drive of the computer.

Gage Installation

The pile bending strain gages were installed first on site. Protective covers were placed over the strain gages prior to pile driving. The strain gage cables were placed into pvc pipes and were brought to the top of the pile. From there, the cables were brought to the data gathering equipment.

The stringer strain gages were installed after the stringers were placed, prior to placing the deck on the stringer. The strain gage cables were secured in place at each gage location until the initial readings are taken. Cables were placed in pvc pipes and brought to the data gathering equipment.

The soil pressure transducers were installed after the abutment, back wall, and deck components were completed and just prior to placing the back fill material. The soil pressure transducers were mounted at the designated location on the back wall with the pressure sensitive surface facing the back fill. The back fill soil was carefully placed up to each pressure transducer and over until all transducers were covered. The individual cables were routed to the central location for soil pressure data monitoring.

The abutment movement measurement devices were installed when the integral bridge construction was completed.

Sensor Design Location and Monitoring

Structural Movement Sensor, I-1478

Design

The structural movement sensor model 10708-2 is a circular ring instrumented with strain gages that measure strains due to the deflections of the ring during horizontal displacements of the bridge. In particular, the ring configuration is a thin-tube section one inch in length and six inches in diameter. Two push/pull rods are attached to the ring section at the zero and 180-degree positions (along the centerline of the bridge). Four strain gages are bonded at the inside and outside diameters of the tube at the 90 and 270-degree positions. Push or pull movement between the rods causes the circular ring to deflect into an elliptical shape. The ring deflection induces bending stress, which are measured by the strain gages at the 90 and 270 degrees locations. The four strain gages were wired into a Wheatstone bridge circuit sensitive to displacement or movement of the push/pull rods. The bridge circuit was insensitive to temperature changes.

Calibration

The sensors were placed in a testing machine using custom fixtures. The sensor bridge circuit output signal was monitored and recorded as the testing machine crosshead was moved over a range of 1.5-inch total travel. A linear regression analysis was performed on the calibration data to determine the best-fit calibration. A calibration certificate was prepared for each structural movement sensor. The nominal full-scale output at 0.75-inch displacement is 3 mV/V.

Mounting Anchors

An “L” shaped bracket was installed on the bottom of the relief slab inline with the sleeper slab. A threaded anchor in the sleeper slab and a clearance hole in the “L” bracket were used for connection to the movement sensor threaded push/pull rods. Flat washers and hex nuts on the rod passing through the “:L” bracket were used to set the sensor zero to the correct value for the bridge deck temperature at the time of the sensor installation.

Monitoring

Two movement sensors were placed on the relief slab. Each sensor was monitored whenever possible during the construction period. A data acquisition system was installed and connected to Stage I movement sensor in December 2002 and to Stage II sensor in December 2003. The data acquisition system has continuously recorded relief slab movement data at two-hour intervals since initiation of the monitoring process in April of 2003. Good correlation of relief slab movement and bridge deck temperature has been observed.

Location

Two structural movement sensors (displacement transducers) were installed on the east and west sides of the North relief slab at elevation 58.5 m. The west side structural

movement sensor was installed during stage I of the project of construction, while the East side on stage II of construction.

Soil Pressure Sensor, I-1477

Design

The soil pressure sensor model 10666-2 is a thin, flat plate, 4-inches in diameter and 5/8-inches in thickness, which houses several strain gages. A 3-inch diameter pressure-sensing element was utilized to provide a relatively large (7.07 square inch) soil pressure area sample. The pressure-sensing element was machined from 630 stainless steel and heat-treated to H900 condition.

Eight individual strain gages were bonded to the sensing element at the center, at the outside diameter and along four equally spaced radial lines. The eight strain gages were wired into a single Wheatstone bridge circuit sensitive to the average soil pressure applied to the 7.07 square inch sensing element. The bridge circuit output signal was, by design, insensitive to temperature changes and mounting configuration.

Calibration

Each soil pressure sensor was calibrated to 50 psig by application of hydrostatic pressure on the face of the pressure-sensing element. The hydrostatic pressure source was an EG&G Chandler Engineering dead weight precision calibrator. A custom pressure adapter fixture was designed for use with the precision calibrator.

Three exercise pressure-load cycles and three calibration data load cycles were performed on each soil pressure sensor. A linear regression analysis was performed on the calibration data to determine the best-fit calibration. A calibration certificate was prepared for each soil pressure transducer. The nominal full-scale output signal at 50 psig is 2 mV/V. The maximum combined error due to non-linearity, zero return and repeatability were less than 0.10 percent of full scale.

Mounting Plates

Steel type ASTM A709 grade 345 mounting plates were provided for flush mounting of the soil pressure sensors. The plates were 360 by 200 by 20 millimeters and were ground flat and smooth within 125 rms finish. A 4-inch diameter counter-bore and a slot were machined into the ground face of the mounting plate to receive the soil pressure sensor and integral cable.

Installation

The exact location of each soil pressure sensor was measured and marked using optical survey techniques. These locations were recorded on the installation log sheets for each soil pressure sensor. Two anchor studs, flat washers and hex nuts were used to hold the mounting plates on the integral abutment structural component being monitored.

The integral abutment back-fill material was placed up to approximately 350 millimeters below the soil pressure sensor. Loose sand was then placed around the sensor within a 350 mm radius. The normal back-fill material placement continued, Figure 3.4.

Monitoring

A total of 18 soil-pressure sensors were installed. Each soil pressure sensor was monitored whenever possible during the construction period. A data acquisition system was installed and connected to the Stage I sensors in December 2002 and to the Stage II sensors in December 2003. The data acquisition system has continuously recorded soil pressure data at two-hour intervals since initiation of the monitoring process in April of 2003. All soil pressure sensors have successfully recorded high quality data throughout the monitoring period.

Location

Nine soil pressure sensors were installed on piles 3, 6, and 9 at elevations 52.6, 54.2, and 55.7 m. Six abutment soil pressure sensors were installed above piles 3, 9, and 14 at elevations 56.5, and 58.0 m. The remaining three sensors were installed on the MSE wall at piles 3, 9, and 14 at elevation 55.7 m.

Several commonly used instrumentations were also used in this project. A brief description of each of these equipment is presented in the next sections.

Tilt-meters

The tilt-meters were equipped with embedded temperature sensors. The data recorded from temperature sensors were in millivolts. The temperature sensors were calibrated such that each mV is equivalent to 0.1 ^{o}C.

Description

The *Tuff Tilt* model 801uniaxial tilt-meter is used in a wide variety of monitoring and measurement applications. The tilt-meter senses angular movement with respect to the vertical gravity vector. It incorporates a high precision electrolytic tilt transducer, similar to a spirit level. When the transducer tilts, internal electrodes are covered or uncovered by a conductive fluid, which induces changes in electrical resistance when an alternate current excitation passes through it. The change in the electrical resistance is measured using a voltage divider network. The resulting signal is then amplified and filtered to form a high level DC signal proportional to the measured angular rotation.

Location

Two tilt-meters installed on the abutment at girders (G2 and G9) at elevation 58.5 m.

Installation

Two concrete anchors are required at each location. The anchors were installed prior to pouring of concrete for the abutment to avoid drilling into concrete.

Temperature Sensors

The tilt-meters were equipped with embedded temperature sensors. The data recorded from temperature sensors were in milli-Volts. The temperature sensors were calibrated such that each mV is equivalent to 0.1^{o}C.

Thermocouples

Description

Temperatures obtained using thermocouples were compared to actual ambient temperature. All temperature measurements were checked for consistency. The consistency test is held to confirm that all measurements are within plus or minus 10 degrees. All temperature measurements in thermocouples were obtained in degrees Farhrenheit (^{o}F).

Location

The eight thermocouples installed for the integral abutment project during Stage I of construction, were at girders (G2 and G5). Four of the thermocouples were positioned at the bottom and top of the girders at elevations 57, and 59 m, respectively. The remaining four were installed at the bottom and top of the deck at elevations 59.1 and 59.26 m, respectively.

Strain Gages for Measuring Lateral Bending of Piles

Four wires were connected to each strain gage forming a Wheatestone bridge. The wires from the strain gages were collected into cables, and curbed into plastic pipes for protection.

Installation of Strain Gages

The steps followed in the instruments of the lateral bending strain gages are described, thereafter. The following procedure was followed for three piles (piles #3, #6, and #9) during (Stage I of construction), and for pile #14 during (Stage II of construction), (Figure 19 to Figure 37).

- Grind the surface, where the strain gages are to be installed with #30 sand paper, Figure 19.
- Grind the surface by hand with #100 fine sand paper, Figure 20.
- Clean the surface with acetone.
- Sand by #320 using conditioner.
- Clean Surface with tissue paper.
- Burnish the surface, i.e. mark using a pencil the location, where the gage is to be installed, Figure 21.
- Clean area very well, until q-tip is free of residue, with M-Prep Conditioner (Acidic), such that that the conditioner does not dry on the surface, Figure 22.
- Clean with M-Prep Neutralizer (Basic), Figure 22.
- Place gage, such that it is precisely aligned with the marked lines on the pile, Figure 23.
- Place a rubber pad over the gage, and apply a pressure of 15 psi, to tighten the gage in place until all other gages are installed, Figure 24 and Figure 25.
- When all gages are placed, prepare the epoxy adhesive.
- Lift gage carefully, and apply the adhesive, while pressing in place, Figure 26 to Figure 28.
- Cure the gage using heating lamps for (110 ^{o}F for two hours), Figure 29.
- Remove the tape, and trim the epoxy around the gage, Figure 30.
- Check the resistance of the gage, to make sure it is reading 350 Ohms, Figure 31.
- Prepare the surface for the installation of Wheatstone Bridge. This process is the same as that of the gages.
- Prepare the surface for welding process (soldering), by removing any oxidation from the gage, Figure 32.
- Clean the surface with acetone to remove any residues, and use the hot sauter to remove any insulation from the magnet wires, Figure 33.
- Sauter magnet wires on the strain gage, Figure 34.

- Sauter red, green, black, and white cables to the gage in order to create Wheatestone bridge, and curb the wires into plastic pipes for protection, Figure 35.
- Check the gage for leakage by using a gage installation tester. The tester used in the installations of the gages; is produced by the Measurement Group, Vishay, Instruments Division, Raleigh, N.C. T. The tester should read a 20 G-Ohms for full signal, however, in case of leakage, lower readings are obtained due to the presence of moisture. The leaking gages were dried using drying guns and re-measured. This process was repeated until the full signal was read, Figure 36.
- Check the ability of the gage to measure strains by applying positive and negative moments. The applied moments were induced manually by repeated push/pull process at the end of the pile in the positive and negative directions. The measuring device was a P-3500 strain indicator, produced by Measurement Group, Vishay, Instruments Division, Raleigh, N.C.T.
- Examine the continuity of the Wheatstone Bridge with a WAVETEK DM27XT device. The resistance between the (black and red) wires or the (white and green) wires is supposed to be 350 Ohms.
- Apply two coats of poly-urethane. Let it dry for 15 minutes to an hour, Figure 37.

Figure 19. Grinding the surface using sand paper #30, at the location of installing the gage

Figure 20. Grinding the surface with sand paper #100 at the location of installing the gage

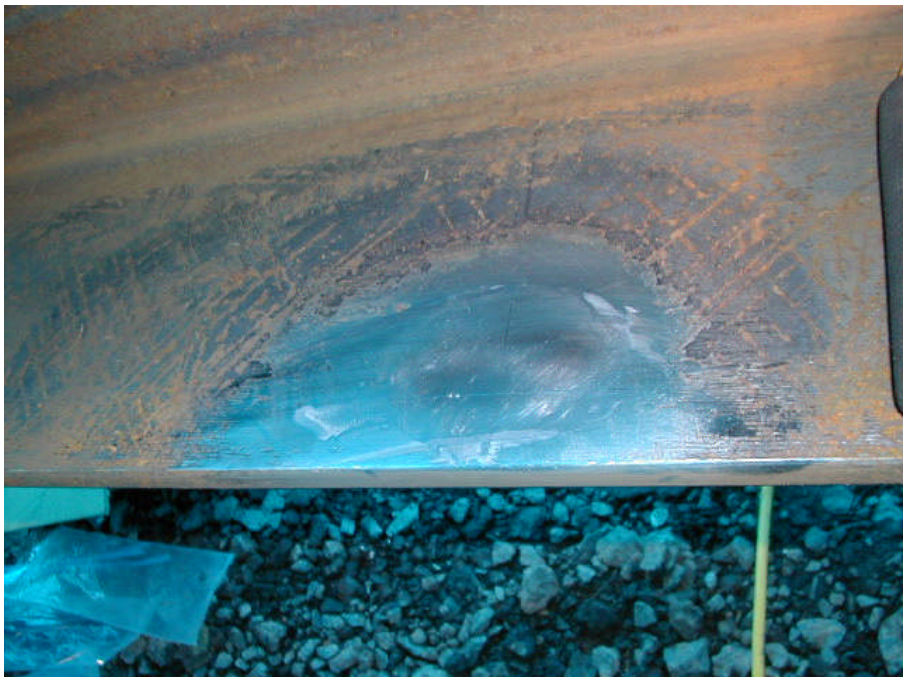

Figure 21. Burnishing the surface using a pencil, at the location of gage installation.

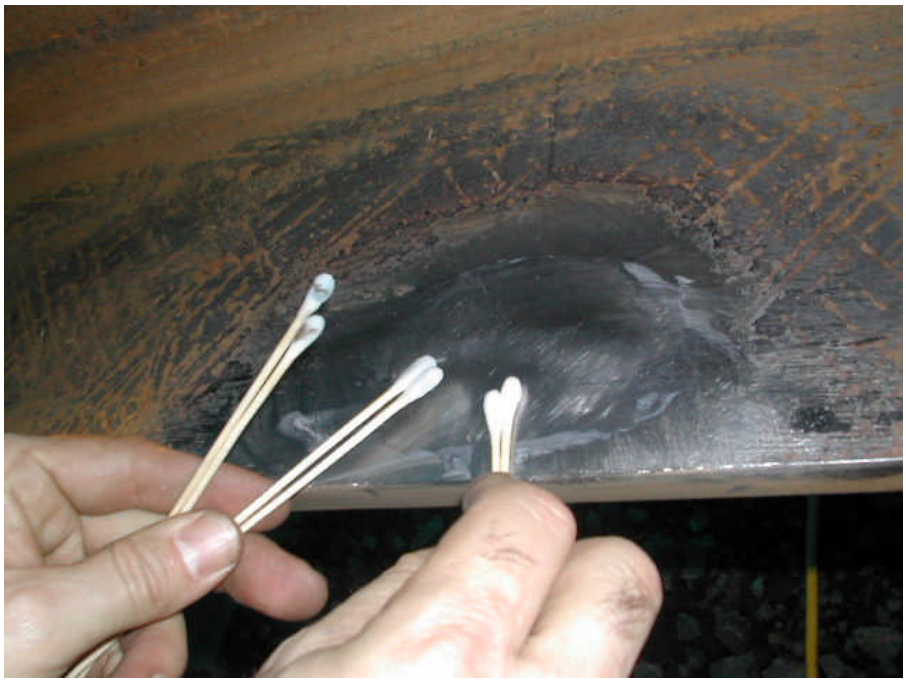

Figure 22. Cleaning the surface from any residue with M-Prep Conditioner (acidic) followed by M-Prep Neutralizer (neutral)

Figure 23. Installing the strain gage

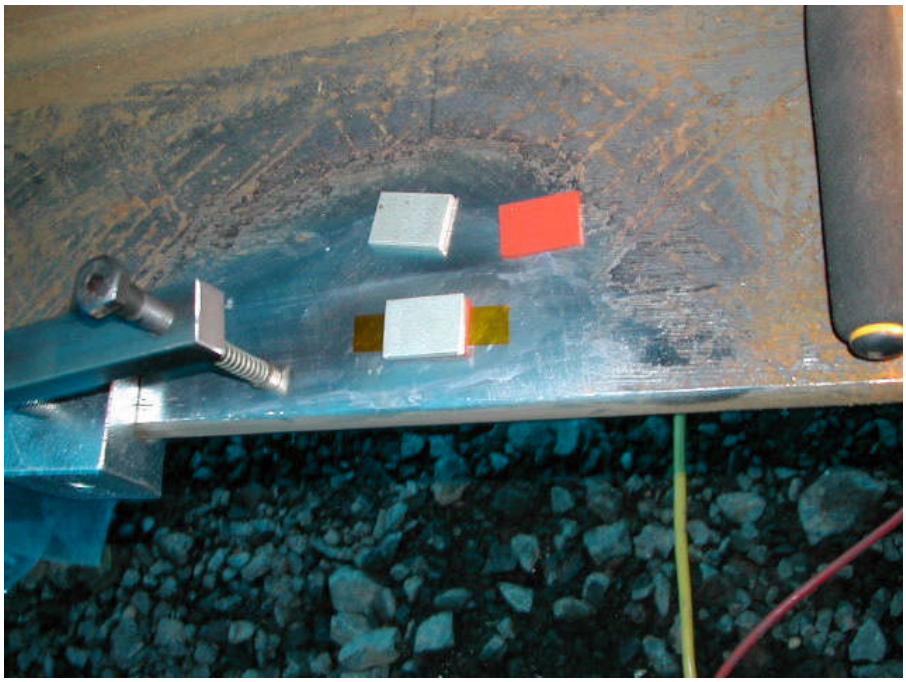

Figure 24. Mounting a rubber pad on the gage

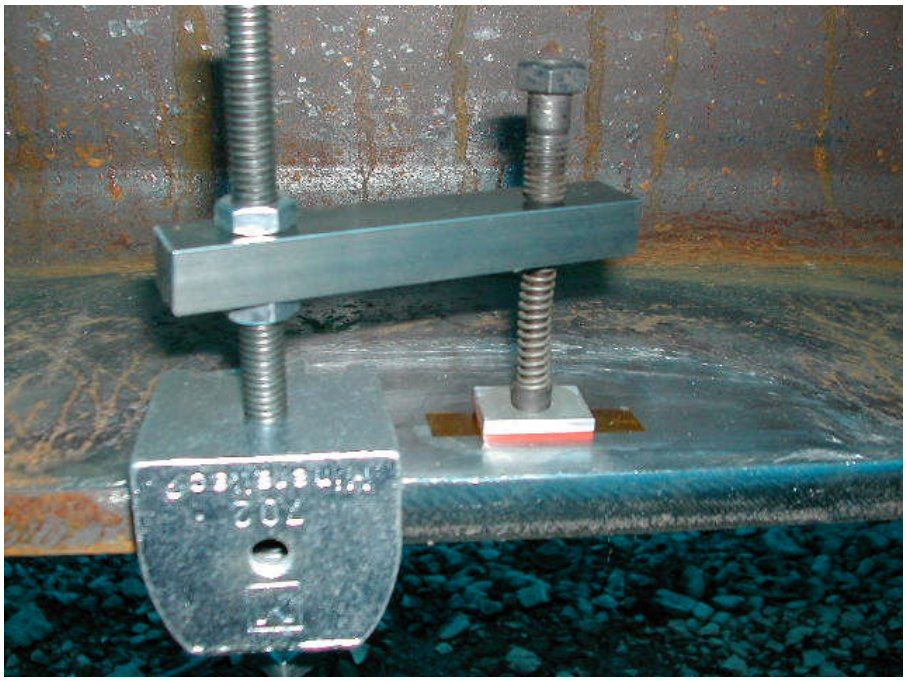

Figure 25. Holding the strain gage in place by applying pressure on rubber pads.

Figure 26. Lifting the gage and spplying the epoxy adhesive

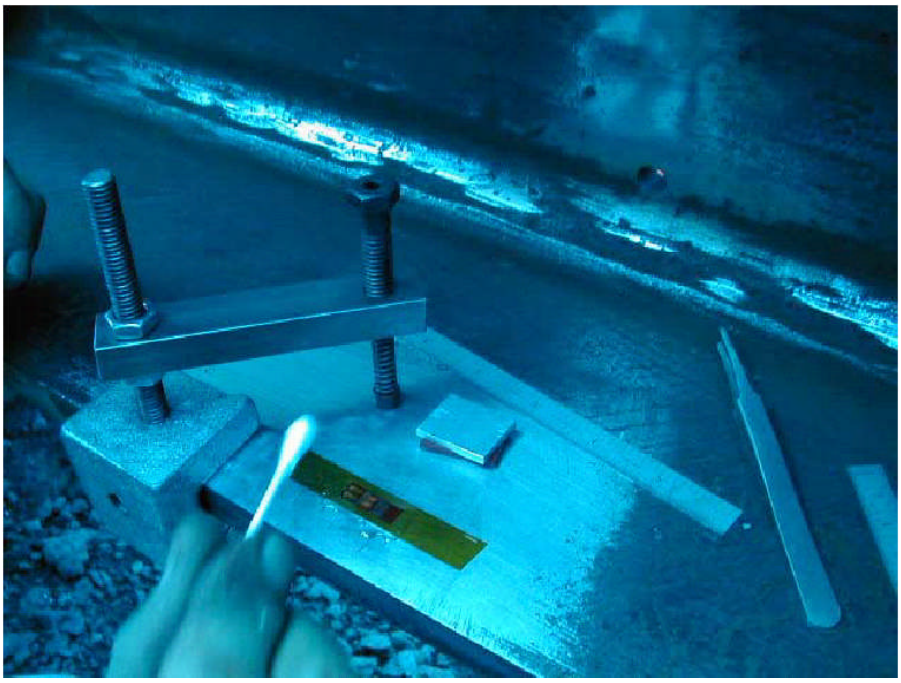

Figure 27. Cover the gage with wide tape following the application of the epoxy adhesive.

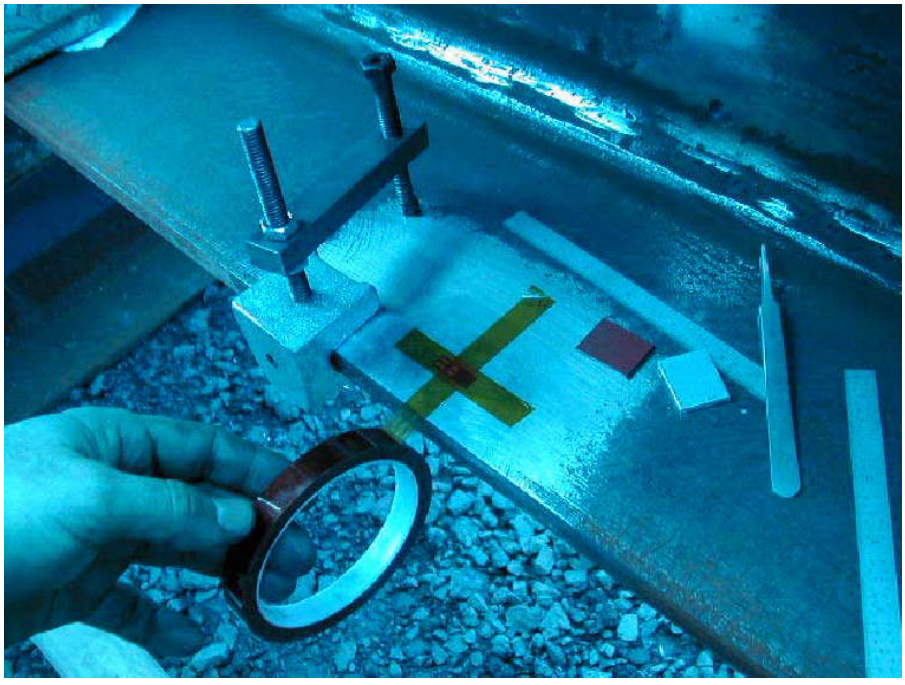

Figure 28. Press the gage in place following the application of the epoxy adhesive

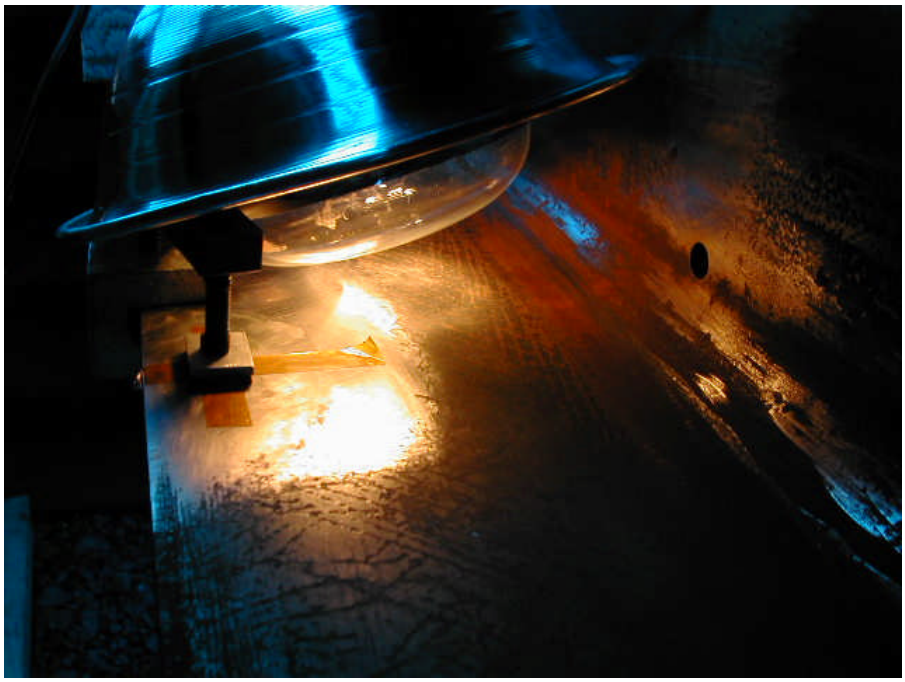

Figure 29. Curing the strain gage under heating lamps.

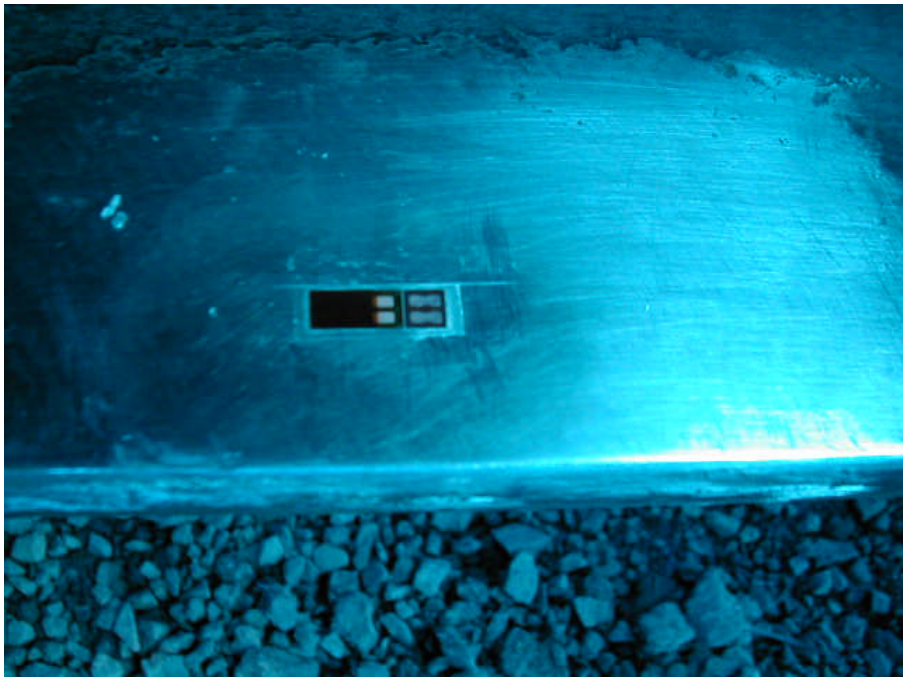

Figure 30. Trimming the surface around the gage

Figure 31. Testing the resistance of the gage

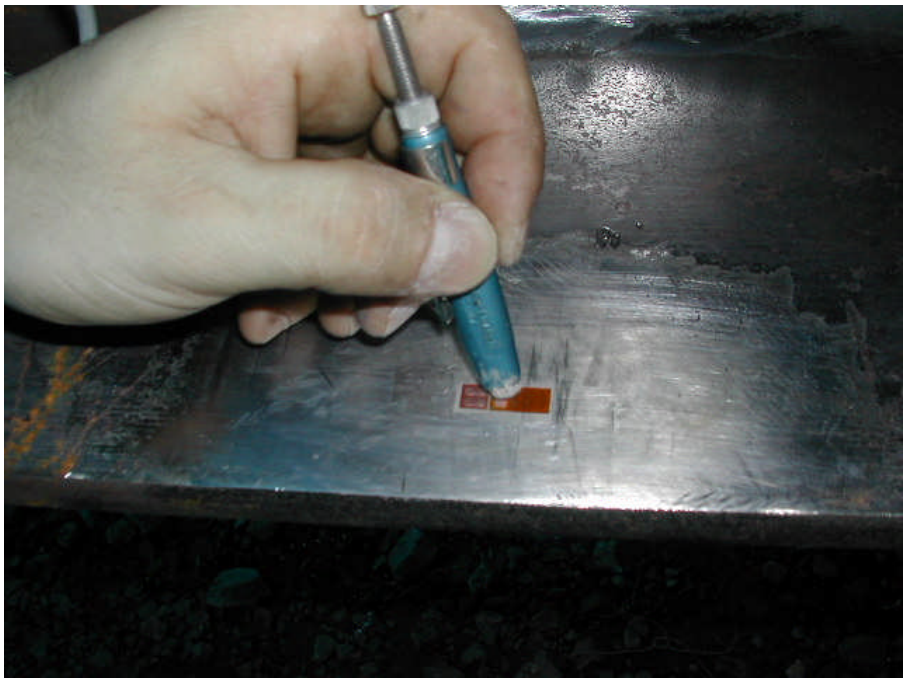

Figure 32. Preparing the surface for welding by removing any oxidation from the gage

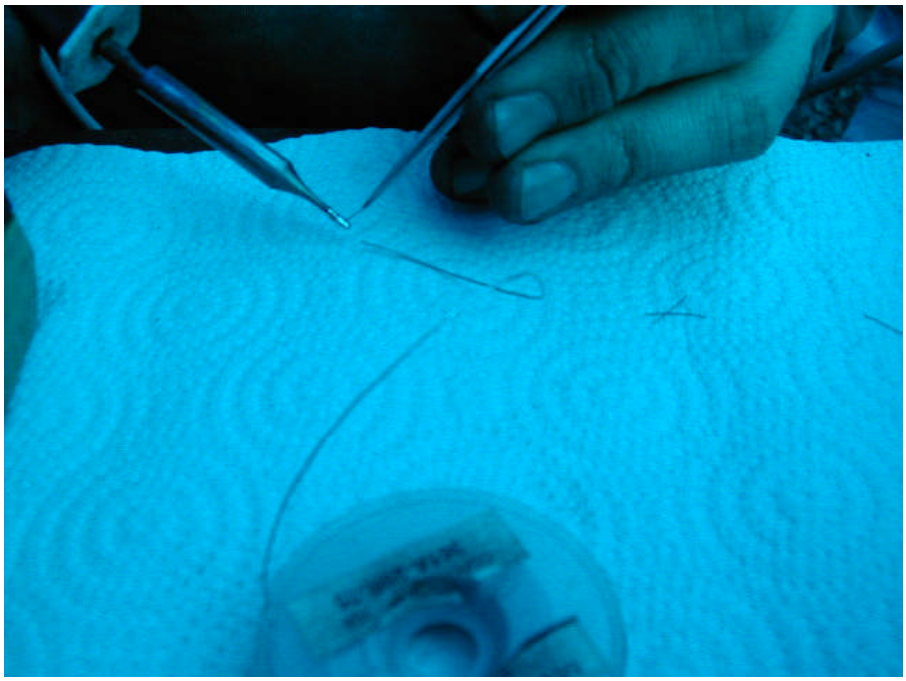

Figure 33. Clean the surface with acetone to remove any residues, and use the hot welder (Sauter) to remove any insulation from the magnet wires.

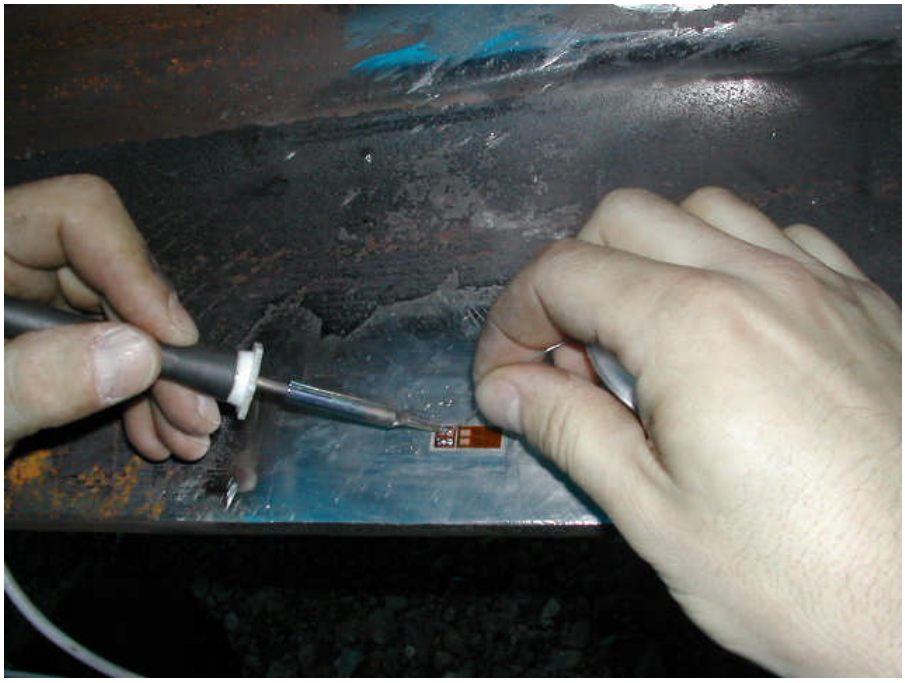

Figure 34. Sauter magnet wires on the strain gage

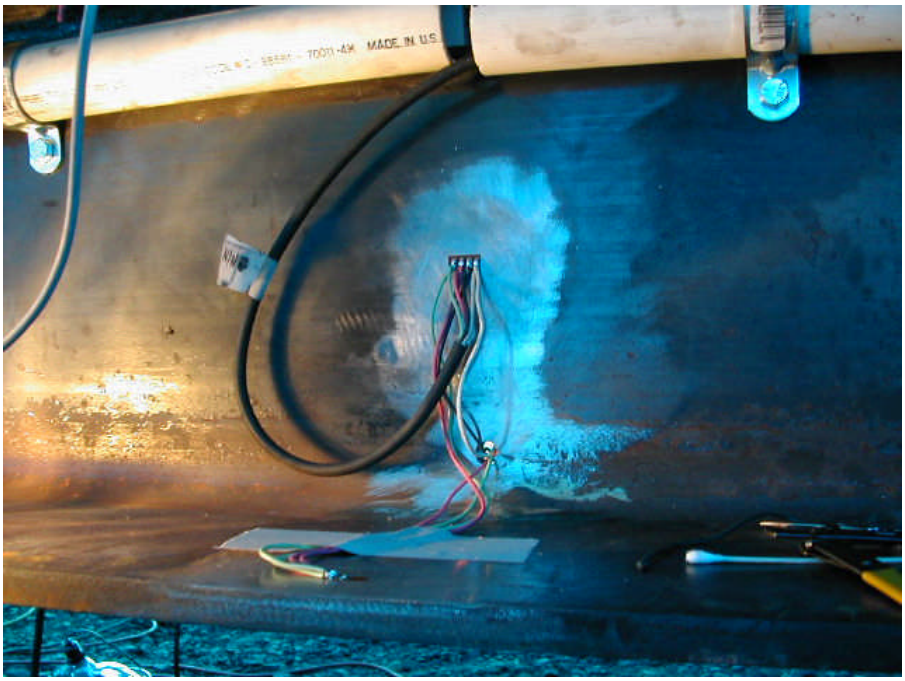

Figure 35. Sauter red, green, black, and white wires to the gage to form Wheatstone-Bridge resistance.

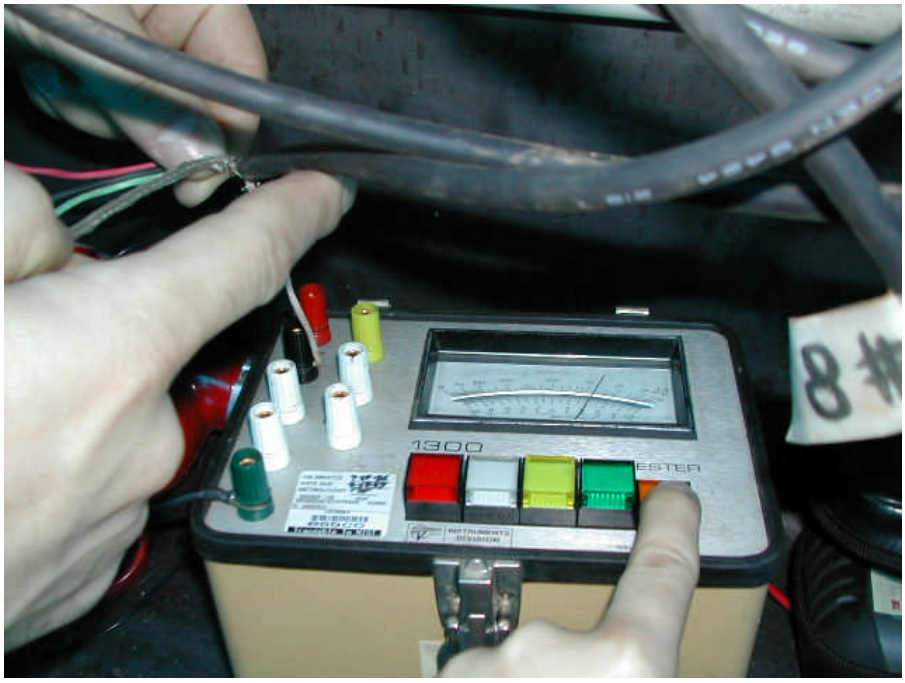

Figure 36. Checking the gage for leakage using a gage installation tester

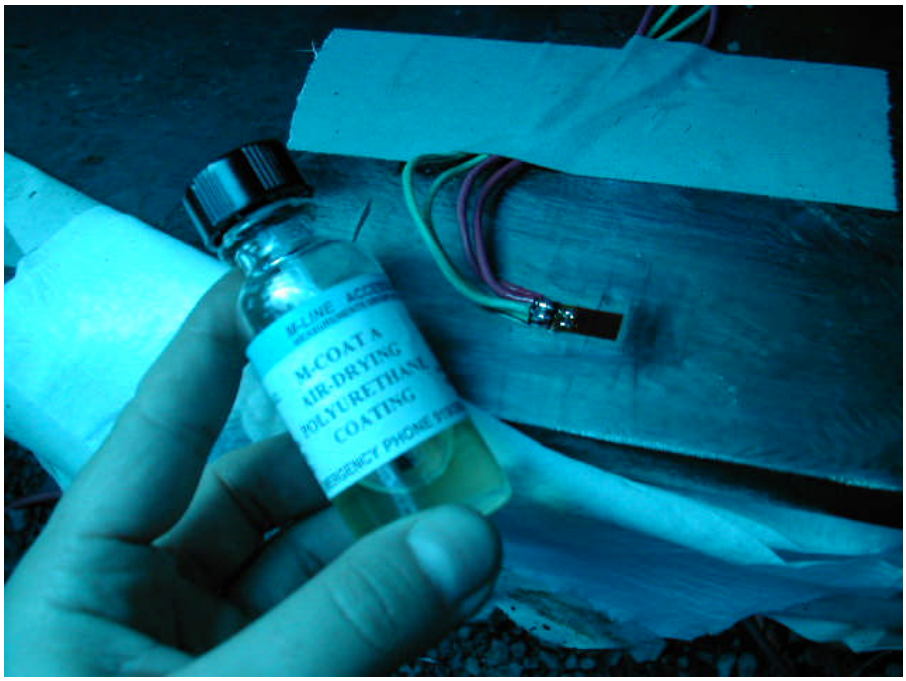

Figure 37. Drying the gage using application of two coats of polyurethane

APPENDIX B - APPLICATION OF L-PILE

The objective in this section is to evaluate available software, such as L-PILE that has been traditionally used in the design of piles, for its ability to predict the behavior of the laterally loaded piles that support the abutment. We accomplish this by comparing the measured bending stress diagrams of the HP steel piles with those calculated by L-PILE [43].

Characteristics of L-PILE

L-PILE is commercial software developed to analyze laterally loaded piles and drilled shafts. The program utilizes the finite difference method to solve a set of differential equations for a beam-column. The software assumes linear elastic behavior of the pile. The program simulates the soil behavior by a series of discrete non-linear springs, where the deformation at one level doesn't affect another. The development of a set of p-y curves can provide a solution to the differential equation of a beam column. Integration of the soil pressures around the pile will eventually result in an unbalanced force per unit length, of the pile caused by the lateral deflection of the pile. L-PILE can provide adequate p-y curves based on the soil information provided by the user or can allow the user to develop his own specific p-y curves. In most practical purposes, the p-y curves inherent into the program provide reasonably accurate prediction of the behavior of the pile. The program supports nine types of soils, including loose, medium, and dense sand. L-PILE assumes four alternatives for the boundary conditions at the top of a pile: (1) shear and moment, shear and slope, shear and rotational stiffness, or deflection and moment.

Comparison Between L-PILE and Field Data

The axial (bending) stresses, S33, diagrams along the depth of the piles were calculated for piles 3, 6, and 9 using L-PILE and compared with those calculated based on the strain data collected at the field. The pile data collected in the field were somewhat limited such that the exact displacements and rotations at the top of the piles are not known. In addition, the properties of the sand that surrounds the piles are not known exactly and they are predisposed to change with time.

The first step in the pile-design is to calculate the displacement of the superstructure and apply this displacement as a boundary condition at the top of the pile. As such, the measured displacements were first applied at the top of the pile, while maintaining a zero slope at the top of the pile.

The pile bending stresses versus depth curves didn't match those from field tests. This is readily justified, because the applied displacements don't take into consideration the resistance of the soil backfill, nor does it consider the rotation of the abutment. The question then becomes, what is the correct boundary condition that can be used with L-PILE in order to better predict the behavior of the pile. To answer this question, we imposed several boundary conditions.

First, the measured bending moments near the top of the piles were imposed into the model, while varying the lateral deflections until the bending stresses diagram

calculated by L-PILE approximately matched that obtained from the field data. Another successful alternative was to use the rotational stiffness and vary the shear force until matching the bending stresses curves obtained from the data, Ingram (2002). The rotational stiffness is calculated by dividing the bending moments near the top of the pile by the rotations measured in the abutment. However, the first alternative is more accurate in predicting the bending stresses behavior of the piles. This is due to variation between the rotation at the top and the bottom of the abutment, the lack of displacement measurements at the top of the pile, and the insufficient information pertaining to the soil profile.

Figure 38 and Figure 39 show the comparison between the bending stresses along the depth of the piles for the three studied piles at two different instances. Table 2 demonstrates the variation between the measured displacements those required as inputs into L-PILE in order to match the bending diagram. It shows that 60 to 65 percent of the horizontal displacement of the superstructure is delivered to the pile head. The full study is found in Khodair (2004). Despite the insufficient data collected on the loading of the pile and the profile of the soil, the results obtained from L-PILE approximately match the field data provided that one of the procedures suggested in this chapter is followed in loading the pile.

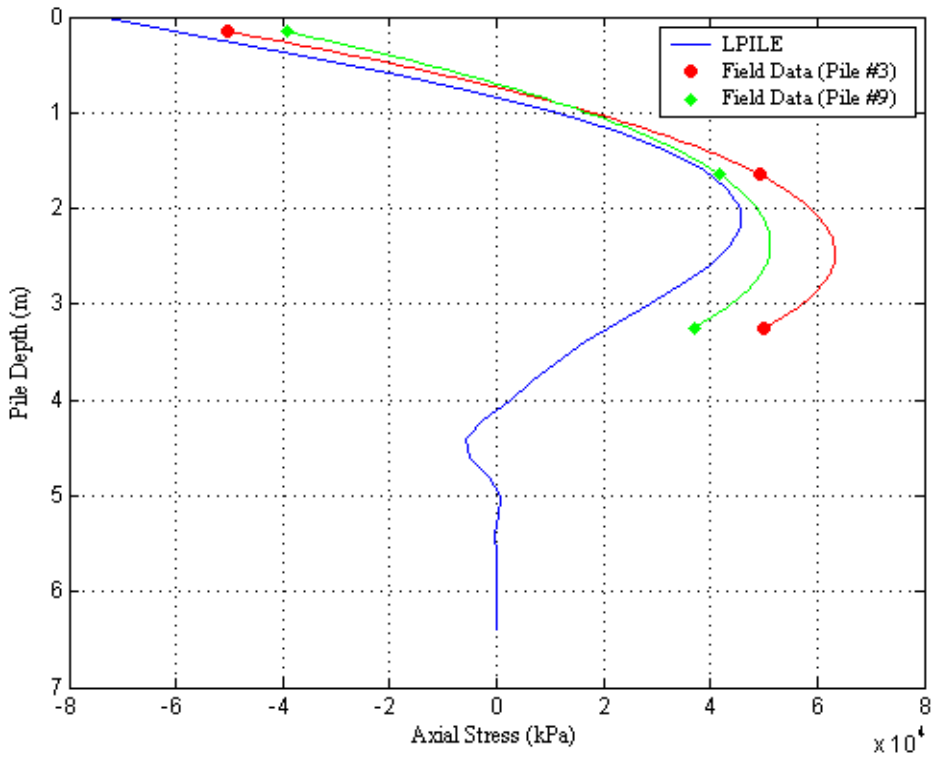

Figure 38. Axial Stresses versus depth for Pile 3, after thermal loading ΔT= 0.98°C at Stringer 2; Passive Pressure Cycle 8/15/03 14:00 p.m.

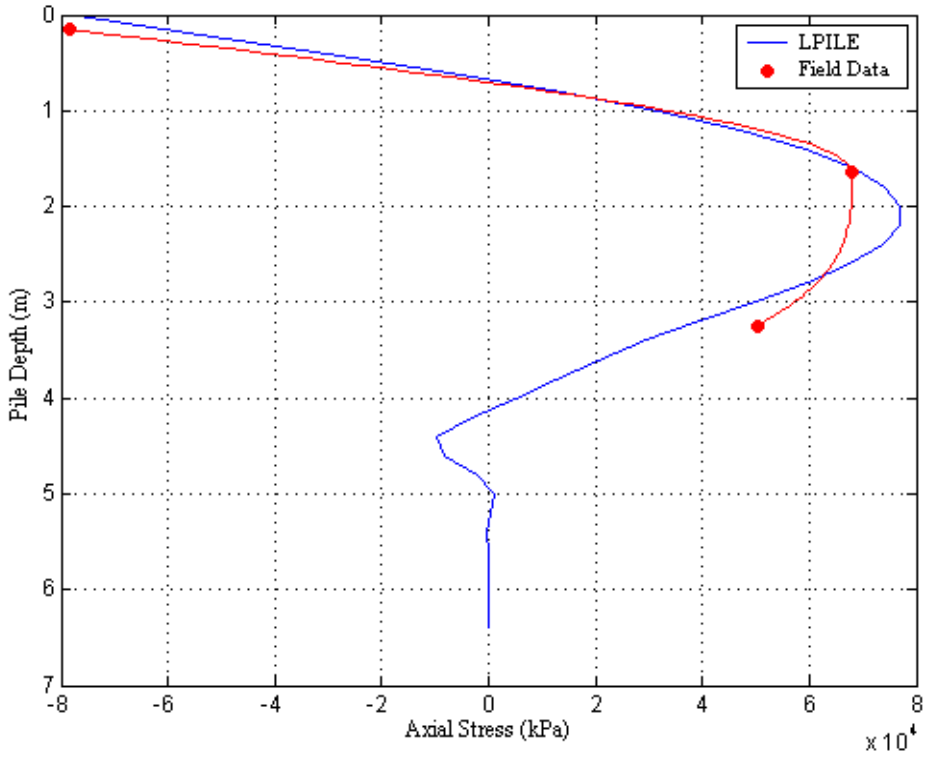

Figure 39. Axial Stresses versus depth for Piles 3 and 9 after thermal loading ΔT= 2.22 °C at Stinger 2; Active Pressure Cycle 9/6/03 0:00 a.m.

Table 2 - Summary of the variation between the measured displacements at the west-end of the approach slab and those obtained from numerical analyses

Date	Disp. from Field Data (m)	Disp. From Numerical Analyses (m)			Avg. Disp. (m)	% Diff. Bet. Avg. Disp. And Field Data Displacement
		Pile 3	Pile 6	Pile 9		
8/15/2003 14:00	0.0133	0.0088	0.00028	0.0048	0.0046	0.6517
9/6/2003 0:00	0.00963	0.0048	0.0017	0.0048	0.0038	0.6085

Conclusions

L-PILE is considered a practical tool in the design of piles supporting integral bridges. The capability of L-PILE to produce fairly accurate bending moment diagram for piles has been corroborated by comparing the output from L-PILE to field data. The key factor in obtaining accurate results is the choice of the correct boundary conditions. The design engineer can rely on L-PILE substantially in predicting the behavior of laterally loaded piles. Despite the lack of information regarding the displacements, shear, and bending moments at the top of the pile, several alternatives are available to obtain one or more of these parameters. Modeling the superstructure of the bridge using the finite element method can provide approximate displacements and rotations at the top of the pile. Using empirical equations such as equation (2.1) to predict the thermal expansion of the bridge could produce an approximate value for the movement of the bridge substructure.

APPENDIX C - FINITE ELEMENT MODELING OF SOIL-PILE INTERACTION

In total, three models were developed in this research. One of them focuses on the pile-soil interaction of a single pile, the other on the pile-soil interaction of a group of piles and the third on the behavior of the superstructure. Detailed information is found in [3]. In this section, a summary of the finite element analysis is presented with conclusions about the behavior of the substructure.

Introduction

In this chapter, analysis of the soil-structure interaction of the Scotch Road integral abutment bridge using experimental measurements, finite difference, and finite element solutions is presented. The objectives of this chapter are to: (1) to use the experimental data to update the FE model; (2) determine the bending stresses on the piles during thermal loading; (3) study the transfer of lateral loading from the piles to the MSE (Mechanically Stabilized Earth) wall that supports the foundation of the bridge; (4) conduct a limited sensitivity analysis pertaining to the effect of the amount of soil surrounding the pile on the induced stresses and displacements; and (5) study the buckling potential of the piles. Three different piles were studied in this part of the research, which are piles 3,6, and 9 shown in Figure 17.

The load case that is of major concern for integral abutment bridges is due to the displacement associated with thermal expansions and contractions. In addition to the displacements, small rotations were also present. This loading varied in magnitude and directions. The measured axial stresses in the pile correlated to the change in displacements and rotations. As the temperature increases (10:00 a.m. to 6:00 p.m.), the displacements and rotations transferred to the abutment increase in magnitude and so do the bending stresses on the piles. In the same trend, the axial stresses in the piles decrease in magnitude as the displacements and rotations decrease.

Pressure on the sleeve that surrounds the piles, and by extension, the transfer of pressure between the abutment and the MSE wall, remained small at all times. This suggests that regardless of the changes in the magnitude of the stresses in the piles supporting the integral abutment, the bridge does not transfer loading to the MSE wall. As expected, the soil pressure cells located on the MSE wall, (piles 3, 9, and 17, elevation 55.7 m), are also reading insignificant soil pressures.

Analysis of Pile Bending

Based on the experimental analysis, three load cases have been studied for the single pile analysis:

- Loading Case (1): The measured displacements at the relief slab and the rotations at the connection between stringers 2 and 5 9, (Figure 40), were applied to the abutment.
- Loading Case (2): A displacement of 0.023 m corresponding to a temperature increase of 26.7^{o} C was applied to the abutment. Table 3 shows a

representative sample of the data collected and analyzed close to the maximum temperature during the day and the minimum temperature at night in the summer

- Loading Case (3). The field bending moment values measured at the top of the pile and a displacement were applied to the pile top. The displacement values were adjusted until the bending moment curves matched those obtained from the field data.

Piles 3 and 9 are positioned with their longitudinal axes aligned with those corresponding to girders 2 and 5 respectively. However, pile 9 is positioned with its longitudinal axis corresponding to the middle of girders 3 and 4. The piles are spaced with a distance of 1.733 m along the skew angle of the bridge.

Due to the different positioning of the piles with respect to the bridge girders*, two models were used in order to capture the magnitudes of the axial stresses of the piles.* A "rigid abutment model" assumes full rigidity of the whole abutment, Figure 41 (a). A "partitioned abutment model" provides rigidity only for the portion of the abutment that corresponds to the area that the girders are embedded into the abutment. The degrees of freedom of the rest of the abutment are released, , Figure 41 (b). Neither, these two models nor the L-PILE model provide accurate matches with the field data. This is due to the fact that abutment is not acting rigidly as previously expected. The resistance of the soil backfill behind the abutment is substantial, and the displacement and rotations at the top of the abutment differ significantly from those at its bottom.

The soil reaction due to the lateral loading associated with the expansion and contraction of the bridge varies from active (soil moving outward in the direction of the deck) to passive (abutment movement into the soil). Figure 41 shows the exaggerated deflected shapes of the pile movement towards the sand (passive pressure cycle) for the different loading runs.

Table 3 - Representative magnitudes of measured displacements and rotations applied to the abutment. Case-2 Loading

Date/Time	Change in Temp. ΔT (^oF)	Displacement (in)	Rotation (rad)
8/15/2003 14:00	33.77	0.52	0.0013
9/6/2003 0:00	36.00	0.38	0.00052

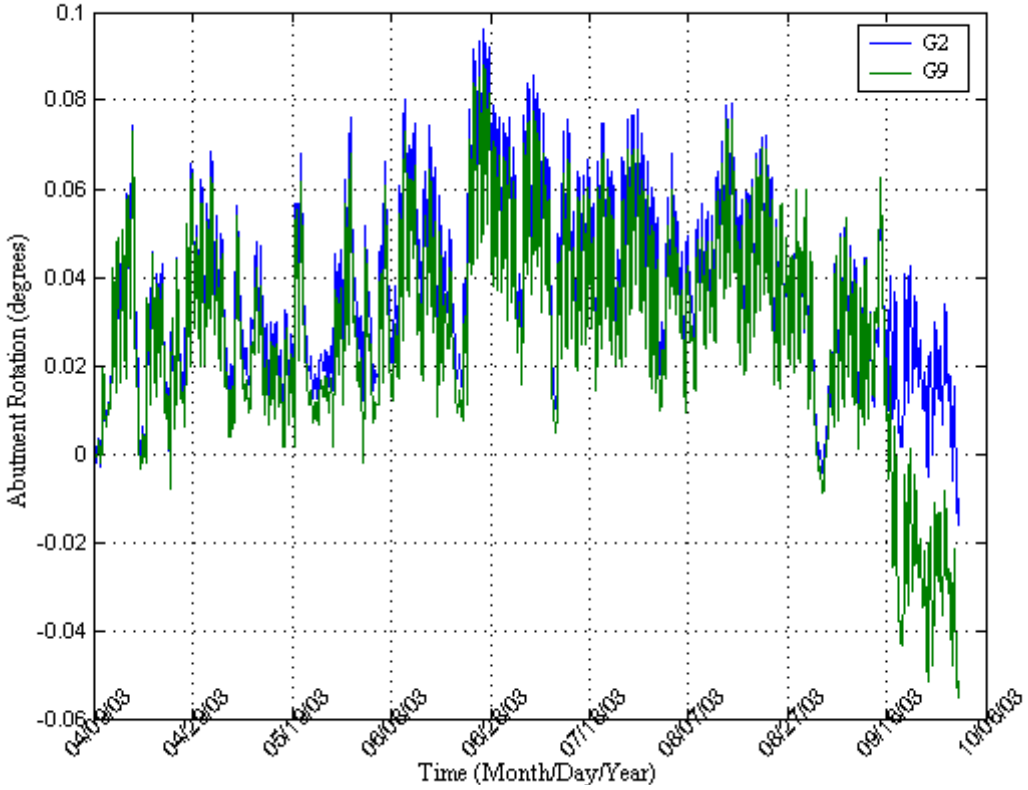

Figure 40. Time variation in measured rotations in Stringers 2 and 5

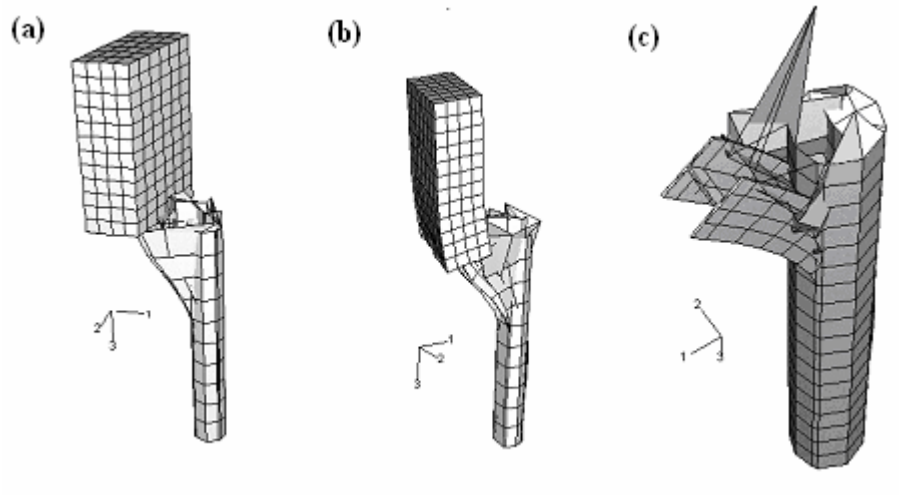

Figure 41. (a) Rigid abutment model. Deformed shape after load cases 1 and 2. (b) Partitioned abutment model. Deformed shape load case 2. (c) Deformed shape after loading application directly on pile top, load case 3

Verification of Finite Element Model; Effects of a Flexible Abutment on Pile Bending

The validity of the results obtained from the finite element model depends essentially on its accuracy in mapping real-life conditions. Therefore, the FE model verification is a prerequisite to implementation of the model in analysis. Two methods were used for the verification of the finite element modeling: (1) The results from the FE model were compared to measured experimental data (loading Case 1), and (2) solutions from FE model produced by ABAQUS were compared to those produced by L-PILE [43], using loading Case (2).

Static lateral displacements and rotations corresponding to the different experimental measurements were applied to the abutment (Case 1). The calculated axial stresses from the FE model compare poorly for the FE Model 1, where the abutment is assumed totally rigid without any lateral resistance, as shown in Figure 42 and Figure 44. However, the results from FE Model 2 are much better, where the abutment was assumed partially rigid at the embedment of the girder. These results substantiate the assumption that the loads applied on the pile during the analysis are much higher than the loads the pile is actually subjected to in the field. Moreover, it suggests that the rotation at the top of the abutment is not constant along it whole depth. The resistance of the soil changes the rotation values transmitted to the top of the pile. This justifies the better accuracy obtained in Figure 43 and Figure 45. Great improvement in the accuracy of the results was achieved by adopting the third alternative as shown in Figure 46.The variation between the magnitudes in the bending stresses of the three piles can be readily justified by considering the effect of the bridge skew and the positioning of the piles with respect to the girders. Pile 3 is located at the obtuse side of the skew, where the resistance to movement of the abutment is less pronounced compared to that at the acute side. In other words, the confinement of the soil towards the acute side of the abutment precludes the full range of movement of the abutment. Therefore, the bending stresses in pile 9 are greater than those at pile 3 in most of the measurements. However, piles 3 and 9 have one thing in common. They are located directly along the axes of girders 2 and 5. Therefore, the bending stresses for these two piles are greater than those for pile 6, which is located between two girders.

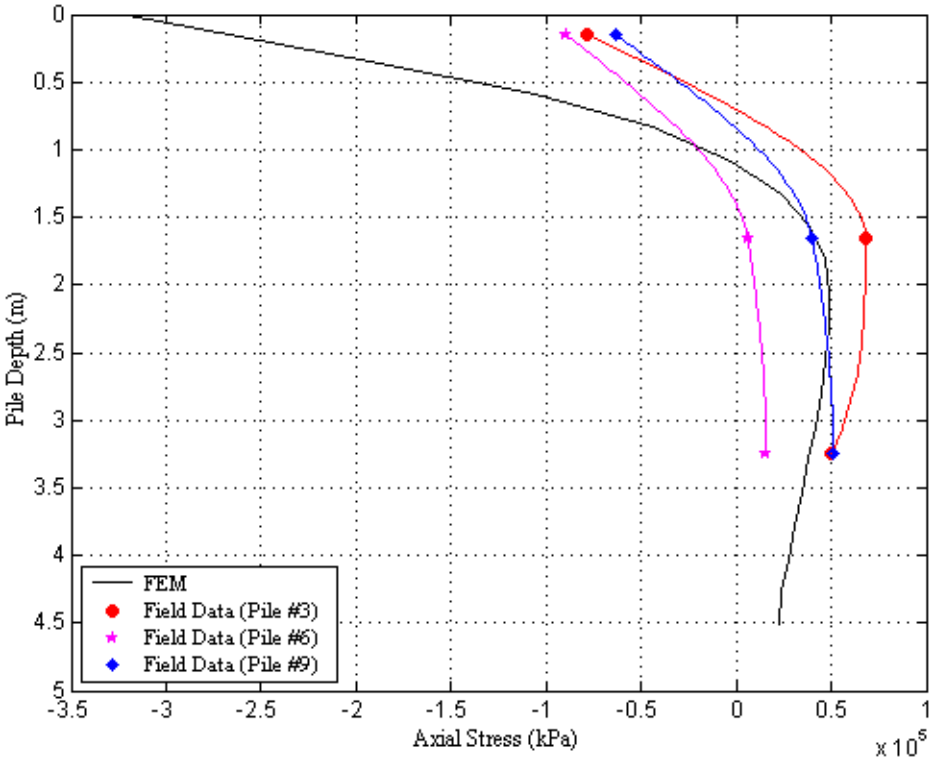

Figure 42. Axial stresses versus depth after thermal loading ΔT= 0.983°C at Stringer 2; passive pressure cycle, model 1, load case 1; 8/15/03 2:00 p.m.

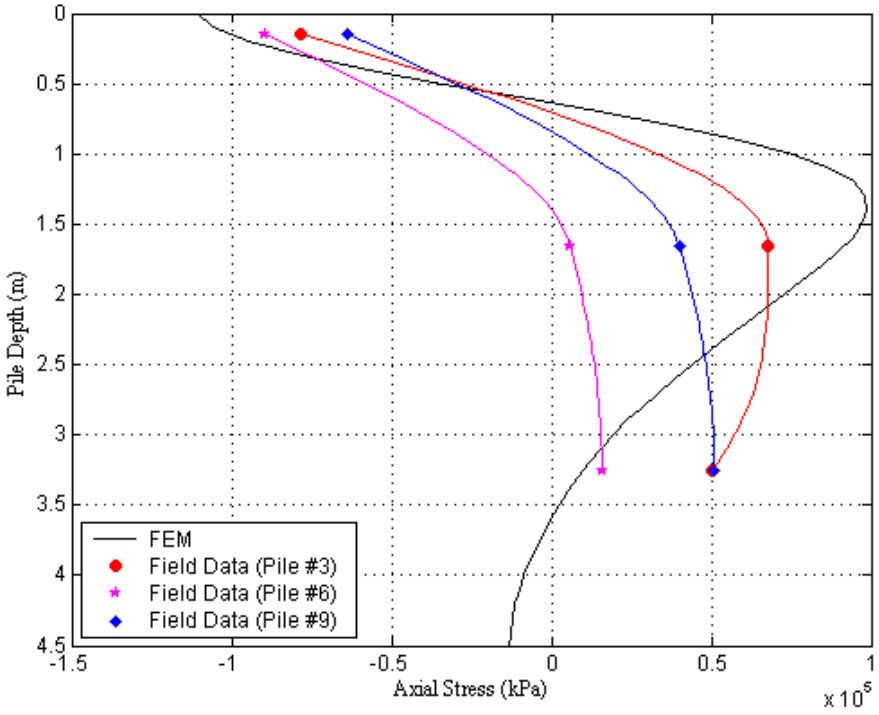

Figure 43. Axial stresses versus depth after thermal loading ΔT= 0.983°C at Stringer 2; passive pressure, model 2, load case 1; 8/15/03 2:00 p.m.

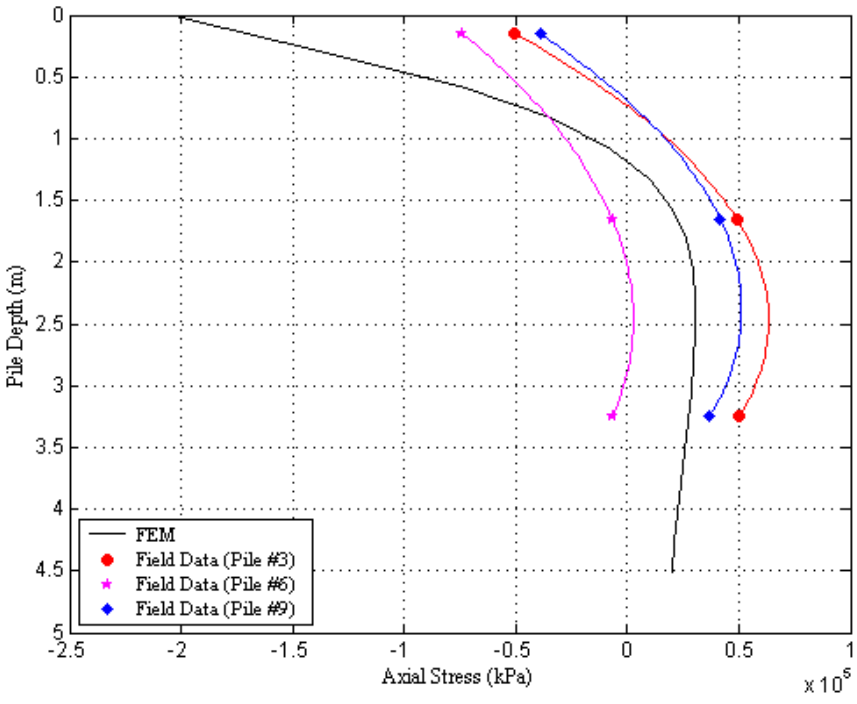

Figure 44. Axial stresses versus depth after thermal loading ΔT= 2.22 °C at Stinger 2; active pressure cycle, model 1, load case 1; 9/6/03 12:00 a.m.

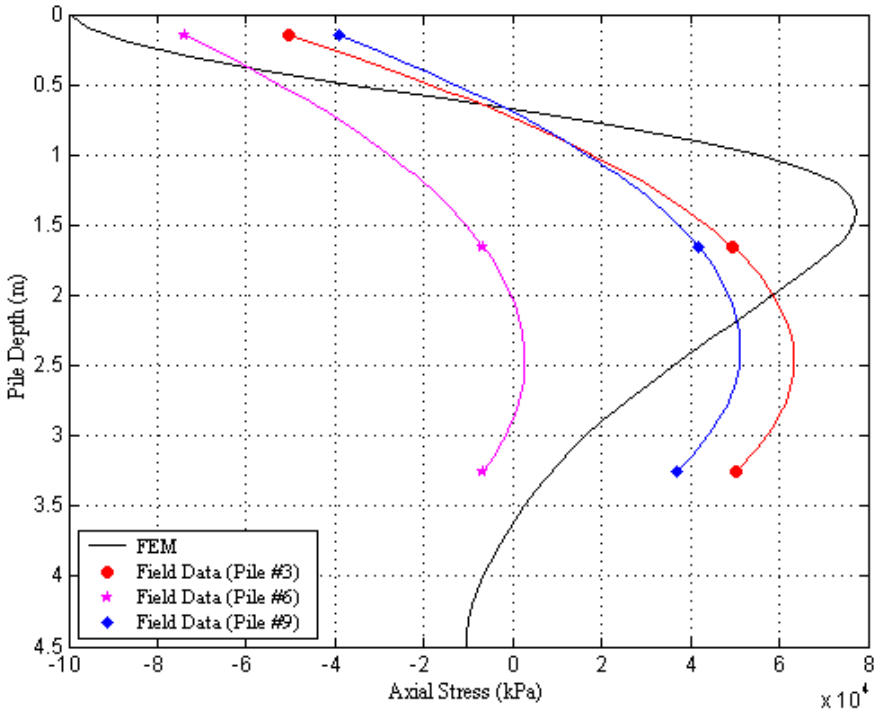

Figure 45. Axial stresses versus depth after thermal loading ΔT= 2.22 °C at Stinger 2; active pressure cycle, model 2, load case 1; 9/6/03 12:00 a.m.

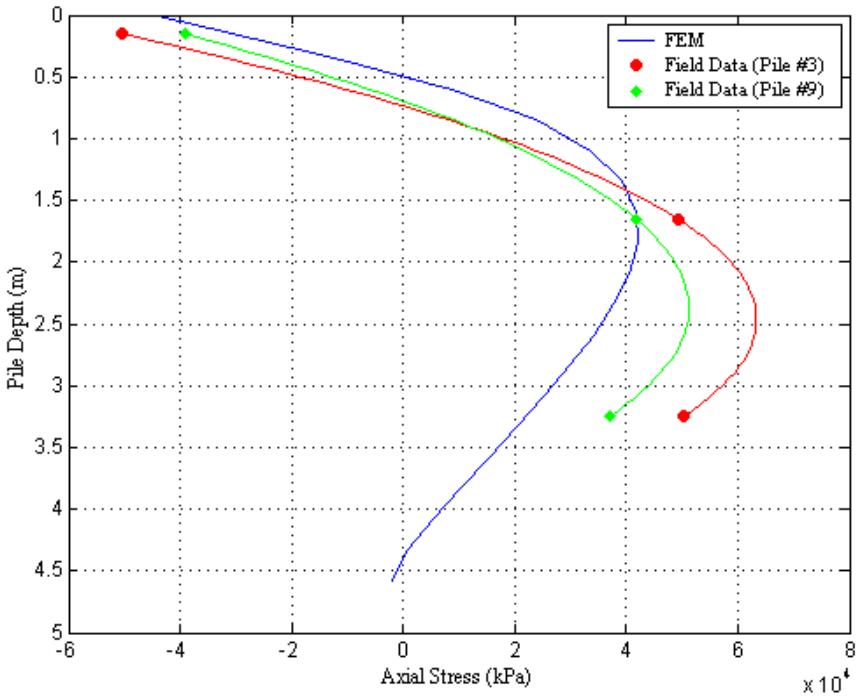

Figure 46. Axial stresses versus depth for piles 3 and 9 after thermal loading ΔT= 2.22 °C at Stringer 2, active pressure cycle, model 3, load case 3; 9/6/03 12:00 a.m.

Influence of Sleeve Diameter to Bending Stresses of Pile and Pressure Transmission to the MSE Wall

A parametric study was conducted to (1) study the effect of the size of the galvanized steel sleeve, and hence, the amount of sand surrounding the pile on the induced axial stresses in the pile and (2) find the magnitude of the pressure transferred to the surrounding soil and the MSE wall.

A lateral loading was applied to the rigid abutment FE model (Figure 47), while changing the diameter of the steel sleeve surrounding the piles from 0.6 m to 2.5 m. The results from the FE analysis shows that the calculated axial stresses along the pile decrease significantly, as the sand sleeve surrounding the pile increases in diameter, Figure 48. This can be justified, because the sand is a malleable media that absorbs the energy in the steel pile as a result of the imposed displacement at its top. However, the deflection along the depth of the pile increases at any elevation, as the size of the galvanized steel sleeve increases. Furthermore, the maximum axial stress in each case occurs at a deeper level along the pile. At its limit, the stresses approaches the results produced by L-PILE (4.0), which analyzes an extended single layer of sand. The same trend takes place for the calculations of the displacements, where the consistent increase in the diameter of the sleeve significantly reduces the discrepancy in the results between the FE and the L-PILE analyses, decreases as the size of the sleeve surrounding the pile increases and the model approaches a single pile in an extended single layer of sand, Figure 49.

This suggests that, for the displacement that was input in this study, a galvanized sleeve of 0.6 m in diameter is sufficient in eliminating development of stresses in the crushed stone and hence, the struts tying the MSE walls. However, increasing the amount of sand surrounding the pile increases the pile capacity for lateral loading.

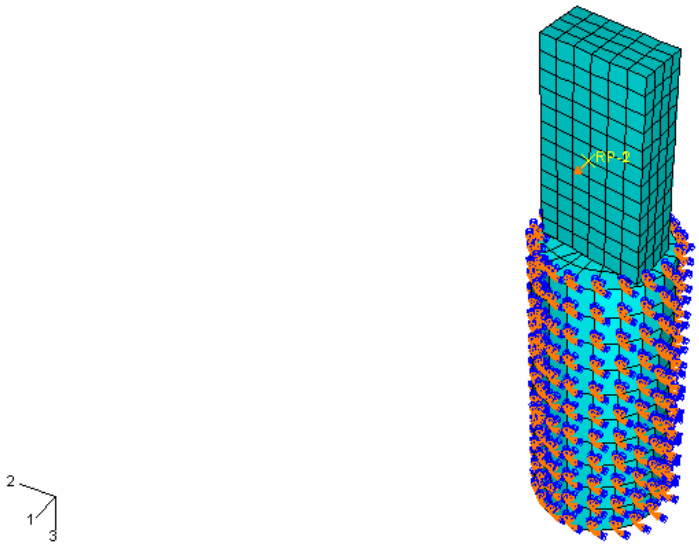

Figure 47. Finite element mesh of HP pile embedded in 2-m diameter sand sleeve

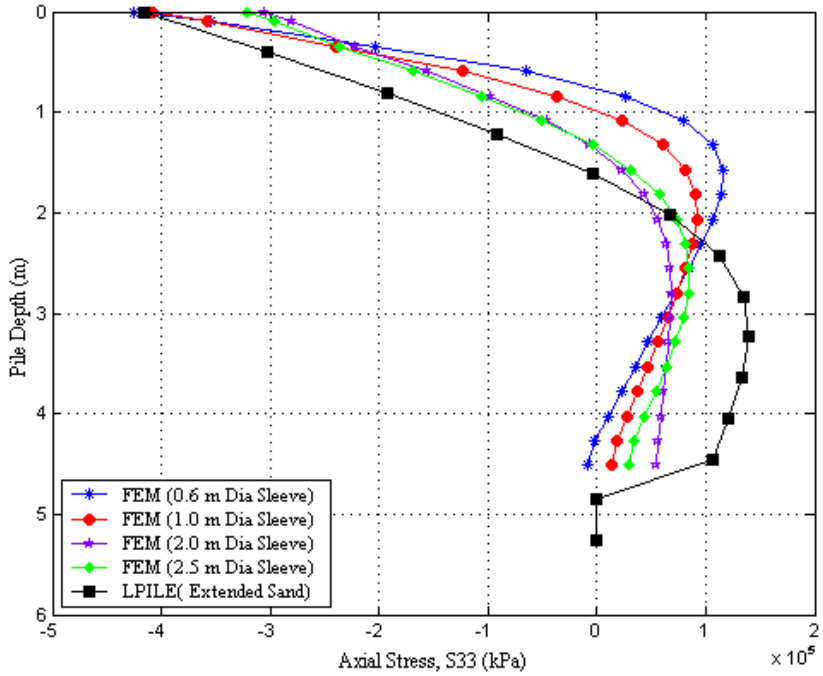

Figure 48. FE versus L-PILE at different sand-sleeve diameters. Axial stresses for an extended single layer of sand subjected to thermal loading, ΔT= 27 °C

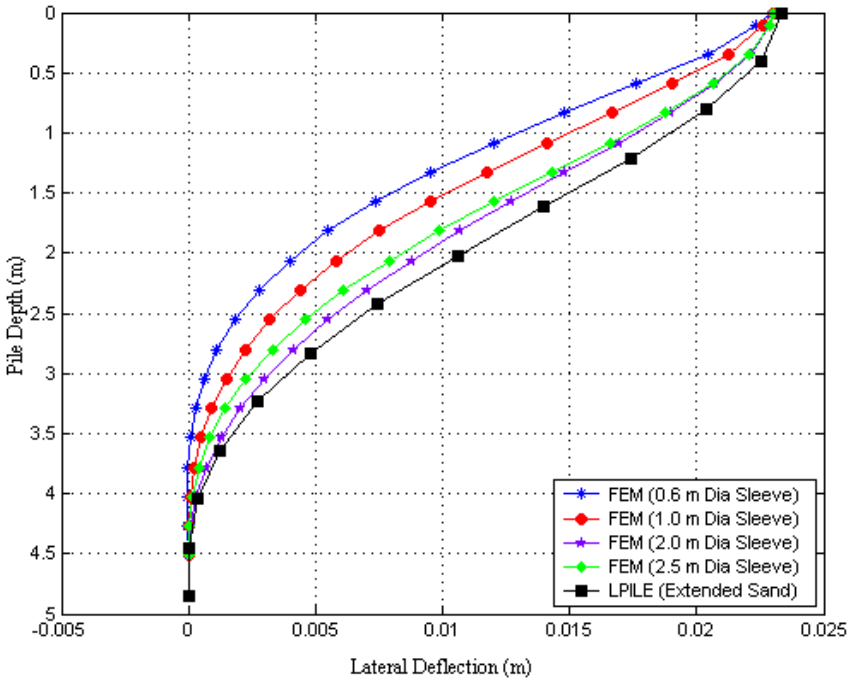

Figure 49. FE versus L-PILE at different sand-sleeve diameters. Lateral deflections, for an extended single layer of sand subjected to thermal loading, ΔT= 27 °C

Buckling of Piles

The buckling behavior of a single pile and pile-bent was studied using the finite element method. Three-dimensional, finite element models for single pile and pile-bent have been developed to study the buckling behavior of single piles and pile-bent. An iterative linear analysis based on extracting the pile(s) eigenvalues has been adopted. The finite element model consists of soil continuum elements. Material non-linearity is accounted for both, the piles and the soil in the base state of the model. A parametric study has been utilized to determine the effect of the geometric and material properties of the pile and the surrounding sand on the predicted critical buckling loads of the piles. We found that the group effect in the pile-bent increases the magnitude of the critical buckling loads, and the capacity of pile-bent to buckle as compared to single piles.

The use of integral abutments supported by steel H-piles has become a common practice in most of the states. In general, stiff piles can buckle under axial stresses before the material of the pile yields. A finite element model for the analysis of fully and partially embedded compression members has been developed in [94]. The mode shapes corresponding to the critical buckling loads were among the most important outputs of this work. The method relied on extracting the eigenvalues by a matrix iteration procedure satisfying the boundary conditions specified at the ends of the slender members. The authors declared that the effect of axial load transfer could be taken into consideration.

Several experimental and numerical approaches were developed for the prediction of pile buckling. A model for evaluating the critical buckling capacity of long slender piles using the sub-grade reaction method is found in [95]. The method relies on using deflection functions developed by the minimum potential energy concept. The effect of the distribution of the horizontal sub-grade reaction on the buckling capacity of the pile has been conducted through a parametric study. Moreover, the authors compared their findings to a pile load test results reported in the literature.

In this chapter, we present a study of the buckling behavior of steel H-piles supporting the integral abutments of the Scotch Road, bridge using the finite element method. The HP steel piles are laterally supported by soil along their depths and subjected to both axial and lateral loads. The dead and live loads on the superstructure cause the axial loading. The thermal expansions and contractions of the bridge cause the horizontal loading. The analysis is based on extracting the pile buckling eigenvalues that corresponds to the pile buckling mode shapes (eigenvectors). A parametric study is conducted to study the buckling sensitivity of a single pile and pile-bent to the geometric and material properties of the pile and sand surrounding it. Four parameters are studied: (1) the effect of the stiffness of the sand surrounding the pile, (2) the effect of the pile length, (3) the effect of the combined axial and vertical loads, and (4) the effect of the type of boundary conditions at the pile ends.

Finite Element modeling

A 3D finite element model was developed to study the buckling of single piles and pile-bent using the finite element software, ABAQUS/Standard [(96)]. The FE model focuses on modeling HP steel piles supported laterally along its depths by sand confined within galvanized steel sleeves.

Euler Formula for Buckling of Columns

The Euler buckling formula was introduced by the Swiss mathematician; Leonhard Euler in 1759. The Euler critical buckling load for a pinned-pinned pile is defined as:

$$P_{cr} = \frac{\pi^2 EI}{L^2} \tag{3}$$

where, *E* is the modulus of elasticity of the pile material, *I* is the moment of inertia of the cross-sectional area with respect to the minor principal axis, and *L* is the length of the member if simply supported.

Comparison between Euler and FE

The purpose of this comparison is to establish the soundness of the FE model in its ability to predict the critical buckling load for the pile. As such, the results from a FE analysis are compared with closed form solution for an HP pile not embedded in soil. A concentrated load equivalent to the Euler critical buckling load (1.485E4 KN/m^2) for a pinned-pinned boundary condition was applied at the reference point at the top of the pile. Table 4 shows that a fixed-pinned pile buckles at a load corresponding to twice the Euler critical buckling load, and a fixed-fixed pile buckles at four times the Euler buckling load. Figure 50 shows the first buckling modal shapes of a single pile with different boundary conditions, corresponding to the smallest eigenvalues. The variation in the magnitudes of the critical buckling load computed by Euler formula and those by the FE model are minimal. Any difference between the two methods can be attributed to the three dimensional nature of the model in (ABAQUS\Standard).

Table 4 - Comparison between the magnitudes of the critical buckling load obtained from Euler formula and FEM

Type of Connection	Eigenvalue (λ)		Critical Buckling Load (KN/m^2)		% Difference Between Methods
	Euler Formula	FEM	Euler Formula	FEM	
Pinned-Pinned	1	0.8995	1.486E+04	1.336E+04	0.10
Fixed-Pinned	2.04	1.867	3.031E+04	2.774E+04	0.08
Fixed-Fixed	4	3.787	5.943E+04	5.627E+04	0.05

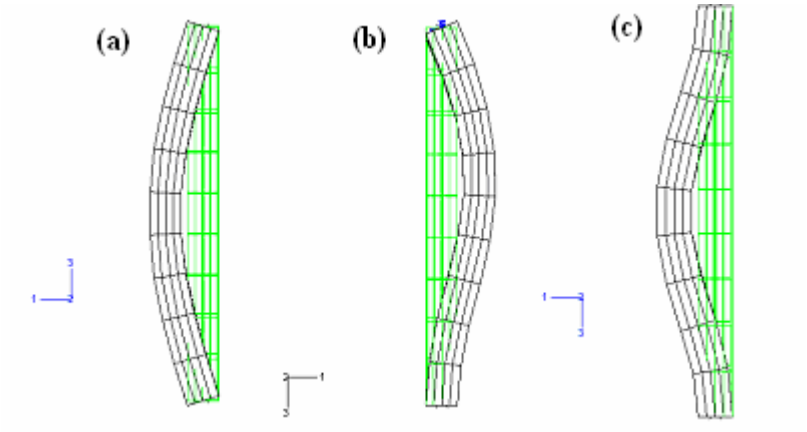

Figure 50. First buckling modes. (a) Pinned-Pinned; (b) Fixed-Pinned; (c) Fixed-Fixed

Since the validity of the FE model has been established, the sand surrounding the pile has been incorporated and the updated model that closely simulates actual construction was utilized to conduct the parametric study.

Buckling Analysis Using Abaqus

The analysis is based on extracting the pile eigenvalues. ABAQUS/Standard has the capability of estimating the critical buckling loads of stiff structures by eigenvalues extraction. The computed eigenvalues are the multipliers of a perturbation load, which added to a base state load to form the critical buckling load. The base state corresponds to response history of the structure prior to the application of the perturbation load, including non-linear effects. The perturbation load is the added load during the buckling step. In ABAQUS/Standard, the eigenvalue-buckling problem, is solved by finding the load that makes the stiffness matrix singular.

$$K^{MN}V^{N} = 0 \tag{4}$$

where, K^{MN} is the tangent stiffness matrix when the loads are applied, and V^{N} are the nontrivial displacement solutions. Equation (4), only applies for a structure with no load history prior to the application of the perturbation load.

However, for structures with load histories, the eigenvalue buckling problem is defined by equation (5):

$$(K_o^{NM} + \lambda_i K_\Delta^{NM})V_i^{M} = 0 \tag{5}$$

where K_o^{NM}, is the stiffness matrix corresponding to the base state, which includes the effects of the preloads, K_Δ^{NM} is the differential initial stress and load stiffness matrix due

to the incremental loading pattern (Q^N), λ_i are the eigenvalues, V_i^M are the buckling mode shapes (eigenvectors), *M* and *N* refer to the degrees of freedom of the whole model, and i, refers to the ith buckling mode.

The perturbation load, Q^N, is defined during the buckling analysis. However, the magnitude of this loading is not important, because it will be scaled by the load multipliers, λ_i, found in the eigenvalue problem. The critical buckling loads are calculated according to the following equation:

$$P^N + \lambda_i Q^N \quad (6)$$

where, P^N, is the base state load.

Loading and Buckling Modes

The 3D finite element models of the piles were subjected to a vertical incremental load, Q^N, equivalent to critical buckling load of a single pile with pinned ends. In addition, a lateral displacement calculated from thermal contractions and expansions of the bridge superstructure was imposed at the top of the pile. Figure 51 (a) and (b) demonstrate the deflected shapes of the buckling of single pile and pile-bent respectively.

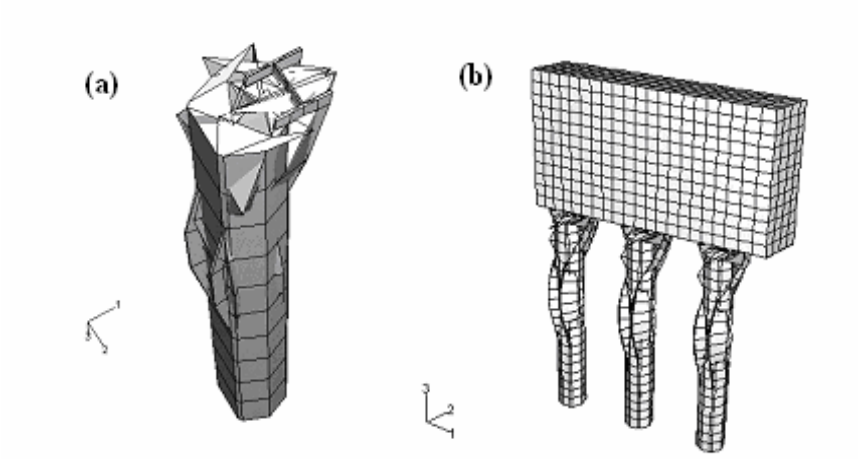

Figure 51. Buckling of a single pile (a) and a pile-bent (b) during a clamped-guided boundary condition

Parametric Studies

The purpose of the parametric study is to investigate the sensitivity of the pile foundation to some crucial design parameters. Several factors are involved in the prediction of the buckling behavior of single pile and pile-bent. The effect of some of these factors on the buckling behavior of the HP 360x152 steel piles used to support the Scotch Road, integral abutments are presented below.

Effect of Soil Stiffness on Critical Buckling Load

The values used in this section are intended to study the effect of the different (low, medium, and high) densities of the sand surrounding the piles on the critical buckling load, Table 5. The results from the finite element model show that lateral support provided by the sand along the depth of the pile has increased the critical buckling load by 17 times compared to that calculated for the pile alone. Table 5 shows that as the soil stiffness increased, the critical buckling load increased accordingly. The relationship is slightly nonlinear for loose sands and it becomes linear for denser sands. Moreover, the critical buckling load increases drastically for the case of a pile-bent, which illustrates the effect of having more of one pile in a row, on increasing the resistance of piles to buckle. However, the early slope of the curve for the pile-bent case is slightly higher than that for the single pile, which indicates a greater increase in the critical buckling load with the increase in the sand stiffness.

Table 5 - Summary of the variation in the critical buckling load due to change in sand stiffness for single pile and pile-bent

Sand Stiffness (KN/m^2)	Eigenvalue (λ)		Critical Buckling Load (KN)	
	Single Pile	Pile-Bent	Single Pile	Pile-Bent
2.70E+04	17.304	43.812	2.570E+05	6.508E+05
3.00E+04	18.107	45.450	2.690E+05	6.751E+05
4.00E+04	19.785	47.754	2.939E+05	7.093E+05
5.00E+04	20.852	49.752	3.097E+05	7.390E+05
7.00E+04	22.804	51.309	3.387E+05	7.621E+05
9.00E+04	24.690	52.533	3.667E+05	7.803E+05

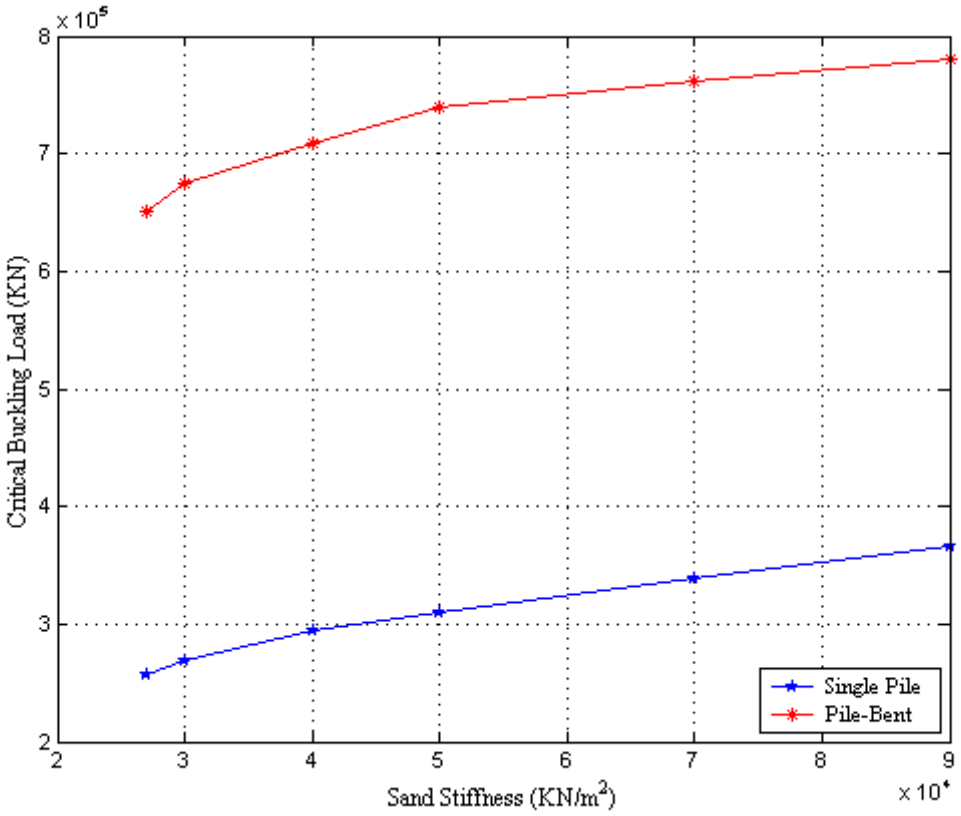

Figure 52. Effect of variation in sand stiffness on the critical buckling load for single pile and pile-bent

Effect of Pile Length on Critical Buckling Load

The values used to vary the length of the pile are shown in Table 6. Expectedly, it is concluded that as the length of the pile increases, the critical buckling load decreases in magnitude, Figure 53. Furthermore, the gap between the values for the single pile and pile-bent, indicates an increase in the critical buckling load for the pile-bent as compared to that of a single pile. This suggests an increase in the buckling capacity of the piles in a pile-bent as compared to a single pile. However, Table shows that the decrease in the magnitudes of the piles critical buckling load in a pile bent (1.825E5 kN) is greater than that of a single pile (1.013E5 kN), as the length of the piles changed from 2.58 m to 12.58 m in both cases. This discrepancy in the critical buckling load (0.445 %) indicates that the piles in a pile-bent are more sensitive to the change in their lengths than a single pile.

Table 6 - Summary of the variation in the critical buckling load due to change in pile length for single pile and pile-bent

Pile Length (m)	Eigenvalue (λ)		Critical Buckling Load (KN)	
	Single Pile	Pile-Bent	Single Pile	Pile-Bent
2.58160	21.569	50.553	3.204E+05	7.509E+05
4.58160	17.304	43.821	2.570E+05	6.508E+05
6.58160	16.072	44.013	2.387E+05	6.538E+05
8.58160	15.802	39.996	2.347E+05	5.941E+05
10.58160	14.924	12.918	2.217E+05	5.757E+05
12.58160	14.751	12.756	2.191E+05	5.684E+05

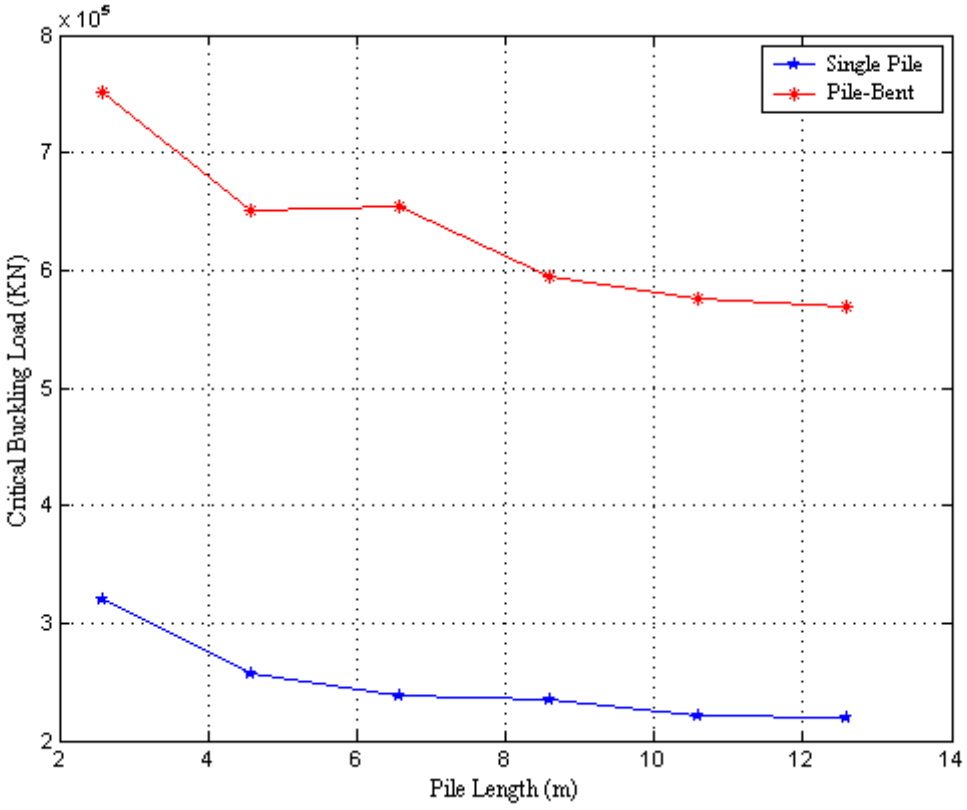

Figure 53. Effect of variation in pile length on the critical buckling load for single pile and pile-bent

Effect of Type of Connection on Critical Buckling Load

In the Scotch Road, I-95 integral abutment bridge, the top of the piles are embedded into the abutments to ensure total fixity of the pile head into the abutment. The movement of the abutment laterally results in the formation of fixed with sway connection between the pile head and the abutment. However, due to excessive loading, a plastic hinge may develop, and this fixed with sway connection may change to pinned with sway. Three different end connections are studied as shown in Table 7; Fixed with Sway-Fixed; Pinned with Sway-Pinned; and Pinned with Sway-Pinned.

Figure 54 shows that the critical buckling load decrease when the rotational degrees of freedom are released at the top of the pile in the case of a Pinned with sway-Fixed connection. The same trend follows with further decrease in the critical buckling load as the rotational degrees of freedom are released at both the top and bottom of the pile for the case of Pinned with sway-Pinned connection, Figure 54. The differences in the critical buckling load between the Fixed with sway-Fixed, and the Pinned with sway-Fixed connections are 0.27 percent, and 0.053 percent for the cases of single and pile-bent respectively. However, the difference in the critical buckling load is significantly smaller between the Pinned with sway-Fixed, and the Pinned with sway-Pinned connections, which amounts to 0.002 percent for a single pile and 0.07 percent for the pile-bent. The pile-bent maintains higher buckling strength as compared to the single pile.

Effect of Combining Vertical and Lateral Loads on Critical Buckling Load

Several displacement magnitudes are applied together with the vertical load representing the critical buckling load for the pile alone. The magnitude of the displacements was chosen based on the probable temperature variations that the bridge might be subjected to during the seasons and is tabulated in Table 8. The equivalent lateral reaction of the applied displacement was calculated from a general static step and included in the buckling step along with the vertical load. Figure 55 shows that as the displacement combined with the vertical load increases, the buckling load decreases. This is readily justified because the lateral displacement developing along the depth of the pile due to the imposed displacement boundary condition is added to the displacement resulting from applying the vertical load at the top of the pile.

Table 7 - Summary of the variation in the critical buckling load due to change in type of connection for single pile and pile-bent

Connection Type	Eigenvalue (λ)		Critical Buckling Load (N)	
	Single Pile	Pile-Bent	Single Pile	Pile-Bent
Fixed with sway-Fixed	17.304	43.812	2.570E+05	6.508E+05
Pinned with sway-Fixed	12.658	41.481	1.880E+05	6.162E+05
Pinned with sway-Pinned	12.631	38.46	1.876E+05	5.713E+05

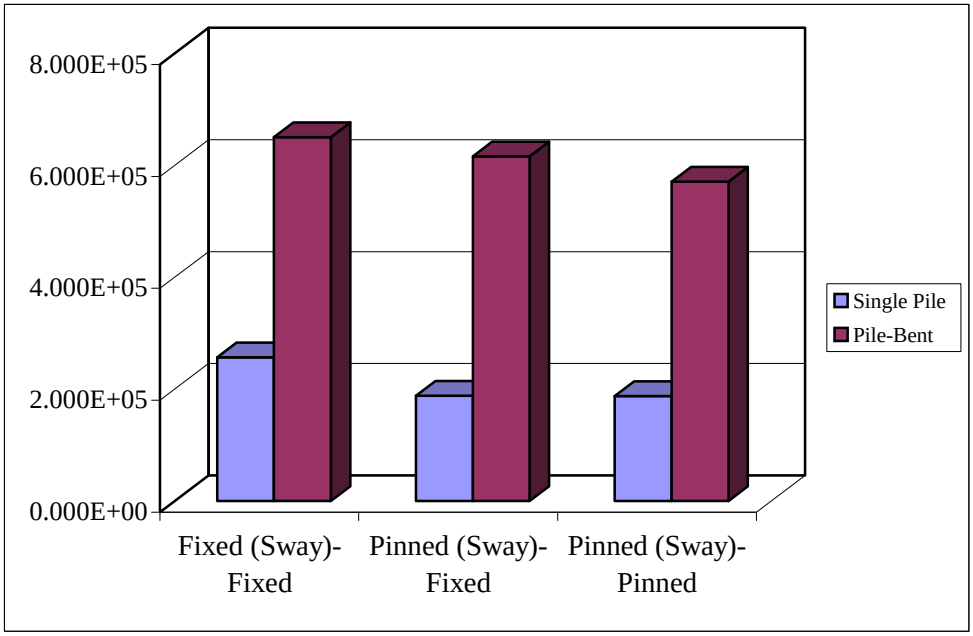

Figure 54. Effect of variation in type of connection at pile ends on the critical buckling load for single pile and pile-bent

Table 8 - Summary of the bariation in the critical buckling load due to change in combined axial and lateral loading for single pile and pile-bent

Displacement (m)	Eigenvalue (λ)		Critical Buckling Load (N)	
	Single Pile	Pile-Bent	Single Pile	Pile-Bent
0.001	12.97	31.976	1.926E+05	4.750E+05
0.00543	12.95	32.2300	1.923E+05	4.787E+05
0.01300	12.92	32.2540	1.919E+05	4.791E+05
0.02000	12.87	32.2760	1.911E+05	4.794E+05
0.02300	12.88	32.3090	1.912E+05	4.799E+05
0.02800	12.85	32.0690	1.908E+05	4.763E+05

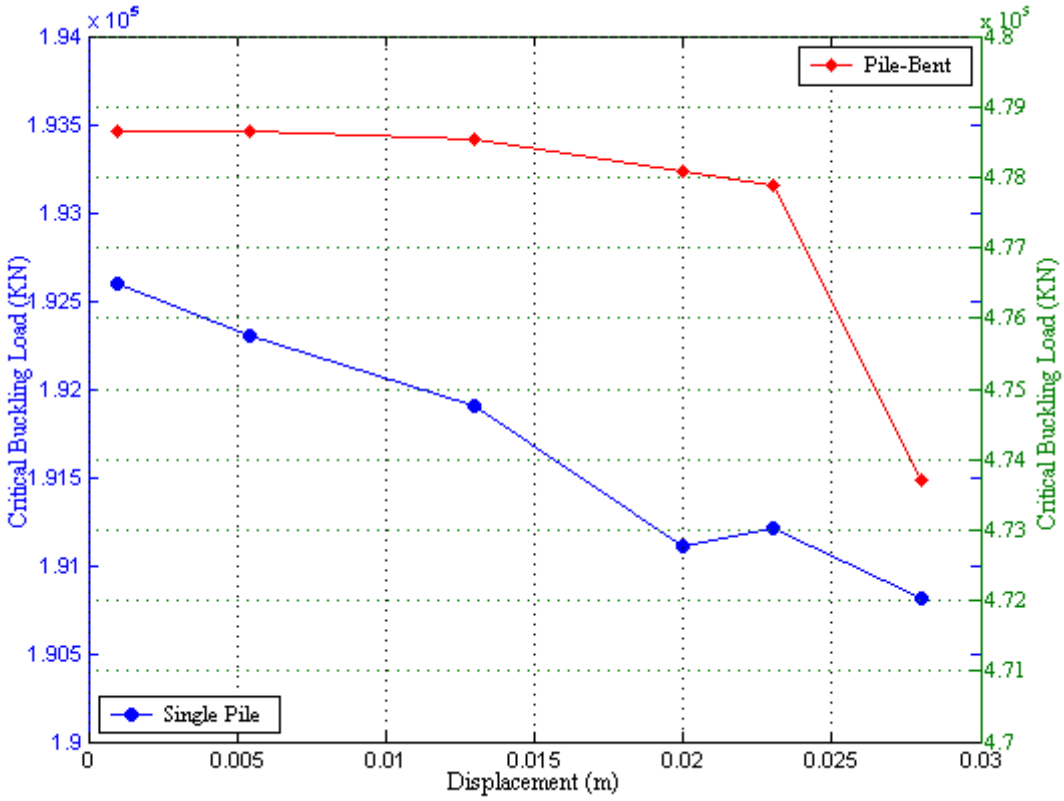

Figure 55. Effect of variation in combined axial and lateral loading at pile ends on the critical buckling load for single pile and pile-bent

Summary and Conclusions

A single pile and pile-bent buckling models were developed using the finite element software ABAQUS/Standard. The method used relied on extracting the buckling eigenvalues of the pile. The non-linear response of the soil was incorporated into the base state of the model, by adopting a solid continuum model defined by the Mohr-Coulomb failure criterion. Eight nodded, solid continuum elements were used to model the piles. A parametric study was conducted to study the effect of the stiffness of the soil surrounding the pile, the pile length, the boundary conditions at the top and bottom of pile, and the effect of combining axial and lateral loads.

The parametric study revealed that all four factors studied, significantly affected the magnitudes of the critical buckling load of the pile. The single-pile buckling model showed that the pile globally buckles at a vertical load of approximately 1.49E4 kN for (fixed with sway-fixed) boundary conditions. However, embedding the pile into a 0.6 m galvanized steel sleeve filled with sand increased the pile capacity against buckling by 17 times.

The results from the parametric study for the pile-bent model also emphasized that the group effect substantially increases the buckling capacity for each of the piles (2.53 times that of a single pile embedded in sand with fixed with sway-fixed boundary

conditions). However, applying combined axial and vertical loading has an adverse effect on the pile capacity for buckling, and the critical buckling load decreases significantly under this type of loading.

Geometry and Element Characteristics of FE Modeling

Introduction

The objective of this chapter is to present the characteristics of the finite element models developed to analyze the soil-pile interaction and the buckling behavior of piles. The models developed in this research are (1) The first model focuses on modeling the pile-soil interaction for single piles. (2) The second model sheds light on the different aspects involved in modeling group of piles.

Geometry and Element Characteristics

In this section, the different aspects related to constructing the geometry of the model and the choice of elements used to model the pile and the surrounding sand are discussed.

Geometry

The entire Scotch Road, integral abutment bridge was modeled using ABAQUS/Standard. Figure 56 shows the geometry of the bridge superstructure. The bridge has six lanes, each having a width of 3.6 m. The shoulders are 3 m in width. Two integral abutments at ends and eight piers at mid span support the bridge. The thickness of the bridge deck is (0.26 m) and the thickness of the approach slabs is (0.45). The girders of the bridge are spaced at a distance of 3.35 m. Figure 57 shows a cross

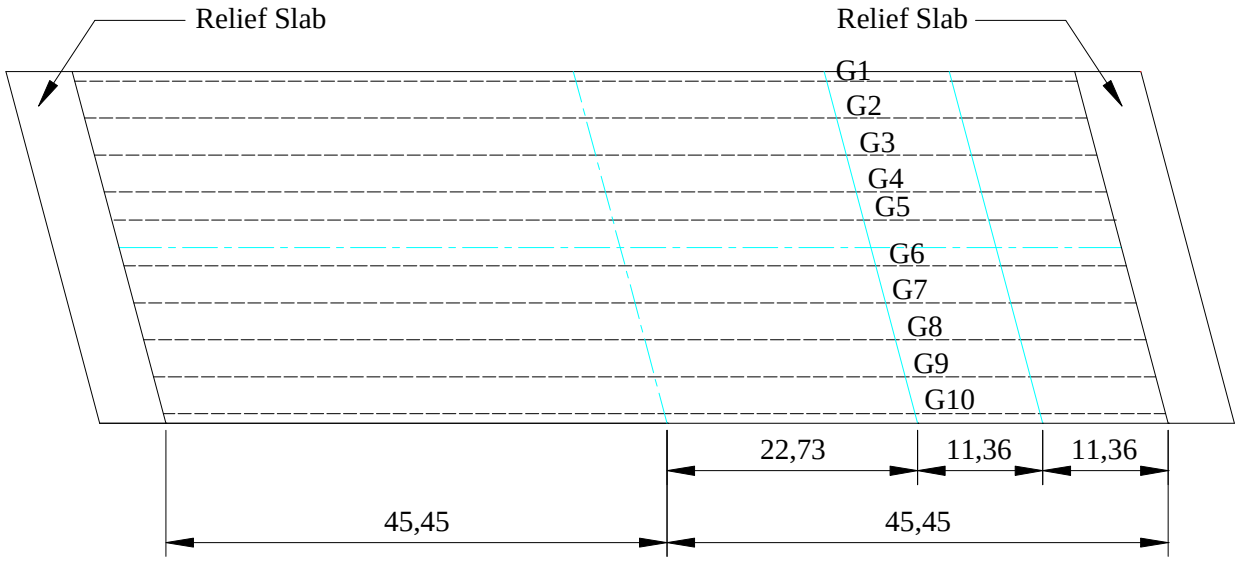

Figure 56. A Plan view of the Scotch Road, Integral Abutment Bridge

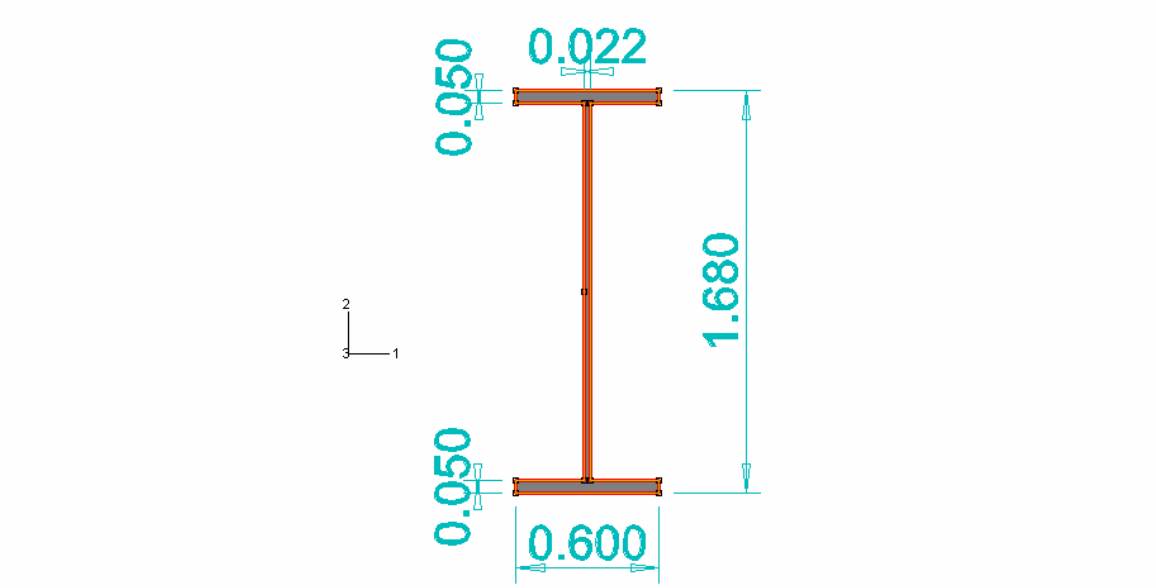

Figure 57. Cross section of steel girders supporting bridge deck

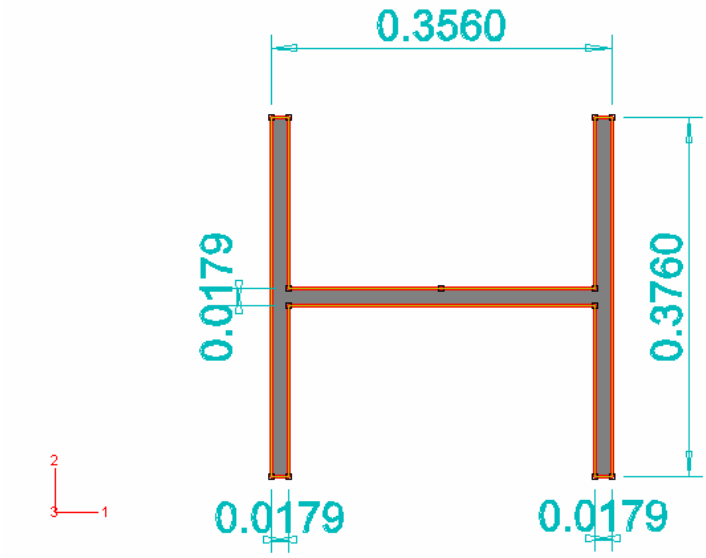

Figure 58. Cross section of HP 360X152 steel piles

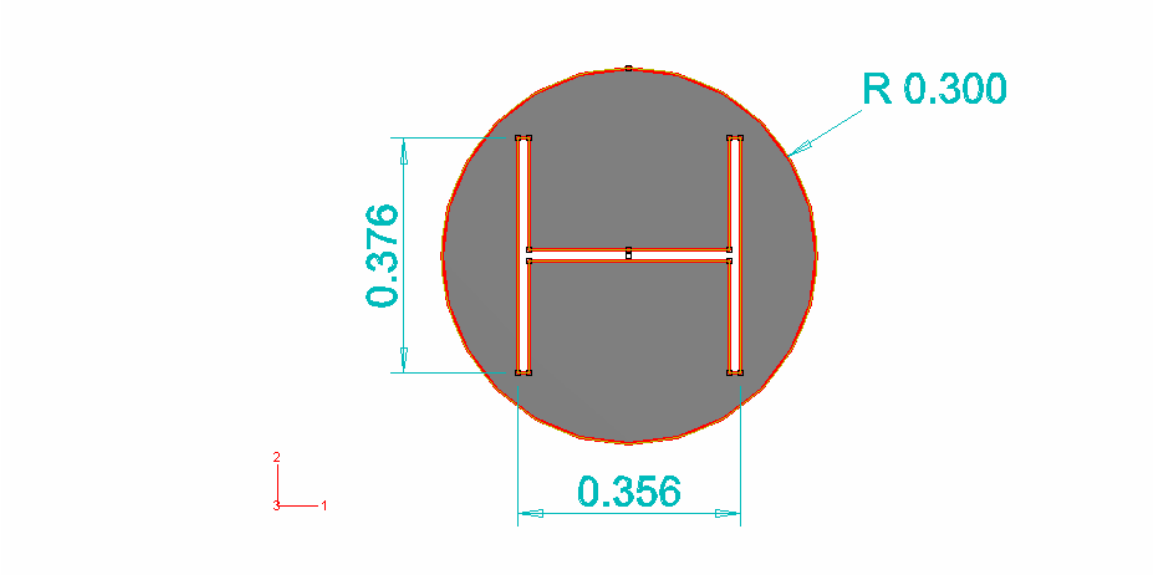

Figure 59. Cross section of the sand sleeves surrounding the piles

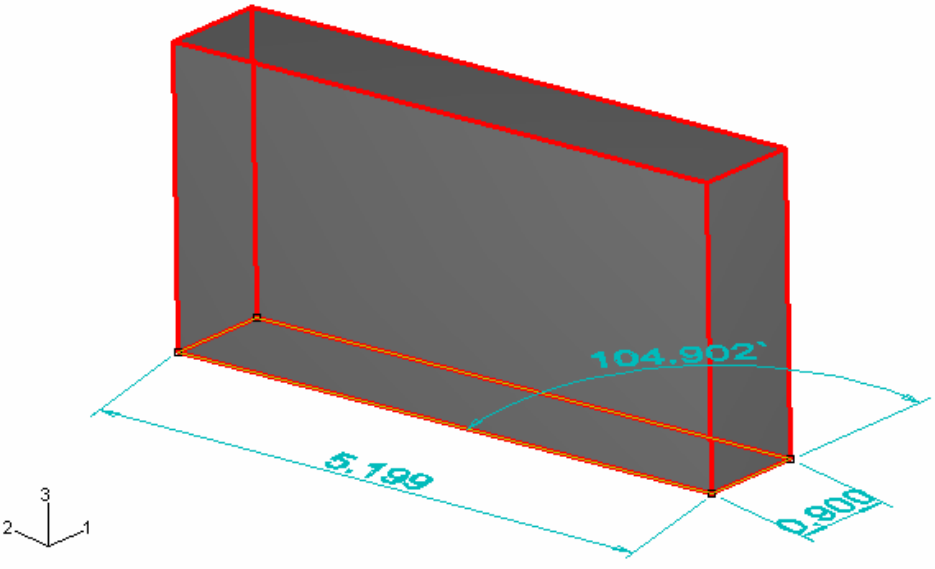

Figure 60. An isometric view of the integral abutment

section of the girders. Furthermore, a full 3D finite element model was developed for the substructure of the bridge simulating the behavior of soil-pile interaction for a single and group of piles. The geometry was modeled according to the exact dimensions of the substructure of the Scotch Road integral abutment bridge, Figure 58 to Figure 60. The pile length used for the model, however, is shorter than its actual length, because the pile was embedded in plain Concrete for a distance of (7.62 m) to ensure its bottom rigidity beyond a depth of (5.1816 m). The dimensions of the sand surrounding the pile and the reinforced concrete integral abutment were modeled according to the design drawings.

Node and Element Numbering

The finite element model for the full bridge model consists of 28473 nodes, and 7898 elements. Figure 61 and Figure 62 demonstrate a portion of the bridge deck with the sequence of nodes and elements numbering.

The single pile finite element model consists of 2134 nodes, and 1032 elements, while it is composed of 7955 nodes, and 3480 elements for the group of piles model. The nodes and elements numbers were, automatically generated by ABAQUS/CAE. Figure 63 and Figure 64 show elements numbering in the pile and sand sleeve, respectively.

Element Family

Full Bridge Model

Three types of elements were used in the full bridge model. The four-nodded, shell elements (S4R) were used to model the bridge deck. Six-nodded triangular elements were used for modeling approach slabs. Three dimensional three-nodded beam elements (B32) were used to model the I-shaped steel girders. Moreover, two nodded beam elements (B31) were used to model the reinforced concrete abutment and piles. Furthermore, the soil behind the abutments and under the approach slabs were modeled using (Spring1) elements, which connect from the defined node to the ground, Figure 65. Although, beam elements in ABAQUS are wire elements, it has the capability of adopting the stiffness of 3-D sections, such as the I-shaped girders of this bridge.

Pile-Soil Interaction Models

Since modeling pile-soil interaction usually involves defining contact behavior between materials, and plastic properties, solid continuum are the best choice for conducting such analysis. The eight nodded, linear brick, reduced integration (C3D8R) element was used to model both the pile and soil behavior, Figure 65.

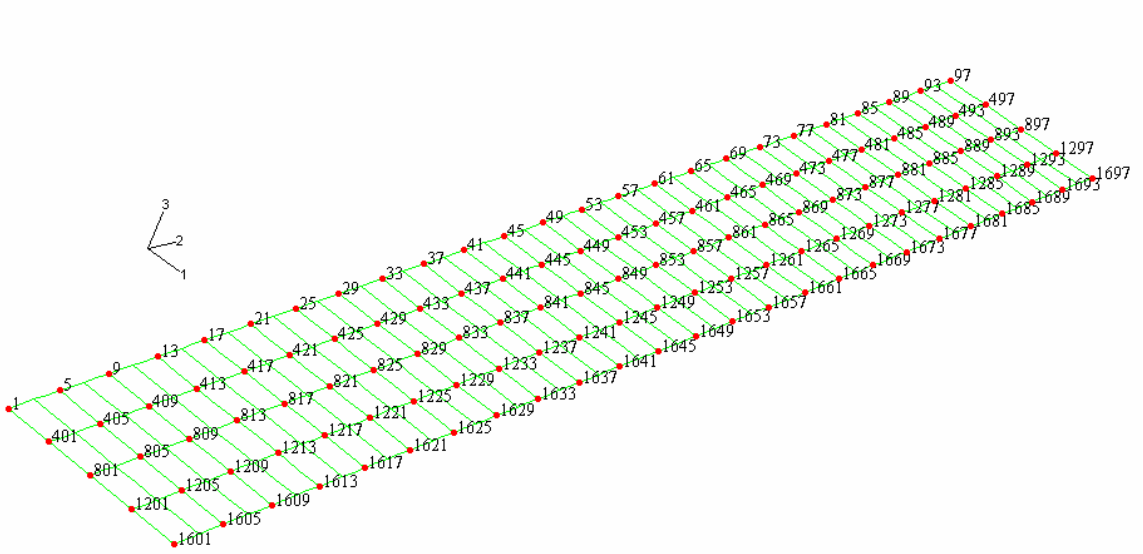

Figure 61. Node numbering in FE mesh of bridge deck

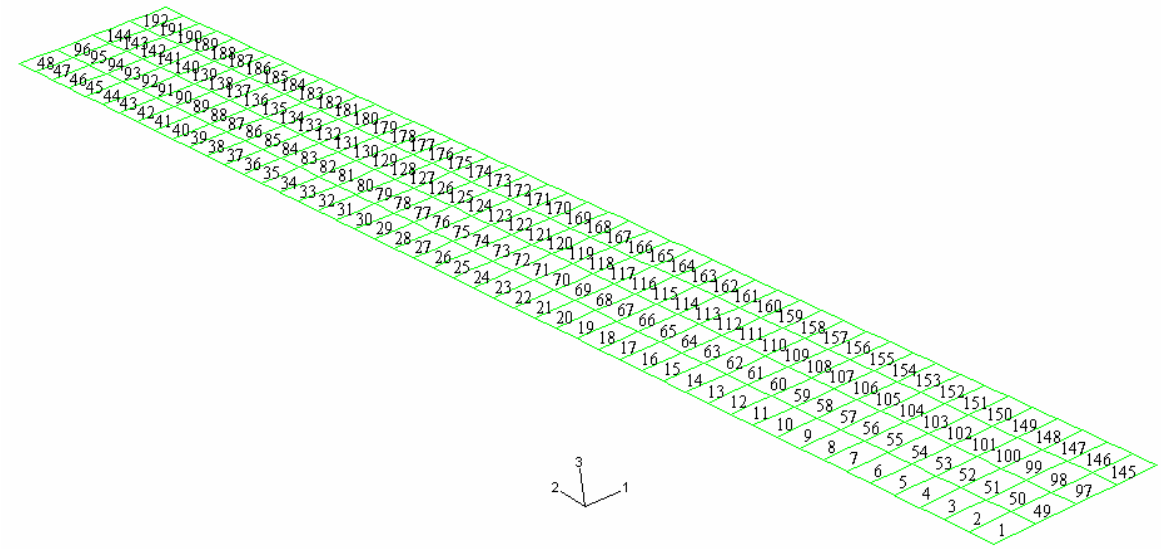

Figure 62. Element numbering in FE mesh of bridge deck

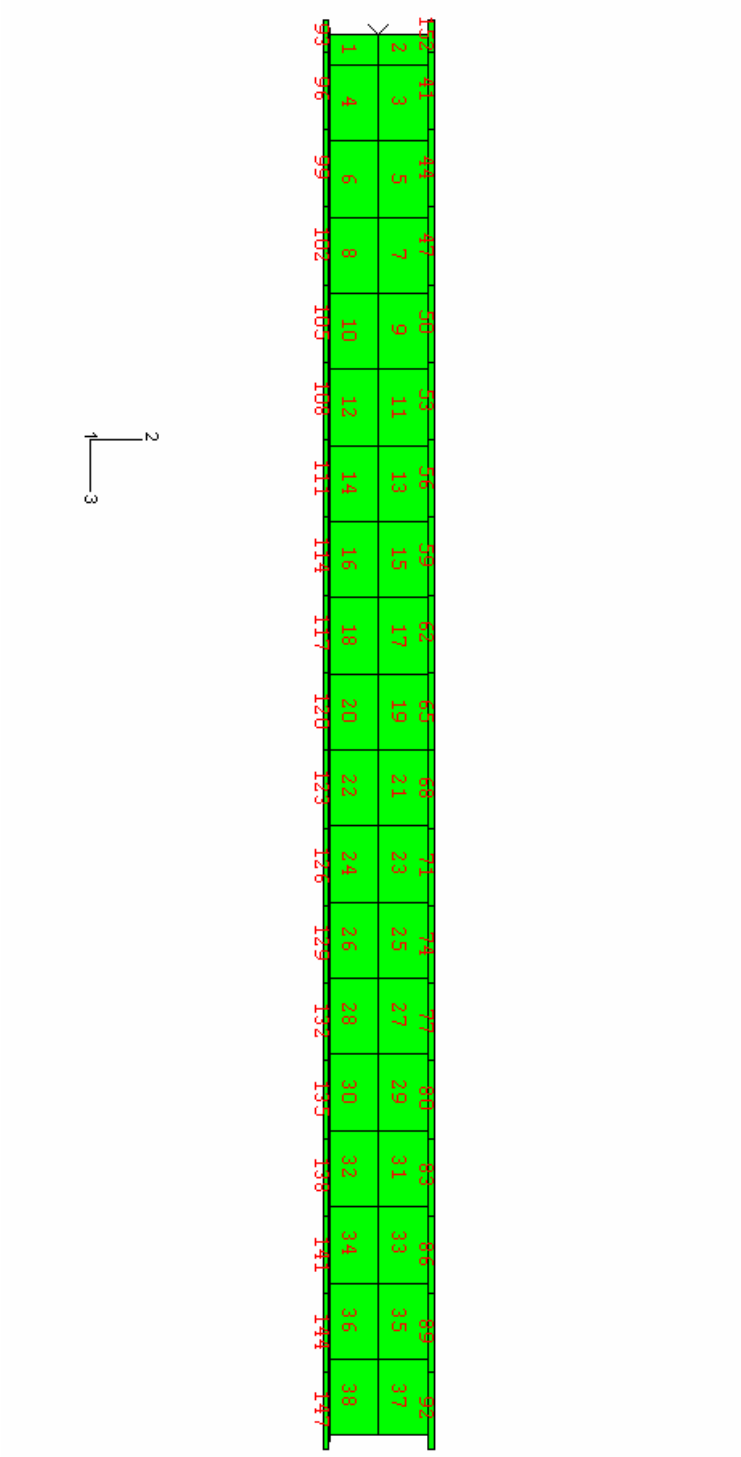

Figure 63. Element numbering in HP steel pile

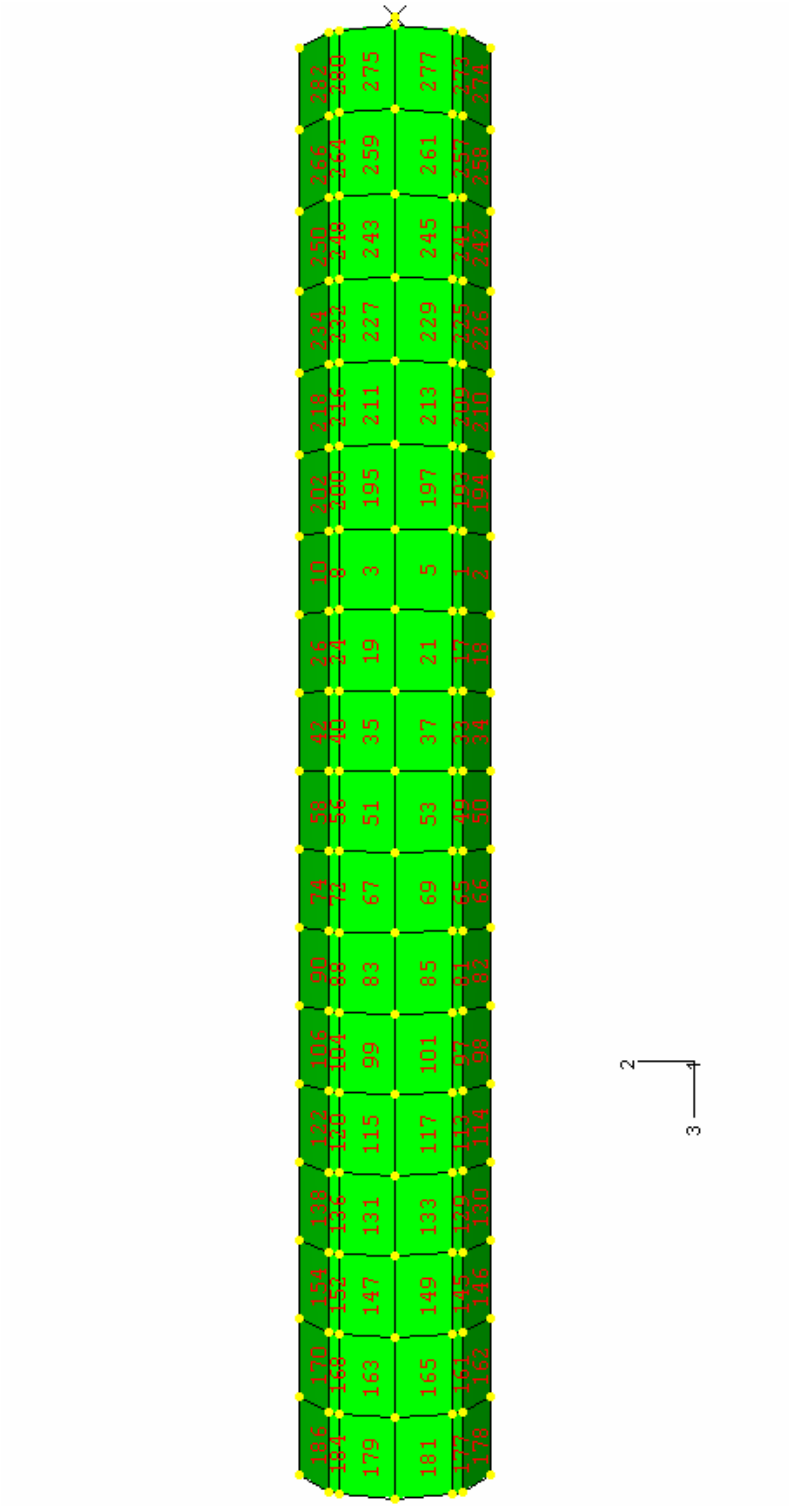

Figure 64. Element numbering in sand sleeve surrounding the pile

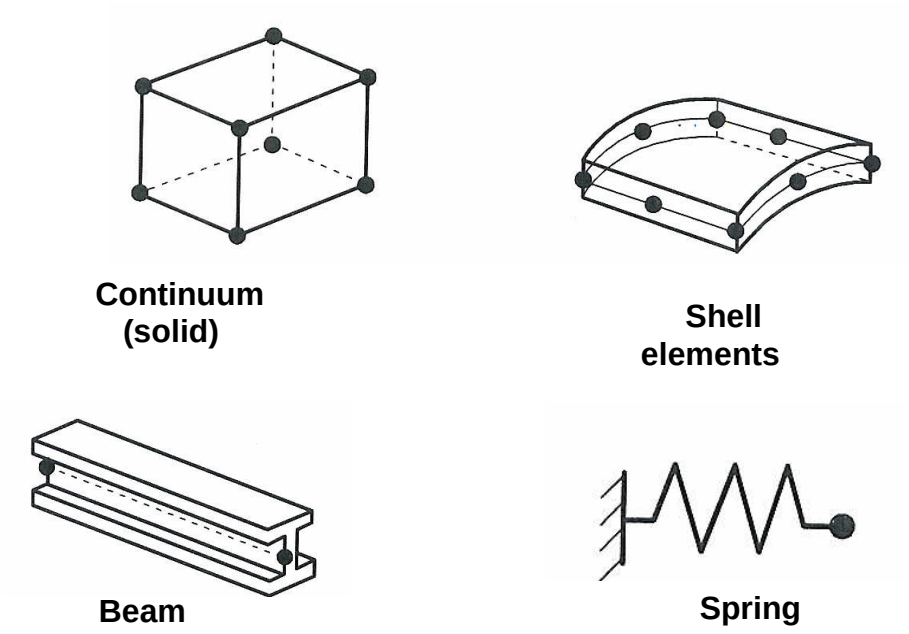

Figure 65. Element family in FE models

Material Properties

The reinforced concrete material definition for the bridge deck was assumed to be elastic-plastic. The modulus of elasticity of concrete was considered to be (4.15E6 kN/m^2) corresponding to f'c of (36513 kN/m^2). The first yielding of the material occurs at a stress of (20684 kN/m^2). Then the concrete is assumed to harden to a stress of (37921 kN/m^2) at a plastic strain of 0.0015. Grade 50 steel I-beams were used to model the steel beams with a modulus of elasticity of 2.0E6 (kN/m^2). An elastic-perfectly plastic material modeling was adopted for the steel beams. The spring elements used to model the soil were presumed to be linear springs with constant modulus of subgrade reaction. The values suggested in (L-PILE 4.0 User's manual) were implemented in the model. Dense sand was utilized behind the integral abutment and under the approach slab of (61000 kPa/m) modulus of subgrade reaction.

The material for the steel pile was assumed to be elastic perfectly plastic. An elastic-plastic model was adopted for the reinforced concrete integral abutment. The soil was modeled with strain hardening model according to Mohr Coulomb failure criterion (Bowels, 1996, Bardet, 1997, and Das, 1998, Coduto, 2001), defined by,

$$\sigma_1 = \sigma_3 N_\phi + 2c\sqrt{N_\phi} \qquad (7)$$

Where, σ_1 and σ_3 are the major and minor principal stresses, respectively, c, is the effective cohesion of the soil, $N_\phi = (45^\circ + \phi/2)$ is the flow value, ϕ is the angle of internal friction of the soil. The sand surrounding the pile was assumed to vary from loose to dense with an angle of internal friction, ϕ of (30° to 38°). Young's modulus for the sand was varied between (27000 and 69000 kN/m^2) along the depth of the pile. The

modulus of elasticity of steel piles was taken to be ($2x10^8$ kN/m^2) and a yielding stress of 344,750 kN/m^2 was used. An elastic-plastic model was adopted for the reinforced concrete abutment. The modulus of elasticity for the concrete was considered to be ($2.86x10^7$ kN/m^2).

Boundary Conditions and Loading

The boundary conditions in the finite element model were implemented according to the type of analysis conducted. Three load conditions were implemented in the finite element model: (1) dead load from the superstructure, the abutment, and self weight of pile and sand, (2) vehicular live load on the bridge, and (3) lateral displacement due to thermal loading on the bridge superstructure.

Full-Bridge Model

Boundary Conditions

Three boundary conditions were imposed on this model, corresponding to modeling the bridge as a frame-like structure. The embedment of the piles beyond a depth of 5.18 m into plain concrete was modeled using a fixed-type connection. Moreover, a roller support was imposed at the middle of the bridge corresponding to the support provided by the piers for the bridge superstructure, Figure 66. The composite section between the steel girders and the bridge deck was modeled by using multi-point constraints. "MPC type BEAM provides a rigid beam between two nodes to constrain the displacement and rotation at the first node to the displacement and rotation at the second node, corresponding to the presence of a rigid beam between the two nodes", (ABAQUS/Standard 6.3.3 User's Manual). This is not a perfectly accurate representation of the composite section, since only the degrees of freedom of the top flange of the girder is tied to those of the bridge deck using shear studs. Nevertheless, this configuration provides an acceptable approximation in case of studying a general property of the bridge such as thermal expansions and contractions.

Loading

The field data collection started on December 2002, which is not sufficient to determine the movement of the bridge, during its predicted lifetime. Therefore, it was necessary to

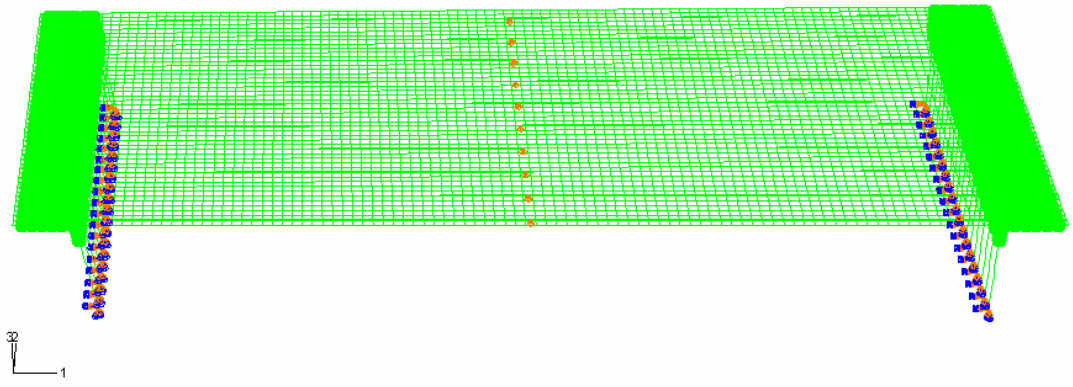

Figure 66. Boundary conditions for full-bridge model

predict the deflections that the bridge undergoes, as subjected to extensive thermal expansions or contractions. The finite element model of the full bridge was utilized to predict such situations. A temperature increase of 27 ^{o}C was applied to the bridge deck assuming an isotropic material behavior.

Pile-Soil Interaction for Bending Analysis Model

Boundary Conditions

Three boundary conditions were implemented for this analysis:

Fixed conditions at the bottom of the pile (restraining all displacement and rotational degrees of freedom), modeling the embedment of the pile into plain concrete for a distance of (7.62 m)

Fixed conditions along the surface volume of the sand, simulating the confinement of the galvanized steel sleeves surrounding the pile by the crushed stone backfill.

The guided fixation at the top of the pile was modeled using rigid body motion, by tying the top surface of the pile to the bottom surface of the abutment. In such a case the abutment is utilized as the rigid body, where the degrees of freedom of a defined reference point control all degrees of freedom of its elements to ensure maintaining zero slope at the top of the pile, and hence full fixation of the piles into the abutment walls. This method is only necessary for the partitioned abutment model, Figure 67. However, if the discrepancy between the transitional and rotational effect between the top and bottom of the abutment is assumed to be negligible, then the guided fixation at the top of the pile can simply be modeled by tying the pile top nodes to a defined reference point in the middle of the pile as shown in Figure 68.

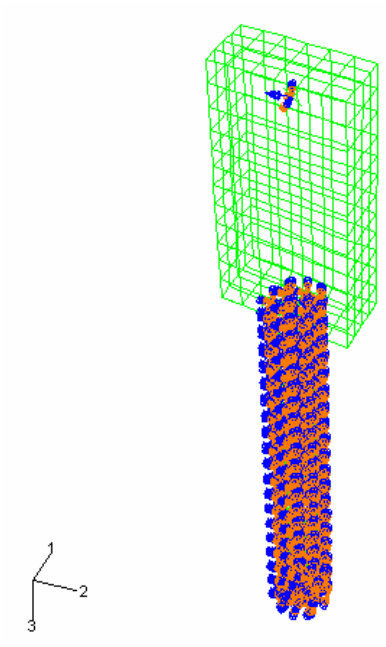

Figure 67. Boundary conditions for single pile model

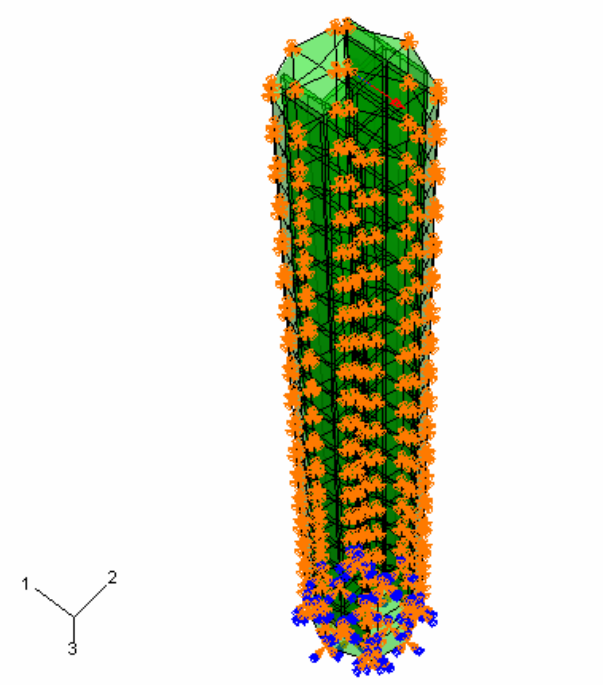

Figure 68. Boundary conditions for single pile with rigid surface at its top.

Loading

The computed dead and live loads per pile (692 KN) were applied as a concentrated load to the reference point of the rigid body along the global (3 direction). The self-weight was incorporated into the model by using the (gravity step), where the density of the materials and gravity acceleration are specified. The dead and live loads are applied prior to the application of the lateral loading to maintain their effect in full during lateral deflection step. The FE model was subjected to several lateral displacements according to the values measured from the displacement rings positioned at the north end of the bridge approach

slabs at the different seasons. Moreover, lateral displacements computed from thermal expansion equation (2.1) were imposed as displacements at the reference node controlling the rigid body motion at the top of the pile, Figure 69.

Single and Group of Piles for Buckling Analysis Model

Boundary Conditions

The same boundary conditions were applied to abutment and the piles as described above for the case of clamped-guided at the top of the pile and clamped at the bottom of the pile. The rigid body motion in this case was achieved by tying all three top surfaces of the piles to the bottom of the abutment, with a reference point controlling the degrees of freedom of the abutment elements as before, Figure 70. However, in order to study the effect of the boundary conditions on the buckling capacity of the piles, fixed-pinned, and pinned- pinned connections were also modeled.

Loading

The FE models for single and group of piles were subjected to a concentrated force

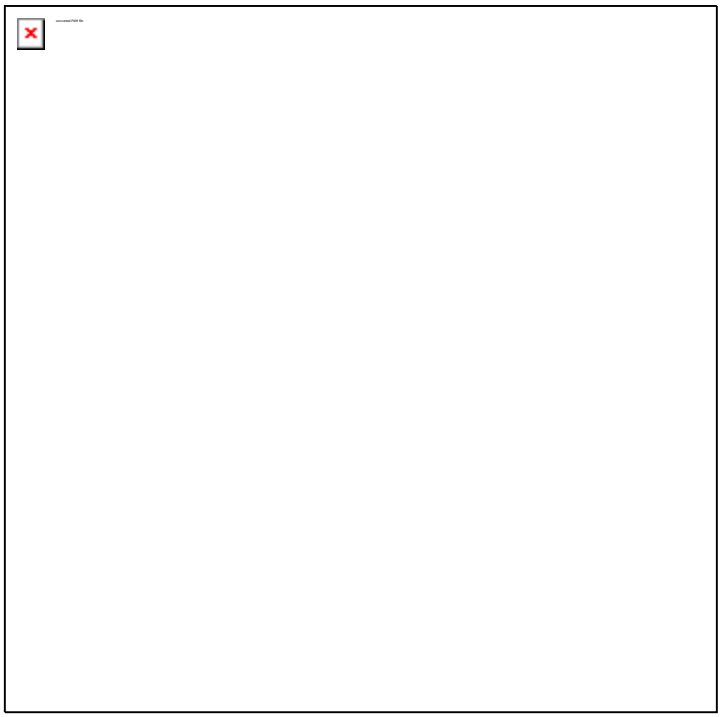

Figure 69. Applied lateral and vertical loading for single pile model

equivalent to the buckling load of an Euler column at the top of the pile. The reaction of the lateral displacement was determined in a separate general step and also applied at the reference point of the pile, Figure 71.

Soil-Structure Interaction

The sand-pile interaction was modeled using surface-to-surface contact algorithm in ABAQUS/Standard (6.3.3). Two surfaces have been identified; the exterior surface of the pile was modeled as the master surface and the interior surface of the sand as the slave, Figure 72. This kind of contact is based on defining the tangential and normal behaviors of the contact between the surfaces. The friction angle, (ϕ), for loose sand was assumed to be (30^{o}), and hence the coefficient of friction can be estimated, as the tangent of the

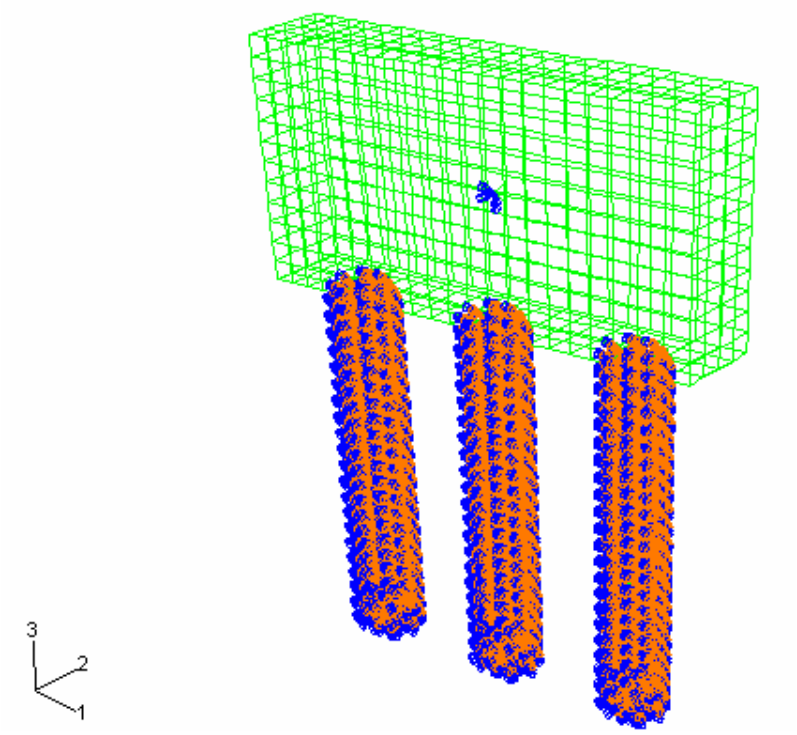

Figure 70. Boundary conditions for group of piles model

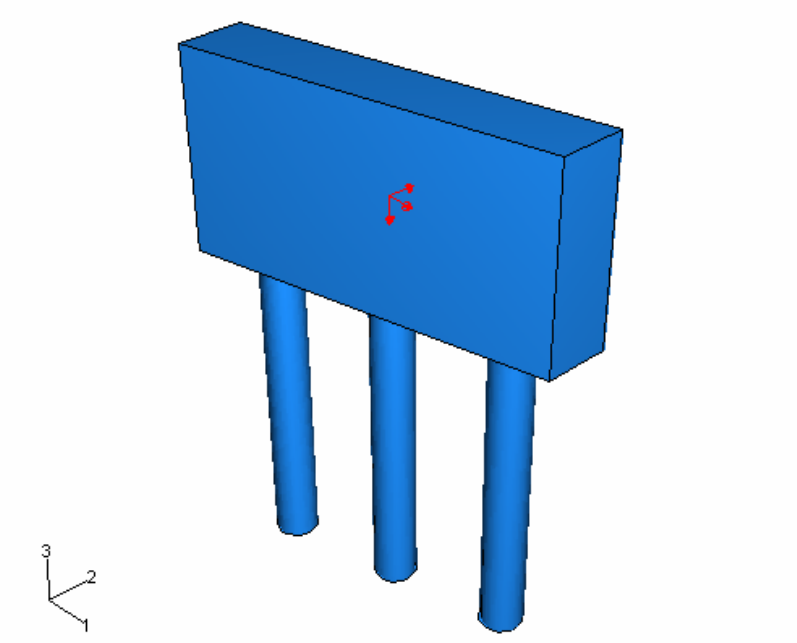

Figure 71. Applied lateral and vertical loading for group of piles model

friction angle. However, since the friction between the sand and steel pile is less in value, a friction coefficient of 0.44 was assumed between the two materials

corresponding to a friction angle of (24^{o}). The tangential behavior was defined using a friction coefficient of

(0.44) between the steel pile and the sand. Two types of normal behavior were defined in the FE models: (1) Hard contact behavior where penetration of the slave nodes into the master surface is prohibited and no transfer of tensile stresses is allowed, Figure 73, (2) A softened contact normal behavior, where the contact pressure transmitted is defined as an exponential function between the clearance of the surfaces in contact, Figure 74 (ABAQUS/Standard user manual version 6.3.3). The softened contact behavior proved to be useful in overcoming numerical problems.

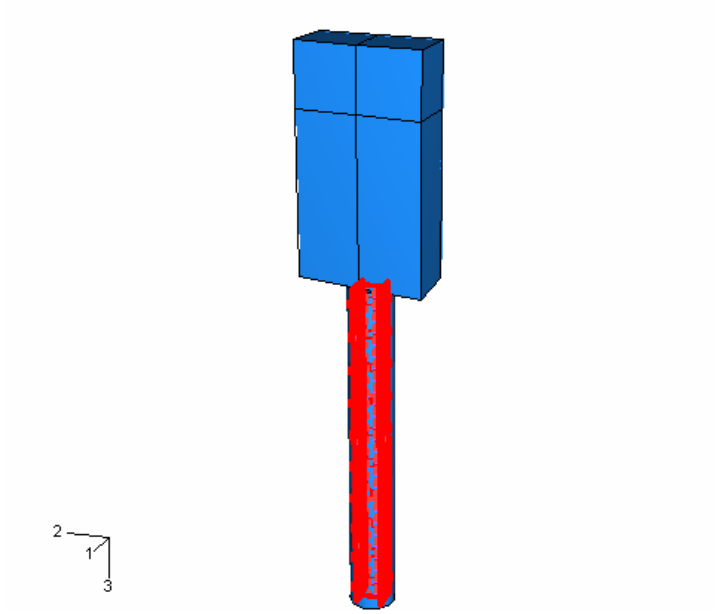

Figure 72. Contact definition in FE model (master and slave surfaces)

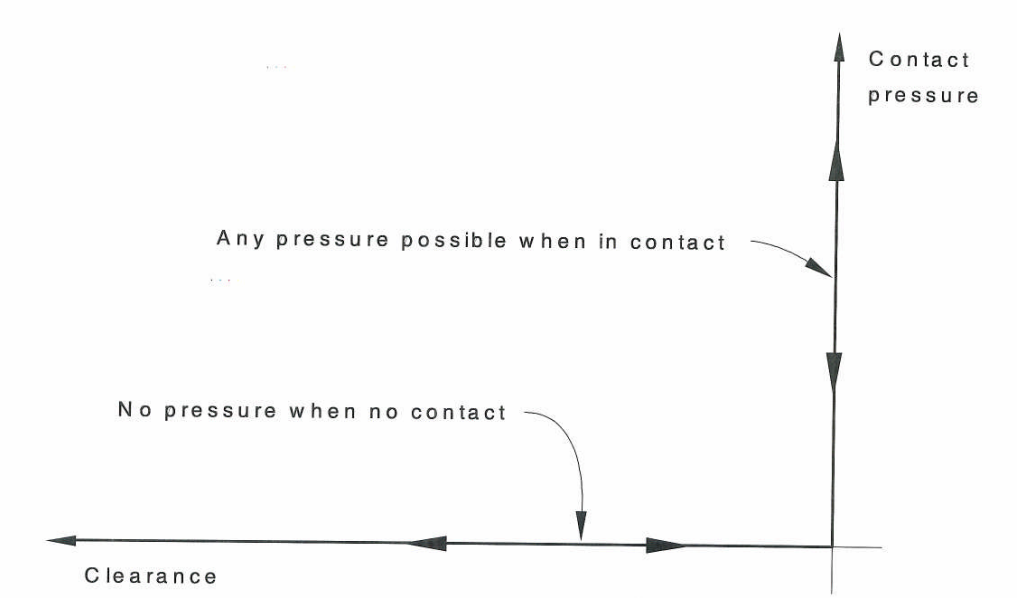

Figure 73. Hard contact characteristics in ABAQUS

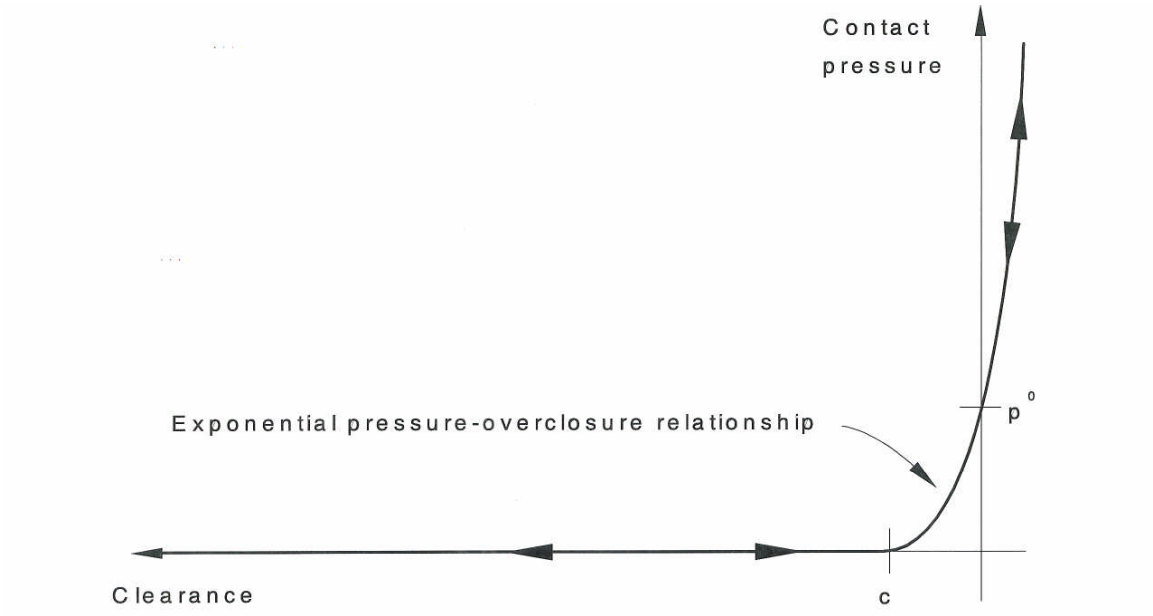

Figure 74. Exponential soft contact characteristics in ABAQUS

Non-Linear Analysis

In non-linear analysis, the solution cannot be obtained by solving a single set of equations. The commercial finite element program (ABAQUS) uses the Newton-Raphson method to solve non-linear problems. The program divides the loads into load increments and attempts to find an acceptable equilibrium solution during each increment within certain tolerances. The summation of the responses during all the increments becomes the overall approximate solution to the load. Figure 75 shows the application of the process.

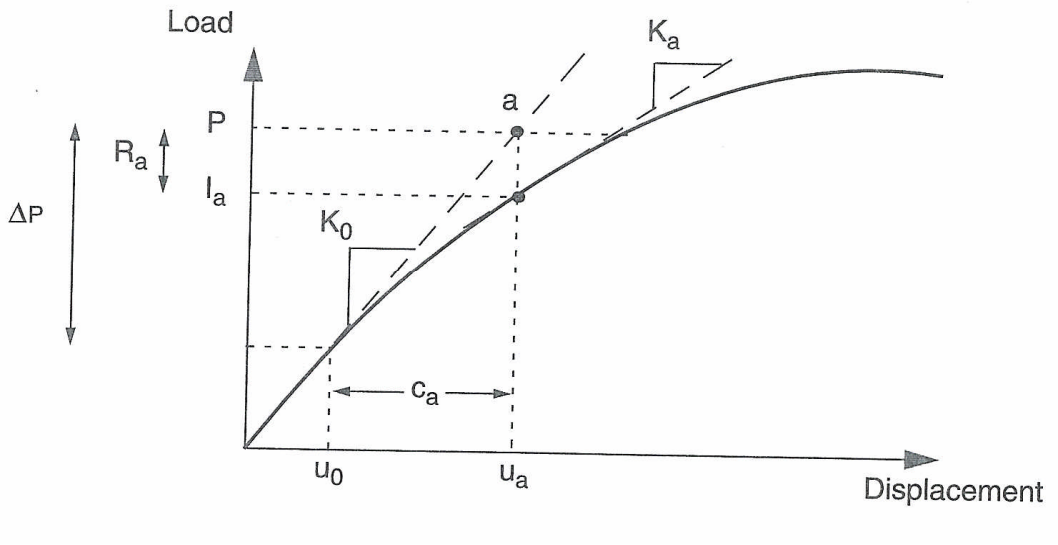

Figure 75. Algorithm of incremental loading in ABAQUS

Results

Figure 76 shows contour plots of the exaggerated deflected shapes of the bridge when subjected to thermal expansion loading. The induced displacement on the bridge as calculated by the finite element analysis was estimated to be (0.154 m) for the case of

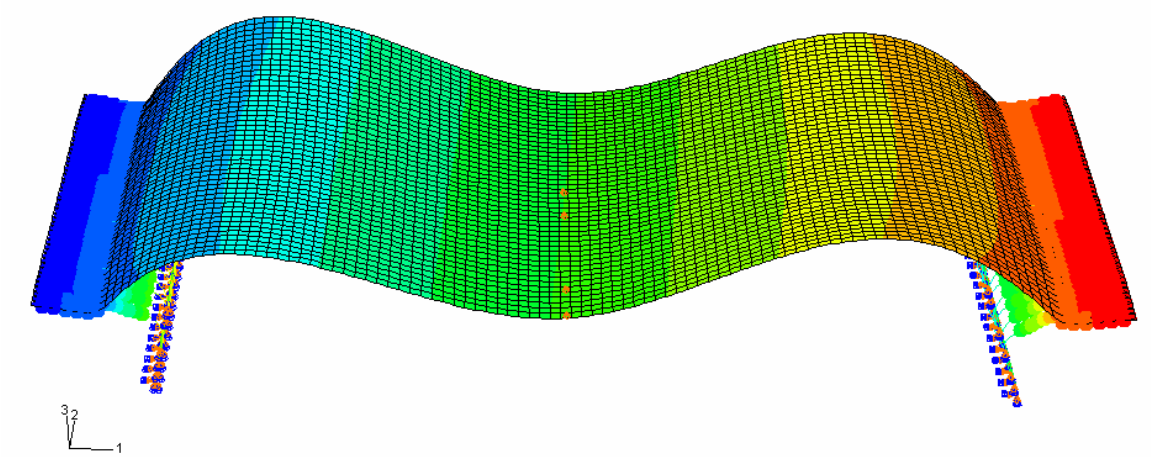

Figure 76. Contour plot of thermal expansion of the bridge (ΔT= 27°C)

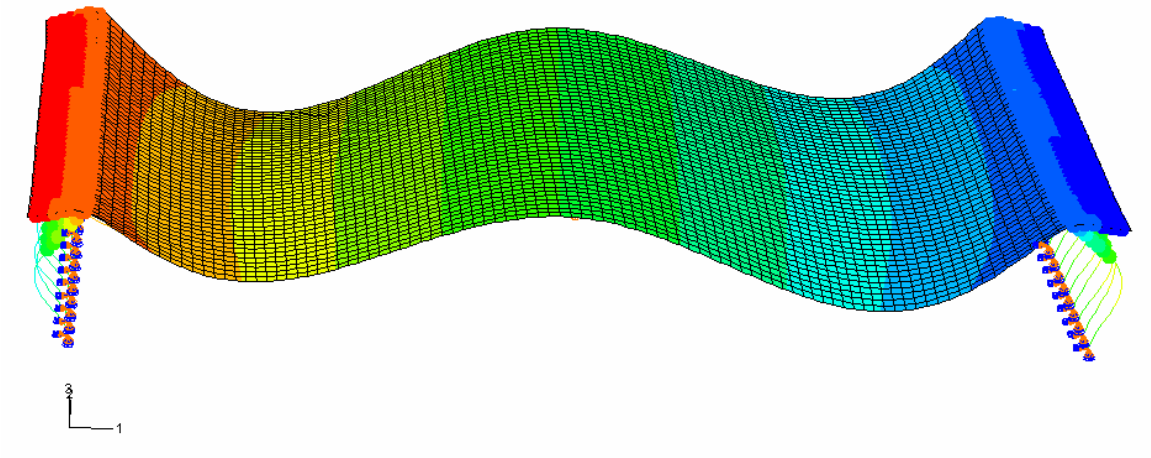

Figure 77. Contour plot of thermal contraction of the bridge (ΔT= -27°C)

dense sand behind the abutments and under the approach slabs. The variation between the value obtained from the finite element model versus that obtained by the thermal expansion empirical equation in (2.1), (0.1458 m) is almost negligible (5%). Figure 77 shows the contour plot of the exaggerated deflected shape of the contraction of the bridge. The bending inward rather than outward delineates the contraction of the bridge elements towards the middle of the bridge.

APPENDIX D - LATERAL EARTH PRESSURE BEHIND INTEGRAL ABUTMENT WALLS

Integral abutment bridges are becoming widely accepted for new construction of short to medium length highway bridges of limited skew. Although they offer an economical alternative to the use of bearings, integral abutments present their own unique challenges. One of the major areas of research is the development of soil pressure behind the abutment due to the cyclic loading of the soil during thermal movement of the superstructure. In this chapter, we compare soil pressure data from the Scotch Road Integral Abutment Bridge with theoretical and empirical soil pressure magnitude and distribution. We conclude that a Rankin pressure distribution for dense sands fits the soil pressure profile of the abutment, which is undergoing translation and rotation.

Introduction

Integral abutments are becoming the first option for short to medium length bridges in the United States because they reduce maintenance problems associated with bearings. Due to the lack of bearing, the superstructures transfer the horizontal movement to the abutments and the soil behind them. The cyclic motion of the abutments on the retained granular soil results in a gradual increase of earth pressure.[64,97,98] There are uncertainties in calculating the distribution and magnitude of the earth pressure behind an integral abutment. In general, the pressure is a function of the type of soil, its unit weight, the friction angle, the degree of compaction, the location of the ground-water table, the magnitude and location of surcharge loads and, to a greater extent, the degree of displacement and rotation of the retaining structure. Conventionally, Coulomb or Rankine theories have been used for the design of retaining walls. A pressure envelope that combines a passive pressure envelope using Rankine passive pressure coefficients (K_p) in the upper third of the wall and Rankine active pressure coefficients (K_a) towards the base of the abutment has been developed.[99] This method is based on the premises that higher lateral earth pressures develop at the top of the wall, and less pressures at the bottom as the movement of the wall subsides at its base. Approximate methods for estimating the displacement-dependent earth pressures have also been developed. (See references 100,101,102and 64) In practice, most transportation departments design for passive pressures.[38,57] At least two agencies neglect soil pressure in smaller bridges and three agencies neglect earth pressure in all their designs.[38]

Many theories exist for the calculation of the coefficients of active and passive earth pressures and for the distribution of the pressure behind the abutment. In what follows we will summarize some of the theories that may apply to a vertical wall undergoing translation and rotation, supporting drained granular soil, and horizontal, uncompacted backfill.

A frictionless wall that is in static equilibrium and has a horizontal backfill experiences a linear variation in horizontal stress of

$$\sigma_o = K_o \ \gamma \ z \tag{8}$$

where γ is the unit weight of the dry soil, z is the depth along the wall, and K_o is the at-rest earth pressure coefficient and is given by [103]:

$$K_o = 1 - \sin \phi \tag{9}$$

for a cohesionless soil of drained friction angle ϕ. Sherif [104] showed that the equation above gives good results for loose sands but underestimates the pressure for dense sands. The following equation *for* K_o for dense sands is proposed instead:

$$K_o = (1 - \sin\phi) + [\frac{\gamma_d}{\gamma_{d\min}} - 1]5.5 \tag{10}$$

where γ_d is the actual compacted dry unit weight of the sand behind the wall and γ_{dmin} is the dry unit weight of the sand in its loosest state.

The classical theories of Coulomb and Rankine can be used to calculate the minimum active and maximum passive pressures. These theories are based on the assumption of a linear failure surface. Rankine's theory assumes a linear variation of stress behind a frictionless wall with horizontal backfill as:

$$\sigma_a = K_a \ \gamma \ z \tag{11}$$

$$\sigma_p = K_p \ \gamma \ z \tag{12}$$

in which K_a and K_p are the active and passive earth pressure coefficients defined as: $K_a = (1-\sin\phi)/(1+\sin\phi)$ and $K_p = (1+\sin\phi)/(1-\sin\phi)$.

In Coulomb's theory of active and passive pressure for a vertical wall with horizontal backfill, we can use the wall friction, δ, to reduce the active and passive earth pressure coefficients:

$$K_a = \frac{\cos^2\phi}{\cos\delta[1 + \{\sin(\delta+\phi)\sin\phi/\cos\delta\}^{1/2}]^2} \tag{13}$$

and

$$K_p = \frac{\cos^2\phi}{\cos\delta[1 - \{\sin(\phi-\delta)\sin\phi/\cos\delta\}^{1/2}]^2} \tag{14}$$

For zero wall friction, these reduce to the Rankine coefficients. For loose granular backfill, δ is approximately equal to ϕ. For dense granular material, δ is in the range of $\phi/2 < \delta < 2/3\phi$.[105]

The assumption of plane failure surfaces gives reasonable estimates of the active earth pressure but overestimates the passive pressure. Theories based on curved failure theories have been accepted as producing more accurate passive pressures. Caquot and Kerise[106] determined the earth pressure coefficients assuming a failure surface in the shape of a log-spiral. Shields and Tolunay[107] obtained passive pressure coefficients using the method of slices.

In general, the development of earth pressure is a function of the wall displacement. The lateral wall movements needed to create active and passive pressures in sand is shown in Table 9.[101] Here, Δ is the horizontal displacement at the top of the wall due to rotation or translation and H is the height of the wall. The assumption is of a rigid wall.

Table 9 - Approximate displacements to achieve minimum active or maximum passive pressures in sand[101]

Backfill	Δ /H	
	Active	Passive
Dense Sand	0.001	0.01
Medium Sand	0.002	0.02
Loose Sand	0.004	0.04

In presence of flexible walls, the problem becomes more complicated. Although the assumption for integral abutment design is that the abutment is rigid, this is not the case Data and finite element analyses has shown that the abutment transmits only part of the bridge displacement to the piles supporting the abutment, pointing to a flexible behavior of the abutment. [108] This, coupled by the fact that the pressure behind an integral abutment is developing during daily and seasonal cyclic loading, creates a pressure distribution behind the abutment that is difficult to predict. It was not until recently that experimental work and modeling concentrated in defining the mechanics of the soil behind an integral abutment.

For the design of integral abutments, the displacement Δ at the top of the abutment is found by assuming that the total bridge displacement is divided equally between each abutment:

$$\Delta = 1/2\, L\, \alpha\, \Delta T \qquad (15)$$

where L is the length of the continuous bridge; α is the coefficient of thermal expansion; and ΔT is calculated as the difference between the temperature during construction and the maximum (or minimum) temperature expected at the site (Figure 78).

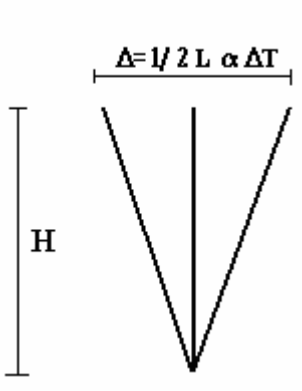

Figure 78. Definition of wall-top displacement

In the design of integral abutments, Massachusetts uses a magnitude of lateral earth pressure that depends on the movement of the backfill. The value is assumed to be somewhere between at-rest conditions and passive pressures. Used with the Mass Highway's standard compacted gravel borrow, a pressure coefficient K is proposed as:[28]

$$K = 0.43 + 5.7[1 - e^{-190(\Delta / H)}] \tag{16}$$

The pressure varies linearly at the back of the abutment.

The British Code BA42 proposes an upper limit of the passive coefficient as

$$K^* = (\frac{\Delta}{0.05H})^{0.4} K_p \tag{17}$$

where a maximum value for Kp ,derived after cyclic loading of Leighton Buzzard sand, is taken to be 12.5. The minimum K* is constrained to Kp/3. The pressure distribution in this code is linear down to H/2 and constant to H.

The same pressure distribution and a new equation for the passive pressure coefficient has also been proposed as:[64]

$$K^* = K_o + (\frac{\Delta}{0.03H})^{0.6} K_p \tag{18}$$

where the constrain for the minimum K^* is removed. The work is based on testing of a model rigid wall that was used to study the effects of thermal loading on integral abutments. The model simulated an abutment, which was free to rotate about its base due to thermal movements of the bridge deck. As such this coefficient may not be directly applicable to an integral abutment supported on piles. Such abutments experience translation as well as rotation. However, the tests give a good understanding about the built up of lateral soil stresses that result from the induced cyclic loading. This work has been instrumental in illustrating the densification and the

granular flow of the sand behind the abutment. To quote: “During the early cyclic wall rotations, the backfill soil densifies and the soil stress acting on the wall increases. The different ratcheting strain effects close to the wall and away from the wall lead to a continuous flow path which is downwards and away from the wall (close to the wall) and away from the wall and upwards (away from the wall). The resulting effect at the soil surface is settlement close to the wall and possible heave away from the wall.”

The objective of the present study is to present the soil pressure data from a full-scale test of an integral bridge, study the pressure distribution in light of classical and later work on the development of such pressure, and to share our findings with the research and design community.

The soil behind the abutment is porous compacted fill, whose gradation limits, as specified by AASHTO T27, are as shown in Table 10:

Table 10 - AASHTO gradation specification for I-9 porous fill

Sieve Size*	Percent Passing
150 mm	100
75 mm	70-100
4.75 mm	30-80
425 μm	0-25
75 μm	0-10

* 1m=3.2808ft

Analysis of Soil Pressure

Integral abutments are affected by both maximum and minimum daily, and seasonal temperature variations. The temperature increases gradually during the day, which results in the expansion of the bridge superstructure, and hence, the passive movement of the abutment. The cycle is reversed at night, when the temperature decreases and the active movement of the abutment takes place. Figure 79 shows the displacement of the superstructure over a 24-hour period and Figure 80shows the pressure development behind the abutment due to that displacement. Starting at time 00:00 up to 8:00 the displacement decreases due to the night temperatures, pulling the abutment away from the soil. This is reflected in the presence of active pressure behind the abutment. From 8:00 to 16:00 the day temperature increases, pushing the abutment against the soil and creating the highest passive pressure at the maximum displacement at 16:00. From 16:00 to 24:00 the abutment starts pulling away relieving the pressure, which seems to dissipate and reach active values around midnight. Figure 81 and Figure 82 show this correlation over a one-month period.

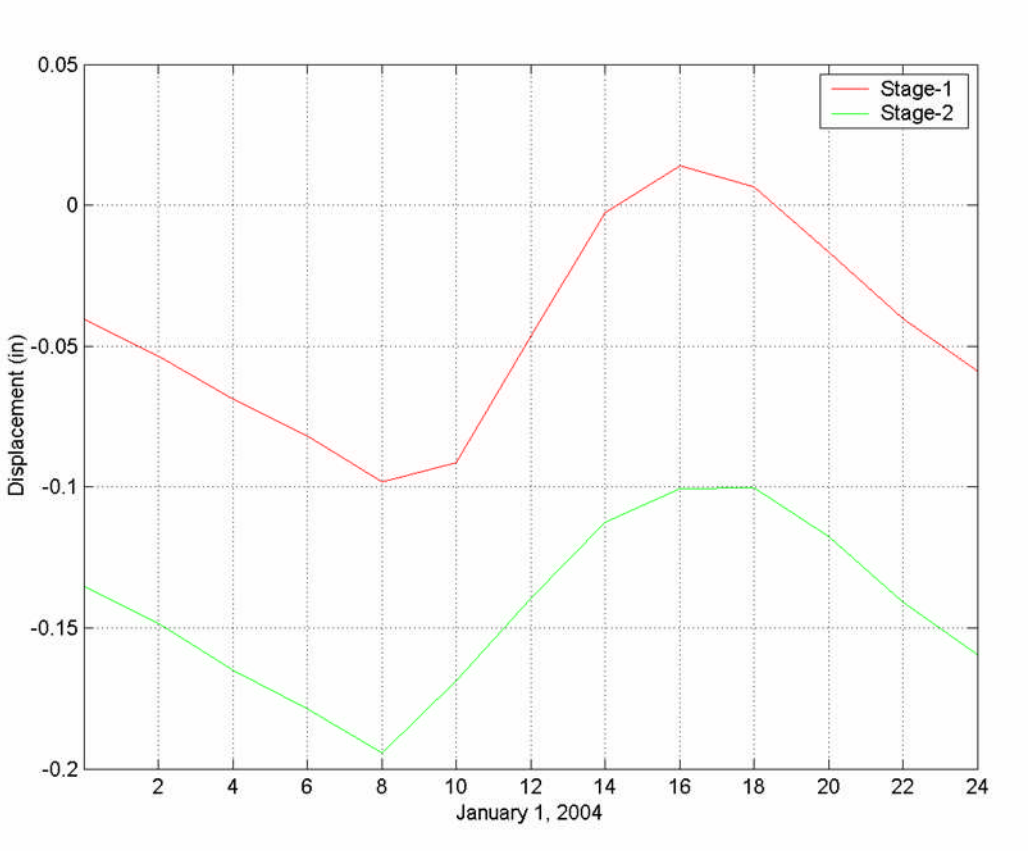

Figure 79. Longitudinal displacement of bridge over 24 hours, January 1, 2004

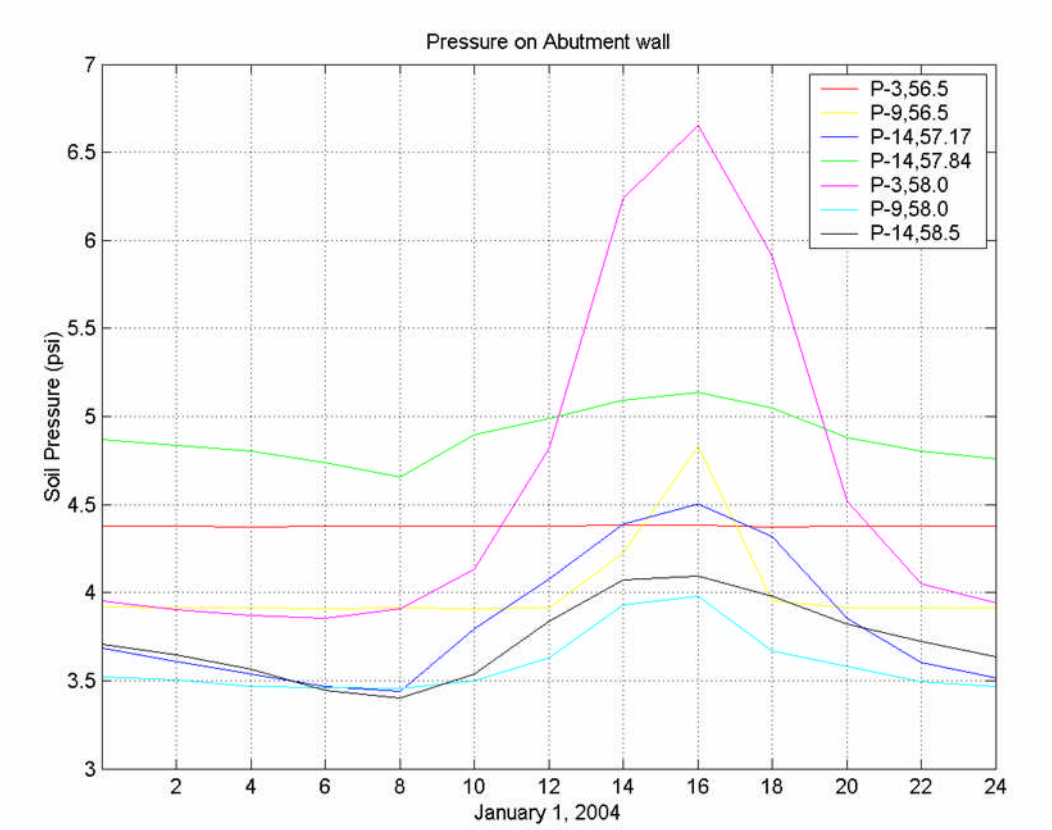

Figure 80. Soil Pressure behind abutment over 24 hours, January 1, 2004

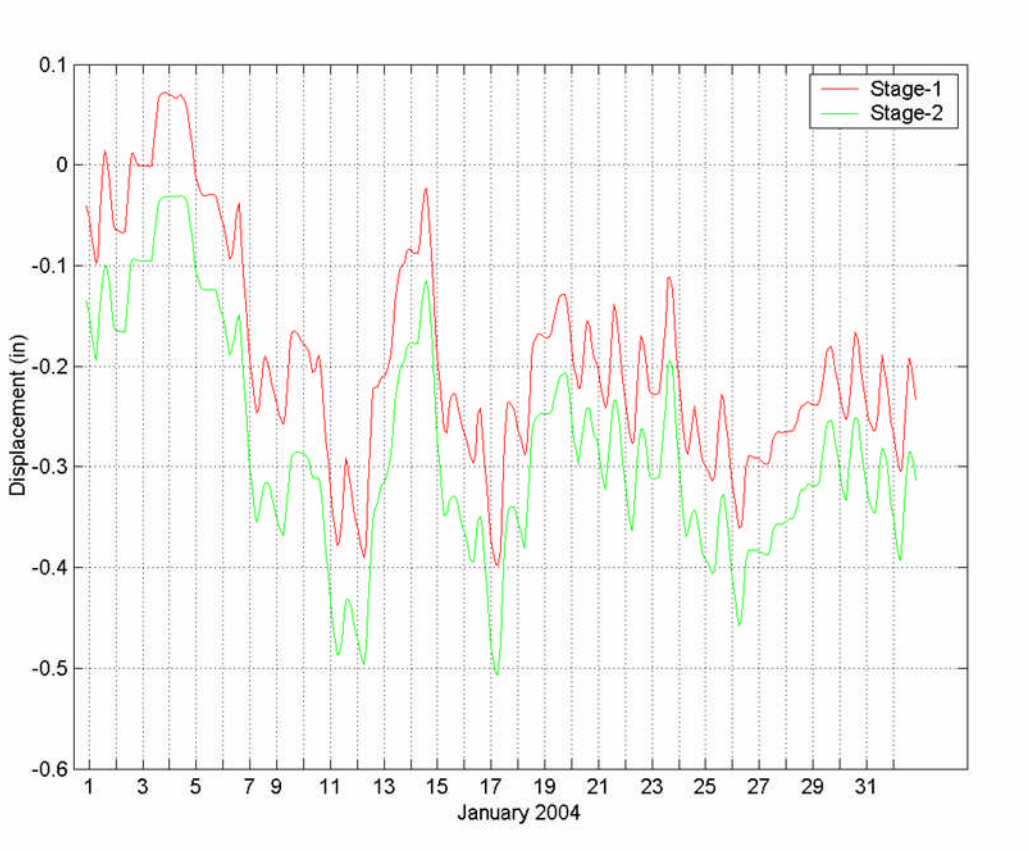

Figure 81. Longitudinal displacement of bridge over one month, January 2004

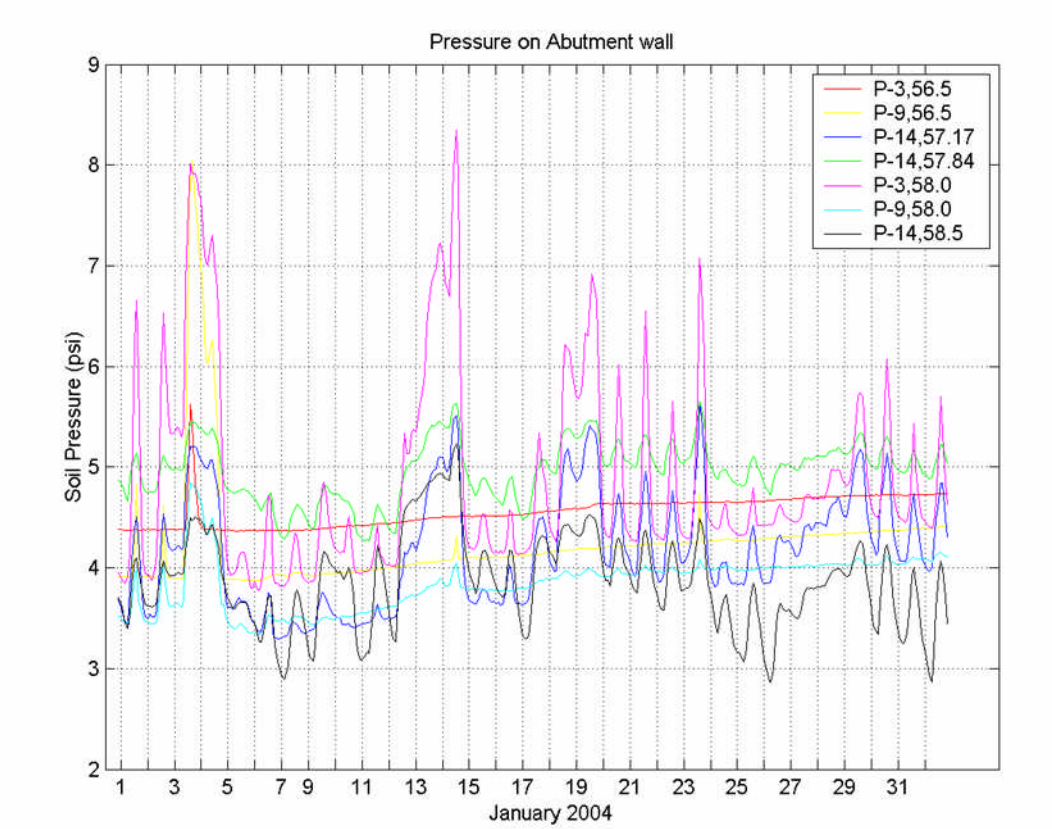

Figure 82. Soil pressure behind abutment over one month, January 2004

The daily cycles are repeated constantly. However over the year, we do not observe an exact correlation of displacement and pressure due to the fact that the soil is not an elastic medium. Figure 83 shows the pressure created behind the abutment due to the displacement and rotation. The data span a period from April 2003 to January 2005. In general, the displacement increases with temperature from January, reaching its highest value in July, and starts decreasing to its lowest value in January. The same is true for the rotations which correlate well to the displacement readings. However, the rotations are very small and do not contribute significantly to the overall movement.

In contrast, the pressure seems to be the greatest at the very beginnings of temperature increase in January or February, reaches its highest value around April and decreases to an average value by July. As the displacement reverses direction in July, the pressure starts to decrease. We can deduce from this that the soil is in its densest state at the end of the seasonal active cycle and it behaves as usual dense sand in shear as the temperatures start to climb and the abutment starts pushing on the soil. The built up of density is a result of the daily cyclic motion during the movement of the structure away from the soil (July to January). The fabric of granular soil changes during the unloading stage, which results in the accretion of permanent plastic deformation, known as strain ratcheting. We can see that at the beginning of each new year (around January or February) the pressure is higher than the year before. We

expect this phenomenon to eventually slow down. In what follows, we will be discussing the observations of the past three years.

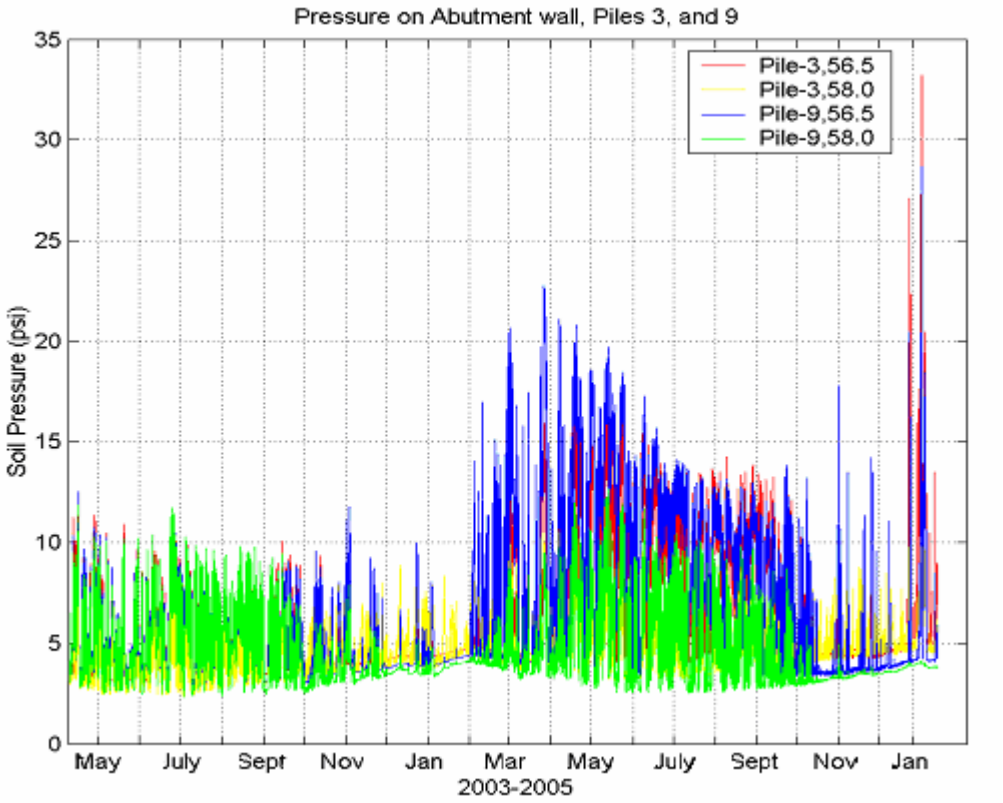

Figure 83. Soil pressure along the abutment wall. Stage I construction

The question of interest is what is the maximum pressure that we should be using to design the abutment. The Scotch Road Bridge was built for a Rankine passive pressure of a soil with an angle of internal friction 30^o. The pressure that has been measured already exceeds the design pressure. At this time, the data and design values are closer if we can assume that the angle of internal friction increased to 40^o due to the densification. To show, the data has been plotted along the depth of the abutment in Figure 84 and is compared to Rankine, Caquot and Kerisel,[106] Shields and Tolunay,[107] and Massachushets Highway Manual.[28] For the calculations, the height of the abutment is 11 ft, the soil density 125pcf, and the angle of internal friction 40^o. The wall is assumed frictionless, and the soil perfectly drained. The passive pressure coefficients are tabulated in Table 11 for several angles of internal friction and angle of friction. A value of 6 was used for K_p in the Mass. Highway equation to reflect maximum passive, in order to compare it to the rest of the classical calculations. The value for Δ/H that was achieved at the abutment is approximately 0.08 so we can assume that we have enough displacement to guarantee that the classical methods are applicable.

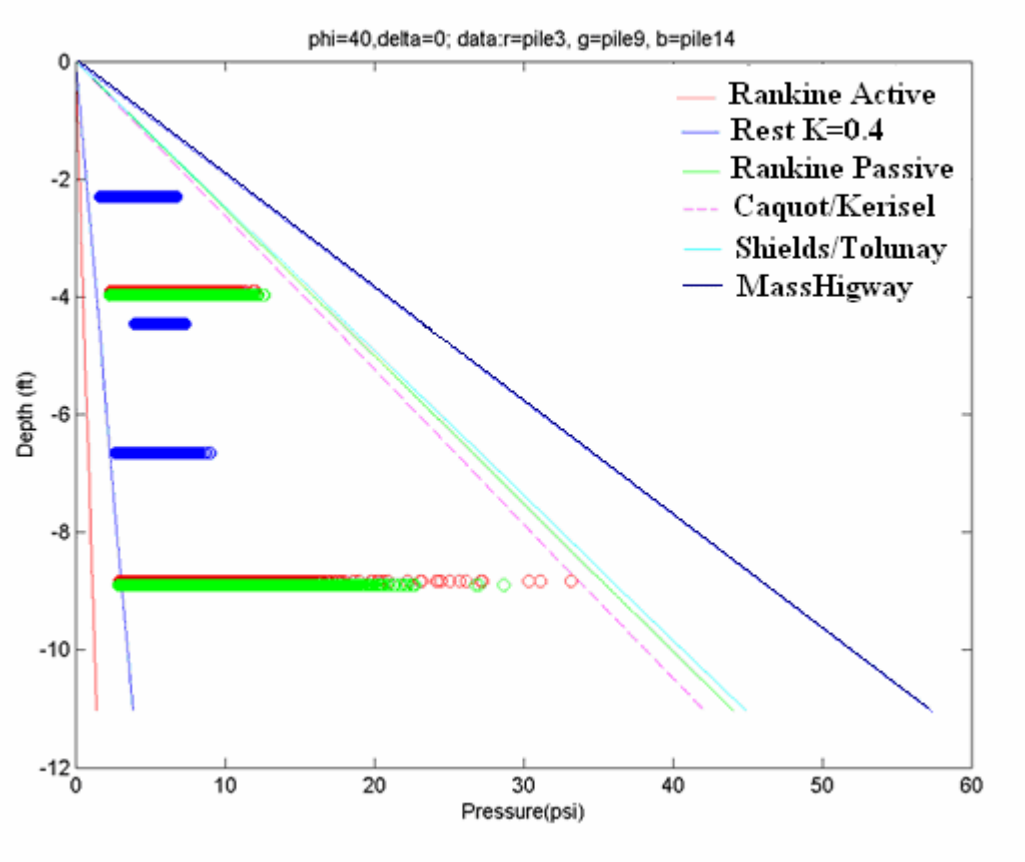

Figure 84. Comparison of data with classical passive pressure

Table 11 - Classical passive pressure coefficients

ϕ	δ	K_p Rankine Coulom.	K_p Caquot/ Kerisel	K_p Shields Tolunay
30	0	3.0	3.0	3.0
	25	7.7	5.7	4.64
35	0	3.69	3.5	3.69
	25	11.0	8.0	6.21
40	0	4.60	4.4	4.69
	25	16.5	11.	8.51
45	0	5.83	5.9	5.83
	25	26.7	19.	12.04

The data shows that the Rankine passive pressure can be used to approximate the pressure behind the abutment, given that we assume densification of the soil with time. Since the data shows a constant increase in pressure during the three winters of data gathering (Figure 83), more *data and observations are needed for a final conclusion about the distribution and magnitude of passive pressure behind the abutment.*

In Figure 85 and Figure 86, the data are plotted against the more recent theories that predict passive pressure as a function of abutment rotation for Δ/H of 0.006 and 0.008 respectively. The coefficients for these methods are tabulated in Table 12. The British code, BA42, and England[64] underestimate the pressures at the base of the abutment. This is due mainly to the fact that the assumption used is of pure rotation and in the pile-supported abutment of the Scotch Road Bridge the motion was mainly translation. The code of the Massachusetts Highway predicts the pressure better, but it is still lacking in accuracy.

Table 12 - Passive pressure coefficients dependent on wall-top displacement

Δ /H	K_p Mass-Highway [28][1]	K^*_p BA 42Code[2] Kp=12.5	K^*_p England [64][2] Kp=12.5
0.001	1.42	4.17	2.02
0.002	2.23	4.17	2.86
0.004	2.90	4.55	4.13
0.006	3.46	5.35	5.16
0.008	3.92	6.00	6.05
0.010	5.27	N/A	N/A
0.020	6.00	N/A	N/A
0.040	6.12	N/A	N/A

[1] Triangular pressure distribution along wall

[2] Triangular pressure down to H/2; constant thereafter.

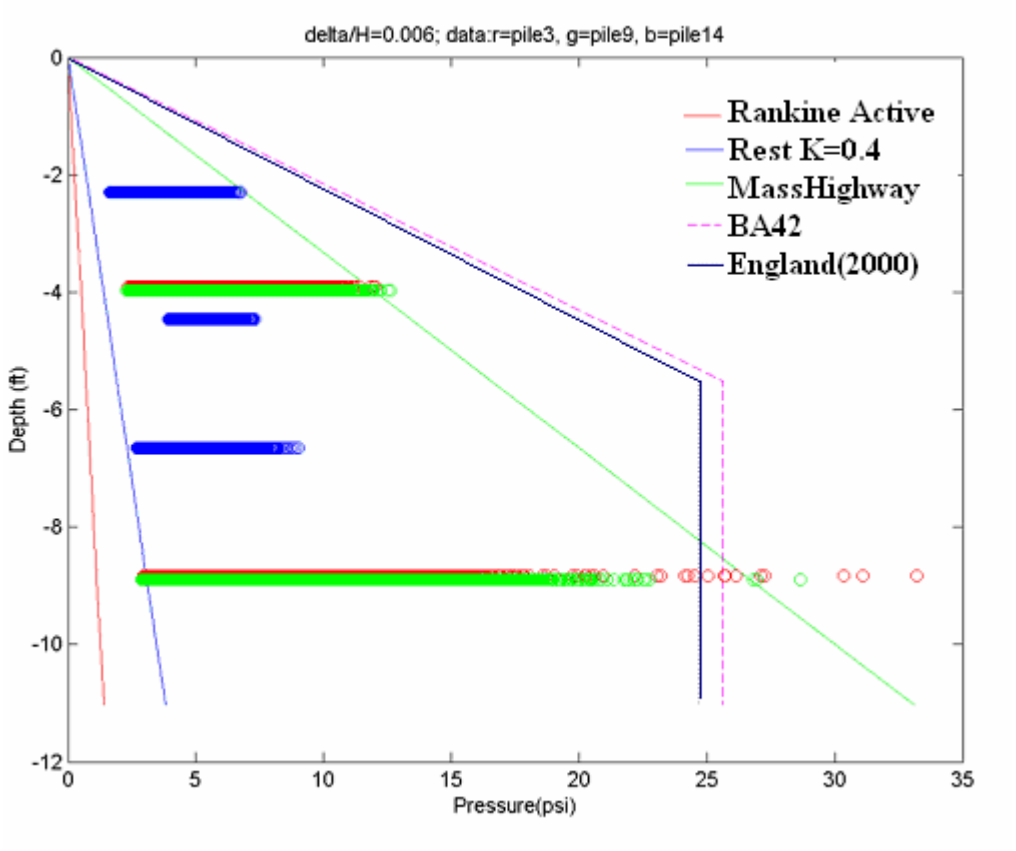

Figure 85. Comparison of data with methods specifically developed to calculate passive pressure behind integral abutments. Δ/H=0.006

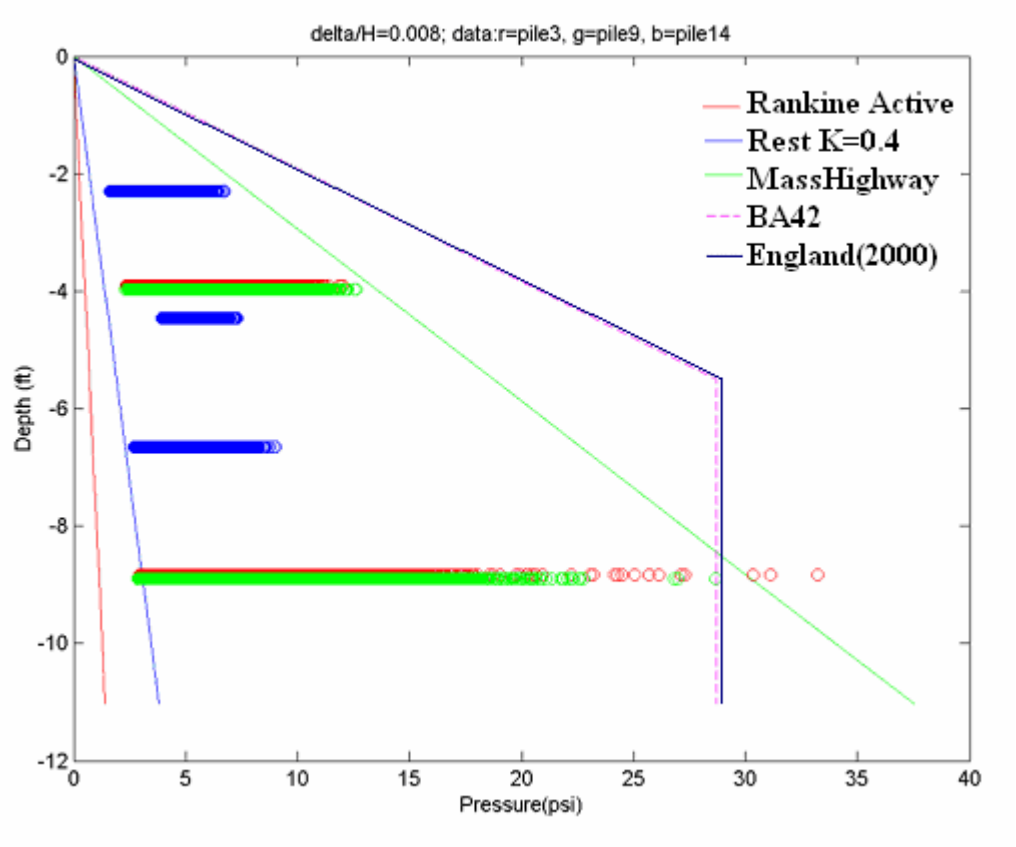

Figure 86. Comparison of data with methods specifically developed to calculate passive pressure behind integral abutments. Δ/H=0.008

Summary and Conclusions

The pressure development behind an integral abutment can be considered to be a function of the soil density and the displacement of the abutment. In classical calculations, an increase of density will inevitably produce an increase in the pressure. It is well documented that granular soils flow and rearrange their fabric during cyclic loading leading to an increase of density and thus pressure. More recent work has tried to link the increase of pressure with the relative displacement of the abutment. Results from the earth pressure measurements behind the Scotch Road integral abutment showed that the soil behind the abutment experiences pressure build-up due to the densification of the granular soil as a result of the daily and seasonal active and passive cycles. The passive stress seems to be well predicted by a Rankine stress distribution for dense sands. However, at the writing of this paper, the pressure may still be increasing. Measurements through the next one to two seasons will be helpful to arrive at a more accurate conclusion about the pressure distribution and magnitude.

APPENDIX E - CONSTRUCTION SEQUENCE

Integral abutment construction sequence

During constructing Scotch Road over I-95 integral bridge a constructions sequence was followed to reduce the effects of thermal movements of the steel girders on abutment fresh concrete and to control moments induced into the supporting pile system. This is a summary of the construction sequence prescribed by Arora and Associates:

- Piles oriented so that the centerline of the pile web is perpendicular the centerline of the girder. Pile driven as per specifications to or below the estimated tip elevation that needed to develop the pile capacity.
- Install 600 mm corrugated steel sleeve around piles. Toe in and secure the sleeve so that the sleeves remain centered around the piles as the MSE wall is constructed. After constructing the MSE wall, back fill the sleeves with cushion sand.
- Pour the pile cap to the required bridge seat elevation. End-welded studs are used as an anchoring system, 22 mm in diameter, attached to the pile. Pour the pap at the same time with the wing-walls.
- Set the girders and anchor them to the abutment. Anchor nuts shall not be fully tightened at this time. Free play for further dead load rotation shall be accounted for. Slotted holes in the bottom flanges are recommended to aid in the erection since the temperature will vary from the time that the anchors are set in the cap to the time that the girders are fully erected. Do not fully tighten the anchor nuts at this time.
- Pour the bridge deck in the desired sequence excluding the abutment back-wall/diaphragm and the last portion of the bridge deck equal to the back-wall/diaphragm width. In this manner, all dead-load slab rotations will occur prior to lock-up, and no dead-load moments will be transferred to the supporting piles.
- Tighten the anchor nuts and pour the back-wall/diaphragm full height. Since no backfilling has occurred to this point, the abutment is free to move without overcoming passive pressures against the back-wall/diaphragm. The wing-walls may also be poured concurrently.
- Place the vertical drain system and backfill in 6-in. lifts until the desired sub-grade elevation is reached. Place a bond breaker on the abutment surfaces in contact with the approach pavement.
- Pour the approach pavement starting at the end away from the abutment and progressing toward the back-wall. If it can be so controlled, approach pavements should be poured in the early morning so that the superstructure is expanding, and therefore, not placing the slab in tension.

Approach slabs construction sequence

- A construction joint should be located at a distance of 150 mm from the back of the back-wall between the approach slab and bridge slab. This will provide a controlled crack location rather than allowing a random crack pattern to develop. Corrosion coated dowels shall pass through the joint and shall be located near the bottom of the slab. This will keep the joint tight but still allow the approach slab to settle without causing tension cracking in the top of the slab.
- The excavation for the approach slabs shall be carefully made after compacted abutment embankment material is in place. The slabs shall be founded on undisturbed compacted material. No loose backfill will be allowed.
- To permit unhindered longitudinal movement of the approach slab, the surface of the sub-base course must be accurately controlled to follow and be parallel to the roadway grade and cross slope.
- A filter fabric or some type of bond breaker such as polyethylene sheets shall be placed on the finished sub-base course the full width of the roadway prior to placement of approach slab reinforcement.
- A lateral drainage system should be provided at the end of the approach slab adjacent to the sleeper slab. Suitable notes should be provided on the plans to incorporate these construction procedures.

Commentary: Typically, the steel girder rests on a bearing pad or plate placed above the pile, and the bearing area is then cast into the abutment. Steel beams can be connected to the pile caps with anchor bolts prior to making the integral connection.[14] This ensures that the superstructure and the abutment move together. Another suggestion is that the girder is welded to the pile. In such cases, holes are cut through the girder web to allow for continuous transverse reinforcement.

Construction details for prestressed concrete girders are similar to that of steel girders. Supplementary details include using grouted pins to connect the beam to the lower portion of the abutment. Sometimes galvanized pipe is run through the web to provide a casing for transverse reinforcing steel.

APPENDIX F - ON-GOING LABORATORY AND FULL-SCALE TESTING

The success of the integral abutment design has incited the Department of Transportation of several states to fund full-scale testing in an effort to create design specifications. Recent publications based on such activities are listed on Table 13. At least ten on-going investigations that were identified are listed on Table 14. In addition, the 2005-FHWA Conference on Integral Abutments and Joint-less Bridges summarizes the results of the latest research efforts.

The projects share similar objectives, namely, to investigate current design and construction practices on integral abutment bridges and to develop or upgrade analysis and design specifications. To this end, the researchers have instrumented full-scale bridges with strain gages, loads cells, thermocouples, displacement gages etc. and are monitoring the response of the bridge and its foundation to variations in temperature and traffic loading.

The full-scale testing includes bridges of either pre-stressed concrete girders or steel girders. The bridge length varies from 25 m (82 ft) up to 820 m (2700 ft); the bridge width varies between 10 m (32 ft.) to 25 m (82 ft.); the skew angle ranges between zero to almost 40^{o}. For the most part, HP piles oriented at either the weak or the strong axes have been used. Concrete-filled steel tubes and concrete friction piles have also been tested.

In addition to full-scale testing, laboratory studies were conducted to test simulated abutments and pile groups, and finite element analyses were performed on sample or full-scale bridges.

Table 13 - Recent articles related to integral abutment bridges

Project Sponsor	**Study Bridge**	**Length of Bridge**	**Bridge Width (out-to-out)**	**Skew Angle/ Curvature**	**Pile Type / Orientation**	**Type of Superstructure**	**Full-Scale/ Field Study/Lab/ FE Analysis**	**Reference**
TDOT/ U of Tennessee	Various Simulated abutments	N/A	N/A	N/A	HP10x42 strong axis	N/A	Lab	[21]
TDOT / U of Tennessee	Kingsport Bridge over Holston River	820 m (2700ft)	13 m (44 ft.)	N/A	N/A	Prestr.concrete box girders	Field Study/ FE Analysis	[21]
NJDOT/ Stevens Institute of Technology	Scotch Road over I-95	90.9m (298ft)	10m (32.1ft)	15^{o}	HP360x52 Weak axis	HPS girders	Field Study/ L-PILE, ABAQUS	[See ref.1,2,3, 60]
VDOT / FHWA/ U of Virginia	Various integral and semi-integral bridges	92 m (301 ft.)	25 m (82 ft.)	0^{o}	HP10x42	Steel girders	Field Study/ FE/Lab SAGE,L-PILE	[22,42]
NA	2 sample bridges	25 m (82 ft.)	13 m (42.7 ft.)	0^{o}	HP305x79	Steel girders	FE Analysis (ALGOR)	[18]
TDOT	Example Steel Bridge	130 m (426 ft.)	13.4 m (44 ft.)	0^{o}	HP 10 x 42/ strong axis	Steel girders	Design/ COM624P	[14]
N/A	U.S. 101/ Painter Street Overpass Rio	80.8 m (265 ft.)	15.85 m (52 ft.)	38.9^{o}	concrete friction piles	Girder:Reinforconcrete multicell box	Full-Scale	[72]

	Dell, CA							
Manhattan College	Hypothetical Bridge (based on Forks Bridge,ME)	50 m (165 ft.)	N/A	N/A	N/A	Steel girders	FEM Analysis ($SSTIPNH^{T}_{M}$)	[109]
U of Mass Transportation Center/MDot	Fitchburg Bridge (F-4-20)	45.7 m (150 ft.)	16.45 m (54 ft.)	0^{o}	HP12x74	Steel girders	FEM Analysis (GTSTRUDL)	[59]
Mn DOT / U of Minnesota	Study Bridge Rochester, MN	66 m (216ft)	12 m (39.4 ft.)	0^{o}	HP 12 x 53, Weak axis	Prestressed concrete girder	Full Scale	61
Tennessee DOT	Tennessee State RT50 over Happy	358 m (1175	14 m (46 ft.)	$4^{o}45'$ (curve	HP10x42/ strong axis	Concrete bulb-tee girders	Full Scale	[20]
VDOT/ VTRC/ FHWA /UVA	Route 257 over Interstate 81	98 m (320 ft.)	25 m (82 ft.)	5^{o}	N/A	Steel Girders	Full Scale	[26]

Table 14 - On-going research projects

Sponsor Agency	Performing Organization	Authors/Investigators	Title Of Project	Start Date	End Date	Study Bridge	Objectives
NJDOT	Stevens Institute of Technology	Sophia Hassiotis	Investigation of the IAB, Scotch Road over I-95	1/1/2002	11/1/2005	Scotch Road over I-95	Full-scale testing, Upgrade NJDOT Design
Louisiana TRC	Tulane University	Baker, Reda	Evaluation of DOTD IAB system	4/1/2002	10/1/03	Various	Evaluate performance of bridge abutments
Iowa / Iowa HRB	Iowa State University	Robert E. Abendroth, L.F. Greimann	An IAB with Precast Concrete Piles(TR 438)	7/1/1999	12/31/02	Tama County Bridge	Investigate performance of IA on PC piles
Mn DOT	University of Minnesota	Catherine French	Investigation No. 700 Field perform. of an IAB.	7/17/1995	4/30/04	N/A	Full-Scale Testing-Evaluate plastification of piles
Alaska DOT		Steve Saboundjian	IAB Design Issues for Alaska (RNS-02-27)	N/A	9/31/03	McClaren River Bridge	Develop special details to minimize lateral resistance
Idaho DOT / FHWA	University of Idaho, Moscow	Richard Nielsen	Development of ITD Design Standards for IAB	9/1/1997	Active	N/A	Develop design practices for the LRFD of integral abutments
Iowa DOT	Iowa State University (ISU)	Robert E. Abendroth	Field Testing of Integral Abutments	2/1/1997	Active	2 bridges	Evaluate the state-of-the-art in IAB-design Pile design

			(HR-399)				
FL DOT	Florida Atlantic U	Madasamy Arockiasamy	Design Consider. for IAB in Florida	8/15/1999	4/30/2003	N/A	Develop analysis and design procedures
Penn DOT	Pennsylvania State University	Jeffrey A. Laman	(1)Methods to Predict Movements and Stresses in IAs (2)Level Analysis Prediction of IAB Behavior	10/25/	12/2006	RSR 6220 at -Blue Spring Hollow Strm - Route 322 - ZendtLane -Wildlife	Monitor 4 full-scale bridges Establish credible verified design procedure
VDOT/ VTRC	N/A	Edward J. Hoppe	Experimental IA with Geofoam	N/A	N/A	N/A	Long-term performance of a IB w/Geofoam at soil interface

APPENDIX G - DATA PLOTS

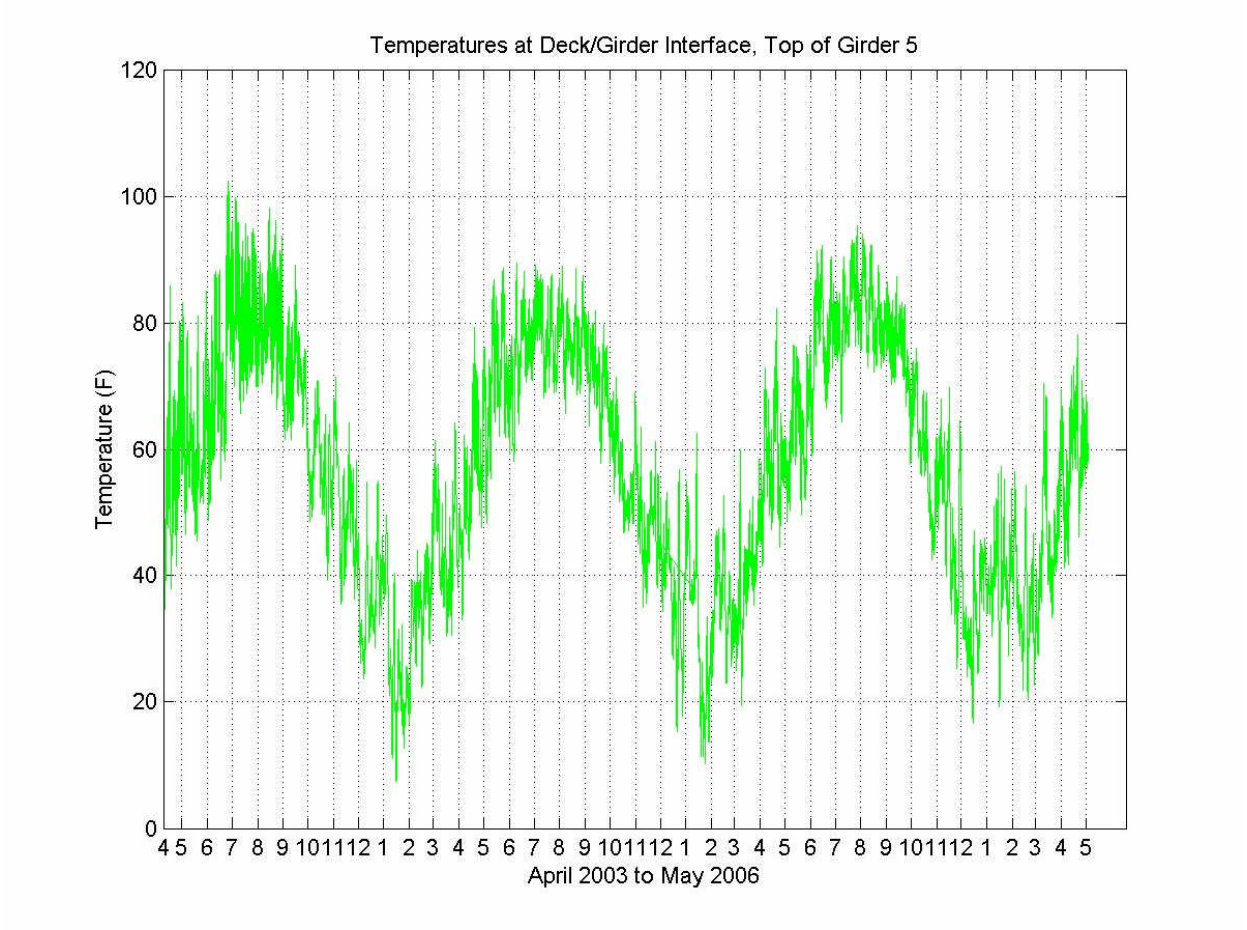

Figure 87. Temperatures at deck/girder interface, top of Girder 5

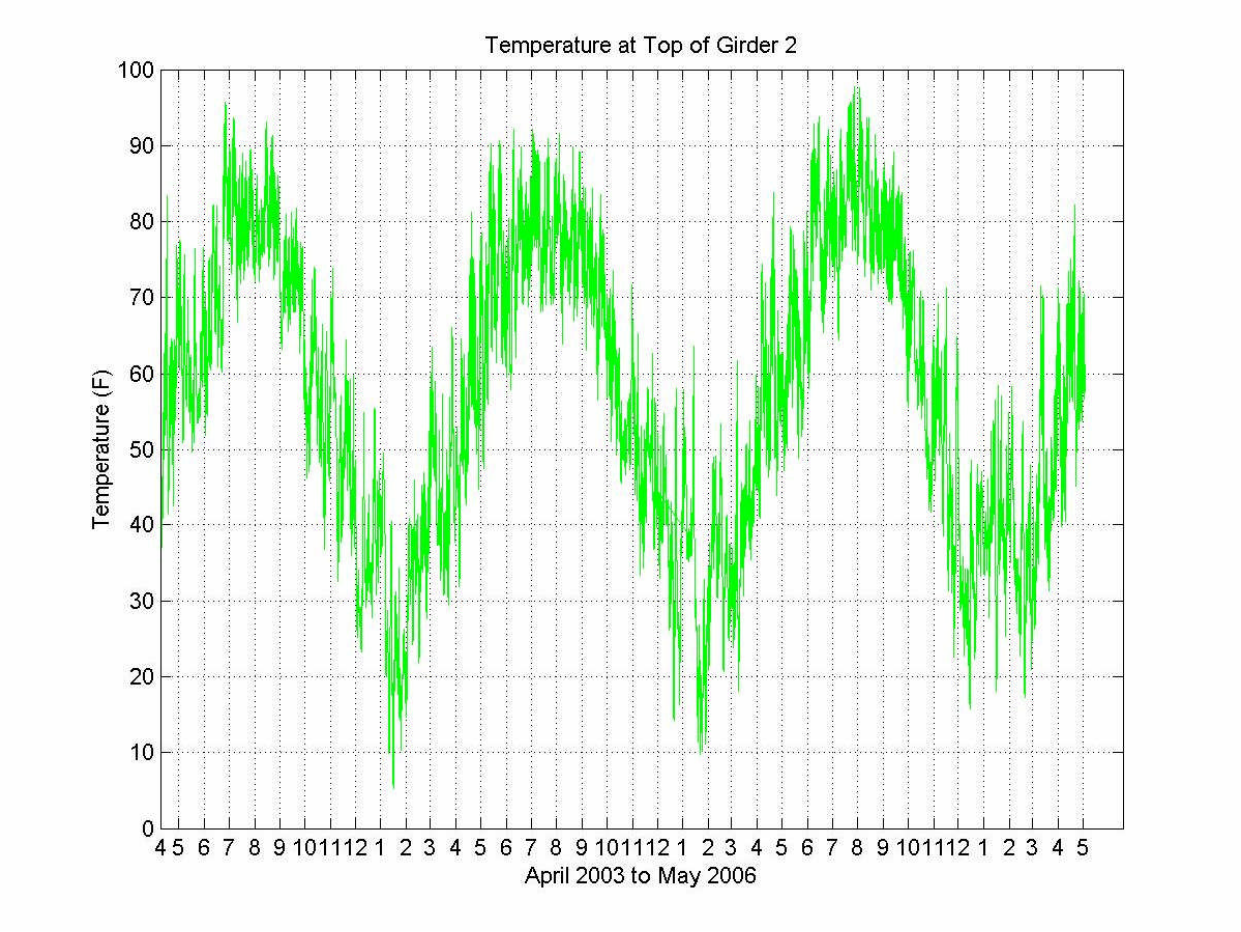

Figure 88. Temperature at top of Girder 2

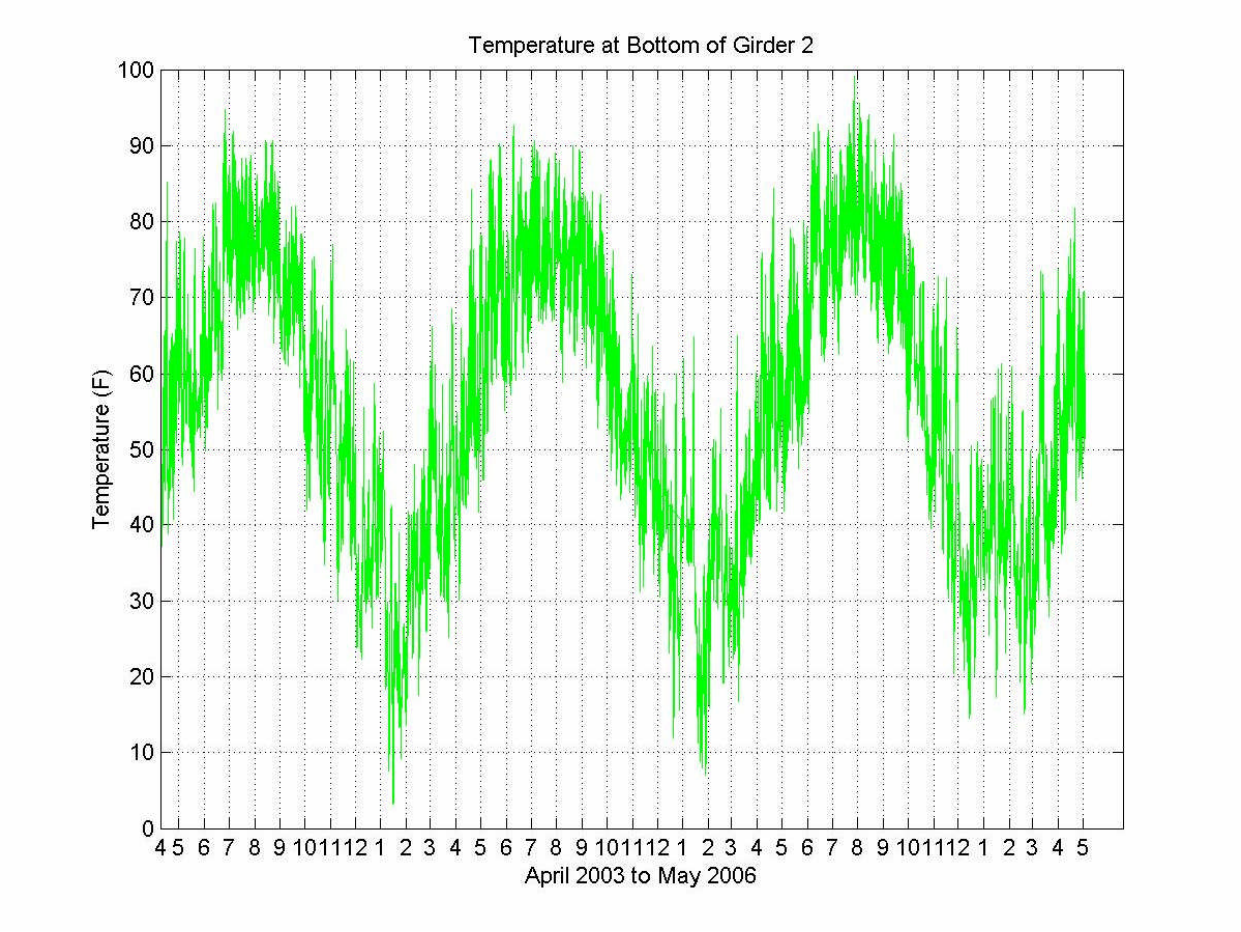

Figure 89. Temperature at bottom of Girder 2

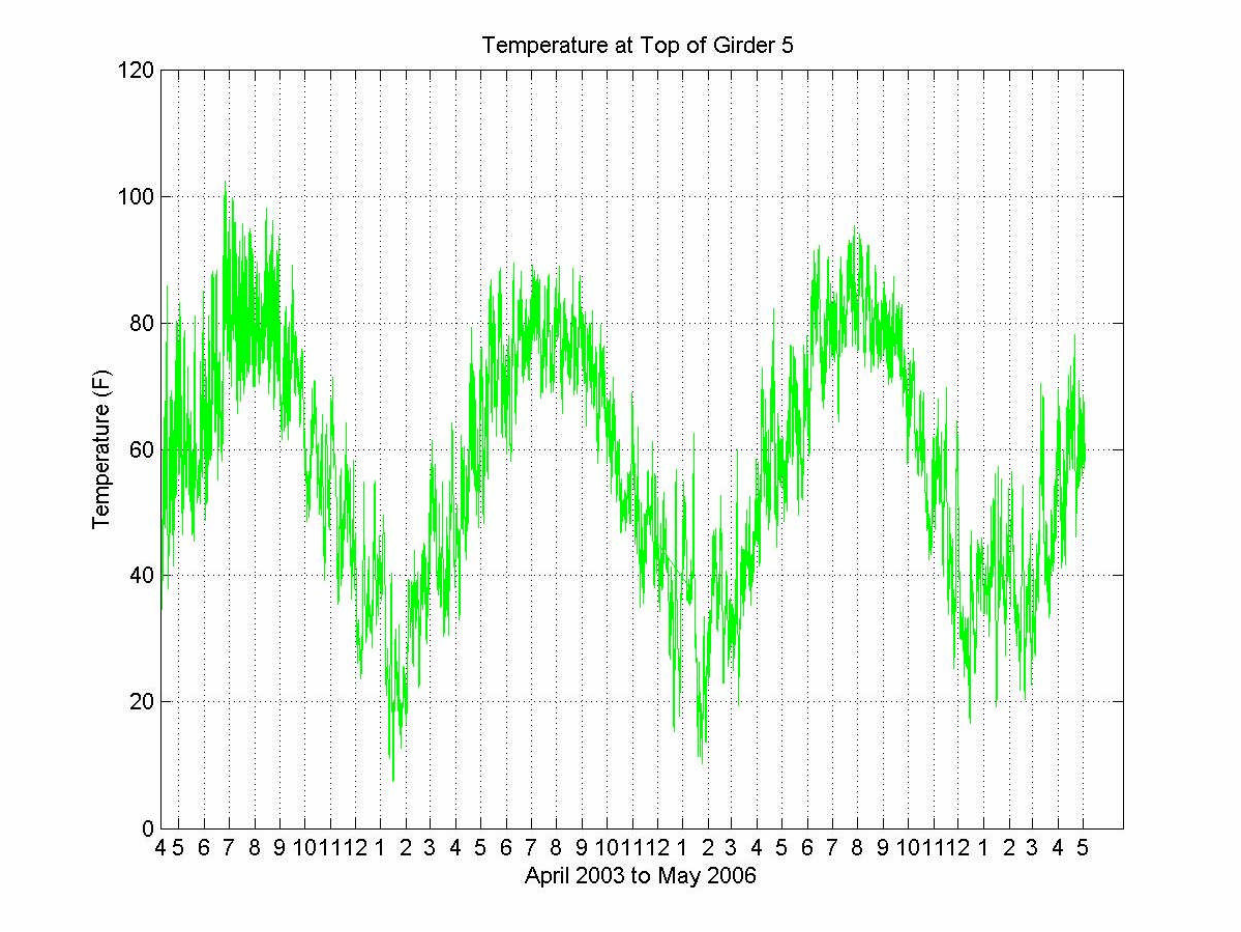

Figure 90. Temperature at top of Girder 5

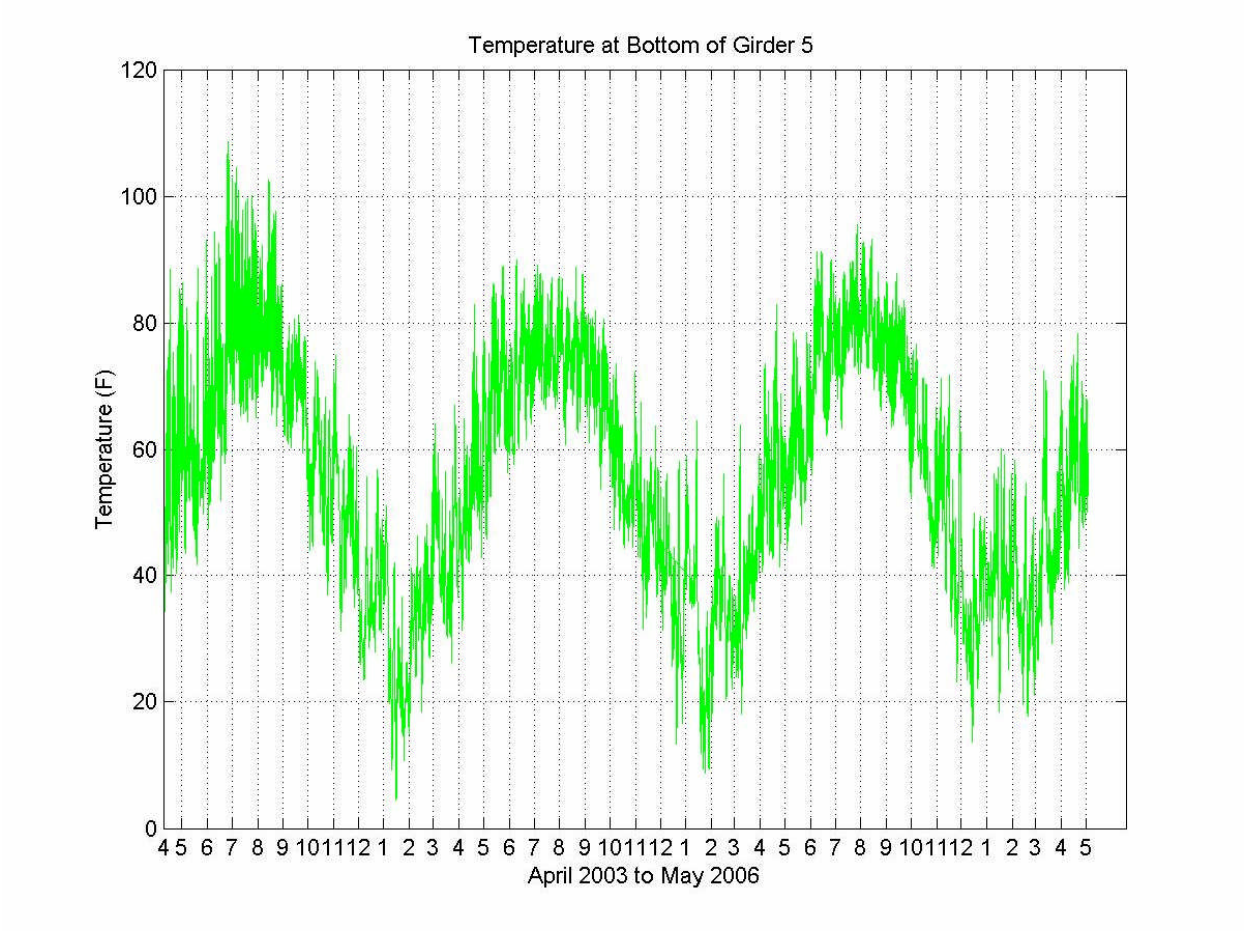

Figure 91. Temperature at bottom of Girder 5

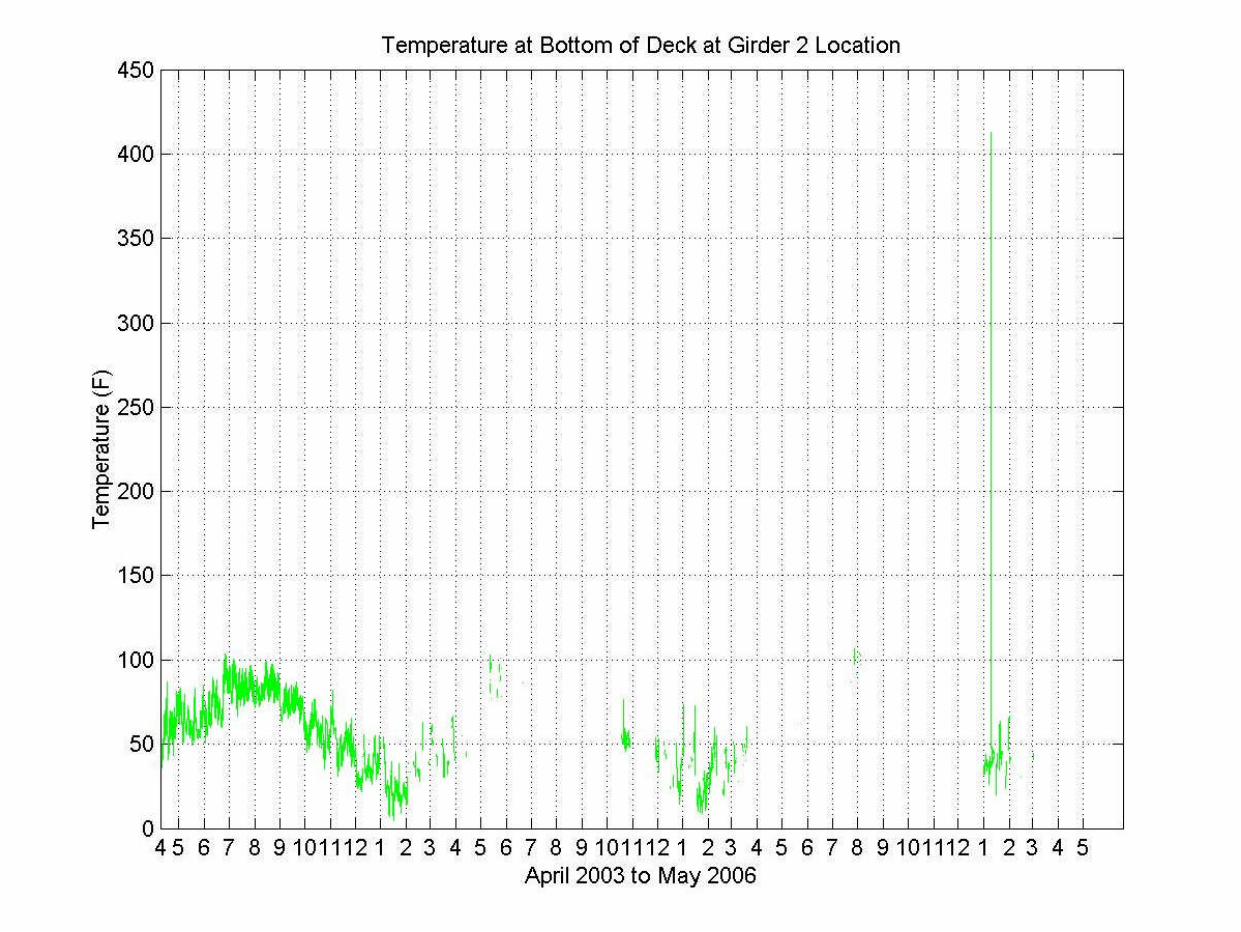

Figure 92. Temperature at bottom of deck at Girder 2

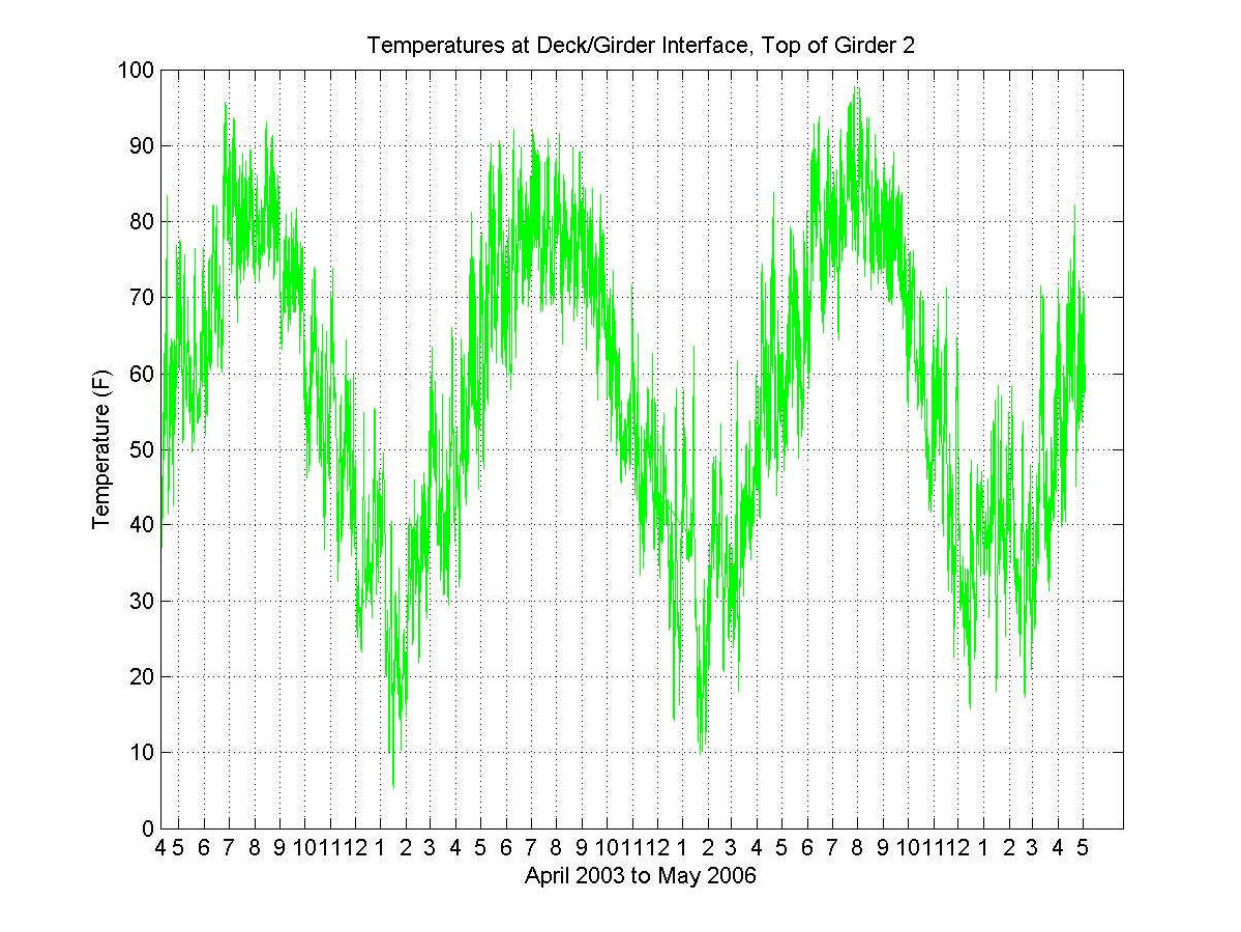

Figure 93. Temperature at deck/girder interface, top of Girder 2

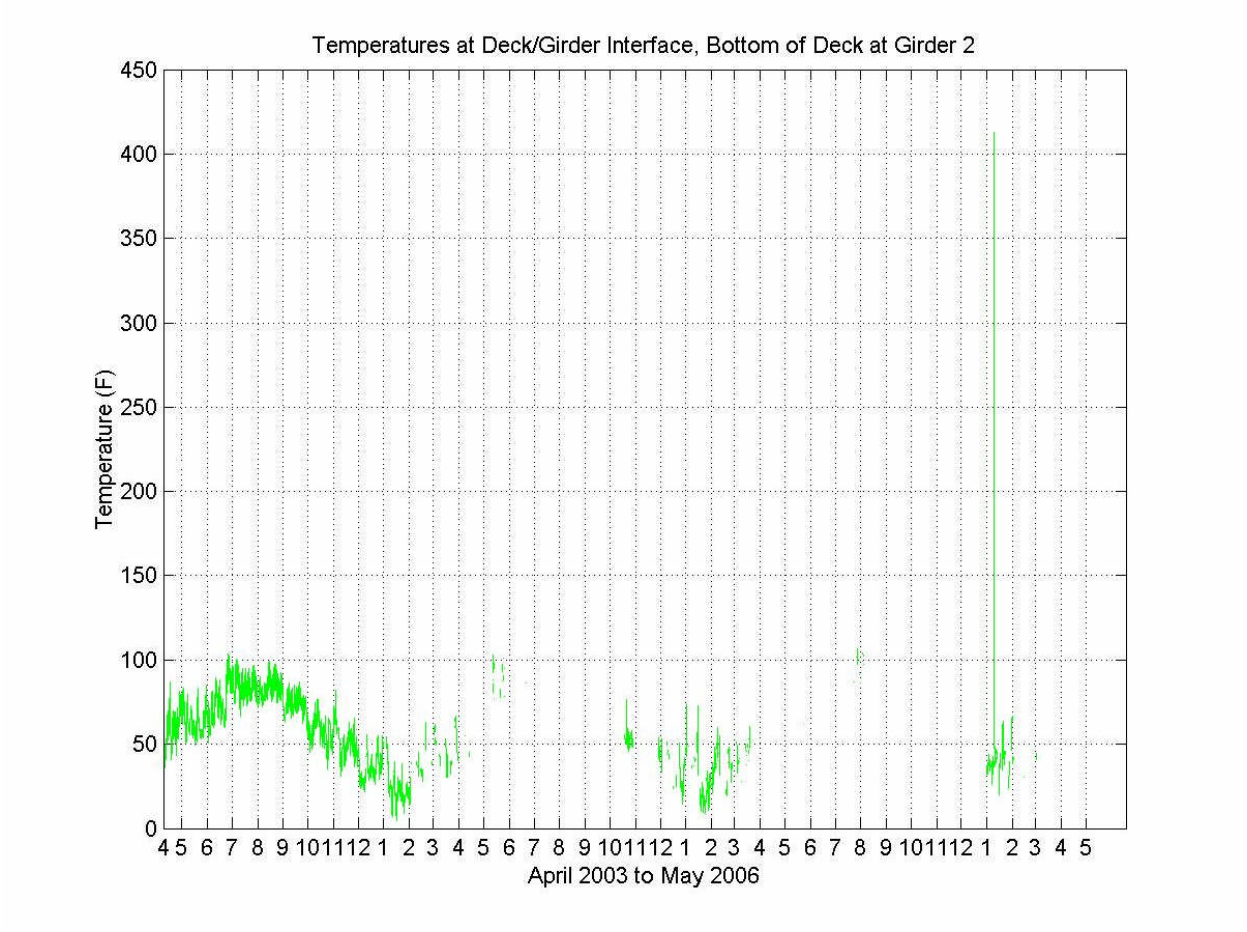

Figure 94. Temperature at deck/girder interface, bottom of deck at Girder 2

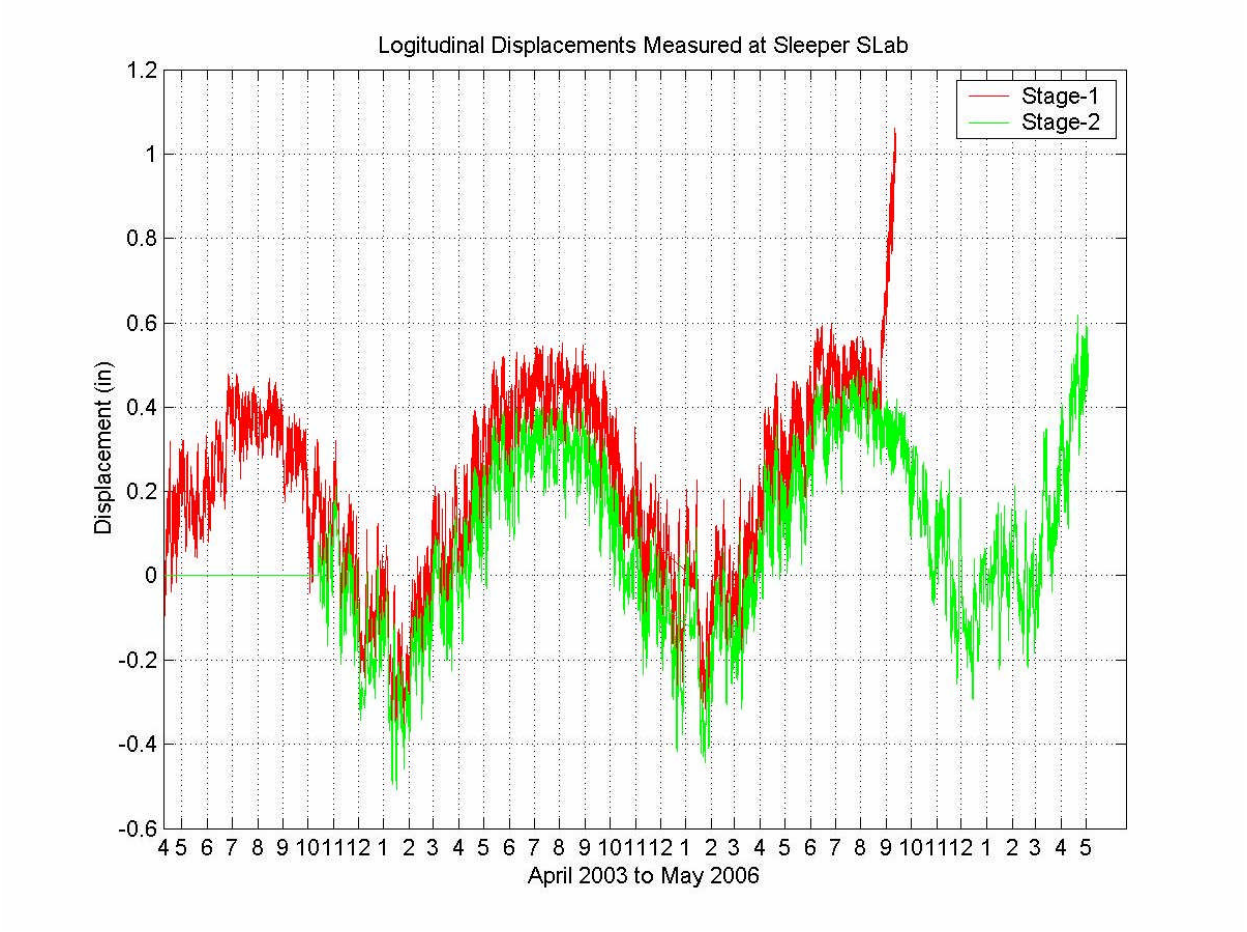

Figure 95. Longitudinal displacements of bridge measured at sleeper slab

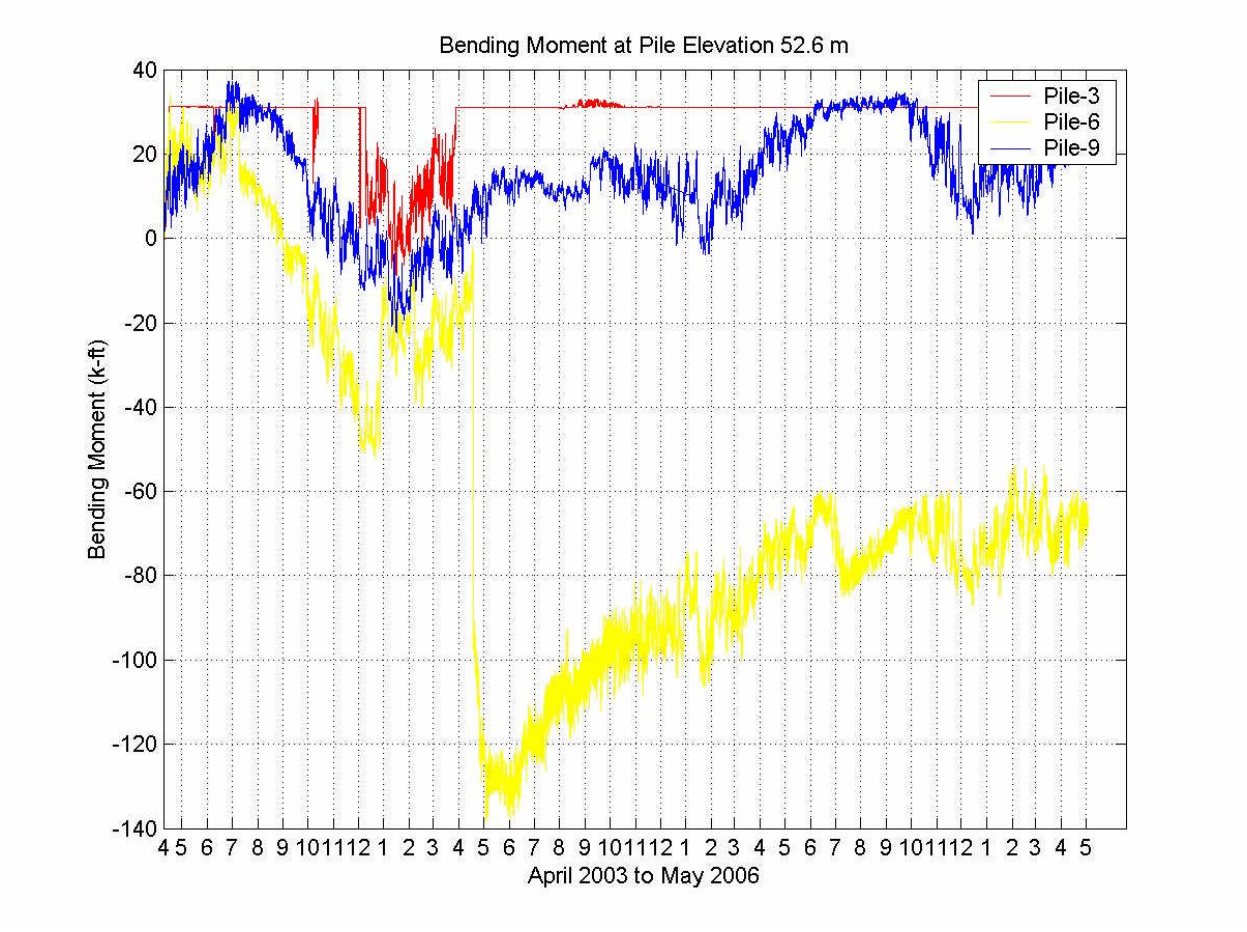

Figure 96. Bending moments of Piles 3, 6 and 9 at the elevation 52.5 meters

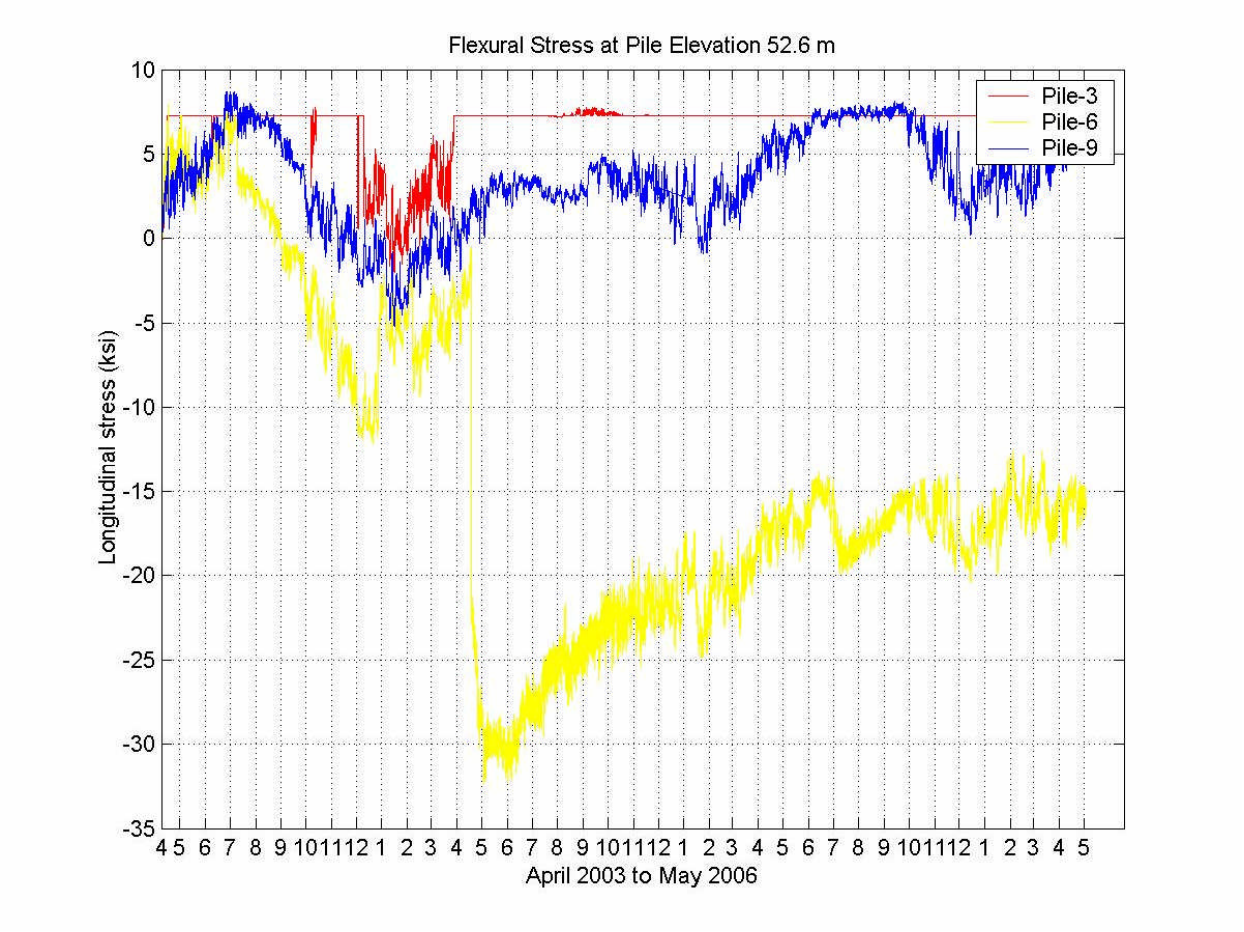

Figure 97. Flexural stresses on Piles 3, 6 and 9 at the elevation of 52.5 meters

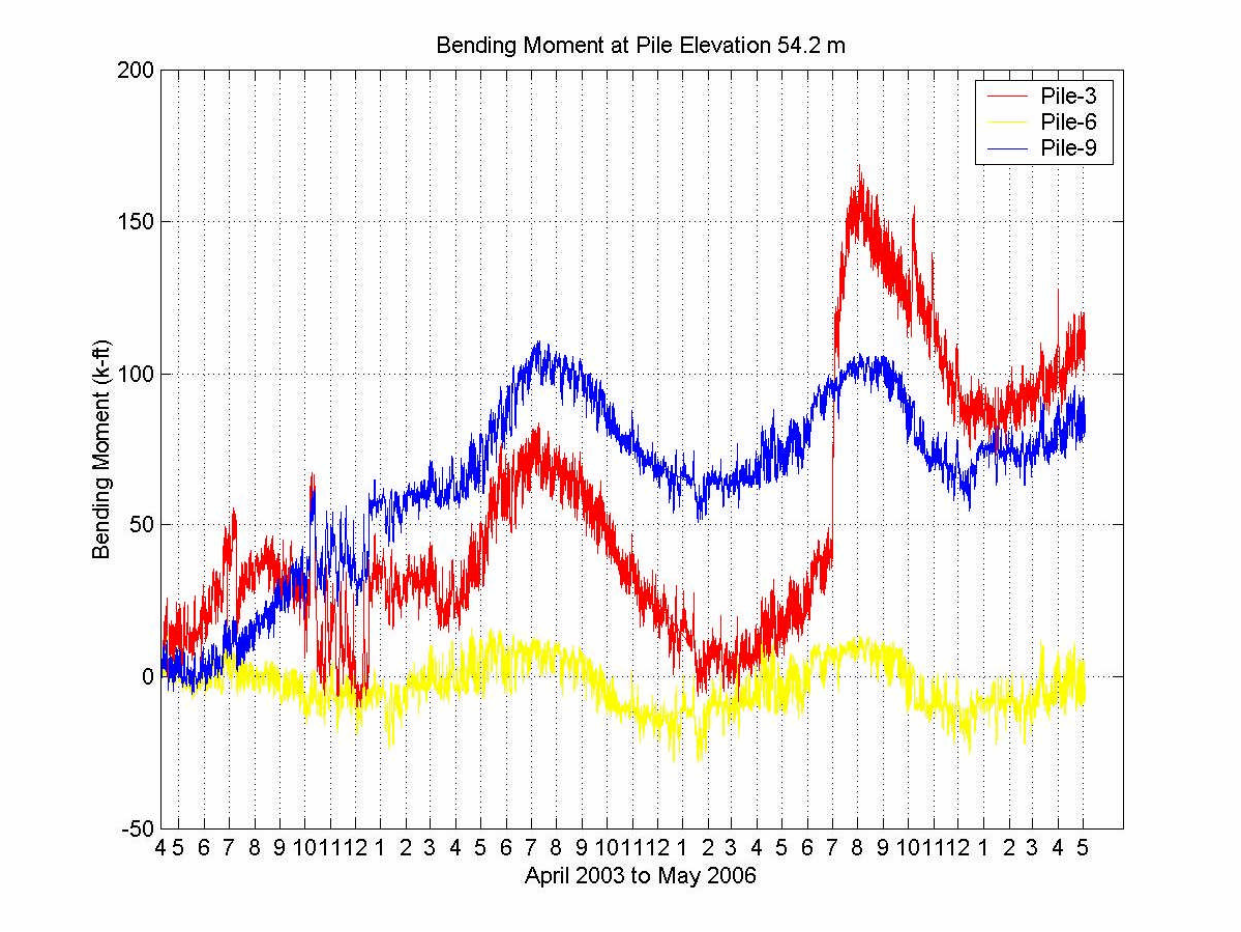

Figure 98. Bending moment of Piles 3, 6, and 9 at the elevation of 54.2 meters

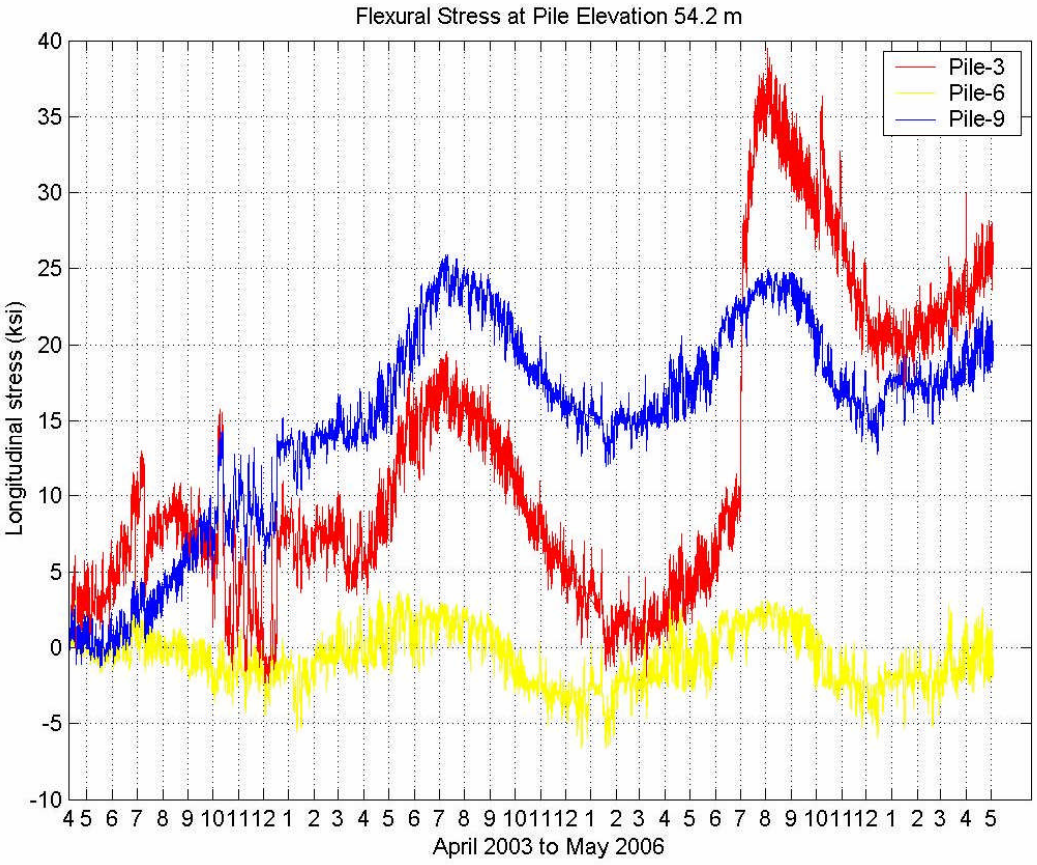

Figure 99. Flexural stresses of Piles 3, 6, and 9 at the elevation of 54.2 meters

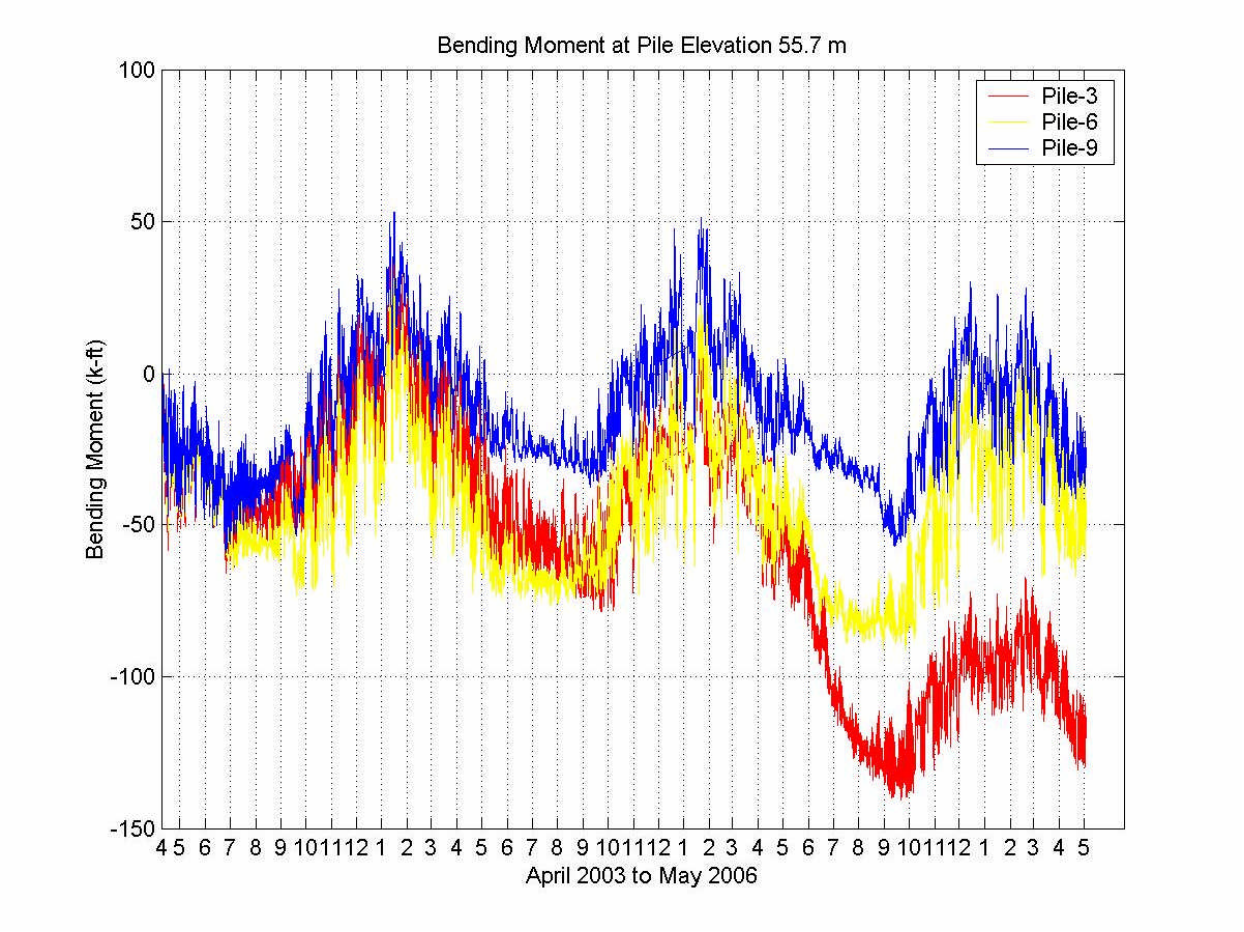

Figure 100. Bending moment of piles 3, 6, and 9 at the elevation of 55.7 meters

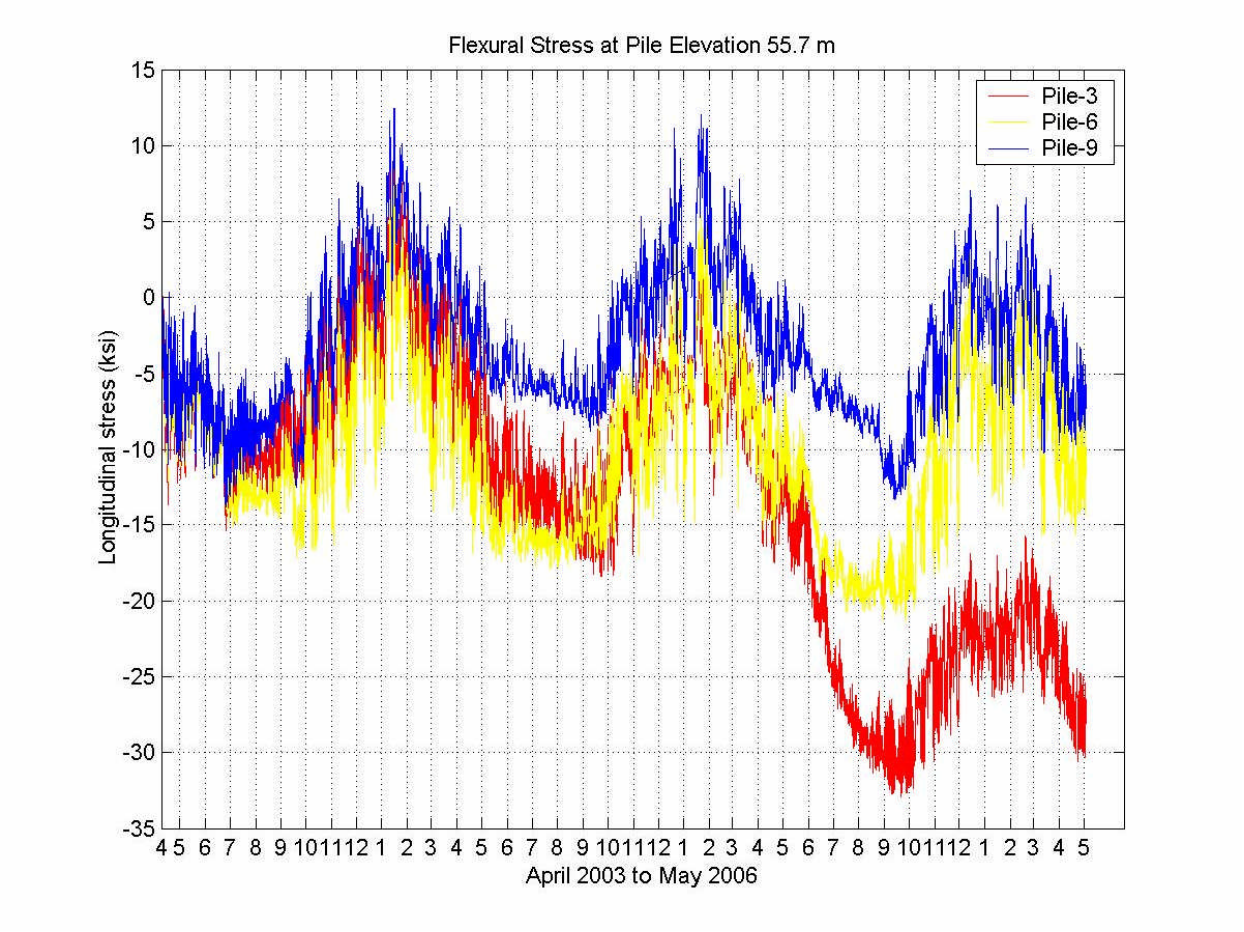

Figure 101. Flexural stresses on Piles 3, 6 and 9 at the elevation of 55.7 meters

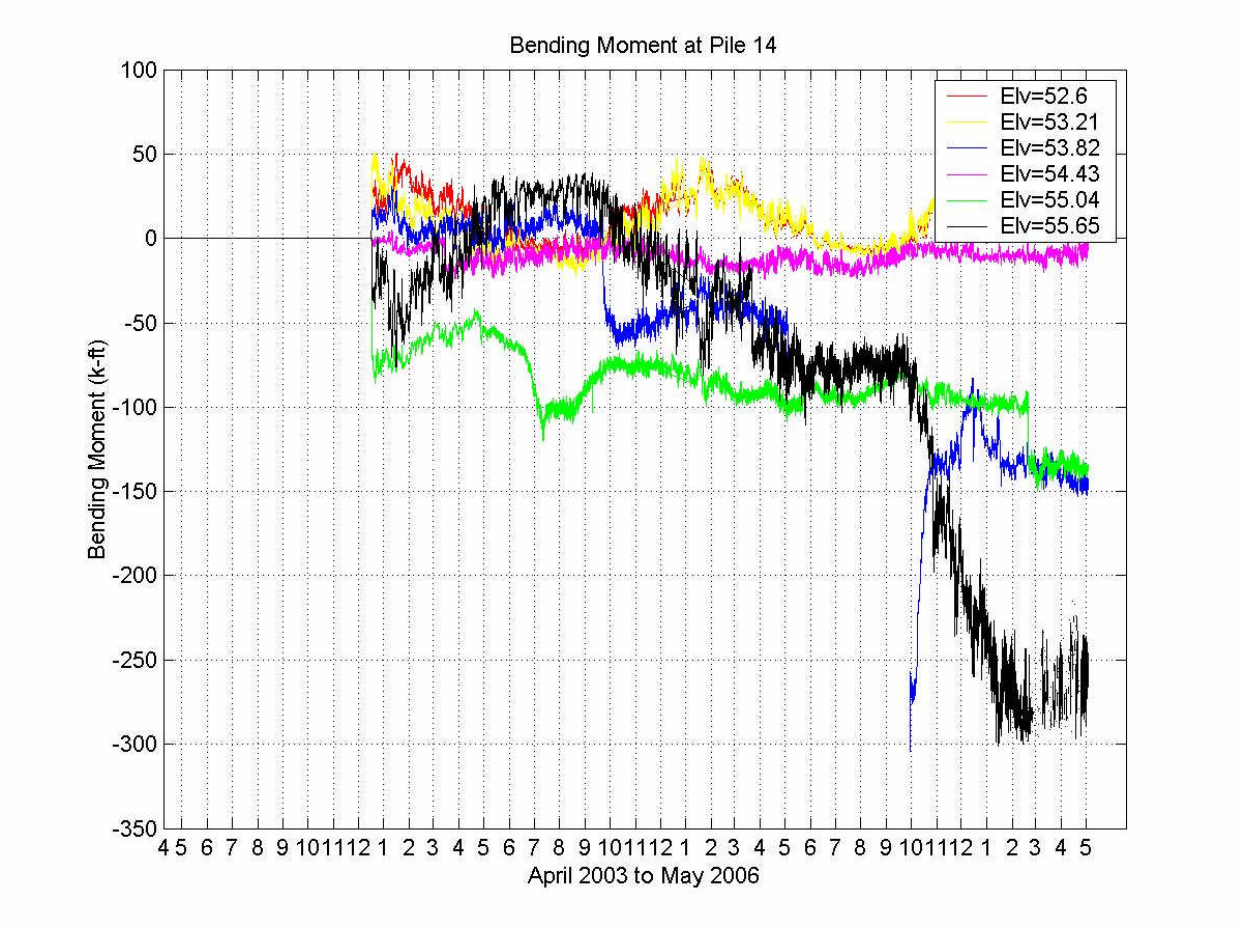

Figure 102. Bending moments along the depth of Pile 14

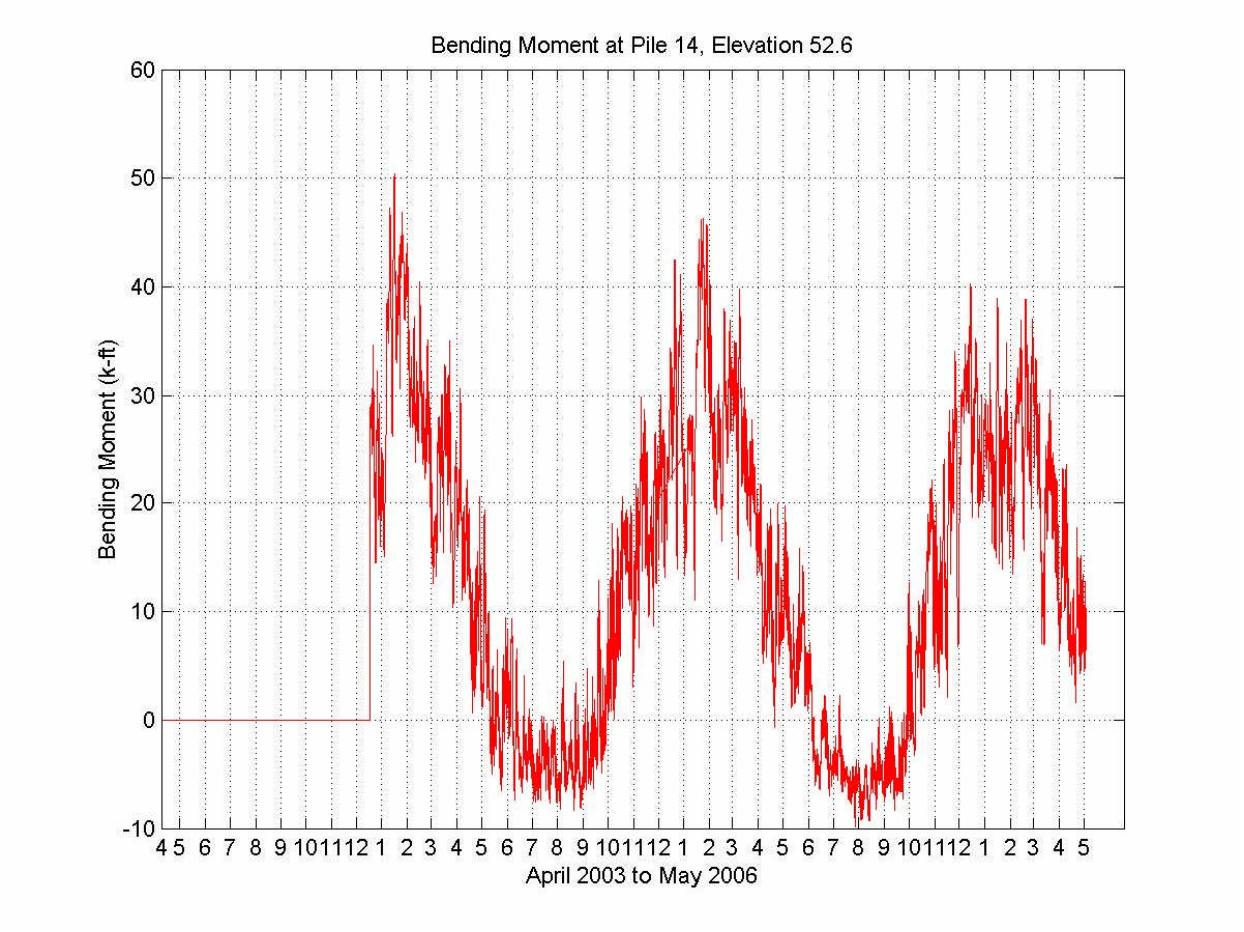

Figure 103. Bending moment of Pile 14 at the elevation of 52.6 meters

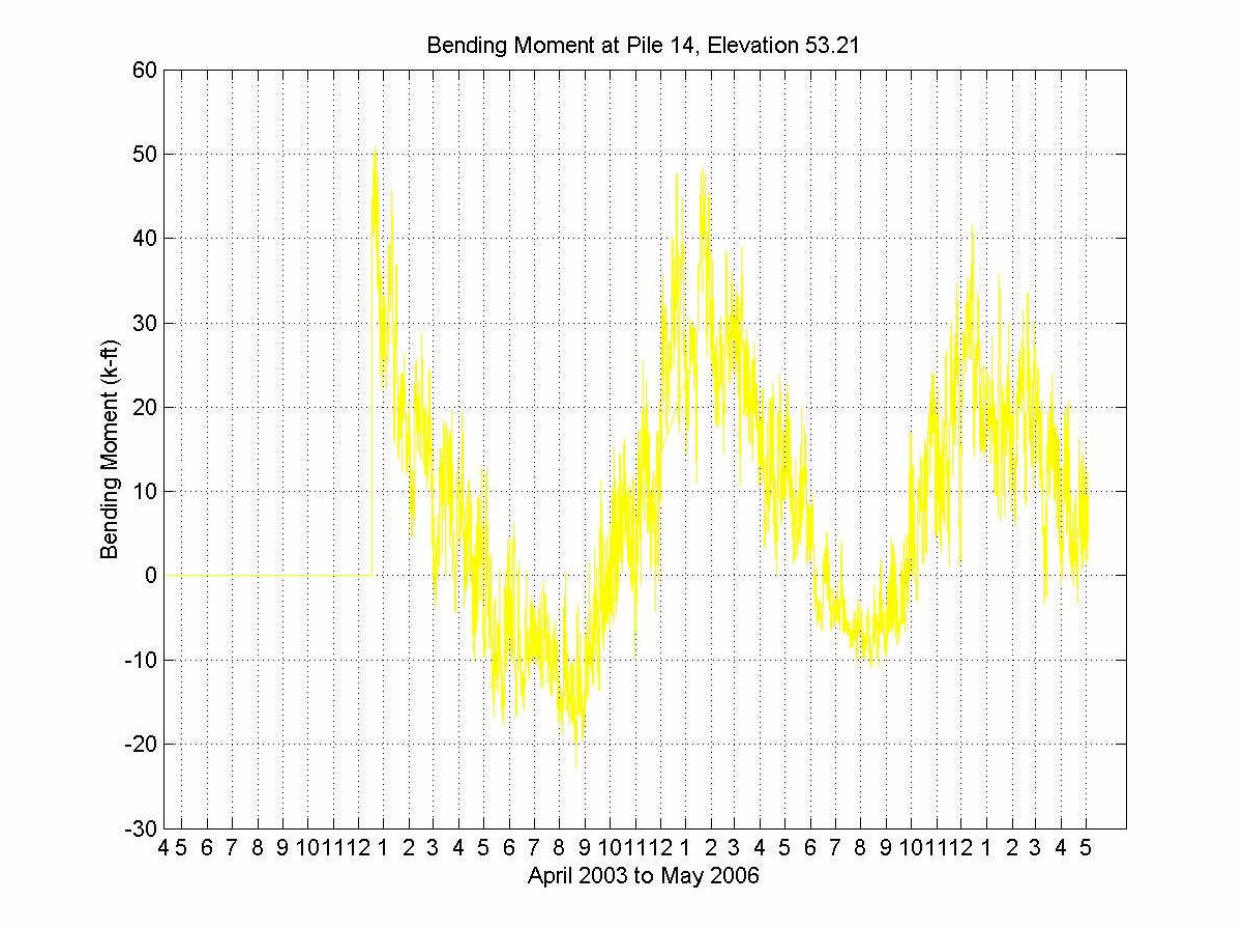

Figure 104. Bending moment of Pile 14 at the elevation of 53.21 meters

Figure 105. Bending moment of Pile 14 at the elevation of 53.82 meters

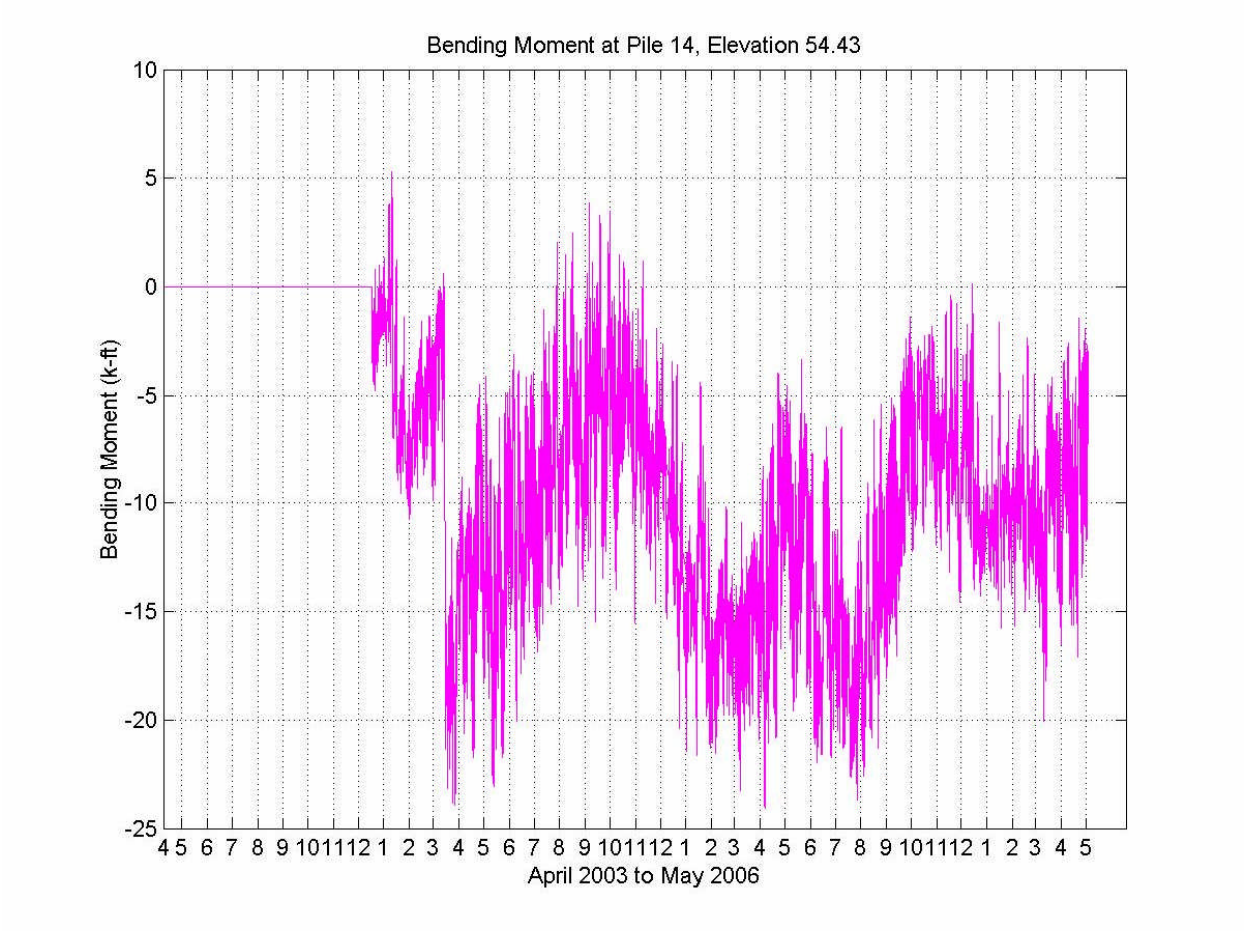

Figure 106. Bending moment of Pile 14 at the elevation of 54.43 meters

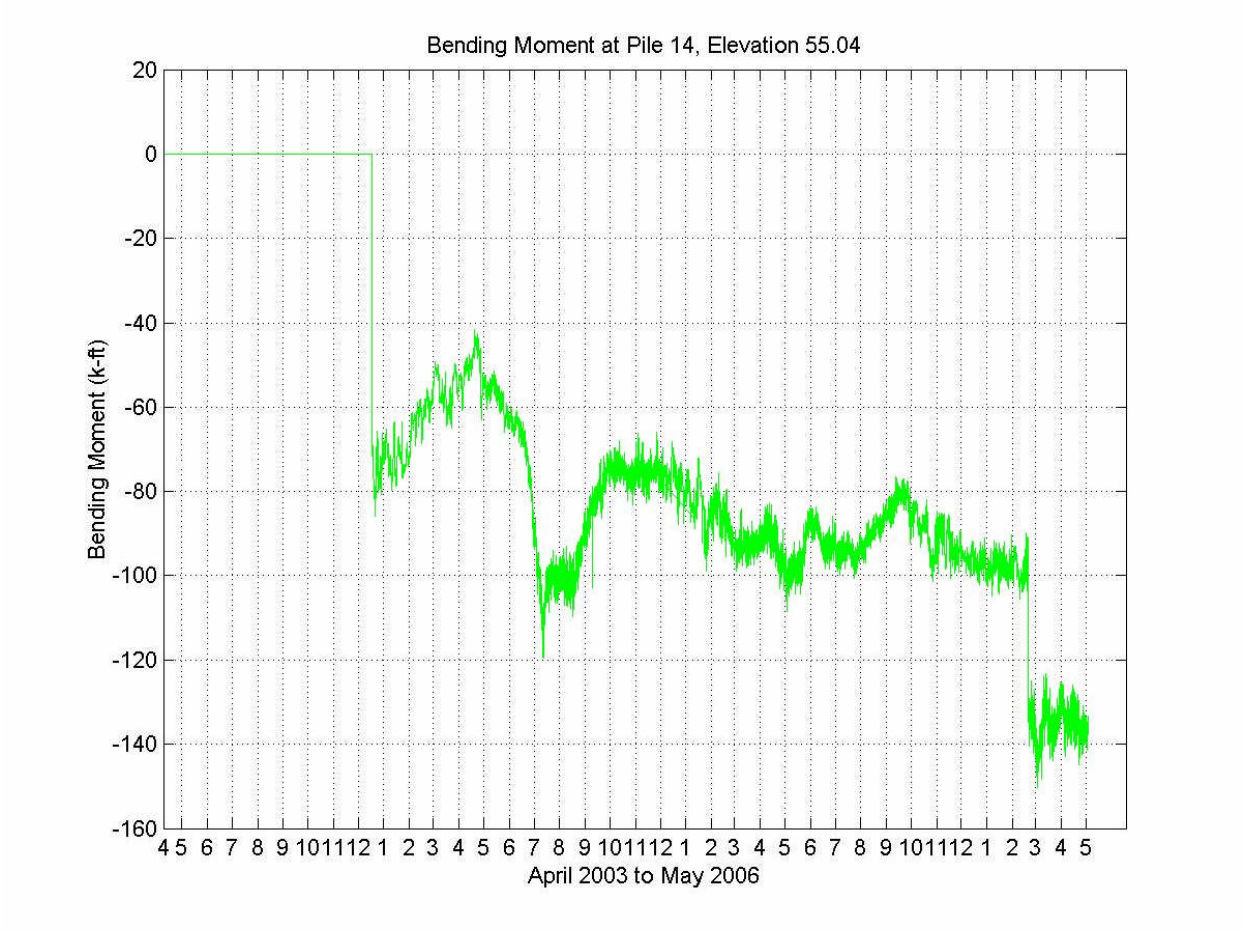

Figure 107. Bending moment of Pile 14 at the elevation of 55.04 meters

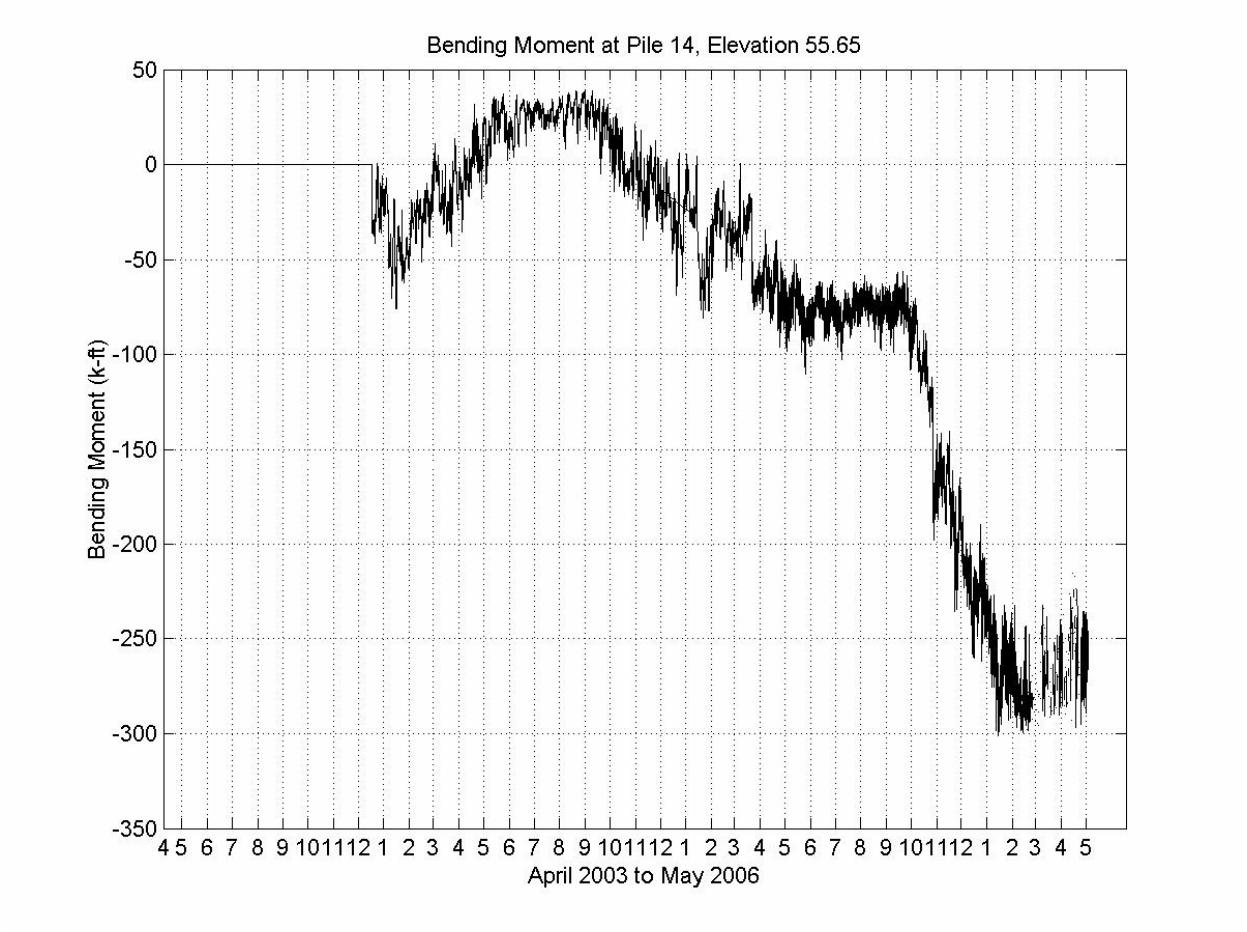

Figure 108. Bending moment of Pile 14 at the elevation of 55.65 meters

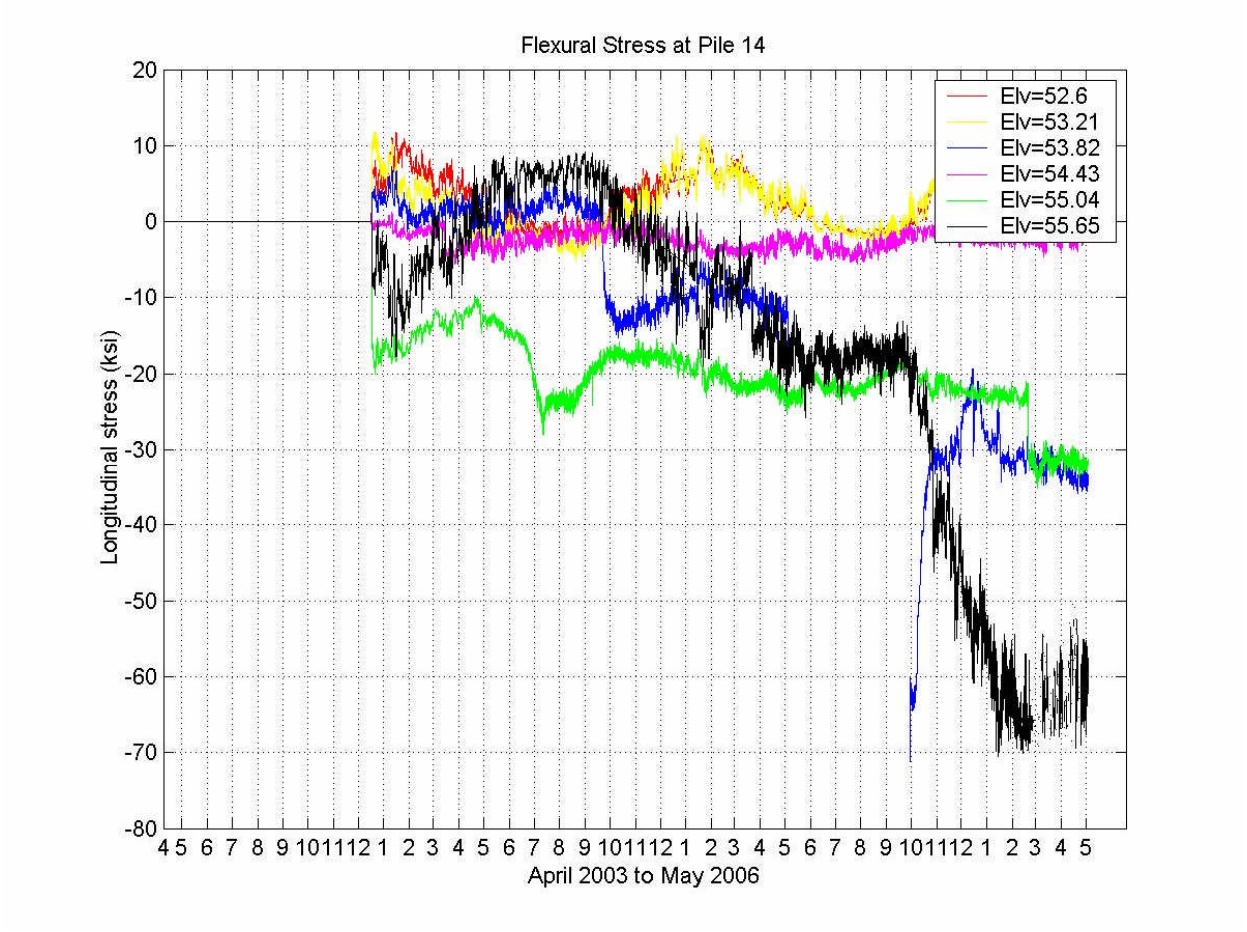

Figure 109. Flexural stresses along the depth of Pile 14

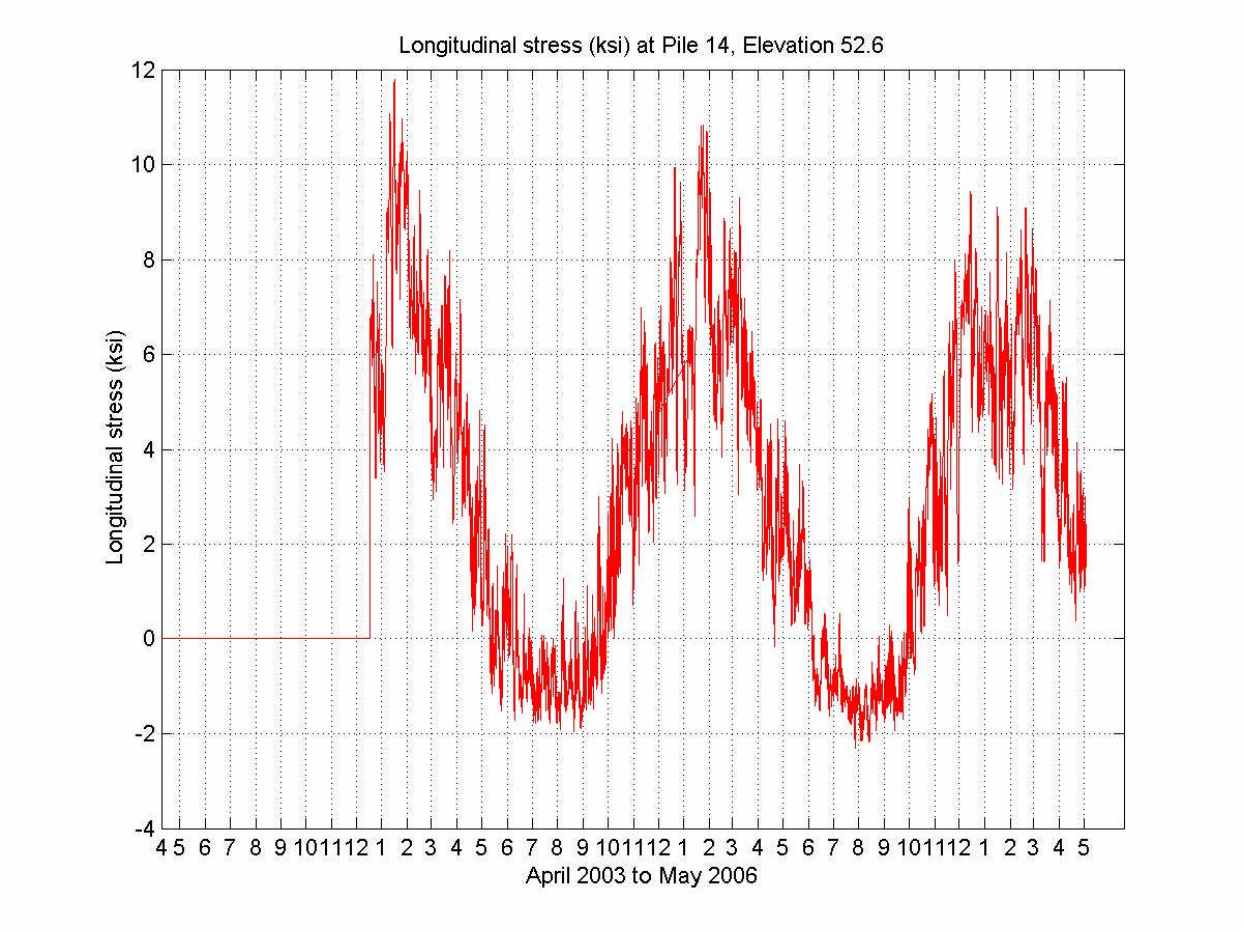

Figure 110. Flexural stress of Pile 14 at the elevation of 52.6 meters

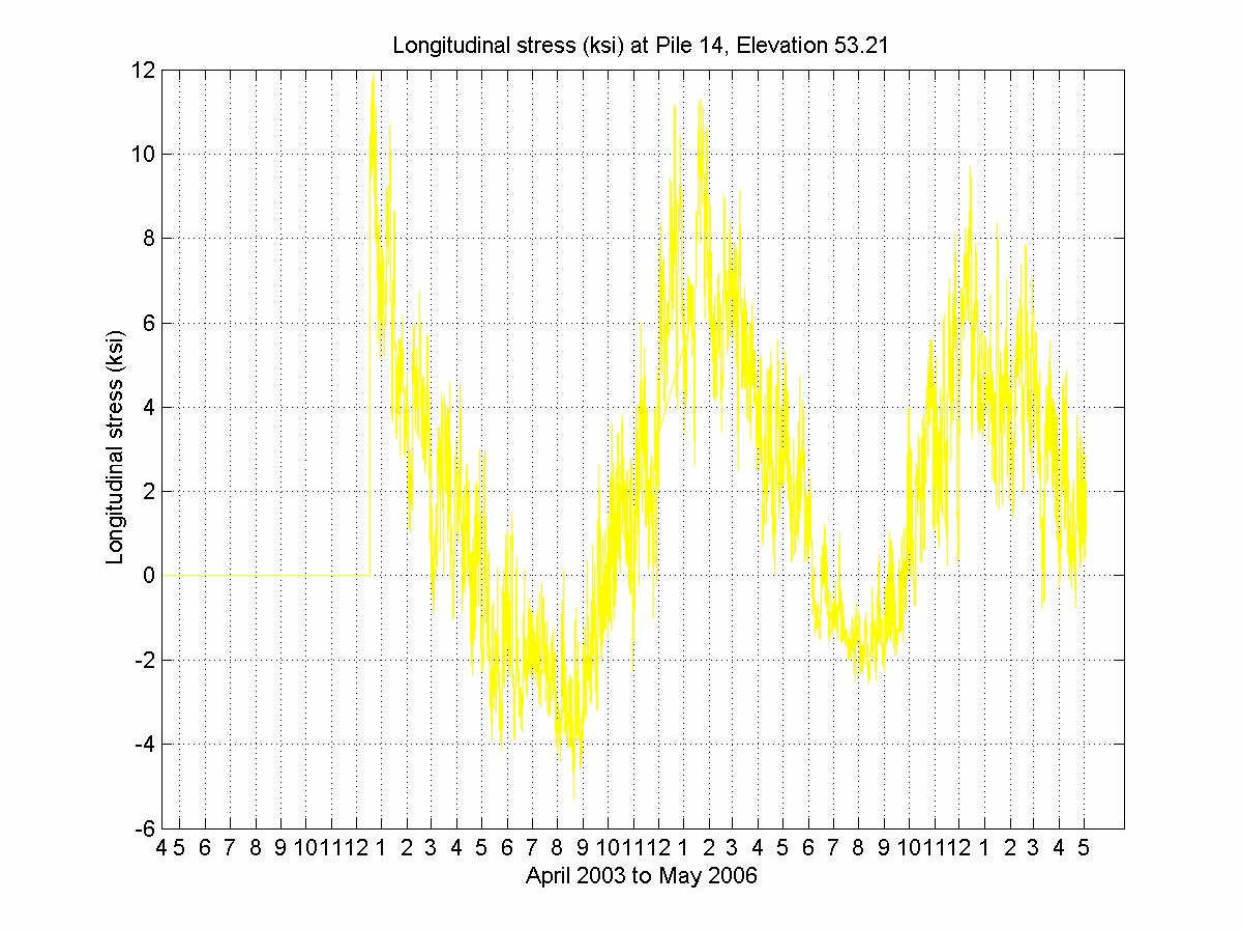

Figure 111. Flexural stress of Pile 14 at the elevation of 53.21 meters

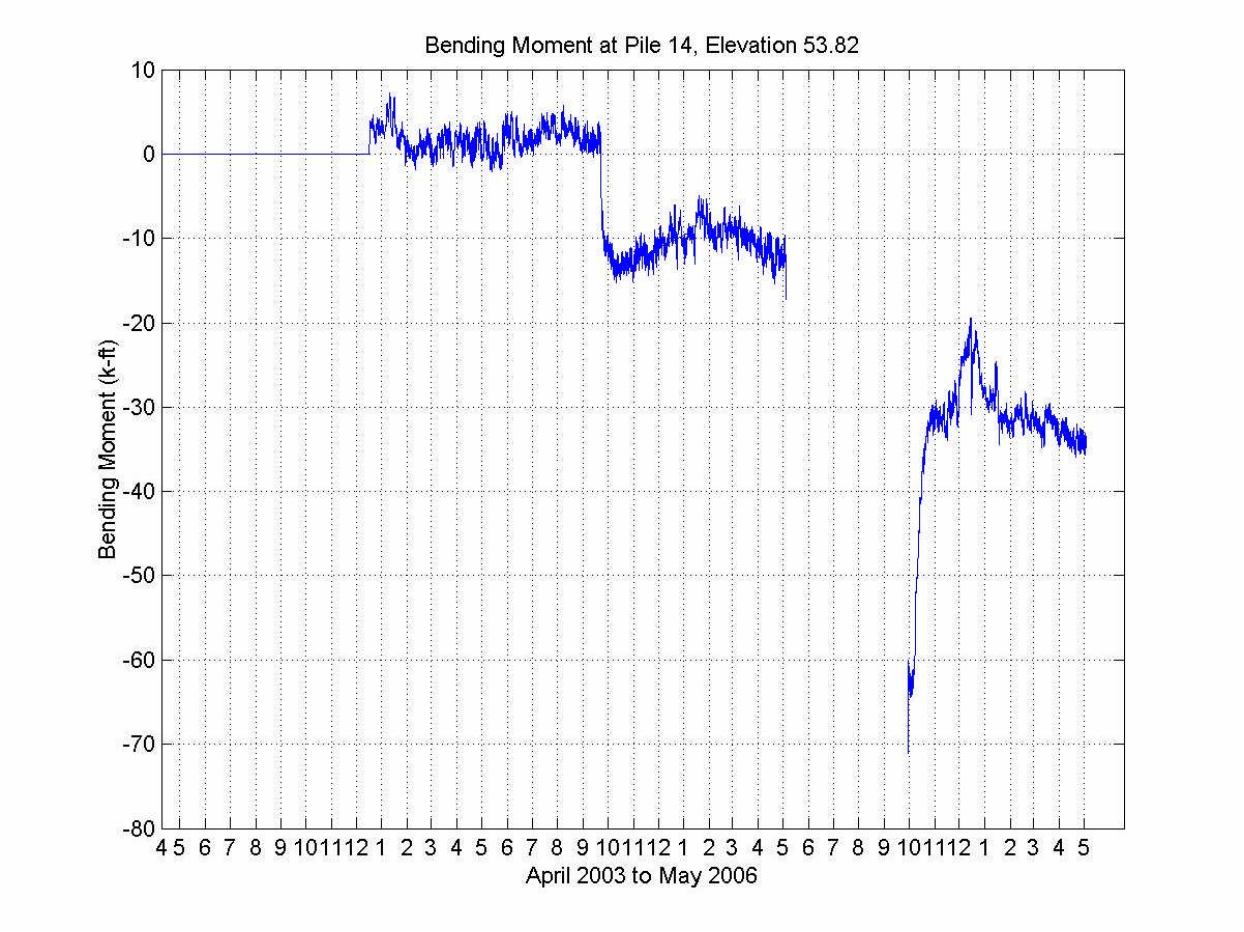

Figure 112. Flexural stress of Pile 14 at the elevation of 53.82 meters

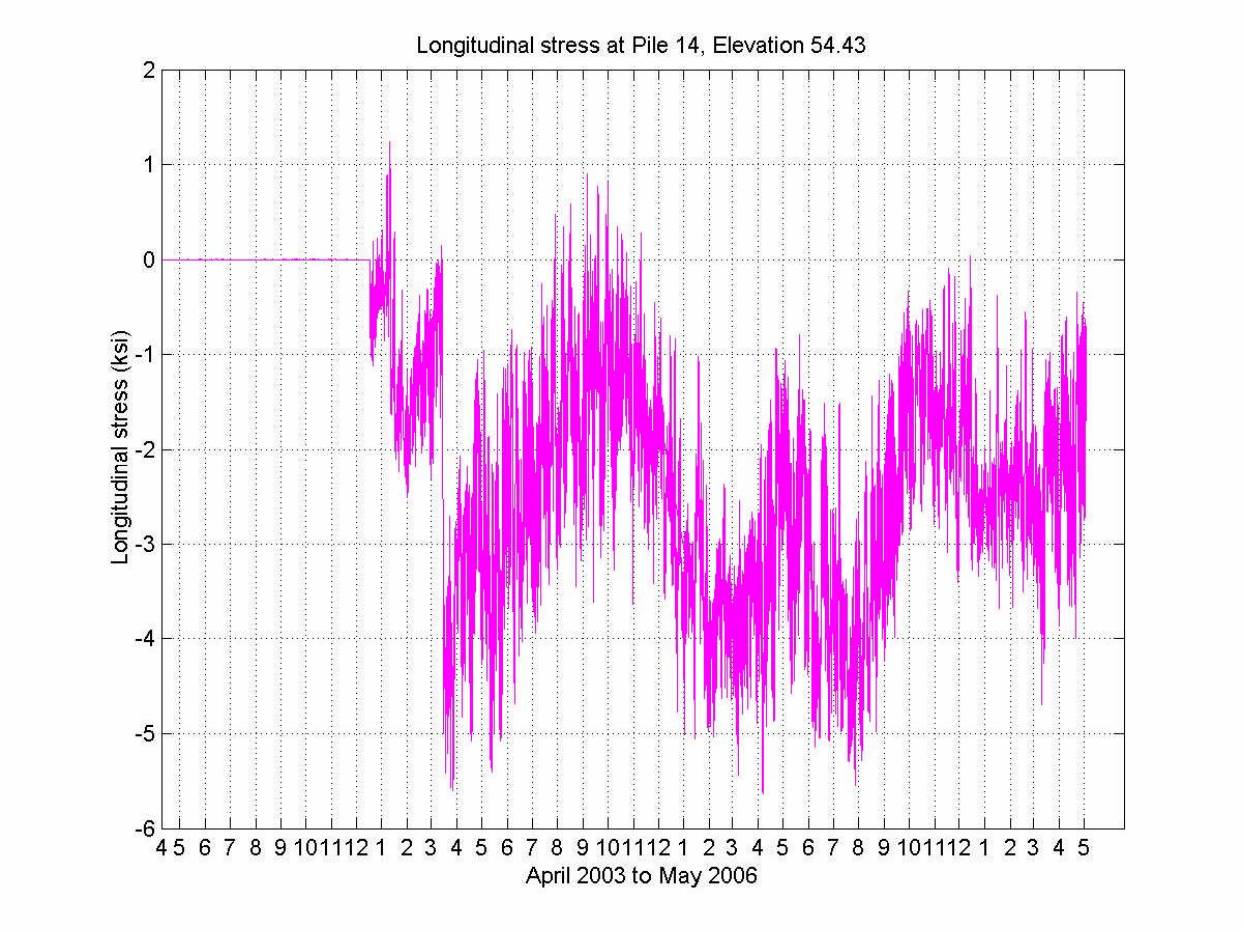

Figure 113. Flexural stress of Pile 14 at the elevation of 54.43 meters

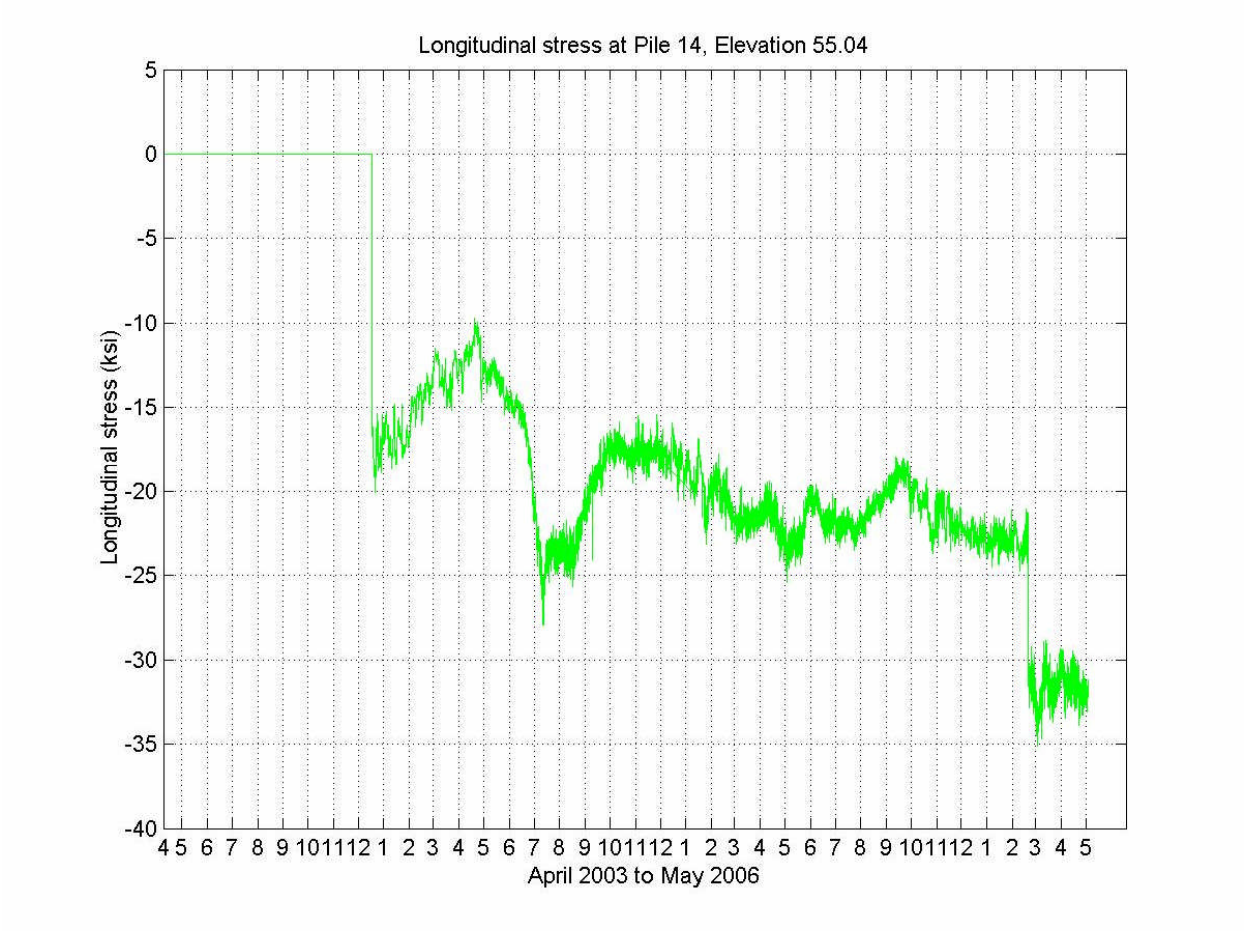

Figure 114. Flexural stress of Pile 14 at the elevation of 55.04 meters

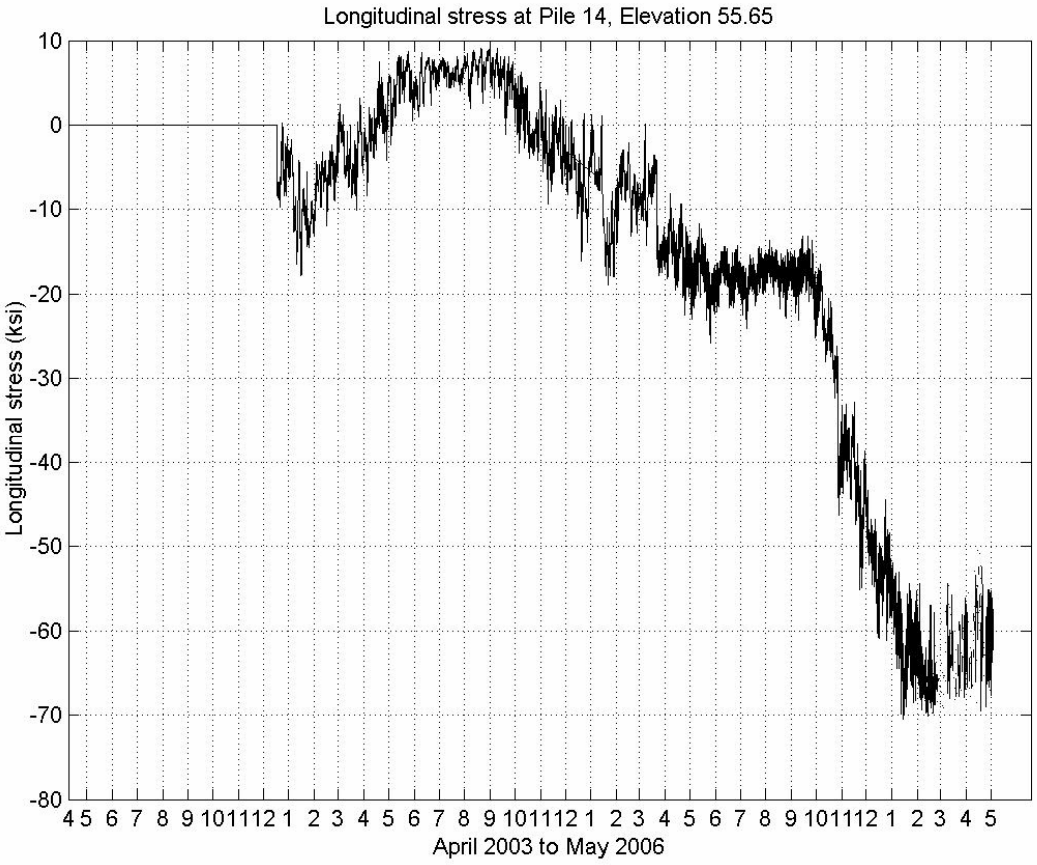

Figure 115. Flexural stress of Pile 14 at the elevation of 55.65 meters

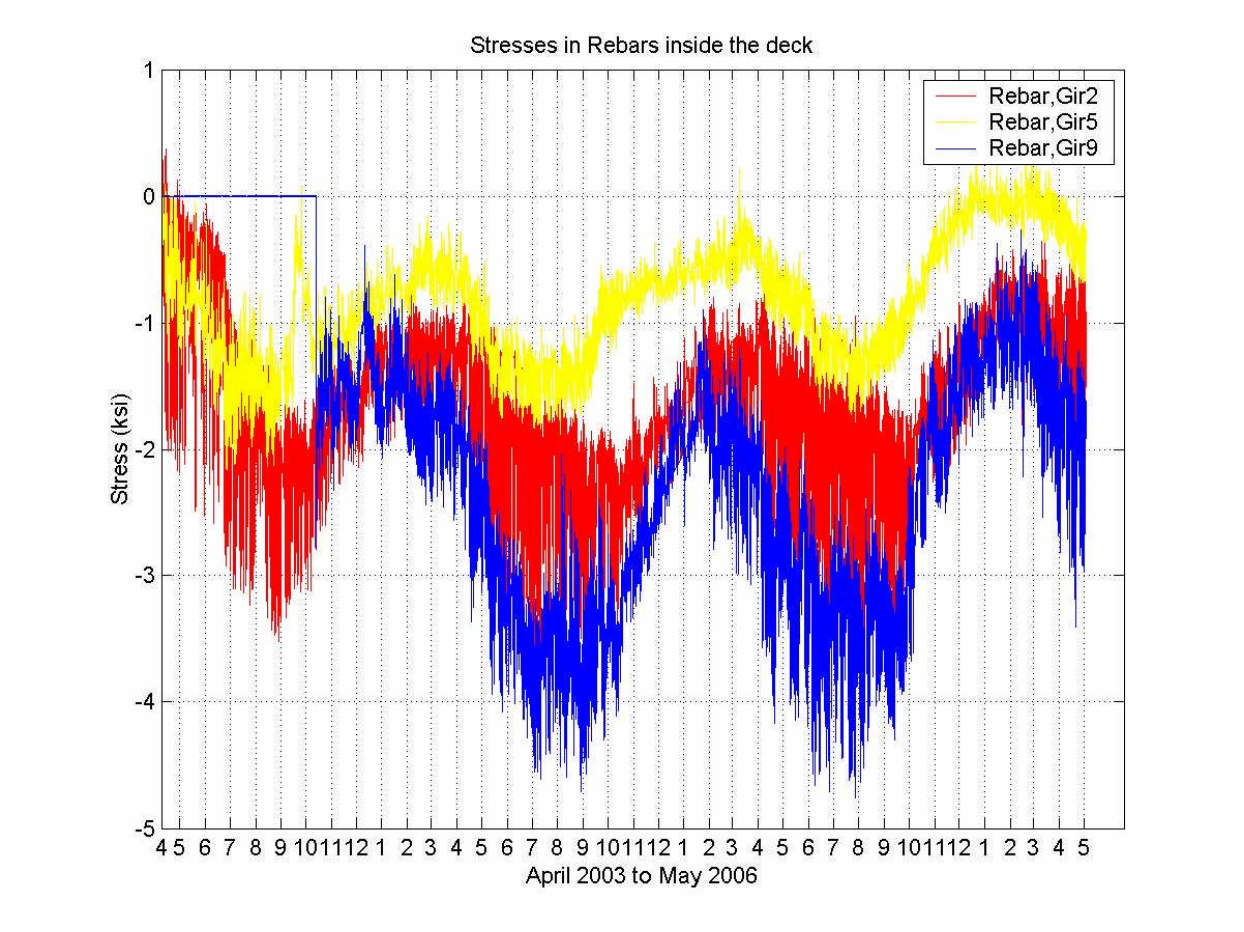

Figure 116. Stresses in rebars inside the deck at girder-abutment connection of Girders 2, 5, and 6

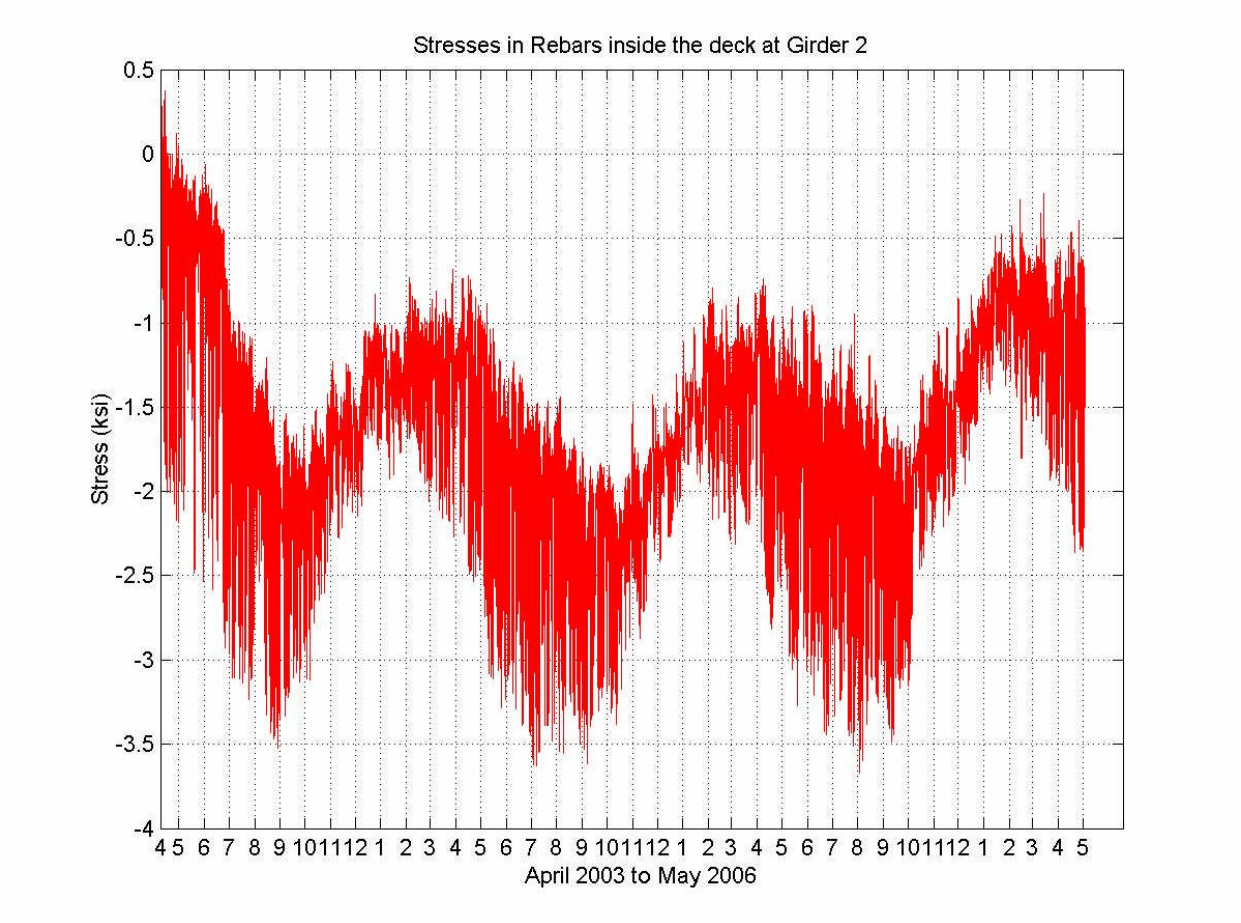

Figure 117. Stresses in rebar inside the deck at girder-abutment connection of Girder 2

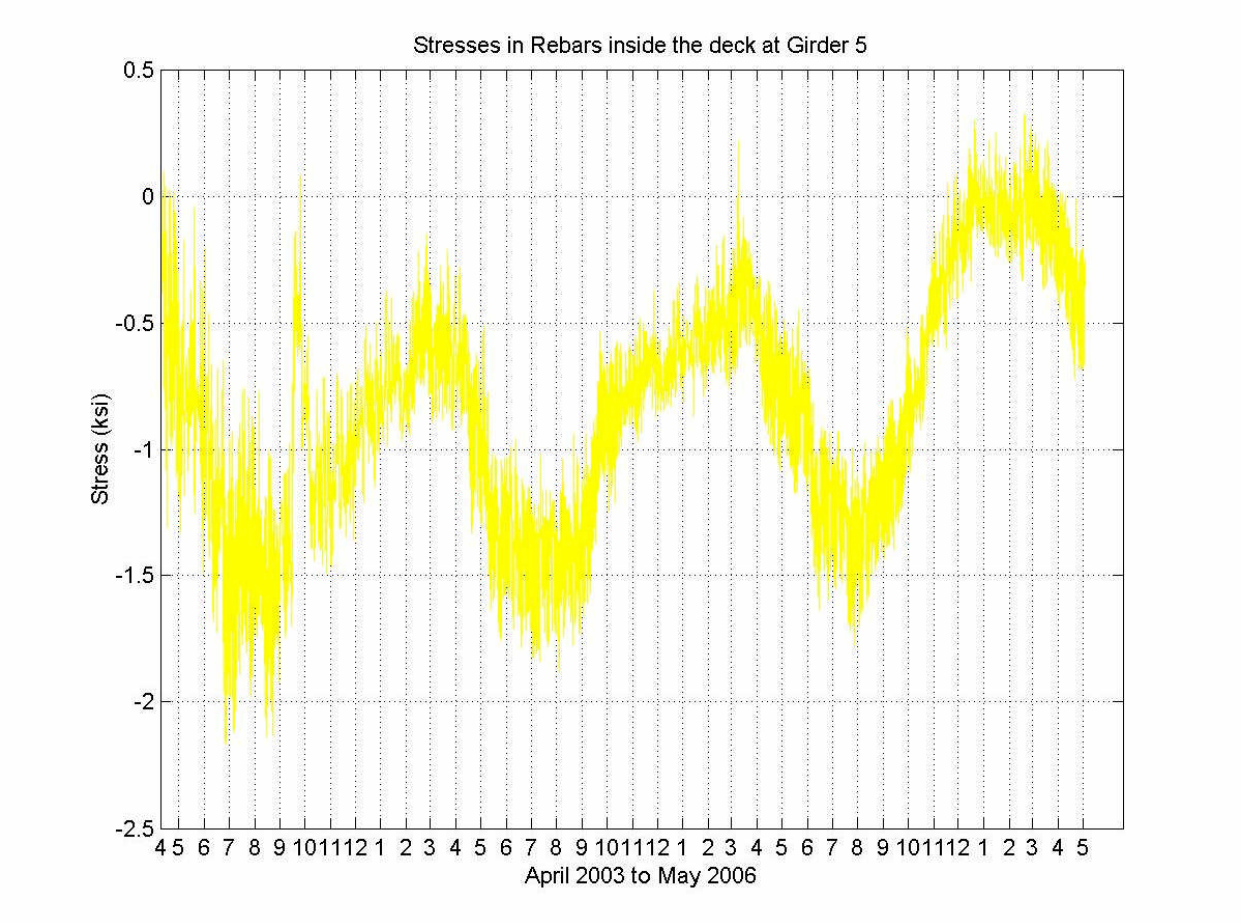

Figure 118. Stresses in rebar inside the deck at girder-abutment connection of Girder 5

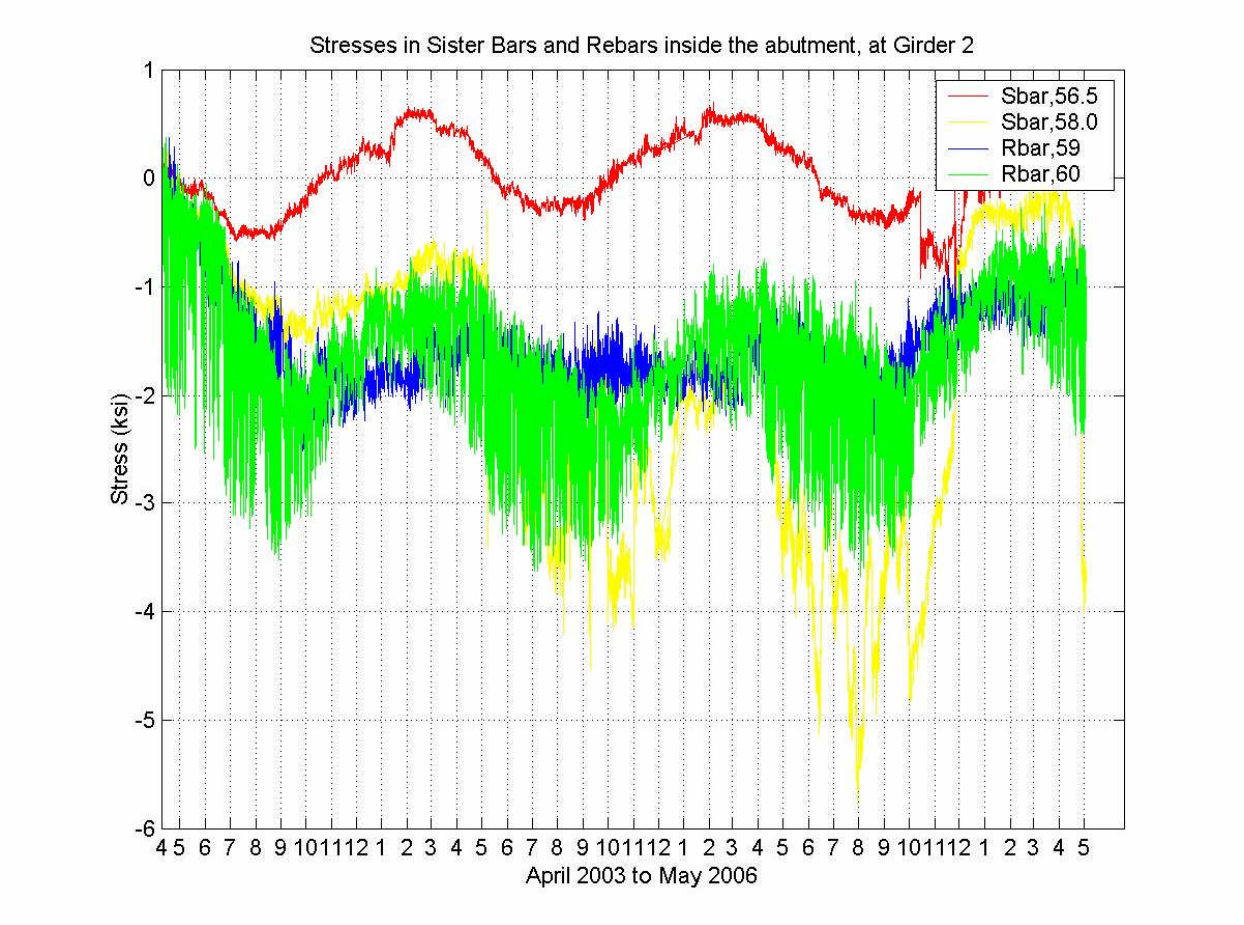

Figure 119. Stresses in rebars inside the abutment at Girder 2 at different elevations

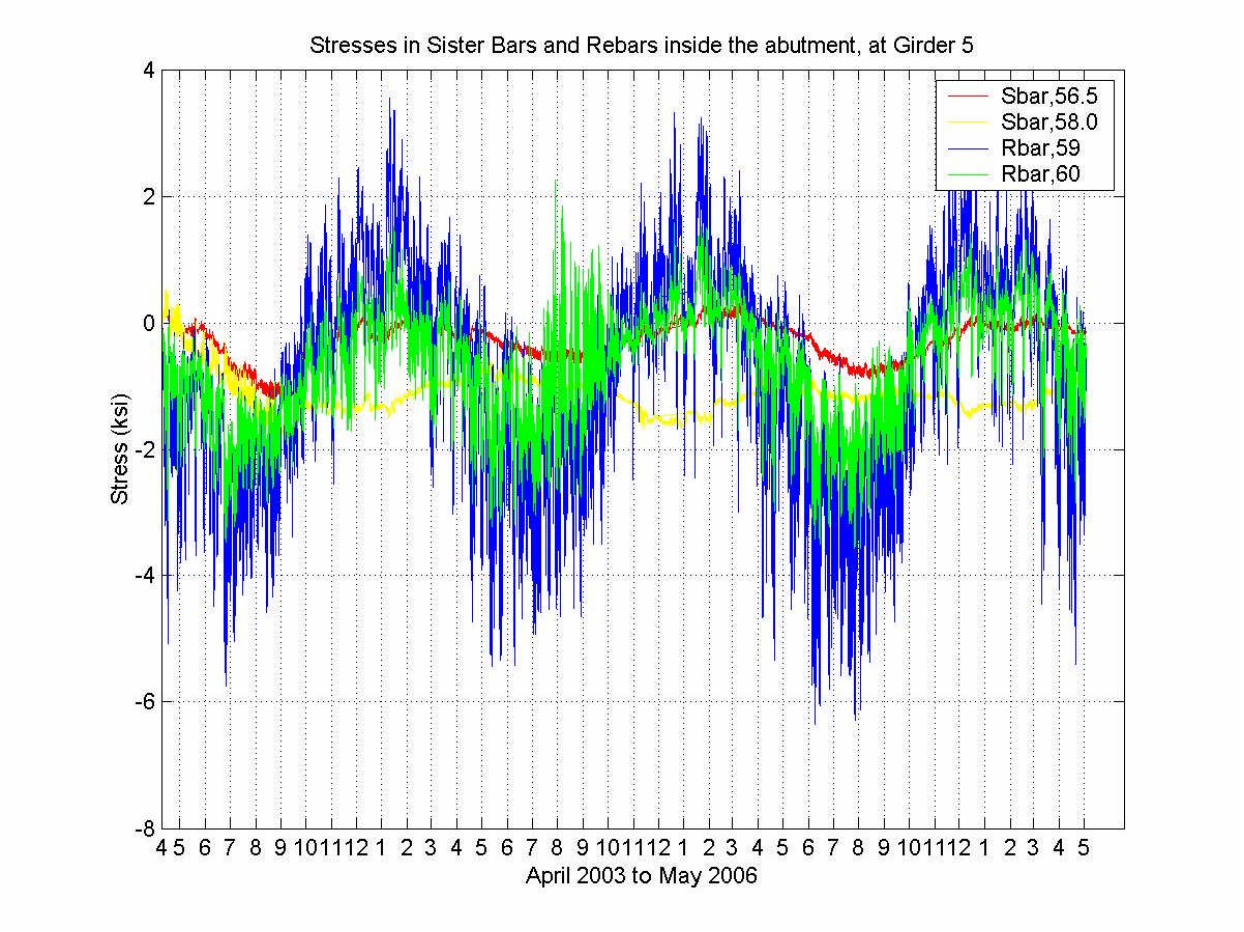

Figure 120. Stresses in rebars inside the abutment at Girder 5 at different elevations

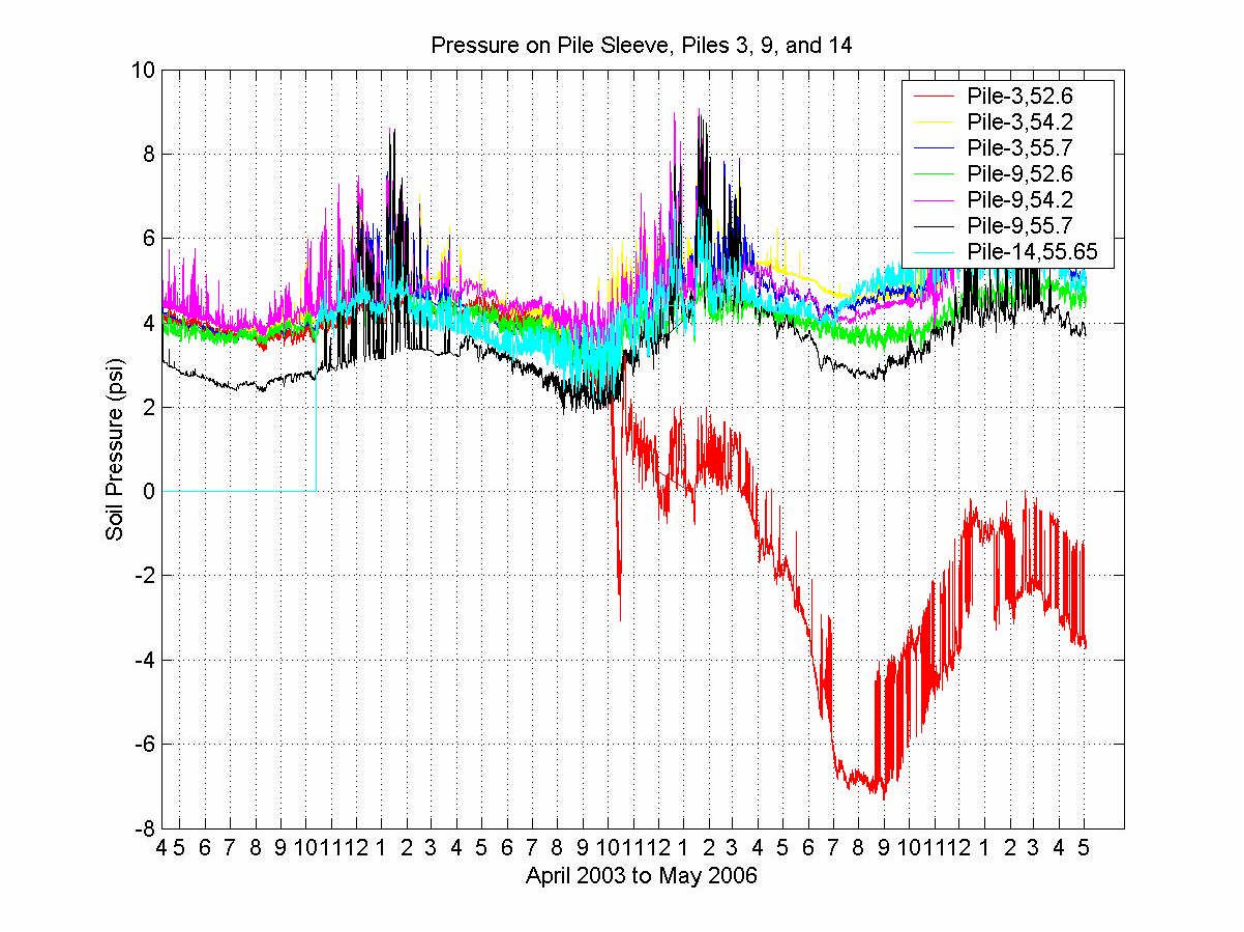

Figure 121. Pressure on sleeves of Piles 3, 9, and 14 at different elevations

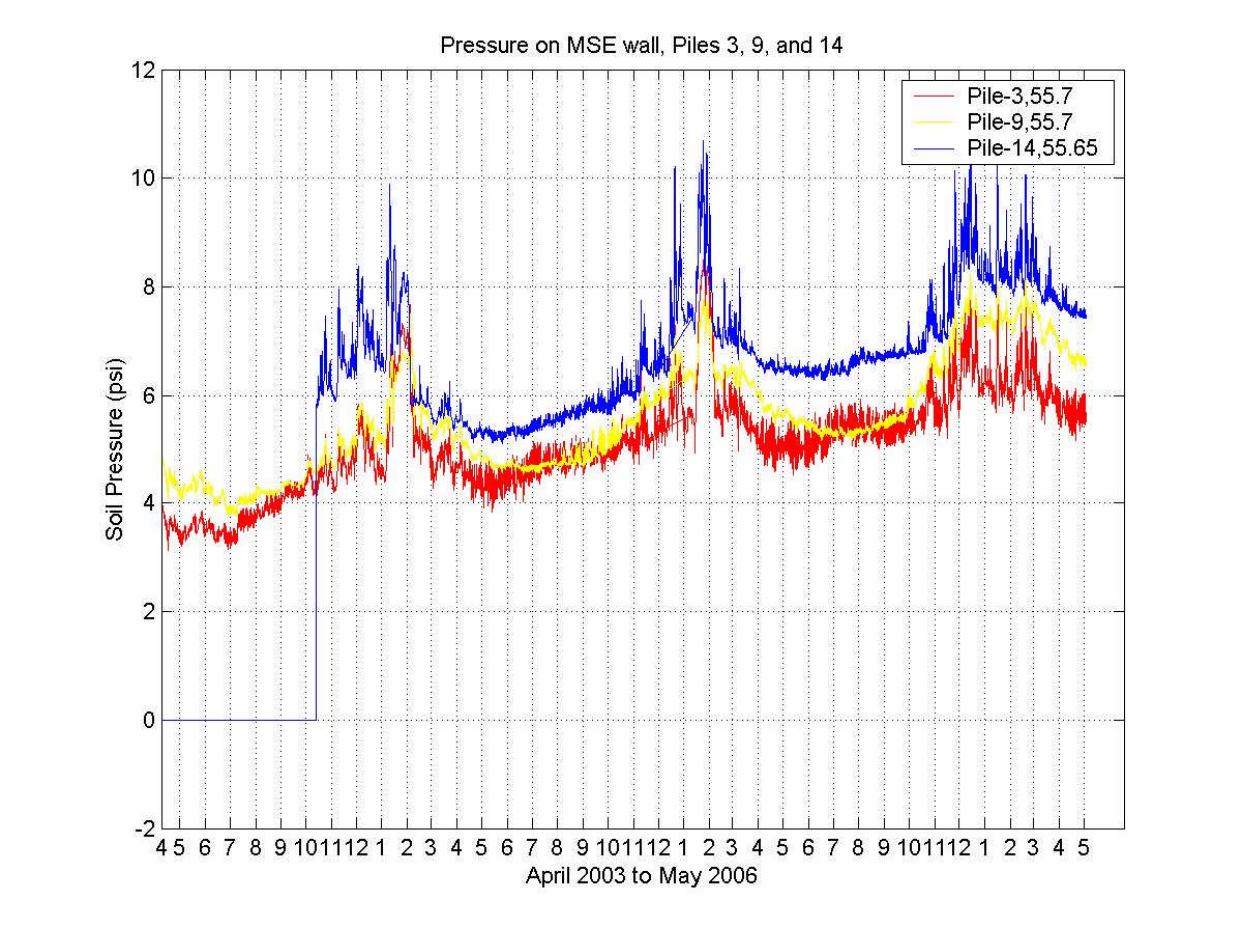

Figure 122. Pressure on MSE wall on plane of Piles 3, 9, and 14

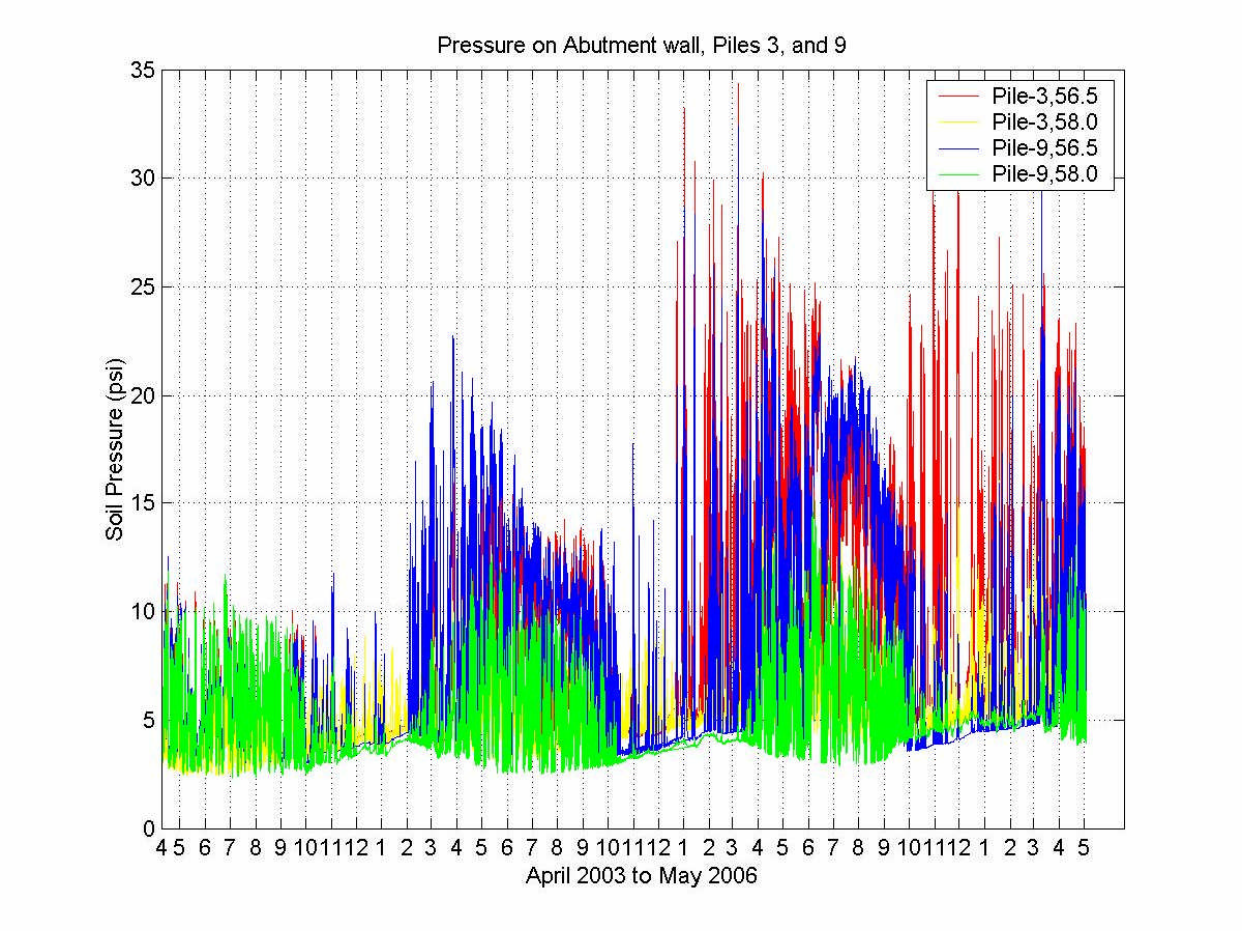

Figure 123. Pressure on the abutment wall at section of Piles 3 and 9

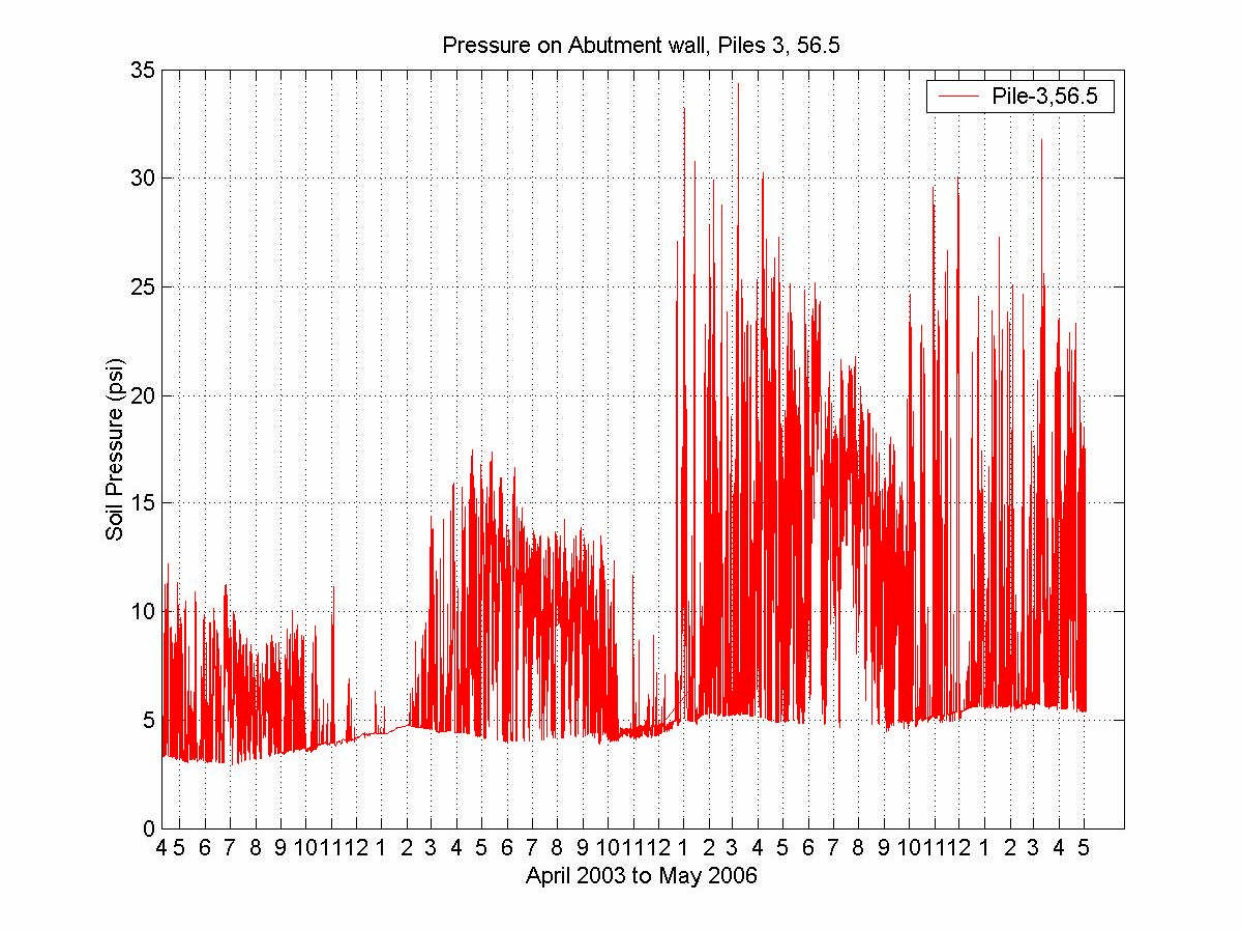

Figure 124. Pressure on the abutment wall at plane of Pile 3, elevation 56.5 meters

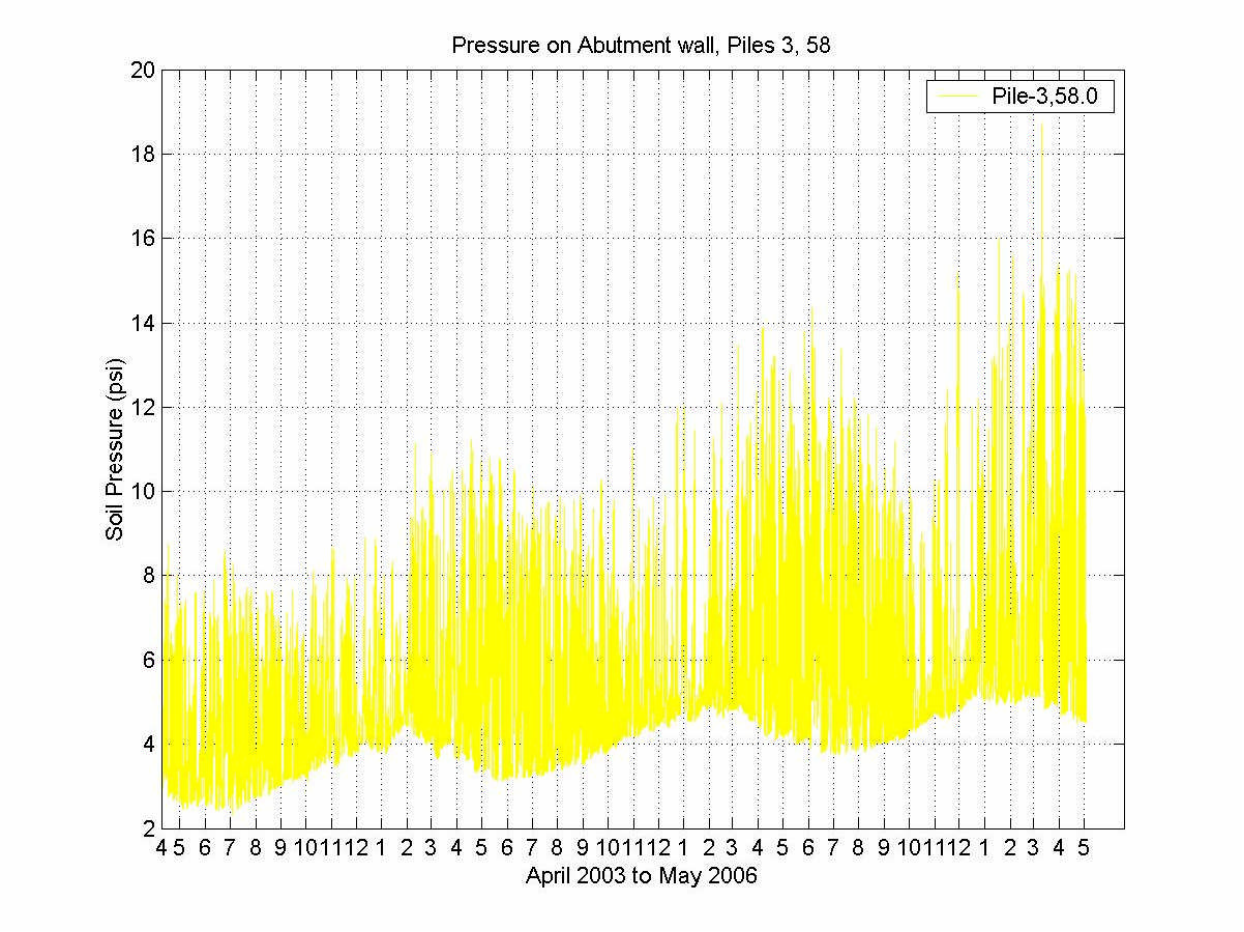

Figure 125. Pressure on the abutment wall at plane of Pile 3, elevation 58 meters

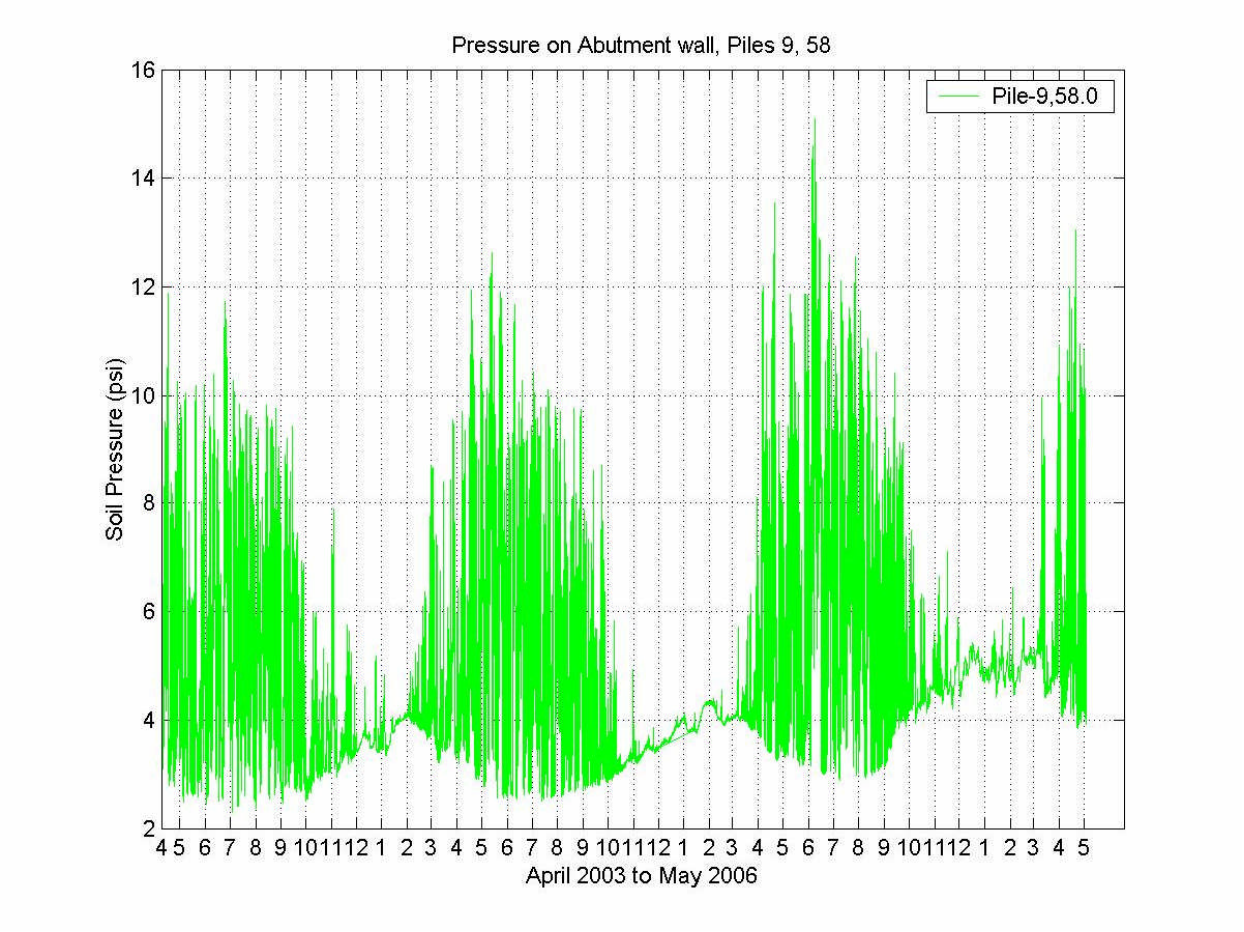

Figure 126. Pressure on the abutment wall at plane of Pile 9, elevation 58 meters

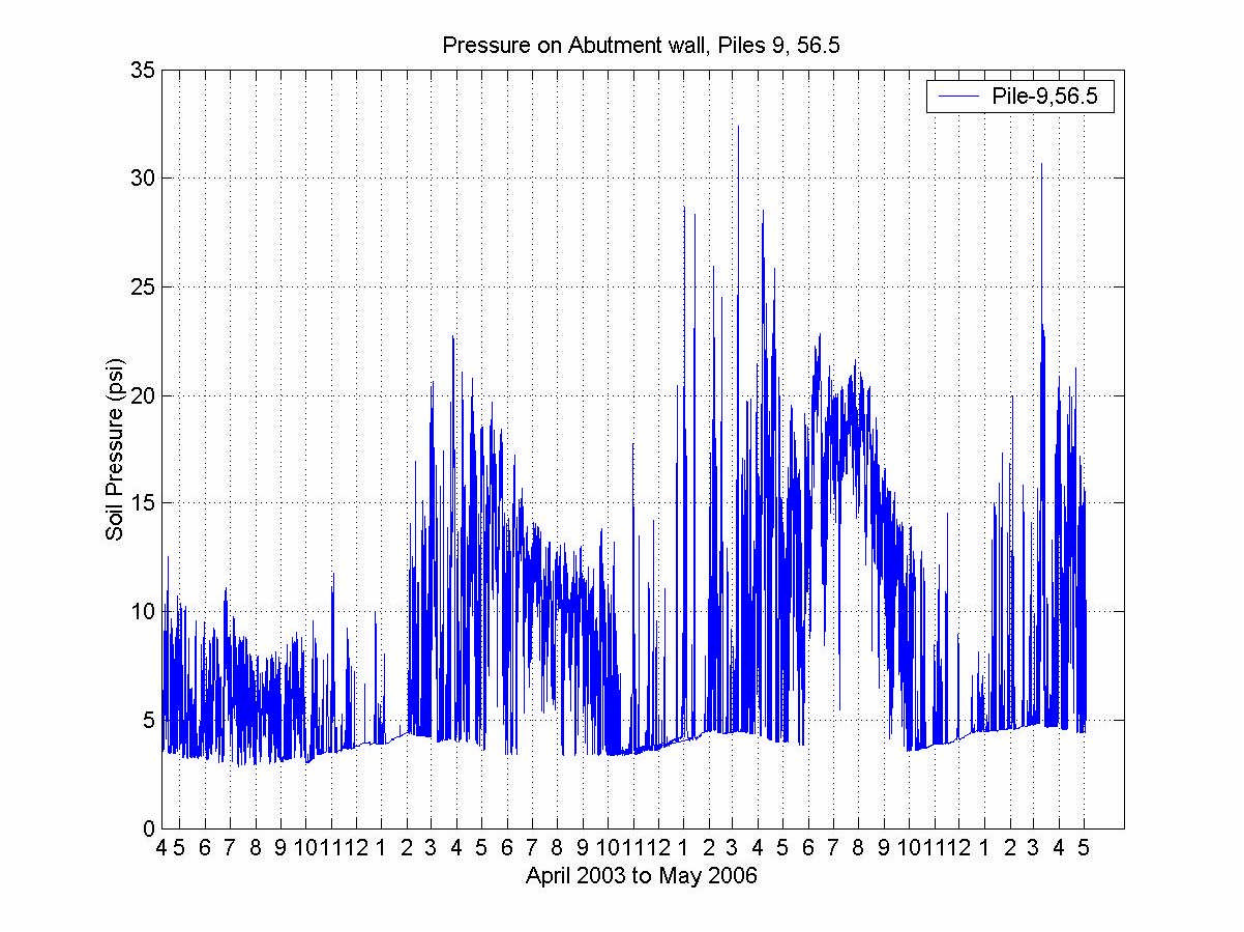

Figure 127. Pressure on the abutment wall at plane of Pile 9, elevation 56.5 meters

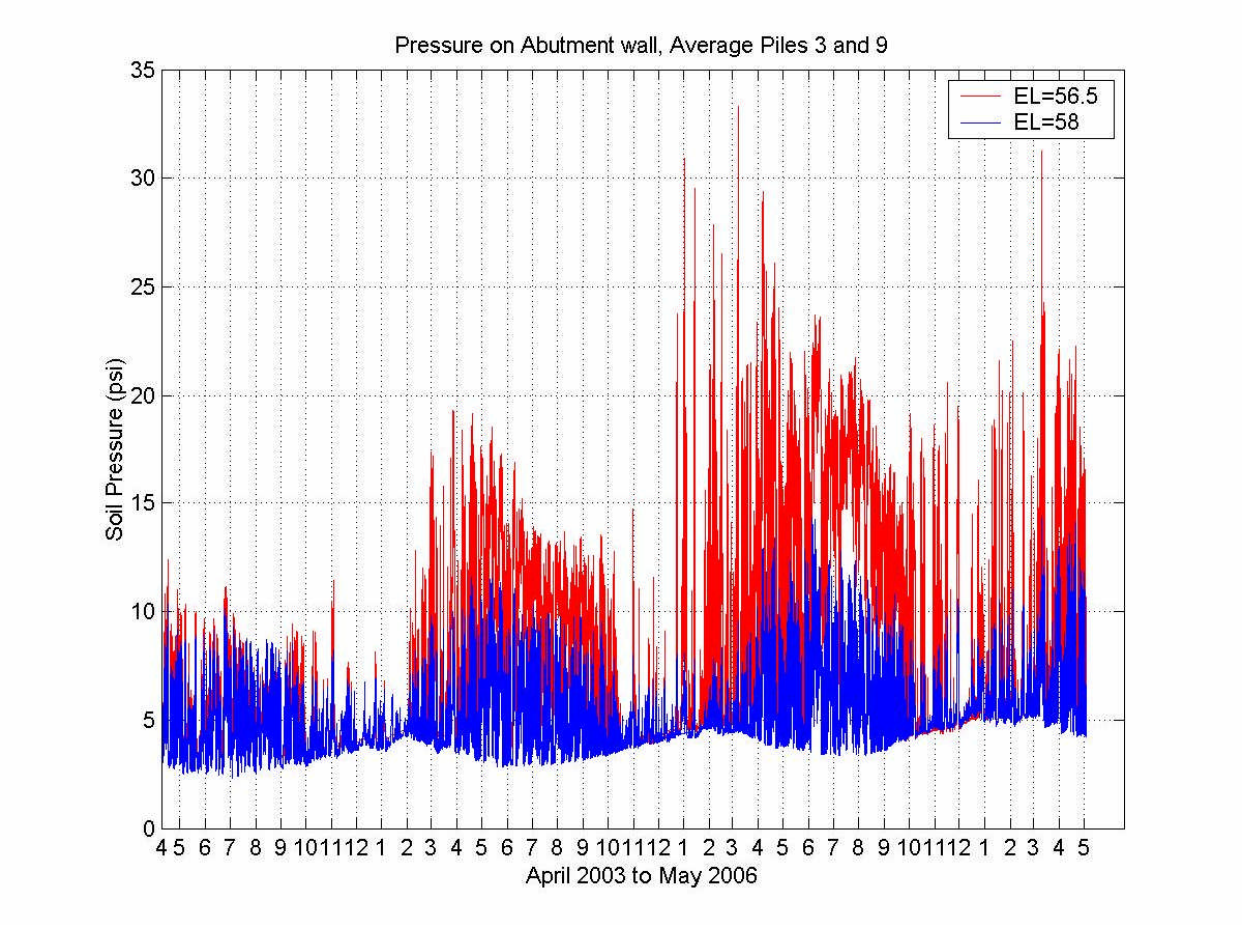

Figure 128. Pressure on the abutment wall at plane of Piles 3 and 9, elevation 56.5 and 58 meters

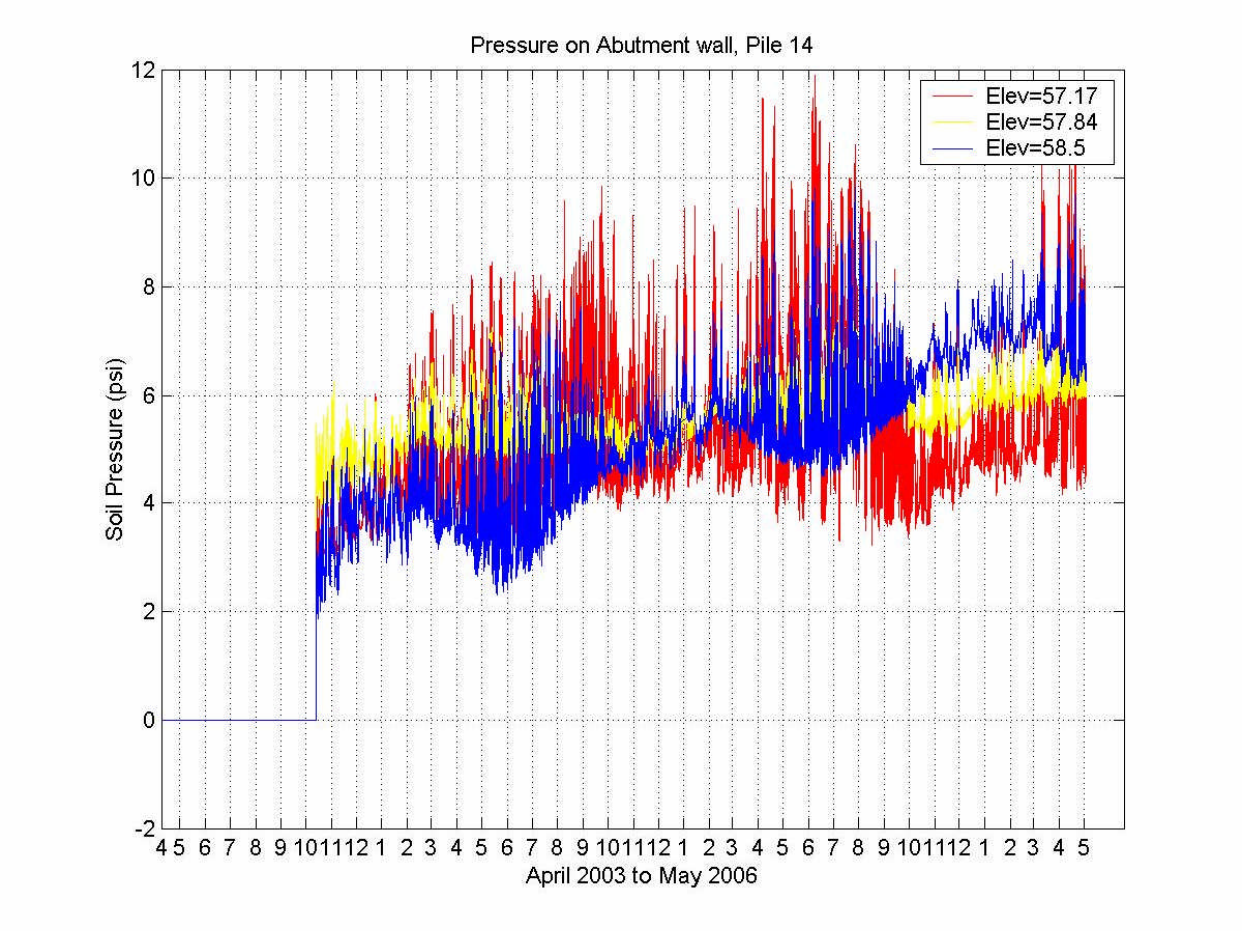

Figure 129. Pressure on Abutment Wall, Pile 14, all elevations

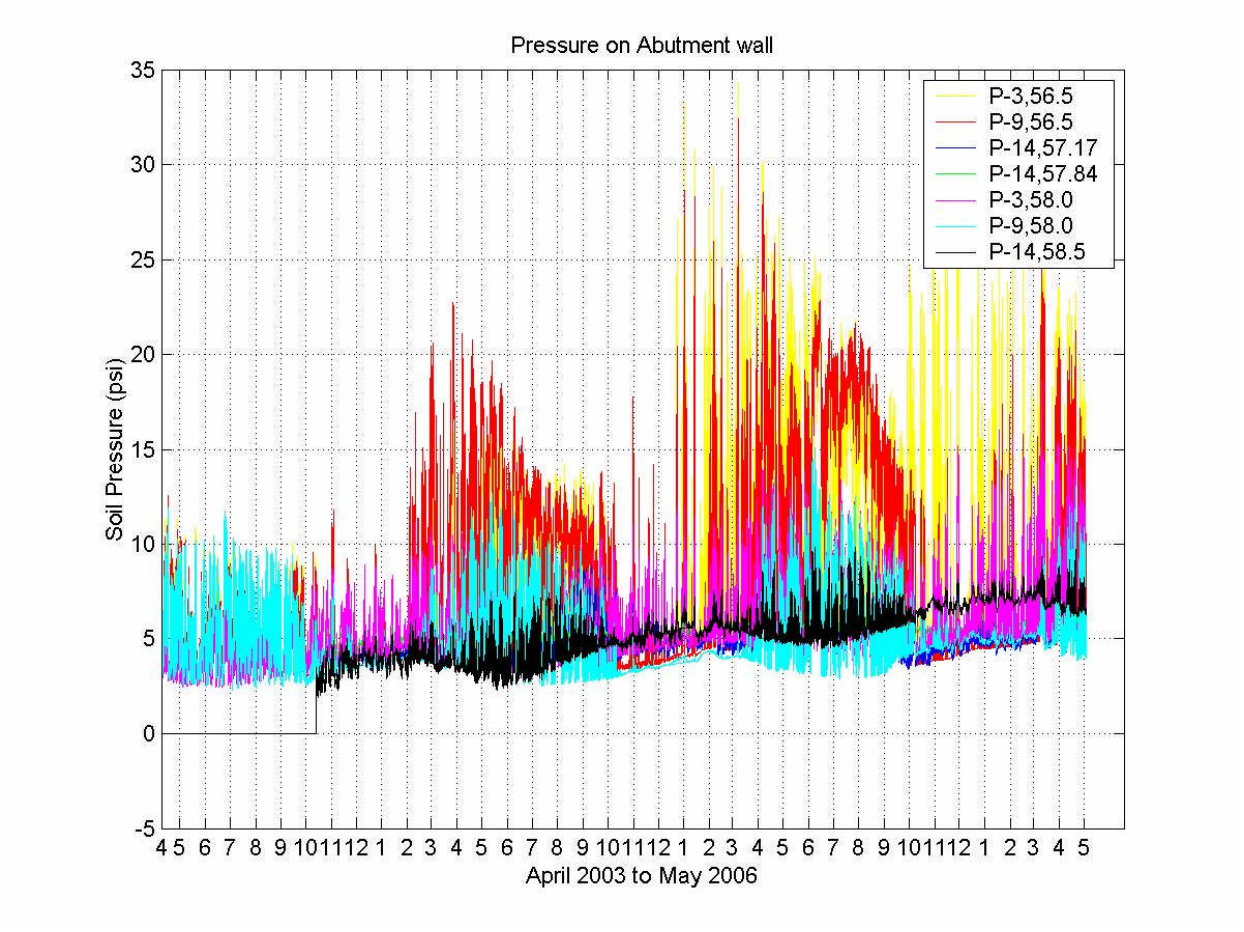

Figure 130. Pressure on Abutment Wall, all locations

CHAPTER 6 - REFERENCES

[1] Roman, E. K. "Evaluation of integral abutments." MS Thesis, Stevens Institute of Technology, Hoboken, N.J. 2004.

[2] Dehne, Y. "Design Procedure for integral abutment bridges." MS Thesis, Stevens Institute of Technology, Hoboken, N.J. 2005.

[3] Khodair Y. A. "Numerical and experimental analysis of integral abutment bridge." PhD Dissertation, Stevens Institute of Technology, Hoboken, N.J., 2005

[4] Rabe, W.H., and Overman, D.H. Long Concrete-Arch Viaduct Built Near Cleveland. Engineering News Record, October 1934. p. 468.

[5] Burke, M. P. Integral Bridges. Transp. Res. Rec. 1275, TRB 1990. Washington, D.C., 53-61.

[6] FHWA. Integral, No-Joint Structures and Required Provisions of Movement." Technical Advisory T5140.13, U.S. Department of Transportation 1980. Washington, D.C.

[7] Wasserman E. Jointless Bridge Decks. AISC Eng. J. 1987; 24(3), pp 93-100.

[8] Hamley E.C. Integral Bridges. Proc. Instn Civ. Engrs, Transp. 1997; 123, Feb. pp. 30-38.

[9] Alampalli, S. and Yannotti, A.P. In-Service Performance of Integral Bridges and Jointless Decks. Transp. Res. Rec. 1624, Transportation Research Board 1998; Washington, D.C., 1-7.

[10] Pezze F.P III Feasibility of Jointless Bridge Decks for Rehabilitation Projects. Client Report 60. Engineering Research and Development Bureau, New York State Department of Transportation, July.1992.

[11]Boardman W.G. North American Bridge Deck Joint Elimination Survey Results Summary. Rhode Island Department of Transportation, Feb. 1997.

[12]Maruri, R.F. and Petro, S.H. "Integral Abutments and Jointless Bridges (IAJB)2004 Survey Summary," FHWA, Integral Abutment and Jointless Bridges Conference, 2005, pp12-29.

[13] FHWA/RD-86/102 Seismic Design of Highway Bridge Foundations, Vol.II. 1986.

[14] Wasserman, E.P., and Walker, J.H. Integral Abutments for Steel Bridges, Highway Structures Design Handbook, Vol. II, Chapter 5, American Iron and Steel Institute (AISI), Chicago, IL.1996

[15] Porter, J.C., Morvant, M.J. and Moon, R.J. Back to the Future for Abutment Design. Concrete International, June 1992, pp. 29-35.

[16] Oesterle, R.G., Tabatabai, H., Lawson, T.J., Refai, T.M., Volz, J.S., and Scanlon, A. Jointless and Integral Abutment Bridges Summary Report." CTL of Skokie, IL, to be published, under review by FHWA. 1998

[17] NJDOT abutment detail

[18] Mourad, S. and Tabash, S.W. Pile Forces in Integral Abutment Bridges Subjected to Truck Loads. Transp. Res. Rec. 1633, TRB 1998, Washington, D.C., 77-83.

[19] Burke, M.P. Bridge Approach Pavements, Integral Bridges and Cycle Control Joints." Transp. Res. Rec. 1113, TRB 1987. Washington, D.C., 54-65.

[20]Wasserman, E.P. Tennessee State Route 50 Bridge Over Happy Hollow Creek, PCI Journal, September-October 1999, pp. 26-36.

[21] Burdette, E.G., Ingram, E.E., Goodpasture, D.W., and Deatherage, J.H Behavior of Concrete Integral Abutments. Concrete International, July 2002, 59-63.

[22] Arsoy, S., Barker, R.M., and Duncan, J.M. The Behavior of Integral Abutment Bridges. VTRC 00-CR3. Virginia Transportation Research Council 1999; Charlottesville, Va.

[23] FHWA. Integral, No-Joint Structures and Required Provisions of Movement." Technical Advisory T5140.13, U.S. Department of Transportation 1980. Washington, D.C.

[24] Robison, J.L. and Luna, R. Deformation Analysis of Modeling of Missouri Bridge Approach Embankments. ASCE Proceedings Geo-Trans 2004. 2020-27.

[25]Stewart, C.F. Highway Structures Approaches, California Department of Transportation, Sacramento, CA. 1985.

[26] Hoppe, E.J. and Gomez, J.P. Field Study of An Integral Backwall Bridge. VTRC 97-R7. 1996. Virginia Transportation Research Council, Charlottesville, Va.

[27] Ohio Department of Transportation (ODOT). Bridge Design Manual, Sections 204.6, 204.7, 205.8 and Sheets 1 to 5 of File ICD-I-82, 2003.

[28] Mass Highway design manual

[29] Hoppe, E.J. Guidelines for the Use, Design and Construction of Bridge Approach Slabs. VTRC 00-R4, Final Report. 1999. Virginia Transportation Research Council, Charlottesville, Va.

[30]Stewart, C.F. Highway Structures Approaches, California Department of Transportation, Sacramento, CA. 1985

[31]Briaud, J.L., James, R.W., and Hoffman, S.B. Settlement of Bridge Approaches (The Bump at the End of the Bridge). Nat. Cooperative Hwy. Res. Program Synthesis of Highway Practice 234, Transportation Research Board 1997; Washington, D.C.

[32] Wahls, H.E. Design and Construction of Bridge Approaches. NCHRP Synthesis of Highway Practice 159, TRB 1990, Washington, D.C.

[33] Stark, T.D., Olson, S.M., and Long, J.H. Differential Movement at the Embankment/Structure Interface: Mitigation and Rehabilitation. Report No. 93-IAB-H1, Illinois Department of Transportation 1995.

[34] Wolde-Tinsae AM, Greimann L.F., and Yang P.S. Nonlinear Pile Behavior in Integral Abutment Bridges. Iowa State University, Ames, Iowa, 1982.

[35] Wolde-Tinsae, A.M., Greimann, L.F., and Johnson, B.V. Performance of Integral Bridge Abutments. J. of the Inter. Assoc. for Bridge and Struct. Engrg. 1983; 17-34.

[36] Wolde-Tinsae A.M., and Klinger J.E. Integral Bridge Design and Construction. Report FHWA/MD-87/04. Maryland Department of Transportation, Jan 1987.

[37] Jorgenson J.L. Behavior of Abutment Piles in an Integral Abutment Bridge. Transportation Research Record 903, TRB 1983, Washington, DC.

[38]Kunin, J. and Alampalli, S. Integral Abutment Bridges: Current Practice in the United States and Canada. Transportation Research and Development Bureau, New York State Department of Transportation 1999.

[39] Abendroth R.E., Greimann, L.F. A rational design approach for integral bridge piles. Transportation Research Record no 1223. Washington, DC: NRC 1989, pp12-23.

[40]Abendroth, R.E., Greimann, L.F., and Ebner, P.B. Abutment Pile Design for Jointless Bridges. ASCE J. Struct. Engrg. 1989; 115 (11), 2914-29.

[41]Girton, D.D., Hawkinson, T.R., and Greimann, L.F. Validation of Design Recommendations for Integral-Abutment Piles. ASCE J. of Struct.Engrg. 1991; 117(7), 2117-34.

[42] Mokwa, R.L. and Duncan, J.M. Investigation of the Resistance of the Pile Caps and Integral Abutments to Lateral Loading. VTRC 00-CR4. Virginia Transportation Research Council, Charlottesville, Va., 2000.

[43] L-PILE Plus 4 for Windows-A Program for the Analysis of Piles and Drilled Shafts Under Lateral Loads", Ensoft, Inc., http://www.ensoft.com, May, 1999.

[44] Wang, S.W. and Reese, L.C. COM624P-Laterally Loaded Pile Analysis Program for the Microcomputer-Version 2.0, U.S. Department of Transportation, Federal Highway Administration, Office of Engineering, Washington, D.C. 1993.

[45]Yee, W.S. Lateral Resistance and Deflection of Vertical Piles – Phase 1. Bridge Department, Division of Highways, California Department of Transportation, Sacramento, CA.1973.

[46] Greimann, L.F., Wolde-Tinsae, A.M., and Yang, P.S. Nonlinear Analysis of Integral Abutment Bridges. ASCE J. of Struct.Engrg 1986; 112(10), 2263-80

[47] Greimann, L.F., Abendroth, R.E., Johnson, D.E. and Ebner, P.B. Pile Design and Tests for Integral Abutment Bridges. Project HR-273, 1987 Iowa Department of Transportation.

[48] Arsoy, S., Barker, R.M., and Duncan, J.M. Experimental And Analytical Investigations of Piles and Abutments of Integral Bridges. VTRC 02-CR6. Virginia Transportation Research Council 2002; Charlottesville, Va.

[49]Coduto, D.P. Foundation Design Principles and Practices. Prentice Hall, Englewood Cliffs, NJ. 1994

[50] Hooper, J.D., Roeder, C.W., Klemencic, R., and Nordquist, K. Best of Both Worlds. Civil Engineering, January 1999, pp. 40-42.

[51] Prakash, S., and Sharma, H.D. Pile Foundations in Engineering Practice, John Wiley & Sons, Inc., New York, NY, 1990.

[52] Burke, M. P. and Gloyd, C.S. The Emergence of Semi-Integral Bridges. TRB 76th Annual Meeting, January 1997.

[53] Burke, M.P. Cracking of Concrete Decks and Other Problems with Integral-Type Bridges. Transp. Res. Rec. 1688, TRB 1999, Washington, D.C., 131-138.

[54] Dicleli, M. and Albhaisi, S.M. Maximum Lengths of Integral Abutment Bridges Based on the Strength of Abutments and the performance of Steel H-Piles under Cyclic Thermal Loading. BU-CEC-03-01, Dept. of Civil Engineering and Construction, Bradley University, Peoria, IL, 2003.

[55] Dicleli, M. and Albhaisi, S.M. Effect of cyclic thermal loading on the performance of steel H-piles in integral bridges with stub-abutments." Journal of Constructional Steel Research 2004, 60(2):161-182.

[56] Yang, P.S., Wolde-Tinsae, A.M., and Greimann, L.F. Effects of Predrilling and Layered Soils on Piles. ASCE J. of Geotech. Engrg. 1985; 111(1), 18-31.

[57] Wasserman, E.P. Design of Integral Abutments for Jointless Bridges, Structure Magazine, May 2001, pp. 24-33.

[58] Wolde-Tinsae, A. and Greimann, L.F. General Design Details for Integral Abutment Bridges. Civil Engineering Practice, Fall 1988, pp. 7-20.

[59] Faraji, S. Behavior of Integral Abutment Bridges in Massachusetts. Project UMTC-96-5, Massachusetts Highway Department.1997

[60] Khodair, Y. and Hassiotis, S. Analysis of Pile-Soil Interaction". 16th Annual ASCE Engineering Mechanics Conference, University of Washington, July 16-18, 2003.

[61] Lawver, A., French, F. and Shield, C.K. Field Performance of an Integral Abutment Bridge." Transp. Res. Rec. 1740, TRB 2000. Washington, D.C., 108-117.

[62] Brown, D.A., Morrison, C., and Reese, L.C. Lateral Load Behavior of Pile Group in Sand. ASCE J. of Geotech. Engrg. 1988, 114(11), 1261-76.

[63] Dicleli, M. and Albhaisi, S.M. Maximum Length of Integral Bridges Based on the Performance of Steel H-Piles at the Abutments", ASCE Journal of Structures 2004

[64] England, G. L., Tsang, N.C.M. and Bush D.I. Integral Bridges, A fundamental approach to the time-temperature loading problem. Imperial College. Thomas Telford Publishing. (2000)

[65] AASHTO LRFD Bridge Design Specifications, 3rd Edition with 2005, 2006 Interims

[66] Burdette, E.G., Goodpasture, D.W., and Deatherage, J.H. A Half-Mile of Bridge Without a Joint. Concrete International, February 2003, 47-51.

[67] Schaefer, V.R. and Koch, J.C. Void Development Under Bridge Approaches. South Dakota Department of Transportation, Office of Research 1992.

[68] Kramer, S.L. and Sajer, P. Bridge Approach Slab Effectiveness. 1991 Final Report, Washington State Department of Transportation.

[69] Lock, R.J. Integral Abutments. M. Eng. Project Report, CUEC/D-SOILS/STR320,2002

[70] Soltani, A.A. and Kukreti, A.R. Performance Evaluation of Integral Abutment Bridges. Transp. Res. Rec. 1371, TRB 1992. Washington, D.C., 17-25.

[71]Greimann, L.F., Wolde-Tinsae, A.M., and Yang, P.S. Skewed Bridges with Integral Abutments. Engineering Research Institute 1982, Iowa State University.

[72] Goel, R.K. Earthquake Characteristics of Bridges with Integral Abutments. ASCE J. of Struct.Engrg. 1997; 123(11), 1435-1443.

[73] Lam, I.P., and Martin, G.R. Seismic Design of Highway Bridge Foundations. Volume II Design Procedures and Guidelines, Report No. FHWA-RD-86-102, June 1986.

[74]Spyrakos, C. and Ioannidis, G. "Seismic behavior of a post-tensioned integral bridge including soil-structure interaction (SSI)' *Soil Dynamics and Earthquake Engineering*, 23 (2003) 53-63.

[75] Burke M.P. The Design of Integral Concrete Bridges. Concrete International, June 1993, 37-42.

[76] Emerson, M. Temperature Differences in Bridges: Basis of Design Requirements. TRRL Laboratory Report 765, Transport and Road Research Laboratory 1977. Croethorne, Berkshore, pp. 39.

[77] Hoffman, P.C., McClure, R.M. and West, H.H. Temperature Study of an Experimental Segmental Concrete Bridge. PCI Journal, March-April 1993, 78-97.

[78] Imbsen, R.A. and Vandershaf, R.S. Thermal Effects in Concrete Bridge Superstructures. NCHRP Report 276, TRB 1985. Washington, D.C.

[79] Potgieter, I.C. and Gamble, W.L. Nonlinear Temperature Distributions in Bridges at Different Locations in the United States. PCI Journal, Precast/Prestressed Concrete Institute, July-Aug 1993, pp. 80-103.

[80] Chen, Y. Important Considerations, Guidelines, and Practical Details of Integral Bridges. J. of Engrg. Tech. 1997, Vol. 14, 16-19.

[81] Barker, R.M., Duncan, J.M., Rojiani, K.B., Ooi, P.S.K., Tan, C.K., and Kim, S.G. Manuals for the Design of Bridge Foundations. Nat. Cooperative Hwy. Res. Program Rep. 343, Transportation Research Board 1991; Washington, D.C.

[82] AASHTO 1994. LRFD Bridge Design Specifications, 1st Edition. Washington, D.C.

[83] Sanford, T.C. and Elgaaly, M. Skew Effects on Backfill Pressures at Frame Bridge Abutments. Transp. Res. Rec. 1415, TRB 1993, Washington, D.C., 1-11.

[84]Roeder, C.W., and Moorty, S. Thermal Movements in Bridges. Transp. Res. Rec. 1290, TRB 1991, Washington, D.C., 135-143.

[85] Tarter JW. A review of jointless-deck designs. Client Report 43. Engineering Research and Development Bureau, New York State Department of Transportation, April 1989.

[86] Oesterle, R.G., and Lotfi, H.R.(2005) “Transverse Movement in Skewed Integral Abutment Bridges”. The 2005 FHWA, IAJB Conference, Baltimore, Maryland 312-322

[87] Weakley, K. “VDOT Integral Bridge Design Guidelines”, FHWA IAJB2005, 61-70

[88] Arrora and Associates, Consulting Engineers, Lawerenceville, N.J. 08648

[89] AASHTO(1996) LRFD Bridge Design Specifications

[90] AASHTO (1998) LRFD Bridge Design Specifications

[91] AASHTO Standard Specifications Bridge Design Manual, 16th Edition

[92] Hassiotis, Sophia and Xiong Kai. (2007) Deformation of cohesionless fill due to cyclic loading” Final Report, UTRC (under preparation)

[93] Sensing Systems Corporation Technical Report 50105-1. Scotch Road Bridge Integral Abutment and HPS/HSC Projects. Stage I Initial Testing. January 15, 2003.

[94]Samanta, A., and Dasgupta, S. (1997). “Finite Element Buckling Analysis of Elastically Restrained Compression Members.” *International Journal of Structures*, 17(1), Jan-Jun, pp.61-81.

[95] Gabr, M. A., Wang, J., and Zhao, M. (1997). “Buckling of Piles with General Power Distribution of Lateral Subgrade Reaction.” *Journal of Geotechnical and Geoenvironmental Engineering*, 123(2), pp. 123-130.

[96] Hibbit, Karlsson & Sorenson, Inc., ABAQUS/Standard 6.3.3 User Manuals, 2002.

[97] Card, G. B. and Carder, D.R. (1993). “A literature review of the geotechnical aspects of the design of integral bridge abutments.” TRL Proj. Rep. 52, TRL, Crowthorne, Berkshire, U.K.

[98] Ng. C.W.W., Springman, S.M. and Norrish, A.R.M. (1998). “Centrifuge modeling of spread-base integral bridge abutments.” Journal of Geotechnical and Geoenvironmental Engineering, V. 124, No. 5., 376-388

[99]Broms, B. B. and Ingleson, I. (1971). "Earth pressure against the abutments of a rigid frame bridge." *Géotechnique*, Institue of Civil Engineeing., U.K., 21 (1), 15-28.

[100] Bang, S. (1984). “Active Earth Pressure behind Retaining Walls.” *Technical note, Journal of Geotechnical Engineering*, ASCE, 111(3), March, 407-412.

[101] Clough, G. W. and Duncan, J. M. (1991). “Earth Pressures, Chapter in Foundation Engineering Handbook.” 2nd edition, edited by Hsai-Yang Fang, van Nostrand Reinhold, New York, NY, 223-235.

[102] Chang, Ming-Fang. (1997). “Lateral Earth Pressures Behind Rotating Walls.” Canadian Geotechnical Journal, Vol. 34, August, 498-509.

[103] Jaky, J. (1944). “The coefficient of Earth pressure at rest,” Journal of the Society of Hungarian Architects and Engineers, Vol 7, 355-358

[104] Sherif, M.A., Fang, Y.S. and Sherif, R.I. (1984). “Ka and Ko behind rotating and Nonyielding Walls,” Journal of Geotechnical Engineering, ASCE, Vol. 110, No. GT1, 41-56.

[105] Das, B.M. (2002) Principles of Geotechnical Engineering, Brooks/Cole Fifth Edition.

[106]Caquot, A., and Kerisel, J (1948). Tables for the calculation of passive pressure, active pressure, and bearing capacity of foundations. Gauthier-Villars, Paris.

[107] Shields, D.H. and Tolunay, A.Z. (1973). “Passive pressure coefficients by method of slices,” Journal of the Soil Mechanics and Foundations Division, ASCE, Vol 99, No. SM12, 1043-1053.

[108] Khodair, Y.A. and Hassiotis, S. (2005) “Analysis of soil-pile interaction in integral abutment.” Computers and Geotechnics, 32, 201-209

[109] Horvath, J.S. (2000). Integral Abutment Bridges: Problems and Innovative Solutions Using EPS Geofoam and Other Geosynthetics.” Rearch Report No. CE?GE-00-2, Manhattan College, Bronx, N.Y.